Application of Carbon-Based Nanomaterials in the field of Enhanced Oil Recovery: An Experimental Approach



Thesis submitted in partial fulfilment for the Award of Degree

Doctor of Philosophy

By

ANURAG PANDEY

RAJIV GANDHI INSTITUTE OF PETROLEUM TECHNOLOGY JAIS, INDIA – 229304

20PE0004 2025

CERTIFICATE

It is certified that the work contained in the thesis titled " Application of Carbon-Based
Nanomaterials in the field of Enhanced Oil Recovery: An Experimental Approach" has been
carried out under my supervision and that this work has not been submitted elsewhere for a
degree.

It i	s further	certified	that	the	student	has	fulfilled	all	the	requirements	of	Comprehensiv	ve,
Car	ndidacy a	nd SOTA	/Ope	n se	minar.								

Supervisor (Dr. Amit Saxena)

Co-Supervisor (**Dr. Shivanjali Sharma**)

DECLARATION BY THE CANDIDATE

I, "Anurag Pandey", certify that the work embodied in this thesis is my own bonafide work and carried out by me under the supervision of "Dr. Amit Saxena and Dr. Shivanjali Sharma" from "August 2020" to "May 2024" at the "Petroleum Engineering & Geoengineering", Rajiv Gandhi Institute of Petroleum Technology, Jais (India). The matter embodied in this thesis has not been submitted for the award of any other degree. I declare that I have faithfully acknowledged and given credits to the research workers wherever their works have been cited in my work in this thesis. I further declare that I have not willfully copied any other's work, paragraphs, text, data, results, etc., reported in journals, books, magazines, reports dissertations, theses, etc., or available at websites and have not included them in this thesis and have not cited as my own work.

Date:	Anurag Pandey
Place:	Roll No: 20PE0004

CERTIFICATE BY THE SUPERVISOR

It is	certified	that	the	above	statement	made	by	the	student	is	correct	to	the	best	of	our
kno	wledge.															

(Dr. Amit Saxena) (Dr. Shivanjali Sharma) (Prof. Satish Kumar Sinha)

(Supervisor) (Co-Supervisor) Head of Department

(PE & GE)

CERTIFICATE

CERTIFIED that the work contained in the thesis titled "Application of Carbon-Based Nanomaterials in the field of Enhanced Oil Recovery: An Experimental Approach" by Mr. Anurag Pandey has been carried out under my supervision. It is also certified that he fulfilled the mandatory requirement of TWO quality publications arose out of his thesis work.

It is further certified that the two publications (copies enclosed) of the aforesaid Mr. **Anurag Pandey** have been published in the Journals indexed by –

- (a) SCI
- (b) SCI Extended
- (c) SCOPUS

Supervisor Co-Supervisor Convener, DPGC

(Dr. Amit Saxena) (Dr. Shivanjali Sharma) (Dr. Hemant Kumar Singh)

COPYRIGHT TRANSFER CERTIFICATE

Title of the Thesis: Application of Carbon-Based Nanomaterials in the field of Enhanced Oil

Recovery: An Experimental Approach

Name of the Student: Anurag Pandey

Date:

Copyright Transfer

The undersigned hereby assigns to the Rajiv Gandhi Institute of Petroleum Technology, Jais, all rights under copyright that may exist in and for the above thesis submitted for the award of the "Doctor of Philosophy".

Anurag Pandey

Place: Roll No: 20PE0004

Note: However, the author may reproduce or authorize others to reproduce material extracted verbatim from the thesis or derivative of the thesis for author's personal use provided that the source and the Institute's copyright notice are indicated.

Dedicated To

My Beloved Grandparents and Parents

For their endless love, support, and encouragement

Acknowledgements

First and foremost, I would want to express my heartfelt gratitude to Dr Amit Saxena and Dr. Shivanjali Sharma, my Doctoral Supervisors, for their patient direction and support, as well as their continuing encouragement, patience, and great confidence in me throughout my research journey. As I go through my studies and daily life, their vast knowledge and experience serve as a source of inspiration. I am very grateful for the many helpful discussions and suggestions that I have received during the thesis preparation process. Every discussion has improved the quality of my work and helped me become a more effective researcher overall. Their guidance also taught me the fundamentals of the workplace. This, I think, will allow me to be a better person in the future, both professionally and personally.

My parents and relatives also deserve the most gratitude from my side as this journey would have been very tough had they not provided emotional support for me throughout it. My grandparents, Pt. Sant Raj Pandey and Mrs. Vidya Pandey and my parents Mr. Ramesh Pandey and Mrs. Nisha Pandey were my rock of Gibraltor, my constant source of strength and faith in myself which propelled me to overcome all hurdles in a short period. A big thanks in my thesis is owed to my sister, Pratibha and Pooja whose efforts and sacrifices on various personal and professional fronts helped me focus on my research work with utmost and ultimate dedication. I would also like to dedicate this thesis to my beloved friend, Shivani, Saurabh, Abhay, Swati, Dheeraj, and Nitish for all their efforts and hard work in being my constant companion through the various highs and the few lows of my PhD journey.

I also sincerely thank the director, Prof. A. S. K. Sinha, of Rajiv Gandhi Institute of Petroleum Technology (RGIPT), Jais, Amethi, for availing research facility and financial support for my experimental work. Furthermore, I would also like to thank Prof. Satish Kumar Sinha (HoD) and Prof. Alok Kumar Singh for providing excellent motivation and encouragement during my research work. I want to express my gratitude to the Department of Petroleum Engineering and Geo-engineering faculty members for their help and support during my research work. I would also like to acknowledge the role of RGIPT, Jais, for providing me with financial aid, laboratory support, and the facilities I need to perform my research successfully. A special note of thanks is also owed to the various research and administrative staff members who ensured that I was never deprived of peace during my stay at RGIPT.

I would also like to take this opportunity to extend my deepest gratitude to the external collaborators in my work. The support and constructive criticism of Prof. Nanda Gopal Sahoo (Kumaun University, Uttarakhand), Prof. Reza Azin (Persian Gulf University Iran), Prof. Jayati Sarkar (IIT Delhi), Prof. Yong Chae Jung (Korea Institute of Science and Technology (KIST), Dr. Chetna Tewari, Dr. Surita Basu, Dr. Himanshu Kesarwani is highly appreciated in making my work more elegant and structured. Thank you all for your time, faith and support.

Finally, I consider myself very lucky to be a member of the Drilling Fluid Design and Cementation Lab and Enhanced Oil Recovery Laboratory (EOR) research group, and the memories, experiences, and knowledge I have acquired from this place will stay with me for a lifetime I would want to express my gratitude to all members of the Drilling Fluid Design and Cementation Lab, and EOR lab for creating and maintaining

a nice environment. For this, my labmates, Dr. Ramesh, Dr. Mukarram Beg, Dr. Ravi, Dr. Krishna, Dr. Himanshu Kesarwani, Vishal, Romy, Anjanay, Alpana, Anirudh, Fahad, Apoorv, Vishnu, Govind, Shivam, Abhilasha, Deepak, Darshan, Shahzar, Zeya, Manoj, Ramaswamy, Saurabh, Devendra, Bidesh Hembram, and Ashim are acknowledged for making this workspace lively and productive. I'd like to also express my gratitude to my seniors and colleagues Dr Alok, Manish Srivastava, Abul Aas, Jitendra Argal, Krishna Kumar Yadav, Arvind, Pooja Pandey, Kumar Nilankar, Divyanshoo, Kaushal, Himanshu, Gyan Prakash, Ayush, Anil, Anas, Abhay, Rajiv and many more whose constant support made my PhD journey, an unforgettable one. I am grateful to them for their support. You fully deserve all of my accolades for support.

......Anurag Pandey

Table of Contents

Acknow	ledgements	i
Table of	Contents	iv
List of F	igures	ix
List of T	ables	xiv
List of A	bbreviations	xv
Preface		xvii
Chapter	: 1 Introduction and Literature Review	1
1.1.	Background	1
1.2.	Challenges associated with cEOR	8
1.3.	Nanoparticles as an additive for Chemical EOR	9
1.4.	Research Gap	13
1.5.	Objective	14
1.6.	Thesis Organization	15
Chapter	: 2 Methodology	20
2.1.	Materials	20
2.2.	Experiment Performed	21
2.2.1	Conductivity measurement	21
2.2.2	2 Dynamic light scattering	26
2.2.3	Surface tension and Interfacial tension	27
2.2.4	4 Contact Angle Measurement	29
2.2.5	5 Rheological analysis	30
2.2.6	6 Recovery test	31
Chapter	: 3 Evaluation of Silicon Carbide Nanoparticles as an Ad	ditive to
Minimiz	e Surfactant Loss during Chemical Flooding	36

3.1. I	ntroduction	36
3.2. E	Experimental section	39
3.2.1	Materials	39
3.2.2	Characterization of Nanoparticles and Adsorbent	39
3.2.3	Critical Micelle Concentration (CMC) Study	40
3.2.4	Adsorption Experiments	41
3.2.5	Impact of SCN on Surfactant Adsorption	42
3.2.6	Impact of Time on Surfactant Adsorption	42
3.3. F	Results & Discussion	42
3.3.1.	Characterization Studies	42
3.3.2 temper	Effect of SCN on Critical Micelle Concentration and its variation variation (CMC)	
3.3.3	Influence of surfactant concentration on the extent of adsorption	48
3.3.4	Impact of time on surfactant adsorption	48
3.3.5	Effect of SCN on surfactant adsorption	49
3.3.6	Effect of temperature on surfactant adsorption	51
3.3.7	Study of adsorption isotherm models	52
3.4.	Conclusion	56
Chapter: 4	Advanced multi-wall carbon nanotube-optimized surfactant-p	olymer
flooding fo	or enhanced oil recovery	58
4.1. I	ntroduction	59
4.2. N	Methodology	63
4.2.1	Materials	63
4.2.2	Methods	64
4.2.3	Modification of MWCNT	64
4.2.4	Dynamic light scattering (DLS) studies	65
4.2.5	Critical micelle concentration measurement	66
4.2.6	Loss of surfactant experiment	67
4.2.7	Effects of Time on the Loss of Surfactant	68
4.2.8	Surface Tension Experiment	68
4.2.9	Analysis of Wetting Behavior	69
4.2.10	Viscometry measurements	70

4.2.11	Core Flooding Experimentations	/ 1
4.3. I	Results and Discussion	72
4.3.1	Characterization of modified MWCNT (mMWCNT)	72
4.3.2	Particle size and ζ-potential of mMWCNT	74
4.3.3	Effect of mMWCNT on CMC	76
4.3.4	Impact of mMWCNT on ST	77
4.3.5	Impact of mMWCNT on IFT	79
4.3.6	Impact of the SDS on the Degree of Adsorption	81
4.3.7	Time effect on adsorption	82
4.3.8	Impact of mMWCNT on surfactant loss	83
4.3.9	Adsorption isotherm model	86
4.3.10	Contact Angle Analysis	90
4.3.11	Viscometry Analysis	93
4.3.12	Dimensional measurement of core	95
4.3.13	Core Flooding Analysis	96
4.4. (00
4.4.	Conclusion	99
	5 Waste Plastic Derived Reduced Graphene Oxide as	
Chapter:	5 Waste Plastic Derived Reduced Graphene Oxide as	A Potential
Chapter:		A Potential
Chapter: Additive f	5 Waste Plastic Derived Reduced Graphene Oxide as	A Potential on102
Chapter: Additive f 5.1. I	5 Waste Plastic Derived Reduced Graphene Oxide as for the Surfactant Polymer Flooding: A Sustainable Solution	A Potential on102
Chapter: Additive f 5.1. I	5 Waste Plastic Derived Reduced Graphene Oxide as for the Surfactant Polymer Flooding: A Sustainable Solution	A Potential on
Chapter: Additive f 5.1. I 5.2. N	5 Waste Plastic Derived Reduced Graphene Oxide as for the Surfactant Polymer Flooding: A Sustainable Solution. Methodology	A Potential on102103108
Chapter: Additive f 5.1. I 5.2. N 5.2.1	5 Waste Plastic Derived Reduced Graphene Oxide as for the Surfactant Polymer Flooding: A Sustainable Solution Introduction Methodology Materials	A Potential on102103108108
Chapter: Additive f 5.1. I 5.2. N 5.2.1 5.2.2	5 Waste Plastic Derived Reduced Graphene Oxide as for the Surfactant Polymer Flooding: A Sustainable Solution Introduction Methodology Materials Synthesis of graphene oxide from waste plastic	A Potential on
Chapter: Additive f 5.1. I 5.2. N 5.2.1 5.2.2 5.2.3	5 Waste Plastic Derived Reduced Graphene Oxide as for the Surfactant Polymer Flooding: A Sustainable Solution Introduction Methodology Materials Synthesis of graphene oxide from waste plastic Dynamic Light Scattering (DLS)	A Potential 103
Chapter: Additive f 5.1. I 5.2. N 5.2.1 5.2.2 5.2.3 5.2.4	5 Waste Plastic Derived Reduced Graphene Oxide as for the Surfactant Polymer Flooding: A Sustainable Solution Introduction Methodology Materials Synthesis of graphene oxide from waste plastic Dynamic Light Scattering (DLS) Surface tension measurement	A Potential on
Chapter: Additive f 5.1. I 5.2. N 5.2.1 5.2.2 5.2.3 5.2.4 5.2.5	5 Waste Plastic Derived Reduced Graphene Oxide as for the Surfactant Polymer Flooding: A Sustainable Solution Introduction Methodology Materials Synthesis of graphene oxide from waste plastic Dynamic Light Scattering (DLS) Surface tension measurement Contact Angle Experiments	A Potential on
Chapter: Additive f 5.1. I 5.2. N 5.2.1 5.2.2 5.2.3 5.2.4 5.2.5 5.2.6 5.2.7	5 Waste Plastic Derived Reduced Graphene Oxide as for the Surfactant Polymer Flooding: A Sustainable Solution Introduction	A Potential n
Chapter: Additive f 5.1. I 5.2. N 5.2.1 5.2.2 5.2.3 5.2.4 5.2.5 5.2.6 5.2.7	5 Waste Plastic Derived Reduced Graphene Oxide as for the Surfactant Polymer Flooding: A Sustainable Solution Introduction	A Potential n
Chapter: Additive f 5.1. I 5.2. N 5.2.1 5.2.2 5.2.3 5.2.4 5.2.5 5.2.6 5.2.7 5.3. I	5 Waste Plastic Derived Reduced Graphene Oxide as for the Surfactant Polymer Flooding: A Sustainable Solution Introduction Methodology Materials Synthesis of graphene oxide from waste plastic Dynamic Light Scattering (DLS) Surface tension measurement Contact Angle Experiments Viscosity Measurement Flooding Experiments Results and Discussion	A Potential 102
Chapter: Additive f 5.1. I 5.2. N 5.2.1 5.2.2 5.2.3 5.2.4 5.2.5 5.2.6 5.2.7 5.3. I 5.3.1	5 Waste Plastic Derived Reduced Graphene Oxide as for the Surfactant Polymer Flooding: A Sustainable Solution Introduction	A Potential n

5.3.5	Rheological analysis	126
5.3.6	Flooding Results	128
5.4. C	onclusion	133
Chapter:	6 Sustainable potassium-doped graphene oxide from	oak fruit
agricultura	al waste for a synergistically improved nanofluid-surfacta	ant slug for
enhancing	oil recovery	134
6.1. Ir	ntroduction	135
6.2. N	lethodology	139
6.2.1	Materials	139
6.2.2	Synthesis of GO from agricultural waste	139
6.2.3	Characterization	140
6.2.4	Hydrodynamic Size and Stability Analysis	141
6.2.5	Surface tension measurement	142
6.2.6	Interfacial tension study	143
6.2.7	Adsorption studies	143
6.2.8	Measurement of contact angle	144
6.2.9	Rheological analysis	145
6.2.10	Core flooding experiments	146
6.3. R	esults and Discussion	147
6.3.1	Characterization of synthesized K-GO	147
6.3.2	Particle Size and Zeta Potential	149
6.3.3	Studies of Surface Tension	152
6.3.4	Impact of nanoparticles on the surface tension	153
6.3.5	Effect of pH on the Surface Tension	154
6.3.6	Analysis of Interfacial Tension	156
6.3.7	Impact of K-GO on Interfacial Tension	157
6.3.8	Impact pH on Interfacial Tension	158
6.3.9	Analysis of Adsorption behavior	159
6.3.10	Adsorption isotherm model of SDS on Sand surface	162
6.3.11	Adsorption kinetics model	166
6.3.12	Wettability modification	168
6313	Rheological Analysis	171

6.3	Recovery test	175
6.4.	Conclusion	177
Chapte	er: 7 Conclusions and Future Directions	178
7.1.	Conclusions	178
7.2.	Potential Areas for Future Study	180
Refere	nces	182

List of Figures

Figure 1. 1. Different types of EOR methods
Figure 2. 1: (a) Conductivity measurement setup, (b) Probe sonicator23
Figure 2. 2: Dynamic light scattering Setup
Figure 2. 3: (a) Wilhelmy plate (b) Du'Nouy ring
Figure 2. 4: Contact angle measurement instrumental schematic
Figure 2. 5: Scientific Rheometer.
Figure 2. 6: Sandpack Flooding experimental setup
Figure 2. 7: Core flooding instrumental setup
Figure 3. 1: Experimental Methodology
Figure 3. 2: Determination of the CMC using conductivity method46
Figure 3. 3: Variation of CMC with the concentration of SCN
Figure 3. 4: Effect of temperature on the CMC of surfactant in the presence of 200 ppm
SCN
Figure 3. 5: Surfactant adsorption variation with different parameters (Time, Surfactant
Concentration, SCN Concentration) at 30° C
Figure 3. 6: Effect of SCN concentration on surfactant adsorption51
Figure 3. 7: Effect of temperature on adsorption of 200 ppm SCN with anionic
surfactant solutions at (a). 30° C temperature, (b). 50° C temperature, and (c). 70° C
temperature
Figure 3. 8: The best-fit model (Langmuir Isotherm Model) for adsorption isotherm
study

Figure 4. 1: Flow chart for experimental methodology.	65
Figure 4. 2: HRTEM images of modified MWCNT (mMWCNT)	73
Figure 4. 3: Raman Spectroscopy of (A) Pristine CNT (B) Modified MWC	CNT
(mMWCNT)	74
Figure 4. 4: XRD analysis of mMWCNT	74
Figure 4. 5: Particle and zeta size of the mMWCNT with anionic surfactants	76
Figure 4. 6: (a) CMC determination of SDS through conductivity measurement	(b)
Effect of mMWCNT concentration on the CMC of the surfactant.	77
Figure 4. 7: (a) Surface tension vs varied surfactant concentration (SDS), (b) the ef	fect
of surface tension using mMWCNT with SDS surfactants (CMC)	79
Figure 4. 8: (a) Interfacial tension of varying SDS concentration, (b) effect of interfa	cial
tension with and without SDS (at CMC)	80
Figure 4. 9: Impact of the duration of ageing on the process of surfactant adsorption	
Figure 4. 10: Surfactant adsorption variation with different parameters (Ti	
Figure 4. 10: Surfactant adsorption variation with different parameters (Ti Surfactant Concentration, mMWCNT Concentration) at 30°C	me,
	85
Surfactant Concentration, mMWCNT Concentration) at 30°C	ime,85
Surfactant Concentration, mMWCNT Concentration) at 30°C	ime, 85 sient 90
Surfactant Concentration, mMWCNT Concentration) at 30°C	85 hient 90 n in
Surfactant Concentration, mMWCNT Concentration) at 30°C	ime,85 sient90 n in92
Surfactant Concentration, mMWCNT Concentration) at 30°C	
Surfactant Concentration, mMWCNT Concentration) at 30°C	ime,85 sient90 n in9293

Figure 4. 15: Displacement efficiency and pressure drop of water, SDS and PAM+
SDS+ mMWCNT (P+S+C), where P stands for polymer, S for SDS and C for
mMWCNT99
Figure 5. 1: Experimental methodology
Figure 5. 2: The Surface tension measurement with the help of Du-Nouy ring111
Figure 5. 3: Measurement setup of the goniometer instruments
Figure 5. 4: Characterization of RGO using Raman spectroscopy114
Figure 5. 5: TEM and SEM analysis of the reduced graphene oxide
Figure 5. 6: (a) FTIR analysis of reduced graphene oxide, (b) TGA analysis of reduced
graphene oxide
Figure 5. 7: Particle size and zeta potential of the RGO
Figure 5. 8: Effect of RGO concentration with surfactant on Surface Tension whereas
G is graphene nanosheets, S is SDS, C is CTAB, and T-is Triton X100119
Figure 5. 10: Wetting characteristics of RGO using contact angle measurements, G is
reduced graphene oxide nanosheets, S is SDS, C is CTAB, T is Triton X100123
Figure 5. 11: Study of the wetting behavior of varying RGO concentration of (a)
Cationic surfactant (CTAB), (b) Anionic surfactant (SDS), and (c) Nonionic surfactant
(Triton X-100) versus time
Figure 5. 12: Study of pH on optimized RGO concentration (100 ppm), although legend
W stands for water, G is RGO, A is acid, and B stands for the base127
Figure 5. 14: Sand pack flooding experiment result. (a) Pressure drops, (b) Oil recovery,
& (c) Water cut
Figure 6. 1: Experimental methodology 140

Figure 6. 2: Graphical representation of sample preparation for Rheological analysis
Figure 6. 3: (a) XRD analysis of K-GO, and (b) FTIR analysis of K-GO149
Figure 6. 4: (a) Characterization of K-GO by Raman spectroscopy, and (b) UV spectra
of K-GO
Figure 6. 5: SEM analysis of K-GO
Figure 6. 6: Particle size and Zeta potential of samples in which K stands for K-GO, S
for SDS, C for CTAB, and T for Triton X100151
Figure 6. 7: Impact of surfactant concentrations on the surface tension, (a) for anionic
surfactant (SDS), (b) for cationic surfactant (CTAB), and (c) for nonionic surfactant
(Triton X100)
Figure 6. 8: (a) Impact of K-GO on the surface tension with and without surfactant. (b)
Role of pH on the surface tension with surfactant at CMC (2500 ppm)156
Figure 6. 9: Effect of K-GO on Interfacial tension (a) without anionic surfactant (SDS)
(b) with anionic surfactant (SDS)
Figure 6. 10: Role of pH with varying K-GO concentrations on Interfacial tension, (a)
Without anionic surfactant (SDS), (b) With anionic surfactant (SDS)159
Figure 6. 11: Role of varying K-GO concentrations on the extent of adsorption, (a) at
aging time, and (b) at varying K-GO concentrations at varying surfactant concentration
Figure 6. 12: Fitting curve of, (a) Langmuir, (b) Freundlich, (c) Temkin, and (d)
Redlich-Peterson isotherm model
Figure 6. 13: The study of anionic surfactant adsorption (SDS) on sandstone revealed a
pseudo-second order kinetics profile i.e., the best fit model

Figure 6. 14: Contact angle, (a) varying anionic surfactant concentration (SDS), and (b)
varying K-GO concentration at CMC of anionic surfactant concentration at different
surface
Figure 6. 15: The viscometry analysis of the K-GO with PAM (1000 ppm) and SDS (at
2500 ppm)
Figure 6. 16: The mathematical fitting of rheological data, (a) Carreau Model, (b) Power
law model
Figure 6. 17: The ultimate oil recovery using water, SDS and Nanofluid (K+S+P)
injection for core ID-1&2.

List of Tables

Table 1. 1. Literature of performed oil recovery experiments on various polymeric	
nanofluid	.18
Table 1. 2. Literature survey of utilized nanomaterials in the field of EOR and their	
findings.	.19
Table 3. 1. Characterstic XRD Peaks and Inference	.44
Table 3. 2. Langmuir adsorption parameters	.55
Table 3. 3. Freundlich adsorption parameters	.55
Table 3. 4. Temkin adsorption parameters	.56
Table 4. 1. Model parameters of Langmuir isotherm model.	.87
Table 4. 2. Parameters of Freundlich isotherm model.	.88
Table 4. 3. Temkin model parameters	.89
Table 4. 4. Rheological analysis of chemical slug	.94
Table 4. 5. Parameters of the core	.96
Table 5. 1. Review of different literature outcomes demonstrating NP (with/ without	ıt
surfactant) effect on wettability modification, IFT reduction, and EOR	107
Table 6. 1. Properties of the Core	147
Table 6. 2. The fitting parameters of the isotherm model	l 66
Table 6. 3. The SDS surfactant adsorption kinetics parameters on sand surfaces1	168
Table 6. 4. Contact angle data for the different substrates with varying K-GO	
concentration1	171
Table 6. 5. Mathematical model fitting of viscosity data	174

List of Abbreviations

ASP Alkaline Surfactant Polymer

CEOR Chemical Enhanced Oil Recovery

CMC Critical Micelle Concentration

SCN/SiC Silicon carbide nanoparticles

CTAB Cetyltrimethylammonium Bromide

mMWCNT Modified multiwall carbon nanotube

DPR Disproportionate Permeability Reduction

EDX Energy Dispersive Xray Spectroscopy

EOR Enhanced Oil Recovery

FESEM Field Emission Scanning Electron Microscopy

FTIR Fourier Transform Infrared Spectroscopy

GCMS Gas Chromatography Mass Spectrometry

HLB Hydrophilic Lipophilic Balance

HPAM Partially Hydrolyzed Polyacrylamide

IFT Interfacial tension

IL Ionic Liquid

IPV Inaccessible Pore Volume

KOH Potassium Hydroxide

NMR Nuclear Magnetic Resonance

NPs Nanoparticles

ONGC Oil and Natural Gas Corporation

OOIP Original Oil in Place

PAM Polyacrylamide

PV Pore Volume

SDBS Sodium Dodecyl Benzene Sulphate

SDS Sodium Dodecyl Sulphate

SP Surfactant Polymer

TDS Total Dissolved Solid

TGA Thermogravimetric Analysis

K-GO Potassium Doped Graphene Oxide

RGO Reduced Graphene Oxide

ST Surface Tension

CA Contact Angle

Preface

The world's energy demand is rising steadily, mainly met by burning fossil fuels like coal, crude oil, and natural gas. Many developing countries rely on imports for their energy needs. Coal, despite its abundance, emits high levels of carbon dioxide when burned, making it an unsustainable option. Natural gas, a cleaner alternative, is still developing, leaving crude oil as the primary energy source. However, extracting crude oil is a complex process, involving drilling wells up to 25,000 feet deep, with reservoir pressures reaching 20,000 psi and temperatures hitting 250°C. Initially, wells can rely on natural reservoir pressure for production, known as primary production. But over time, as reservoir pressure decreases, only about 25% of the original oil in place (OOIP) can be recovered, leaving significant resources untapped. To maintain production, reservoir energy must be enhanced through artificial lift mechanisms or enhanced oil recovery (EOR) methods. Enhanced Oil Recovery (EOR) is segmented into three classifications: Thermal methods, Chemical methods, and Miscible gas injection. The primary objective of enhanced oil recovery (EOR) methods is to enhance the overall efficiency of displacing oil, which depends on both microscopic and macroscopic displacement efficiency. Chemical-enhanced oil recovery (CEOR) entails the introduction of a chemical slug containing various chemicals like surfactants, polymers, nanoparticles, alkalis, etc. CEOR operates on the principle of altering the petrophysical characteristics of the reservoir fluid to enhance flow and increase recovery from the well. This process may include reducing interfacial tension (IFT) and altering the preferential wetting behaviors of the reservoir rock surface. The study focuses on different techniques and additives that can be employed to modify reservoir properties, aiming to achieve a higher recovery factor while minimizing surfactant loss due to

adsorption. The loss of surfactant is a major problem during the surfactant polymer injection, which the help of various additive like nanoparticles, nanotubes and nanosheets can minimize. Chapter 1 provides a concise overview of Enhanced Oil Recovery (EOR), outlining its benefits and categorizing its methods. It also examines the criteria for selecting appropriate EOR techniques based on reservoir conditions. It also delves into the specific type of EOR implemented under varying reservoir conditions. Chapter 2 outlines the methodology involving several experimental techniques utilized in the thesis. It primarily focuses on the criteria for selecting surfactants, which involves conducting experiments using zeta potential, surface tension, and conductivity meters. Additionally, interfacial tension experiments and contact angle experiments were performed to modify the wetting behaviors of the substrate. Adsorption experiments were carried out to minimize surfactant loss with additives. Rheological experiments were conducted to evaluate fluid viscosity. Finally, core flood experiments were undertaken to improve oil recovery with additives. This methodology provides a comprehensive approach to understanding and optimizing surfactant selection and its application in enhancing oil recovery. Chapter 3 investigates the use of silicon carbide nanoparticles to reduce anionic surfactant loss during flooding experiments to enhance flooding efficiency while mitigating environmental concerns associated with nanoparticle application. The study examines the adsorption of anionic surfactants at different concentrations of silicon carbide nanoparticles (100, 200, and 300 ppm) and varying surfactant concentrations. Additionally, surfactant adsorption is studied at elevated temperatures (30, 50, and 70°C), and the surfactant's critical micelle concentration (CMC) is evaluated across different concentrations of silicon carbide nanoparticles and temperatures. Following the adsorption experiments, the data is

analyzed using various adsorption isotherm models. Chapter 4 examined the effects of Advanced multi-wall carbon nanotube-optimized surfactant-polymer flooding on enhanced oil recovery. This study investigates the potential of multiwall carbon nanotubes to enhance the efficiency of oil recovery, alter the interfacial tension (IFT) and perform an experiment to modify the wetting characteristics of the rock surfaces. The adsorption studies were conducted to minimize the surfactant loss during flooding experiments. The adsorption data was analyzed using different adsorption isotherm models after the adsorption experiments. Finally, the core flooding experiments were conducted to maximize the oil recovery at the optimized slug, using a combination of 1000 ppm polymer and anionic surfactant (SDS) at CMC, optimizing the concentration of multiwall carbon nanotube. In Chapter 5, the impact of waste plastic-derived reduced graphene oxide as a potential additive for surfactant polymer flooding was investigated. The reduced graphene oxide was synthesized with the help of waste plastic, and the synthesized particles were used in the field of enhanced oil recovery to maximize oil recovery by reducing the IFT and modifying the wetting characteristics of the rock surface. The surface tension was also explored at various surfactants, which are anionic surfactant (SDS), cationic surfactant (CTAB), and anionic surfactant (Triton X 100), with varying RGO concentrations. This study also investigated the influence of pH on surface tension and wettability at optimized concentrations of reduced graphene oxide (RGO). Ultimately, we performed sand-pack flooding experiments to enhance oil recovery. Chapter 6 examined the impact of sustainable potassium-doped graphene oxide from oak fruit agricultural waste as a synergistically improved nanofluidsurfactant slug for enhancing oil recovery. The potassium-doped graphene (KGO) oxide was synthesized with the help of agricultural waste, and these particles were

further utilized in enhanced oil recovery to maximize production by altering the IFT and modifying the wetting behaviors of the rock surfaces. In this study, surfactant adsorption experiments were also explored to minimize surfactant loss, and the adsorption data was also fitted with the adsorption isotherm model and adsorption kinetics. The DLS experiments were conducted to assess the zeta potential of the fluid, through which we can easily evaluate the stability of the surfactant in the presence of KGO. The rheological properties were also investigated to evaluate the viscosity of the prepared sample, which contained KGO, surfactant, and polymer. Finally, core flood experiments were also conducted to evaluate oil recovery. In Chapter 7, the study will present a detailed compilation of findings from the diverse investigations conducted. Additionally, it will propose potential paths for future research exploring deeper into the practical implementation of enhanced oil recovery techniques.



Introduction and Literature Review

1.1. Background

Hydrocarbon recovery from reservoirs is divided into three distinct stages: primary, secondary, and tertiary. Each stage employs progressively more advanced techniques to maximize oil extraction.

Primary Recovery:

The initial stage, primary recovery, relies on the reservoir's natural energy sources, such as solution gas drive, gas cap expansion, or water influx. These mechanisms provide the necessary pressure differential to drive hydrocarbons towards production wells. However, this method typically recovers only 10-15% of the original oil in place (OOIP).

Secondary Recovery:

As reservoir pressure depletes during primary production, the natural drive becomes insufficient to maintain economically viable production rates. At this point, secondary recovery methods are implemented, primarily through water flooding or gas injection. In water flooding, water is injected into strategically placed injection wells, creating a pressure front that sweeps oil towards production wells. This technique can increase recovery to 20-40% of OOIP depending on reservoir characteristics and fluid properties.

Tertiary Recovery (Enhanced Oil Recovery - EOR):

Despite the effectiveness of primary and secondary methods, a significant portion of oil remains trapped in the reservoir due to capillary forces and heterogeneities in the rock formation. Tertiary recovery, or EOR, aims to mobilize this residual oil. EOR techniques are broadly categorized into thermal, gas injection, and chemical methods, as illustrated in Figure 1.1.

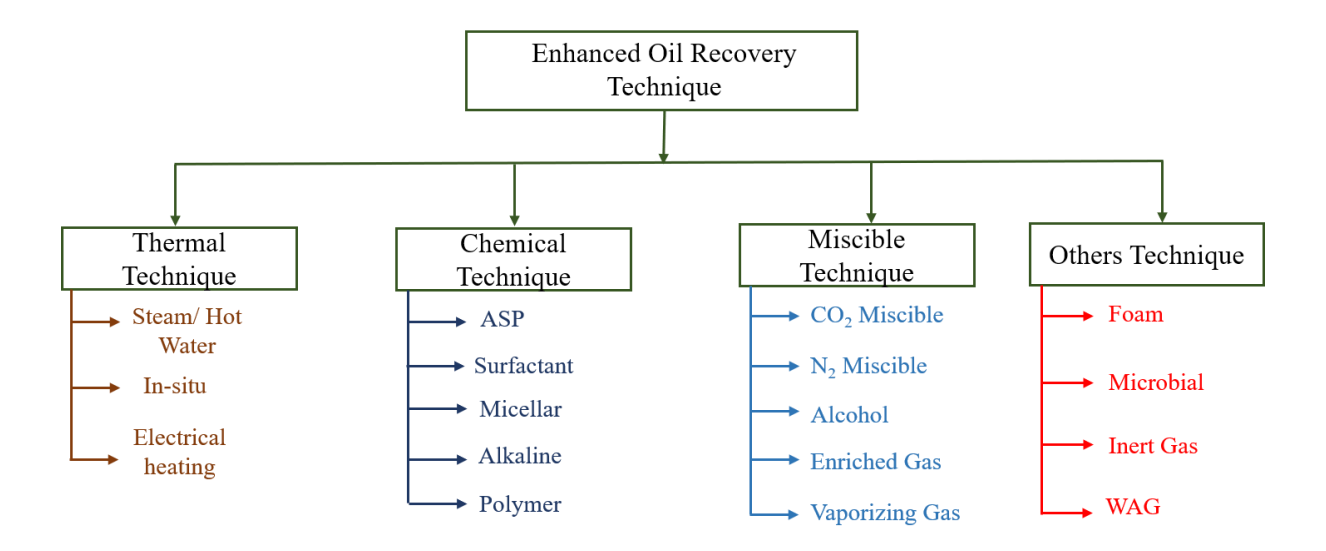


Figure 1. 1. Different types of EOR methods.

Chemical Enhanced Oil Recovery (cEOR):

Among EOR methods, chemical-enhanced oil recovery (cEOR) has gained prominence due to its versatility and effectiveness. cEOR techniques include:

Surfactant flooding: Reduces interfacial tension between oil and water, mobilizing trapped oil.

Polymer flooding: Improves sweep efficiency by increasing the viscosity of the injected water.

Alkaline flooding: Reacts with acidic components in the oil to create in-situ surfactants.

Alkaline-Surfactant-Polymer (ASP) flooding: Combines the benefits of all three methods for maximum oil recovery.

These methods target different oil mobilization and displacement aspects, often achieving recovery factors of up to 60-70% OOIP in favourable conditions. The cEOR technique increases hydrocarbon production by improving microscopic, areal, and vertical efficiencies, resulting in enhanced total displacement efficiency (E), which is mentioned in equation 1.1.

$$E = E_{v} \times E_{d} \tag{1.1}$$

 E_v is the volumetric sweep efficiency, and Ed is the microscopic displacement efficiency. Consequently, volumetric sweep efficiency is represented by equation 1.2.

$$E_{v} = E_{Areal} \times E_{Vertical} \tag{1.2}$$

In equation 1.2, the E_{Areal} is the areal sweep efficiency, and $E_{Vertical}$ is the vertical weep efficiency, giving information about volumetric sweep efficiency.

As global energy demand continues to rise, there is increasing pressure on mature fields to enhance production. cEOR techniques play a crucial role in accessing previously unrecoverable oil, extending the productive life of these fields and contributing to global energy security. The selection and optimization of specific cEOR methods depend on reservoir characteristics, fluid properties, and economic considerations, necessitating thorough laboratory studies and field piloting before full-scale implementation.

Surfactants are crucial in the petroleum industry, particularly in enhanced oil recovery (EOR), drilling, and refining processes. These chemical compounds possess hydrophobic and hydrophilic properties, characterized by a long hydrophobic chain and a hydrophilic head group [1]. Their unique structure significantly reduces surface tension (ST) and interfacial tension (IFT) between immiscible fluids like oil and water. Surfactants are classified into four main categories based on their head group charges:

anionic (negative), cationic (positive), nonionic (uncharged), and zwitterionic (both positive and negative). Each type offers distinct advantages and is selected based on specific application requirements. Anionic surfactants, for instance, excel in stabilizing emulsions and are commonly used in sandstone reservoirs due to their reduced adsorption on negatively charged sand particles. Cationic surfactants, known for their superior cleaning power, are more effective in carbonate reservoirs with positively charged rocks.

Nonionic surfactants are valued for their high salt tolerance and are increasingly used as cosurfactants to enhance the adsorption capabilities of other surfactants. Although more expensive, Zwitterionic surfactants exhibit versatile behavior and increased salt tolerance. They can display non-ionic-cationic, non-ionic-anionic, or cationic-anionic characteristics depending on the environment.

As surfactant concentration increases, the IFT between immiscible fluids decreases until the critical micelle concentration (CMC) is reached. Beyond this point, surfactants form micelles, and further concentration increases do not significantly reduce IFT. Common examples of surfactants include sodium dodecyl sulfate (SDS), sodium dodecyl benzene sulfonate (SDBS), cetyl trimethyl ammonium bromide (CTAB), and polysorbate 20 (Tween 20).

The hydrophilic-lipophilic balance (HLB) is a crucial parameter for categorising surfactants [2], [3]. This numerical scale, ranging from 0 to 60, represents the ratio of hydrophilic to lipophilic components in a surfactant molecule. Higher HLB values indicate greater hydrophilicity, while lower values suggest increased lipophilicity. Emulsions typically require surfactants with HLB values between 10 and 18, with values below 10 indicating lipid solubility and above 10 indicating water

solubility. In enhanced oil recovery, surfactant flooding can typically recover around 10% of the original oil in place (OOIP). This technique and other surfactant applications in the petroleum industry demonstrate these compounds' significant impact on improving efficiency and effectiveness in various operations throughout the sector. The HLB values can be determined with the help of equation 1.3 mentioned below.

$$HLB = \frac{-(\sigma - 45.7)}{2.36} \tag{1.3}$$

Whereas in equation (1.3), σ is the interfacial tension between immiscible fluids.

Surfactant flooding improves the microscopic displacement of crude oil from small areas by decreasing the interfacial tension (IFT) between the crude oil and the fluid displacing it. The decrease in interfacial tension (IFT) may result in the creation of microemulsions. The salinity of the system affects the formation of the emulsion. Under low salinity conditions, a microemulsion of Winsor type I is created, where water acts as the continuous phase, and the emulsion develops as a distinct phase on the surface [4]. High salinity leads to Winsor type II microemulsion formation, where the oil acts as the continuous phase, and the emulsion settles at the bottom. At intermediate salinity levels, a Winsor type III microemulsion is produced, which consists of three separated layers: water at the bottom, an emulsion in the centre, and oil on top. Surfactants also decrease the capillary pressure, facilitating the movement of leftover oil from small areas inside the pores. Moreover, surfactants modify the wettability of the reservoir rock, transforming it from being oil-wet to water-wet. This phenomenon arises from the interaction between the crude oil's non-polar component and the surfactant's hydrophobic portion. As a result, the surfactant adheres to the rock's surface, exposing its hydrophilic head and leading to the rock becoming water wet. This

mechanism exhibits variability in response to cationic surfactants. In addition, the phenomenon of bubble entrapment, which occurs when stationary oil droplets get caught in the displacing fluid, also plays a role in enhancing oil recovery during surfactant flooding.

Polymers are complex compounds with a large molecular weight that consists of repeating components known as monomers. When these polymers are mixed with water, they cause the solution to become more viscous. In the petroleum industry, polymer flooding increases the thickness of the injection fluid by including watersoluble polymers. This process ultimately leads to improved oil recovery. Two main categories of polymers are used: natural biopolymers, such as Xanthan gum, and synthetic polymers, such as Polyacrylamide (PAM). Synthetic polymers are favoured for their cost-effectiveness and efficient performance. Polyacrylamide (PAM) is a commonly used industrial polymer that, when mixed with water, attains the required viscosity for injection fluids. To decrease the amount of adsorption on minerals found in reservoirs, polyacrylamide (PAM) is altered to become partly hydrolyzed polyacrylamide (HPAM), whereby the amide group is transformed into a negatively charged carboxylic group. This alteration in structure reduces the polymer's propensity for adsorption. The viscosity of these polymer solutions depends on the shear rate and decreases as the shear rate increases [5]. Salinity has an impact on viscosity as well. When salts are present, they decrease the viscosity of polymer solutions by reducing the repulsion between molecules, leading to polymer chains' contraction. Divalent salts have a more pronounced influence on lowering viscosity than monovalent salts. The molecular weights of synthetic polymers commonly used in the industry generally fall within the 10^6 to 10^7 Da range. Polymer flooding may increase oil recovery by around 10%.

Polymer flooding improves the viscosity of the injection fluid by adding polymers. This increases the fluid's viscosity and decreases the relative permeability of the displacing fluid by causing polymer adsorption on rock surfaces. This procedure reduces the viscous fingering of the more mobile phase and limits the bypassing of crude oil, consequently enhancing the volumetric sweep efficiency. The primary processes involved in polymer flooding are the lowering of permeability and the control of fluid movement. The fractional flow equation states that water cut is directly proportional to the mobility ratio of water to oil. Therefore, if the viscosity of the injection fluid is increased, its mobility reduces, resulting in a reduced mobility ratio. An optimal mobility ratio should be ≤ 1 . Polymer flooding and controlling the mobility ratio are affected by polymers' adsorption on the reservoir's mineral surfaces. This leads to a phenomenon called disproportionate permeability reduction, where the permeability in specific zones decreases, resulting in a decrease in the relative permeability of water and an increase in the relative permeability of crude oil. The augmentation in the oil's relative permeability may improve the oil cut. In addition, the process of polymer adsorption may slow down the velocity of the injection fluid in these areas, referred to as the permeability reduction effect.

Therefore, an increased polymer viscosity enhances the regulation of the mobility ratio and the efficacy of polymer flooding. Nevertheless, overly long polymer chains might be challenging as they may struggle to enter narrower pore passages inside the reservoir, where oil droplets are confined. This can result in the creation of inaccessible pore volume (IPV). When the length of the polymer chain is greater than

the diameter of the pore, the oil within these pores cannot move. The simultaneous influence of polymer adsorption and mobility control may impede fluid flow between different areas, especially in reservoirs with significant variations in composition.

Integrating two distinct additives governs surfactant polymer flooding, each serving a specific purpose. The primary challenge during the flooding process arises from the higher mobility of the displaced fluid compared to the displaced fluid. This disparity in mobility, characterized by higher relative permeability and lower viscosity, leads to the phenomenon known as viscous fingering, where the less viscous displacing fluid bypasses the more viscous formation fluid. Polymers are added to the displacing fluid to mitigate this issue and increase viscosity, enhancing mobility control. Simultaneously, surfactants alter wettability and reduce surface tension. This dual-additive approach harnesses the benefits of both surfactant flooding and polymer flooding. Ongoing debate points to whether the surfactant and polymer should be premixed into a single slug or injected separately. However, most research indicates that premixing the additives at specific concentrations yields optimal results. This study focuses on surfactant polymer flooding, where the additives are premixed to form a single slug, which is then injected into a sand pack or core to facilitate oil mobilization experiments. A few literature surveys on oil recovery are mentioned in Table 1.1.

1.2. Challenges associated with cEOR

Incorporating different additives to formulate a chemical slug for Chemical Enhanced Oil Recovery (cEOR) is a widely recognized and established approach to recovering larger hydrocarbons. This technique has garnered significant attention and effort from numerous researchers, who have extensively studied and developed various additive combinations to optimize recovery. Their collective work aims to enhance the

efficiency and effectiveness of cEOR, ensuring that a higher volume of hydrocarbons is successfully extracted from reservoirs. The ongoing research in this field highlights the importance and potential of additive incorporation in improving oil recovery rates, thereby contributing to the advancement of cEOR methodologies. Their consensus is that the effectiveness of Surfactant-Polymer (SP) flooding can be significantly enhanced by adding certain chemicals to the slug. However, these chemicals' optimal concentration and selection require extensive laboratory studies. A prevalent issue in cEOR, particularly with the use of surfactants, is the loss due to adsorption onto the rock surface. This adsorption not only diminishes the surfactant's efficiency but also leads to increased costs because higher surfactant dosages become necessary. Researchers in the field have widely acknowledged this challenge. Another critical factor identified in previous studies is the slug's capacity to alter the rock's wettability, which is essential for effective oil mobilization. While some slugs can effectively reduce the interfacial tension (IFT), they often fall short in modifying the reservoir's wettability. Therefore, an ideal CEOR slug should not only minimize IFT but also be capable of changing the wettability of the reservoir while maintaining low adsorption losses. Considering these requirements, various researchers have endeavoured to design suitable slugs for the CEOR process. A thorough literature review indicates substantial potential for improving SP flooding by strategically applying various chemical additives.

1.3. Nanoparticles as an additive for Chemical EOR

Nanoparticles (NPs) have gained significant attention in recent years due to their unique structural and thermal properties, stemming from their small size and large surface area. These properties enhance the efficacy of surfactant-polymer (SP) flooding

in oil recovery. Despite their potential, field trials have been hindered by the extremely high cost of NPs. Nonetheless, laboratory-scale studies have demonstrated the potential of NPs as additives in chemical flooding, drawing considerable interest from researchers. Promising results from these studies have established NPs as viable candidates for improving surfactant flooding efficiency. Researchers have utilized NPs to address the issue of surfactant adsorption losses on rock [6]-[10]. The small size of NPs results in a high surface area and surface charge density, enabling even a small quantity to reduce surfactant loss significantly. Various researchers have combined NPs with surfactants to enhance oil recovery. For instance, Rezk and colleagues used zinc oxide NPs (~50 nm) with surfactants, achieving a 25 mN/m reduction in interfacial tension (IFT) and an additional 8% oil recovery compared to using surfactant alone [11]. Similarly, iron oxide NPs were employed by Kazemzadeh et al. for asphaltene precipitation during carbon dioxide injection. At the same time, Ehtesabi et al. reported a 14% increase in oil recovery with just 0.01 wt% of titanium oxide NPs in the flooding slug [12], [13]. Venancio et al. successfully reduced surfactant adsorption from 28% to 16% using silica NPs [14]. Additionally, Saxena et al. found that alumina and silica NPs reduced the adsorption of soap nut oil surfactants on various mineralogical surfaces [10]. Silica NPs have also been used by Wu et al. to minimize surfactant loss on rock surfaces, resulting in a 4.68% increase in oil recovery [15]. NPs not only aid in reducing surfactant adsorption but also lower the IFT, which would help improve the capillary number, indicating improved oil recovery. Yekeen et al. demonstrated that various NPs effectively reduced IFT between the surfactant-NP solution and n-decane [16]. Nanoparticles (NPs) are highly effective in reducing the interfacial tension (IFT) between water and oil, primarily due to their ability to position themselves at the

interfacial layers [17]. At low concentrations, nanoparticles lower the IFT by adsorbing onto the surface of the liquid. However, as the concentration of nanoparticles increases, they can nearly eliminate surfactants from the bulk aqueous phase, leaving no free surfactant available in the solution [18]. This phenomenon is particularly significant because surfactants are crucial in reducing IFT. Moreover, research has demonstrated that incorporating non-ferrous metal nanoparticles into an anionic surfactant solution can substantially reduce IFT, achieving reductions of 70% to 79% [19]. This highlights the potent synergistic effect between nanoparticles and surfactants in interfacial applications. Giraldo and colleagues conducted a study involving aluminium oxide nanoparticles (Al₂O₃ NPs) combined with an anionic surfactant. Their research highlights the potential of these nanoparticles to alter the wettability of rock surfaces. Specifically, the Al₂O₃ nanoparticles were found to transform the rock surfaces from being oil-wet to water-wet. This change in wettability is crucial in the context of enhanced oil recovery techniques. The transition to a water-wet state facilitates oil displacement from the rock pores, thereby enhancing the efficiency of oil extraction processes. The researchers demonstrated that using Al₂O₃ nanoparticles, along with the anionic surfactant, not only modifies the rock's wettability but also contributes to an increase in the ultimate oil recovery. This finding suggests that such nanofluids could significantly improve the performance of oil recovery operations, offering a promising approach to maximize the extraction of oil from reservoirs. Recent studies have indicated that the inclusion of nanoparticles (NPs) in surfactant flooding processes can lead to substantial rheological alterations, particularly demonstrating as increased viscosity. This enhanced viscosity, while beneficial in certain contexts, can have a profound impact on the efficiency of oil recovery processes. The presence of NPs

modifies the flow characteristics of the surfactant solutions, making them more resistant to deformation and flow. This resistance translates to a thicker, more viscous fluid that can influence the movement and distribution of the surfactant within the oil reservoir. As a result, the altered rheology due to NPs can either improve or impede the displacement of oil, depending on the specific conditions and properties of the reservoir. The overall effect on oil recovery is thus a complex interplay of factors, including the concentration and type of nanoparticles used, the surfactant's nature, and the oil-bearing formation's geological characteristics. Consequently, while NPs have the potential to enhance certain aspects of surfactant flooding, careful consideration and optimization are required to harness their benefits without inadvertently compromising the efficiency of the oil extraction process [17], [18]. Additionally, Suleimanov et al. made a substantial discovery by observing that adding nanoparticles to a surface-active agent solution induced a transformation in the fluid's flow behavior, shifting it from Newtonian to non-Newtonian characteristics. This modification was accompanied by a notable doubling of the solution's viscosity. This breakthrough holds substantial promise for enhanced oil recovery, specifically in surfactant flooding processes. The increased viscosity achieved through this innovative nano-surfactant solution plays a crucial role in effectively controlling the mobility ratio. By enhancing the ability to manage this ratio, the nano-surfactant solution can potentially improve the efficiency and effectiveness of surfactant flooding, thereby optimizing oil extraction and recovery processes [19]. These studies collectively suggest that NPs can significantly enhance surfactant flooding performance in the oil industry by improving oil recovery because of IFT reduction, spontaneous emulsion formation, wettability alteration and Flow characteristics modification. However, the primary challenge remains the costeffectiveness of applying NPs on a large scale. The literature review of some utilized NPs in the field of EOR is mentioned in Table 1.2.

1.4. Research Gap

One of the significant challenges in Chemical Enhanced Oil Recovery (CEOR) is the loss of surfactants and polymers, primarily due to adsorption onto reservoir rock surfaces, degradation, or chemical reactions with reservoir fluids. These processes reduce the effectiveness of the injected chemicals, resulting in diminished oil recovery and increased operational costs. Consequently, minimizing these losses is crucial for improving the efficiency of CEOR operations and ensuring the economic viability of the recovery process. To address these challenges, further research is necessary to develop more efficient surfactants and polymers that exhibit lower adsorption rates, enhanced thermal stability, and reduced interaction with reservoir minerals. This can involve the incorporation of nanomaterials, such as nanoparticles and nanosheets, which have shown potential in improving the performance of surfactant-polymer systems. By minimizing surfactant loss and enhancing the overall efficiency of the Chemical Enhanced Oil Recovery (CEOR) process, these advanced materials can contribute to improved oil recovery while mitigating associated environmental concerns. Nanomaterials have gained significant attention in the field of Enhanced Oil Recovery (EOR) due to their ability to improve oil displacement and recovery. However, despite the successful incorporation of various nanomaterials, carbon-based nanomaterials (such as carbon nanotubes, graphene, and fullerenes) have not been extensively utilized in EOR applications. This lack of integration is largely due to several research gaps that need to be addressed to fully harness their potential. Bridging these gaps could lead to more efficient and sustainable oil recovery techniques.

1.5. Objective

According to the literature survey, researchers have predominantly concentrated on surfactant-polymer (SP) flooding because of its high recovery efficiency and ease of controlling its parameters. This has consequently guided the focus of our work. Although SP flooding is notably effective in extracting a significant portion of the residual oil from reservoirs, it has drawbacks. One major issue is surfactant adsorption, which remains a vital challenge during the process. To address this, the study has shifted towards enhancing SP flooding by incorporating various chemical additives, aiming to improve its effectiveness in maximizing the recovery factor. NPs have been employed in this study to minimize surfactant loss and IFT, which helps improve the capillary number by enhancing recovery efficiency. It also modifies the wetting behavior of the rock surfaces by which the untouched hydrocarbon can be recovered, which also helps to increase the recovery factor. We employed different types of nanomaterials and precise procedures to achieve this objective, as outlined below.

- Silicon carbide nanoparticles are utilized to reduce surfactant loss during chemical enhanced oil recovery (cEOR).
- Modified multi-walled carbon nanotubes (mMWCNTs) are employed in cEOR to mitigate surfactant loss. These nanotubes effectively modify interfacial tension (IFT) and wettability, enhancing the efficiency of the injection slug and improving oil recovery.
- 3. Reduced graphene oxide (RGO) derived from waste plastic is applied in cEOR to optimize the recovery factor.

4. Potassium-doped graphene oxide, sustainably synthesized from agricultural waste oak fruit, exhibits a synergistic effect when combined with a nanofluid-surfactant slug, maximizing oil recovery.

1.6. Thesis Organization

This thesis is composed of seven chapters, each addressing a specific objective related to the research work. Chapter 1 provides a brief overview of Enhanced Oil Recovery (EOR), emphasizing its advantages and categorizing the various EOR methods. It also discusses how to choose the most suitable EOR techniques based on reservoir conditions and explores the specific types of EOR applied in different scenarios. Chapter 2 focuses on the methodology employed throughout the thesis, highlighting the experimental techniques used. The chapter concentrates on selecting appropriate surfactants, conducting experiments such as zeta potential, surface tension, and conductivity measurements. Interfacial tension and contact angle experiments were performed to modify the substrate's wettability, while adsorption experiments were aimed at reducing surfactant loss with the addition of various additives. Rheological studies were conducted to assess fluid viscosity, and core flood experiments were carried out to enhance oil recovery using additives. This methodology offers a comprehensive framework for optimizing surfactant selection in EOR applications. Chapter 3 examines the use of silicon carbide nanoparticles to reduce the loss of anionic surfactants during flooding experiments, improving efficiency and addressing environmental concerns. The study investigates surfactant adsorption at various concentrations of silicon carbide nanoparticles (100, 200, and 300 ppm) and surfactants, as well as at different temperatures (30, 50, and 70 °C). The critical micelle concentration (CMC) of the surfactant is also evaluated in relation to nanoparticle

concentration and temperature. The adsorption data is analyzed using multiple adsorption isotherm models. Whereas Chapter 4 explores the impact of multi-wall carbon nanotubes in optimizing surfactant-polymer flooding for enhanced oil recovery. It investigates how these nanotubes improve oil recovery efficiency by reducing interfacial tension (IFT) and altering the wetting characteristics of rock surfaces. Adsorption studies aimed at minimizing surfactant loss are conducted, and the data is analyzed using different adsorption isotherms. Core flooding experiments are performed with an optimized slug consisting of 1000 ppm polymer and an anionic surfactant (SDS) at CMC, along with multi-wall carbon nanotubes. However, Chapter 5 investigates the use of reduced graphene oxide (RGO), synthesized from waste plastic, as an additive in surfactant-polymer flooding to enhance oil recovery. This chapter examines how RGO reduces IFT and modifies rock wettability. Surface tension experiments are conducted with different surfactants, including SDS, CTAB, and Triton X 100, at varying RGO concentrations. The influence of pH on surface tension and wettability at optimized RGO concentrations is also explored. Sand-pack flooding experiments are performed to evaluate oil recovery. Where Chapter 6 focuses on the use of potassium-doped graphene oxide (K-GO), synthesized from oak fruit agricultural waste, as a nanofluid-surfactant slug to enhance oil recovery. The chapter covers experiments aimed at optimizing surfactant performance and assessing the efficacy of this novel fluid system. Surfactant adsorption experiments are conducted and fitted to adsorption isotherm models and kinetics. Dynamic Light Scattering (DLS) experiments are used to measure the zeta potential and evaluate the stability of the surfactant in the presence of K-GO. Rheological studies assess the viscosity properties of the K-GO, surfactant, and polymer sample. Core flooding experiments quantify the oil recovery

potential of the developed fluid system. Finally, Chapter 7 presents a comprehensive summary of the findings from the research. It also suggests future research directions for further exploring the practical application of enhanced oil recovery techniques.

 ${\bf Table \ 1. \ 1. \ Literature \ of \ performed \ oil \ recovery \ experiments \ on \ various \ polymeric \ nanofluids.}$

NPs Type	Polymer Type	Polymeric NPs	Porous Media	Temperatur e(°C)	IOR (%)	Ref.
6:0	DEOMA	Conc(ppm)	Damas	30	10.00	[20]
SiO_2	PEOMA	10,000	Berea	30	19.80	[20]
G:O	HDDAM	1500	Sandstone	00	16.25	[21]
SiO_2	HBPAM	1500	Berea Sandstone	90	16.35	[21]
SiO_2	Duon 2	8000		80	21.0	[22]
$S1O_2$	Prop-2- enamide/A	8000	Quartz Sand	80	21.0	[22]
	M		Sand			
SiO_2	AMPS	50,000	Quartz	80	23.30	[23]
3102	AIVII 5	30,000	Sand	80	23.30	[23]
SiO_2	HPAM	600	Quartz	80	10.54	[24]
5102	III AWI	000	Sand	80	10.54	[24]
SiO_2	HPAM	1500	Sandstone	NS	13.0	[25]
Clay	111 7 1111	1500	Buildstolle	110	13.0	[23]
SiO_2	HPAM	1000	Glass	25	10.0	[26]
2102	222 2 2272	1000	Micromode		10.0	[=0]
			1			
SiO_2	HPAM	800	Glass	-	10.0	[25]
			Micromode			
			1			
SiO_2	AM/AA	1500	-	-	18.90	[27]
SiO_2	PA-S	3000	-	25	12.82	[28]
SiO_2	AA/AM	2000	Sandstone	65	20.0	[29]
SiO_2	$AMC_{12}S$	1100	Sandstone	110	24.0	[30]
SiO_2	MeDiC ₈ AM	1500	Sandstone	82.3	20.0	[31]
SiO_2	PEG	10,000	Glass	80	20.0	[32]
			Micromode			
			1			
TiO_2	HPAM	800	Sandstone	-	4.0^{*}	[33]
MM	HPAM	1000	Quartz sand	90	33.10	[34]
T						
Clay	:1					

^{*} For heavy oil

Table 1. 2. Literature survey of utilized nanomaterials in the field of EOR and their findings.

Type of NPs	Ref.	Experiment type	Study	
MgO	[35]	Core Flood	Oil recovery and stability of the nanofluid.	
${ m TiO_2}$	[13]	Core Flood	Transport and retention of NPs and sweep efficiency of TiO ₂ with heavy oil.	
Hydrophobic and hydrophilic silica NPs	[36]	Wettability Index measurement	Impact of NPs adsorption on wettability.	
ZnO	[37]	Core Flood	Impact of ZnO on IFT reduction in surfactant flooding.	
MgO	[38]	Core Flood	Study of fines migration and sweep efficiency.	
Fe ₃ O ₄	[39]	IFT measurement	Study of NPs on the asphaltene precipitation.	
Fe, Fe ₃ O ₂ , Cu	[40]	Viscosity measurement using a viscometer	Impact of microwave radiation on NPs to minimize the viscosity of the heavy oil.	
TiO ₂ , Al ₂ O ₃ , and Cu	[41]	Thermal cubical vessel apparatus	Impact of various nanofluids on critical eat flux.	
${ m SiO_2}$	[42]	Contact angle and core flood	Studied the impact of NPs on the wettability modification by spontaneous imbibition process, which helps to recover more oil.	
Non-ferrous metal	[43]	Contact angle and core flood measurement	Using these particles reduces the IFT and alters the rock surface's wetting behavior to improve oil recovery.	
Al_2O_3	[44]	Contact Angle and Imbibition Tests	Altering the wetting behavior of the rock surface by which more oil is recovered from the core.	
ZrO_2	[45]	Conduct micromodel test for oil recovery	Altering the surface's wettability minimized the IFT and recovered more oil by micromodel test.	
mMWCNT	[46]	Adsorption study, IFT, and Wettability measurement	Minimize the surfactant loss, which helps reduce the IFT and modify the surface's wetness to recover more oil.	

2.1. Materials

This study utilized various surfactants, which were anionic, cationic, and nonionic. The anionic surfactant used was SDS (sodium dodecyl sulfate), with a purity greater than 94% and a molecular weight of approximately 289 g/mol, procured from Rankem Chemicals. The cationic surfactant employed was CTAB (cetyl trimethyl ammonium bromide), which had a purity exceeding 98% and a molecular weight of around 364 g/mol, sourced from Molychem Chemicals. The non-ionic surfactant Triton X-100, obtained from Sigma Chemicals, was also used. Sodium hydroxide (NaOH) and hydrochloric acid (HCl) were also employed to study the impact of pH on various nanomaterials. These chemicals were obtained from SD Fine-Chem Limited and Merck Life Science Private Limited. The research included different carbon-based nanomaterials to evaluate their effectiveness in enhanced oil recovery. These nanomaterials included SCN/SiC (silicon carbide nanoparticles), mMWCNT (modified multiwall carbon nanotube), RGO (reduced graphene oxide nanosheet), and K-GO (potassium-doped graphene oxide nanosheet). For sample preparation and cleaning purposes, deionized (DI) water with a resistivity value of 18.2 M Ω ·m was used. The thoroughness of our research process should reassure you about the reliability of our findings.

2.2. Experiment Performed

2.2.1 Conductivity measurement

Conductivity measurements were conducted using a Labman Multiparameter LMMP-30 (Figure 2.1 (a)) conductivity meter to evaluate the surfactant's critical micelle concentration (CMC) and examine surfactant loss on the sand surface during recovery. This comprehensive analysis enabled the precise determination of the CMC, ensuring an accurate understanding of the surfactant's behavior in the solution. Additionally, the assessment of surfactant loss on the sand surface provided valuable insights into the efficiency and effectiveness of the recovery process, highlighting potential areas for optimization and improvement.

2.2.1.1 Critical micelle concentration determination

To determine the critical micelle concentration (CMC), surface tension measurement and a conductivity meter can be utilized. Begin by preparing a surfactant solution with varying concentrations using deionized (DI) water and the surfactant. Once the solutions are ready, measure the conductivity of each solution with a conductivity meter. After each measurement, carefully clean the probe of the conductivity meter with DI water, then gently dry it with tissue paper to ensure that no surfactant molecules remain attached to the probe during the experiments. After recording all samples' conductivity, plot a conductivity graph versus surfactant concentration. By observing the inflection point on this graph, the value of the CMC can be determined. As the surfactant concentration increases, the conductivity initially rises linearly until it reaches a specific point, after which the slope changes, and the conductivity continues to increase but at a lower rate. This point on the graph, where the slope changes, is identified as the Critical Micelle Concentration (CMC). The CMC

signifies that a further increase in surfactant concentration beyond this point does not lead to additional surfactant adsorption onto the interface. Instead, the excess surfactant contributes only to micellization in the solution.

2.2.1.2 Adsorption Studies

Surfactant loss occurs when surfactant molecules accumulate on a reservoir rock surface from the bulk liquid solution, which is crucial in many industrial and scientific applications. This retention at the solid-liquid interface can lead to significant technical and financial issues. Thus, surfactant retention is crucial in surfactant-based chemical EOR processes, including surfactant flooding, surfactant-polymer flooding, and alkaline/surfactant/polymer (ASP) flooding. Adsorption studies were performed to assess surfactant loss and the effectiveness of various additives in minimizing this loss. Initially, 40 ml surfactant solutions of varying concentrations were prepared for the studies. The conductivity of each prepared sample was carefully measured using a conductivity meter. Surfactant loss was monitored over five or three successive days, and a characteristic graph showed conductivity as a function of surfactant concentration. After measuring the conductivity of the sample, 10 wt% sand particles were added to the bulk phase of the surfactant solution and left undisturbed for 24 hours. Following this period, the sand particles were separated from the surfactant solution using a centrifuge operated for 20 minutes at 3000 RPM. The conductivity of the recovered sample was then examined. The loss of surfactant on the sand particles was determined by measuring the change in surfactant concentration before and after adsorption. The adsorption was evaluated with the help of Equation 2.1 below.

$$A = (C_i - C_f) \times \frac{m_{sol}}{m_{sand}} \times 10^{-3}$$
 (2.1)

Where A denotes surfactant loss on the adsorbent (mg/g). C_i represents the initial surfactant concentration in the absence of sand particles, while C_f stands for the final surfactant concentration after adding sand particles to the bulk phase. Also, m_{sol} and m_{sand} refer to the sample's total mass and the sand particles' mass in grams, respectively.

Several additives, including nanomaterials, were employed to reduce surfactant loss. Nanomaterials were introduced into the bulk phase of the solution after surfactant adsorption was assessed. We mixed surfactant samples of varying concentrations with different concentrations of the nanomaterials. The solution was then sonicated with a probe sonicator (Figure 2.1 (b)) to ensure better nanomaterial dispersion. The same procedure was followed to measure the conductivity of each sample, both with and without sand particles. The initial and final values were used to determine the difference in surfactant concentration, with the expected difference indicating the surfactant loss.

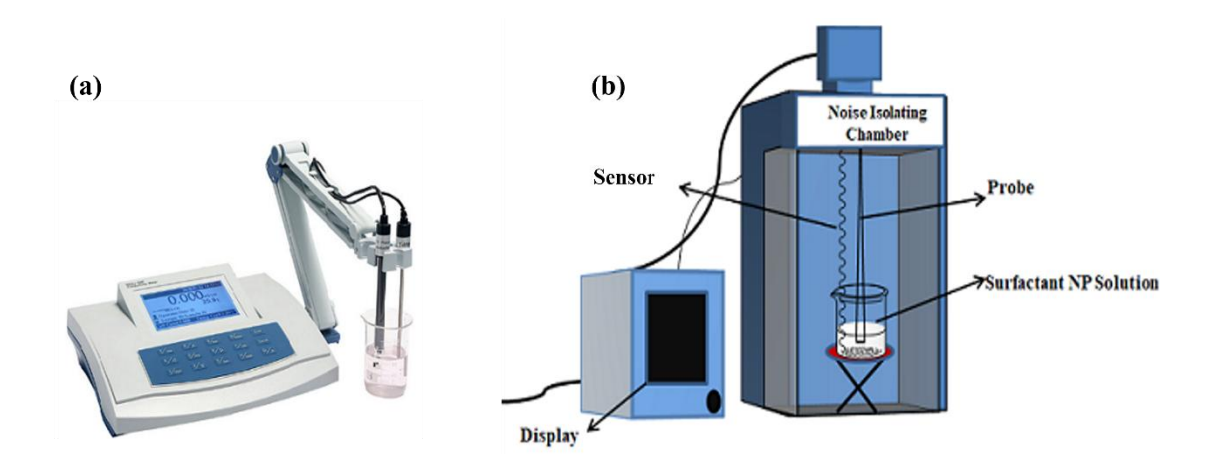


Figure 2. 1: (a) Conductivity measurement setup, (b) Probe Sonicator

2.2.1.3 Adsorption isotherm model

To understand its mechanisms or characteristics, the adsorption data was analyzed using the most employed models, Langmuir, Freundlich, Temkin, and the Redlich-Peterson (R-P) isotherm.

The Langmuir adsorption isotherm assumes a finite number of adsorption sites, with no interactions between adsorbed surfactant molecules. It treats adsorption as a monolayer process, permitting only one surfactant molecule to bind to each site. Additionally, it presumes all adsorption sites are identical and energetically equivalent, with no interaction between adjacent adsorbed atoms. Equations 2.2 and 2.3 give information regarding the Langmuir isotherm model, shown below.

$$q = \frac{q_{\text{max}} C_e K_l}{1 + K_l C_e} \tag{2.2}$$

Or
$$\frac{1}{q} = \left(\frac{1}{K_l q_{\text{max}}}\right) \frac{1}{C_e} + \frac{1}{q_{\text{max}}}$$
 (2.3)

Here, q represents the equilibrium adsorption of the surfactant, and q_{max} denotes the maximum adsorption capacity. Meanwhile, C_e is the equilibrium adsorbate concentration, and K_l is the Langmuir constant, which is associated with the adsorption capacity and depends on the surface area and pore volume.

The Freundlich adsorption isotherm deviates from the assumption of monolayer adsorption, suggesting that the total adsorption across different layers determines the amount of material adsorbed. The Freundlich isotherm model is recognized for describing particle adsorption on heterogeneous surfaces. It characterizes surface heterogeneity and the distribution of active sites and their energies. The mathematical expression of the Freundlich isotherm is represented below in equations 2.4 and 2.5.

$$q = K_f(C_e)^{1/n} (2.4)$$

Or
$$q = \ln K_f + \left(\frac{1}{n}\right) \ln C_e \tag{2.5}$$

 K_f and 1/n are known as the Freundlich constants, providing information about the adsorption capacity and intensity.

The Temkin Adsorption isotherm model is valid for a moderate range of ion concentrations. This model assumes that as adsorption progresses and the surface becomes increasingly covered, the heat of adsorption of the adsorbate molecules decreases linearly. Equation 2.6 represents the mathematical form of the Temkin isotherm model.

$$q = B_T \ln K_T + B_T \ln C_e \tag{2.6}$$

The Redlich-Peterson (R-P) isotherm combines aspects of the Langmuir and Freundlich models, utilizing three parameters to describe adsorption. Unlike ideal monolayer adsorption assumptions, its unique mechanism sets it apart. Equations 2.7 and 2.8 demonstrate the mathematical expression of the R-P isotherm model, as shown below.

$$q = \frac{k_R C_e}{1 + \alpha C_e^{\beta}} \tag{2.7}$$

Or
$$\ln\left(k_R \frac{C_e}{q} - 1\right) = \beta \ln C_e + \ln \alpha \tag{2.8}$$

In the Redlich-Peterson isotherm equation (8), k_R (L/mg) and α [(L/mg) $^{\beta}$] are constants. The parameter β , which ranges from 0 to 1, characterizes the behavior of the adsorption isotherm model. A value of $\beta=1$ corresponds to the Langmuir model, whereas $\beta=0$ represents the linear isotherm model.

2.2.2 Dynamic light scattering

Dynamic light scattering (DLS) accurately measures particle size and zeta potential in suspensions and emulsions. It relies on the Brownian motion of particles, where smaller particles move faster, and larger particles move more slowly in liquids. The light scattered by these suspended particles provides information on their diffusion speed and size distribution. DLS analysis covers particle sizes ranging from 0.3 to 10,000 nm, making it suitable for analyzing and characterizing nanomaterials dispersed in solutions. The particle size distribution of nanomaterials was analyzed via DLS tests, while its zeta potential determined the nanofluid's stability. The Malvern Zetasizer Nano-ZS (Figure 2.2) instrument measured the nanomaterial's mean diameter and zeta potential in aqueous dispersion. About 1.5 ml of the batch of nanomaterials were added to the cuvette at 30°C for particle size measurement. The samples were exposed to a laser beam with a wavelength of 635 nm to observe particles undergoing Brownian motion in a liquid phase. Particle sizes were determined using the Stokes-Einstein equation 2.9 mentioned below.

$$D = \frac{kT}{3\pi nd} \tag{2.9}$$

D represents diffusion coefficients, T denotes temperature, k is the Boltzmann constant, η stands for viscosity, and d indicates hydrodynamic diameter. The cuvette was rinsed twice with methanol to remove any contaminants, and the instrument's 120-second equilibrium period was set to stabilize the temperature for the experiment. Zeta potential was measured using the Malvern Zetasizer Nano-ZS instrument, indicating the potential stability of the colloidal system. Particles with significantly positive or negative zeta potentials will repel each other, preventing agglomeration. Conversely,

particles with low zeta potentials lack forces to avoid flocculation. Stability is typically observed with zeta potential values exceeding +30 mV or more negative than -30 mV.

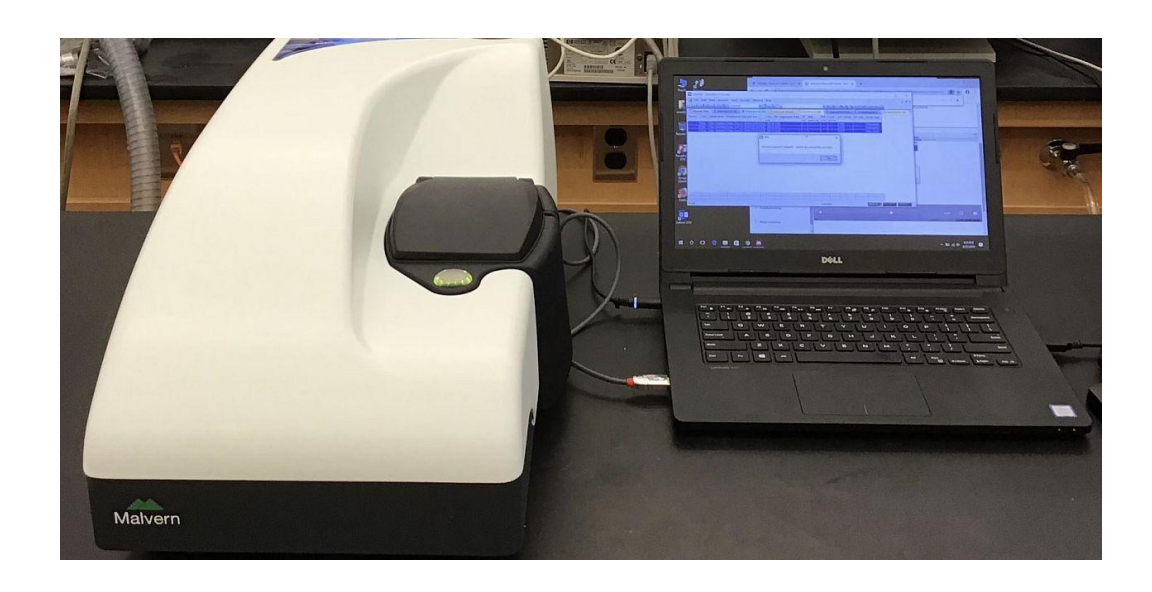


Figure 2. 2: Dynamic light scattering Setup

2.2.3 Surface tension and Interfacial tension

The surface tension of the formulated surfactant mixture in aqueous solution was assessed using the KYOWA DY-500 tensiometer to determine the critical micelle concentration (CMC). The surface tension of differing surfactants was initially measured to explore their respective CMCs. Surfactant solutions of varying concentrations (40 mL) were prepared in deionized water to observe changes in surface tension. Surface tension measurements were conducted using the Du'Nouy ring method, which had a 14.5 mm diameter and 0.4 mm thickness, or Wilhelmy plate, with the ring and plate heated before each test to prevent contamination. In the Wilhelmy plate method for surface tension determination, the plate makes contact with the sample's surface, allowing the liquid to wet the plate and form a lamella around its perimeter. The force needed to break this lamella defines the surface tension of the sample.

In contrast, when using the Du'Nouy ring method, the ring is first submerged in the solution, causing the sample to form a film around the ring. The force required to break this film represents the surface tension of the sample. Figures 2.3 (a and b) illustrate the Wilhelmy plate and Du'Nouy ring setups, respectively. Each surface tension measurement was repeated three times to ensure accuracy and consistency. Solvents such as acetone, hexane, and deionized water were tested to validate the precision of the equipment. The assessment of CMC involved plotting a graph depicting the decrease in surface tension as the concentration of the surfactant mixture increased.

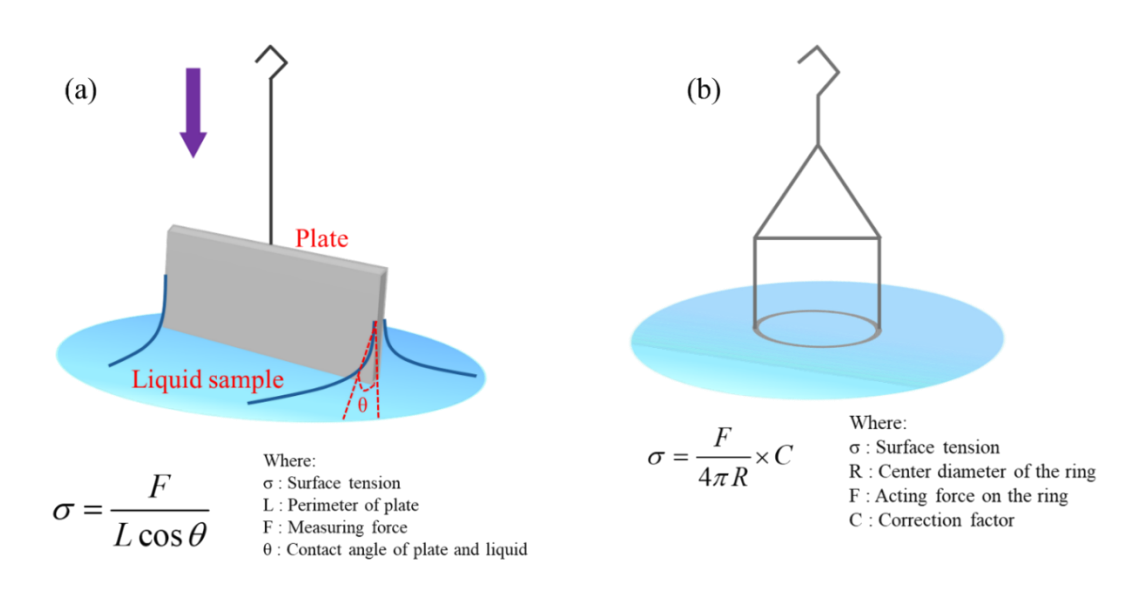


Figure 2. 3: (a) Wilhelmy plate (b) Du'Nouy ring

After finding the CMC of the surfactant, nanomaterials were added into the bulk phase, and the solution was sonicated for better dispersion. Then, the surface tension of the surfactant with nanomaterials was measured. Similarly, the interfacial tension between surfactant and crude oil with and without nanomaterials was measured using a KYOWA DY-500 tensiometer at ambient pressure and room temperature. The IFT experiments employed a platinum Du-Nouy ring with a precision of 0.02 mN/m and also with the help of a Wilhelmy plate. After each experiment, the sample holder was

cleaned with toluene to remove any residual crude oil, followed by acetone to eliminate surfactant remnants, and then dried. Similarly, the ring and plate were cleaned using a burner to remove any traces of crude oil or surfactant from its diameter.

2.2.4 Contact Angle Measurement

Contact angle experiments were conducted to study the wetting behavior of rock surfaces using an Acam-NSC series goniometer from Apex Instruments, India. The goniometer features a flat stage, a backlight, a needle or pipette for dispensing solution onto the rock surfaces, and a recording device for capturing drop images for analysis. The sessile drop method was used to determine contact angles. Based on the contact angle values, the wetting behavior of the rock can be categorized: 0–75° indicates water wet, 75–105° indicates mixed wet, and above 105° indicates oil wet. The instrument's contact angle range is 0 to 180°, with an accuracy of \pm 0.05°. Varying concentrations of different surfactant solutions were prepared to study the wetting behavior of the rock surfaces. Initially, the core was saturated with crude oil for 24 hours, followed by a 2day soaking period. Experiments were conducted using instruments to measure the contact angle of the surfactant solution on the saturated core. Subsequently, nanomaterials were added to the bulk phase of the surfactant solution for further studies. After each experiment, the syringe attached to the instruments was thoroughly cleaned with DI water to ensure no residue remained. The experiments were repeated three times to verify the repeatability of the instruments and schematic of the instruments mentioned below in Figure 2.4.

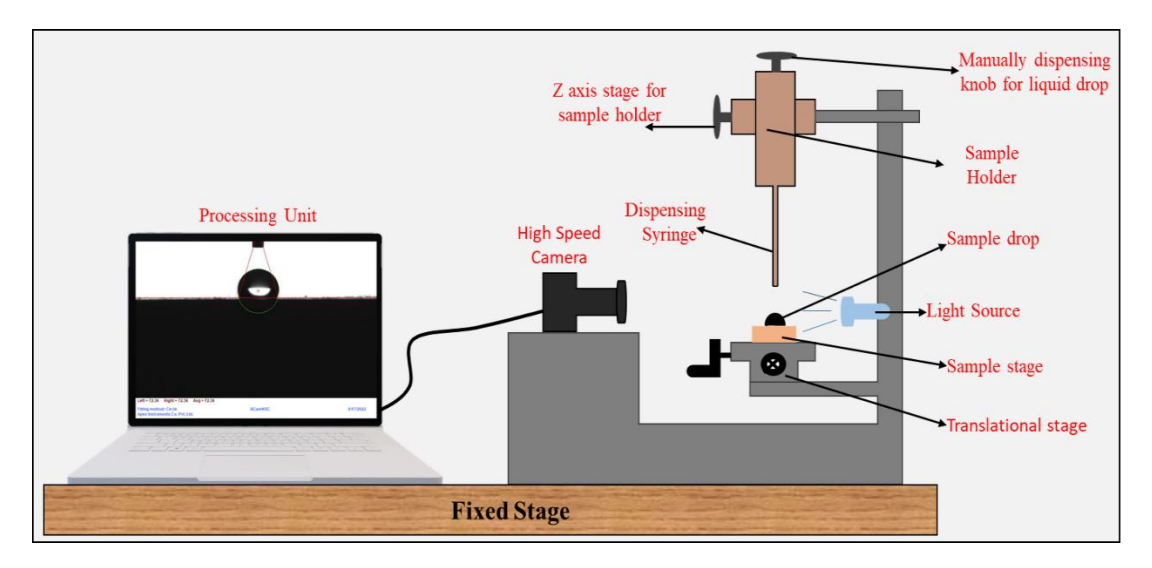


Figure 2. 4: Contact angle measurement instrumental schematic.

2.2.5 Rheological analysis

Rheological analysis was performed to examine the flow behavior and deformation of the prepared slung in response to applied forces, considering factors such as shear rate and temperature. Rheology examines how material shape changes under various forces or stresses, revealing their viscoelastic properties and flow behavior by measuring the applied force and resulting deformation. A modular rheometer (MCR-302e) from Anton Paar (Figure 2.5) determined the samples' viscosity. The rheometer's bob and cup assembly system analyzed the rheological properties of the slug with different polymer and nanomaterial concentrations. After each test, the apparatus was cleaned with DI water and dried. The chemical slug was formulated with the help of polymer and varying nanomaterial concentrations with and without surfactant.



Figure 2. 5: Scientific Rheometer.

2.2.6 Recovery test

2.2.6.1 Sand pack flooding test

Flooding tests were conducted using sand pack flooding equipment purchased from D-CAM Engineers, Ahmedabad, India. This setup includes a sand pack holder, four accumulator cells for chemicals, crude oil, water, and toluene, and a syringe pump maintaining a constant flow rate of 2 mL/min. A heating jacket on the sand pack holder enables experiments at elevated temperatures. A pressure transducer monitors the fluid pressure at the beginning of the sand pack holder. The components are connected with 1/8-inch tubing. The sand pack holder measures 3.81 cm in diameter and 30.48 cm in length. Beach sand (400-500 μm) was cleaned with DI water to remove clay, then dried in an oven at 105°C for 24 hours to eliminate moisture. The sand was manually packed into the holder to create an artificial porous medium. Using Darcy's law, water was first injected to estimate porosity and absolute permeability. Crude oil was then injected, displacing some water to establish initial oil saturation and connate water. Post-

experiment, toluene cleaned the flow lines, and the porous medium was left for five days to become oil-wet. Secondary oil recovery was achieved by injecting water with the syringe pump. The initial oil and irreducible water saturation were obtained using the formula (equations 2.10 and 2.11).

$$S_{oi} = \left(\frac{OOIP}{PV}\right) \times 100 \tag{2.10}$$

$$S_{wi} = 1 - S_{oi} \tag{2.11}$$

 S_{oi} represents the initial oil saturation, while S_{wi} represents the irreducible water saturation. Oil volume is collected at the opposite end of the sand pack holder. Displacing oil via water injection continues until the water cut is nearly 100% achieved. The recovery of oil and water cuts from water flooding was determined using the following formula (equations 2.12 and 2.13).

$$W_{cut}\% = \left(\frac{W_{v}}{N_{v} + W_{v}}\right) \times 100 \tag{2.12}$$

$$O_R\% = \left(\frac{N_v}{OOIP}\right) \times 100 \tag{2.13}$$

Where the OOIP is the original oil in place, PV is pore volume, W_{cut} % is the water cut percentage, W_v and N_v are the produced water volume and the oil volume correspondingly, O_R is the oil recovery factor. The instrumental representation of the sand pack flooding provided below in Figure 2.6.

2.2.6.2 Core flooding test

Core flooding studies evaluated the effectiveness of surfactant polymer flooding for chemical-enhanced oil recovery (CEOR) using nanomaterials. Numerous core displacement tests were conducted at ambient temperature and pressure to assess the efficiency of surfactant and nanomaterial/surfactant slugs in enhancing oil recovery under reservoir conditions. The setup included two transfer accumulators (one for oil and one for nanofluid), a core holder, and an HPLC constant rate syringe pump for injecting water or nanofluid at high pressure. A back-pressure regulator (BPR) maintained the system's pressure at the core's output, while a differential pressure transducer (DPT) measured the pressure drop across the core. First, select the core for the recovery test. Measure its dimensions using vernier calipers and weight using a weighing machine. Then, the porosity of the core was determined using a helium porosity meter provided by D-CAM Engineers, Ahmedabad, India. After assessing porosity, conduct a gas permeability test to estimate the gas permeability of the core. After these experiments, saturate the core with DI water and leave it for one day. Next, saturate the core with crude oil, leave it for two days, and start the experiment. The core flooding setup mentioned below in Figure 2.7.

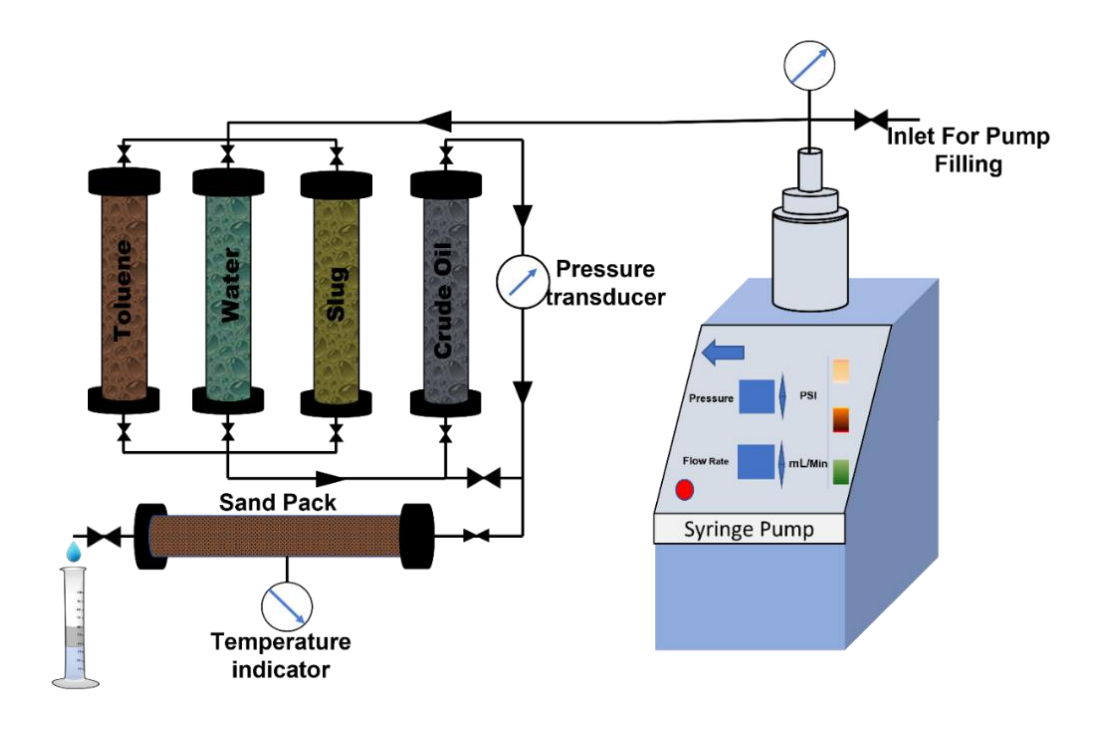


Figure 2. 6: Sandpack Flooding experimental setup.

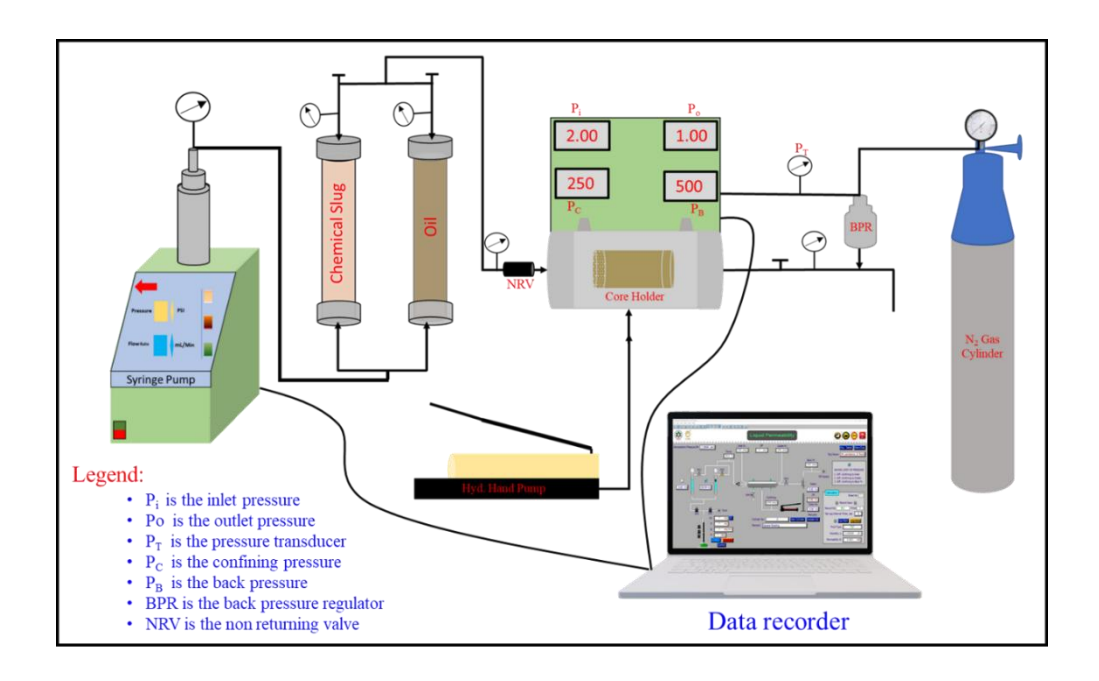


Figure 2. 7: Core flooding instrumental setup.

Evaluation of Silicon Carbide Nanoparticles as an Additive to Minimize Surfactant Loss during Chemical Flooding

Abstract

Surfactant flooding is a prolific enhanced oil recovery technique. It alters the rock fluid interfacial interactions between reservoir fluids and rocks. However, a pair of impeding factors often limit the economic viability of the process and need to be optimized. The first is surfactant loss on the adsorbent surface due to adsorption, a potential environmental problem. The second is the Critical Micelle Concentration (CMC), which governs the amount of surfactant pumped. This study aimed to minimize the surfactant loss and the CMC, thereby optimizing the flooding efficiency and reducing the environmental concerns for nanoparticle applications in the field. To achieve this, Silicon Carbide nanoparticles (SCN) were employed as additives to the surfactant solution. It was observed that using SCN reduces the surfactant adsorption by as much as 44% and the critical micelle concentration by 14%. The studies also observed that the concentration of SCN required to get these results is dramatically (more than 25 times) lower than previously reported literature on other nanoparticles. Adsorption isotherm studies provide insight into the type of adsorption. The adsorption isotherm follows the Langmuir model.

3.1. Introduction

The mature oil fields are witnessing a decline in production with lesser exploration. This has led the energy industry to focus on increasing production using

alternative techniques from the mature fields. The onus is on chemical or other methods to augment the slowing oil production as speculation surrounds oil sustainability [47]. Surfactant flooding is a popular EOR technique that can improve tertiary production [48]–[51]. Surfactants have found their way into numerous industrial applications due to their foam capabilities, reducing the surface/interfacial tension, altering wettability, etc. Sodium dodecyl sulfate is a widely used anionic surfactant for oil field applications.

The surfactant in EOR applications alters the reservoir's solid/liquid and liquid/liquid interactions to improve oil recovery. The charged surface of reservoir rocks tends to adsorb the ionized surfactants onto their surfaces [52]. This adsorption occurs as the liquid-solid interface often provides better thermodynamic stability than the bulk of the liquid phase. Initially, the surfactant adsorption is in the form of a monolayer. However, at higher surfactant concentrations, micelles form, which adsorb in mono or bilayer. To reduce surfactant adsorption, we tend to use surfactants that possess a charge similar to the surface [6]. The surfactant adsorption is affected by many other factors, including salt concentration and pH [53]. Adsorption of surfactant hinders the oil recovery process. It reduces the effective surfactant concentration and restricts the impact of the flood on oil recovery. This also poses an imminent concern for the subsurface environment being polluted by surfactants that are hard to degrade naturally [52]. Numerous studies have been performed to decrease the tendency of the surfactant to get adsorbed on the surface. Al Hashim et al. studied alkali additives at low salinity & recognized the mechanism to be through the change of charge density on the rock surfaces [54]. Wang et al. experimented with polymers to reduce surfactant adsorption in carbonate reservoirs. They ascertained that polymers reduce active adsorption sites by forming a layer on the rock surface [55]. However, other studies

have ended with opposing results, rendering polymers and alkalis ineffective for the desired purpose [15], [56]. Thus, interest has now turned towards studies of nanoparticles and their effects on surfactant adsorption. The use of Silica nanoparticles reduces surfactant adsorption significantly [15], [57]. Wu et al. attributed this to the nanoparticle's adherence to the sand wall. They also studied dynamic adsorption and concluded that the constant friction and collisions between the nanoparticles and the sand wall reduce dynamic surfactant adsorption [15]. In the context of oil and gas recovery, research focusing on nanoparticles like SiO₂, TiO₂, Graphene, etc., has gained traction [48], [58], [59]. However, studies on Silicon Carbide Nanoparticles (SCN) have not yet been conducted in the field of EOR to the best of our knowledge. SiC is a promising material in the nanotechnology domain. It has numerous desirable properties, such as excellent mechanical strength at high temperatures, good heat resistance, good oxidation resistance, low expansion coefficient, and high biocompatibility [60]. Its chemically inert and biocompatible nature also reduces concerns from a formation damage point of view.

The end goal of injecting any surfactant into the reservoir rock is to reduce interfacial tension (IFT). Critical Micelle Concentration (CMC) is the surfactant concentration beyond which the IFT practically remains constant [61], [62]. Injecting concentrations higher than the CMC is deemed unnecessary. Thus, the reduction of any surfactant by CMC enhances the economic viability of the flood. This study aims to test the effects of SCN on SDS adsorption onto the sand surface and its impact on its CMC.

3.2. Experimental section

3.2.1 Materials

SDS, known as Sodium Dodecyl Sulfate of purity ~93%, was acquired from Rankem Chemicals. Silicon Carbide nanoparticles (SCN) of size ~50nm were obtained from Sisco Research Laboratories Pvt. Ltd. Locally procured beach sand was used as the adsorbent surface in the adsorption experiments. The 400 to 500 µm sand was first washed with deionized water and dried at 105°C using a vacuum oven for 24 hours to remove its moisture content. The experimental methodology shown in Figure 3.1.

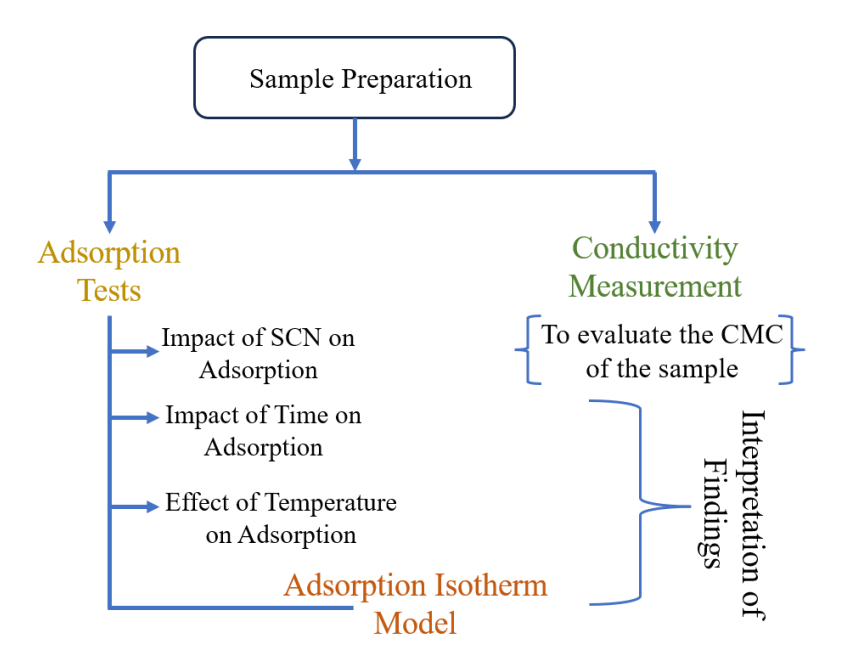


Figure 3. 1: Experimental Methodology

3.2.2 Characterization of Nanoparticles and Adsorbent

Nanoparticles attract the attention of researchers because of their smaller size and high surface area-to-volume ratio. The size of the nanoparticles dispersed in water was measured by Dynamic Light Scattering (DLS) using the Malvern Zetasizer Nano ZS equipment. Brunauer Emmett Teller (BET) analysis using the Belsorp Max II

Analyzer determined the specific surface area of the nanoparticles. DLS is based on the interference of the light scattered by the particles dispersed in a liquid phase. In contrast, the BET is based on the principles of adsorption and desorption to calculate the specific surface area. It assumes the adsorption of gas molecules on the solid surface occurs in layers that do not interact with one another [7]. Apart from this, the mineralogical content of the adsorbent also affects the surfactant's adsorption. Hence, the XRD analysis helped study the mineralogical composition of the sand particles.

3.2.3 Critical Micelle Concentration (CMC) Study

The surfactant CMC was obtained by measuring the conductivity of solutions of various surfactant concentrations and observing the inflection point on the graph. The surfactant concentration was varied from 500 ppm to 4000 ppm. The issue at which a distinct change in the conductivity versus concentration plot slope occurred was noted [9], [63]. Surfactant solutions were prepared in deionized (DI) water using magnetic stirring at 1000 rpm for 15 minutes at room temperature. The Labman Multiparameter LMMP-30 conductivity meter measured the conductivity of the surfactant solution. The instrument was calibrated with the standard solutions. After each measurement, the probe of the conductivity meter was cleaned carefully with DI water and wiped with the help of Kim wipes tissue paper to remove moisture content. The conductivity of the DI water was measured after every measurement to ensure that no surfactant contamination on the probe was present. The measurements were performed at atmospheric pressure and 30°C, 50°C, and 70°C.

3.2.4 Adsorption Experiments

The method of calculating surfactant adsorption on the rock surface was similar to that of past researchers [7], [64]. First, 40 ml surfactant solutions of different surfactant concentrations (500 ppm to 4000 ppm) were prepared. The conductivity of each sample was measured cautiously with the help of a conductivity meter. Surfactant loss was monitored for five consecutive days, and a characteristic curve was generated for the conductivity as a function of surfactant concentration. Adsorbent (sand particles of 400 µm, 10 wt% or 4 grams) was added to every surfactant solution and kept undisturbed for 24 hours. After 24 hours, a centrifuge extracted the sand particles from the surfactant solution by rotating it for 15 min at 3000 RPM, and the conductivity was measured. The remaining surfactant was calculated by using the previously generated characteristic curve. The surfactant adsorption on the sand particles was calculated by evaluating the variation of surfactant concentration before and after adsorption. The surfactant solution's adsorption (Ad) was determined by equation 3.1 [7], [65].

$$A_d = \left(C_i - C_f\right) \times \frac{m_{totalsol.}}{m_{sand}} \times 10^{-3}$$
(3.1)

Where A_d represents surfactant adsorption on the sand (mg/g), C_i is the initial concentration of surfactant solution with no added sand. C_f is the final concentration of the surfactant solution after the sand particle is added to the solution (ppm), m_{total sol}. represents the total mass of the sample(grams), m_{sand} is the mass of the sand particle in grams used in the solution. Various adsorption isotherm models, including Langmuir, Freundlich, and Temkin models, described the surfactant adsorption on the adsorbent. These models are known to determine a relationship between adsorbate (surfactant

concentrations) on different adsorbent surfaces. The effect of temperature was studied with the same adsorption experiments at temperatures of 50 °C and 70 °C.

3.2.5 Impact of SCN on Surfactant Adsorption

Surfactant samples of different concentrations (500-4000 ppm) were mixed with 100 ppm, 200 ppm, and 300 ppm of SCN. The mixture was sonicated using a probe sonicator for better dispersion. A similar routine was followed to measure the conductivity of the sample with and without sand particles. The initial and final conductivity values were used to deduce the difference in the surfactant concentration. The estimated difference in surfactant concentration determines the loss of surfactant in the presence of SCN with the help of the equation. 1.

3.2.6 Impact of Time on Surfactant Adsorption

Surfactant loss was monitored for five days at an interval of 24 hours. The conductivity measurement evaluated the surfactant solution's final concentration after sand particles were isolated using a centrifuge. The measured value was compared with the initial conductivity value, revealing the remaining surfactant concentration. The conductivity measurements of the surfactant solution were performed over 24-hour intervals for five consecutive days.

3.3. Results & Discussion

3.3.1. Characterization Studies

3.3.1.1 BET Analysis

The number of gas molecules that get adsorbed on a surface is a reflection of its surface area. BET analysis relies on measuring the rate of dissolution. In the BET theory, this adsorption rate is assumed to be proportional to the specific surface area [10]. It was observed that the specific pore volume of the SCN was 0.25 cm³/g, and the

BET-specific surface area was 33.4 m²/g. This surface area value lies in the typical nanoparticle range (20 to 60 m²/g) [7]. This high surface area to volume ratio makes nanoparticles special and gives them their unique properties [66]. This increased surface area is crucial for adsorption as the number of adsorption sites drastically increases.

3.3.1.2 DLS and Zeta Potential

The hydrodynamic particle size measures the nanoparticle's size and the surrounding layer's size, influencing its movement [67]. Nanoparticles possess a surface charge owing to which an electrical double layer exists at its surface. This phenomenon gives rise to an electrical potential known as the Zeta potential, which indicates the solution's stability [67]. SCN in an aqueous solution was observed to have a hydrodynamic size of 483 nm. The polydispersity index was found to be 0.28, whereas its zeta potential was -33 mV, showing better system stability.

3.3.1.3 XRD study of the adsorbent

For an adsorption study, it is crucial to understand the surface characteristics of the adsorbent. Generally, owing to the adsorbent's mineralogy, a surface charge is present. This charge gives rise to a coulombic force of attraction/repulsion between the adsorbent and the adsorbate [10]. Thus, an XRD study was conducted to identify the mineralogical composition of the adsorbent. Table 3.1 shows the characteristic peaks that were obtained along with what they indicate. Distinct peaks were observed at 22.39°, 26.97°, 27.80°, 46.06° & 68.44°, which corroborates the presence of quartz [10]. The adsorbent had a high quartz content with a small quantity of Kaolinite as an impurity. Thus, the adsorbent used in this study was clean sand (quartz arenite).

Table 3. 1. Characteristic XRD Peaks and Inference

Serial Number	Major Characteristic Peaks	Inference
1	22.39	Quartz
2	26.97	Quartz
3	27.80	Quartz
4	46.06	Quartz, Kaolinite
5	68.44	Quartz, Kaolinite

3.3.2 Effect of SCN on Critical Micelle Concentration and its variation with temperature (CMC)

The presence of surfactants in an aqueous solution decreases the surface tension because of the micelle's adsorption on the air-water interface. Below CMC, a rise in the surfactant concentration leads to a surge in micelles at the surface. However, the interface gets saturated with micelles at the CMC, resulting in the lowest surface tension. Further increment in the surfactant concentration does not lead to any significant change in the interfacial forces. Thus, CMC is the minimum surfactant concentration, yielding the lowest surface tension. CMC was found by identifying the point of inflection in the conductivity versus concentration plots (Figure 3.2), and Figure 3.3 demonstrates the impact of SCN concentration on the CMC of the surfactant. The CMC of SDS was 2219 ppm at 30 °C and atmospheric pressure. The CMC was reduced to 2035 ppm upon adding 100 ppm CSN to the solution. The CMC decreased to 1905 ppm when the solution contained 200 ppm SCN. The drop in the CMC value is attributed to the decrease in electrostatic repulsion between the like-charged

surfactant head groups. The presence of SCN offers additional repulsive force to the negatively charged surfactant particles due to its negative surface charge [68]. This leads to micellization even at lower concentrations. Another possible reason for the decrease in the CMC is the increase in the ionic strength of the solution in the presence of nanoparticles, which could enhance the surfactant micellization [69]. However, when the NPs concentration was raised to 300 ppm, an increment in the CMC value was noted to 2172 ppm. The sudden increase in the CMC at higher SCN concentrations could be due to the advent of nanoparticles' agglomeration. The aggregation of nanoparticles reduces the Coulombic interaction between the charged surfactant head group and nanoparticles. This interaction causes an increase in surfactant micellization concentration.

On conducting the same experiments at elevated temperatures (Figure 3.4), it was found that the CMC increased from 1905 ppm at 30°C to 2638 ppm at 50°C and 2746 ppm at 70°C. These rises in CMC occur due to the increased repulsion among the ionic heads [70]. For this study, carrying out studies at temperatures below the atmospheric temperature was not deemed necessary. However, Tennouga et al. have shown that the CMC increases even at reduced temperatures. The CMC of SDS is observed to be minimal at the atmospheric temperature. They explained this behavior by stating that the hydrophobic tails confirm at atmospheric conditions, minimizing the occupied volume [70].

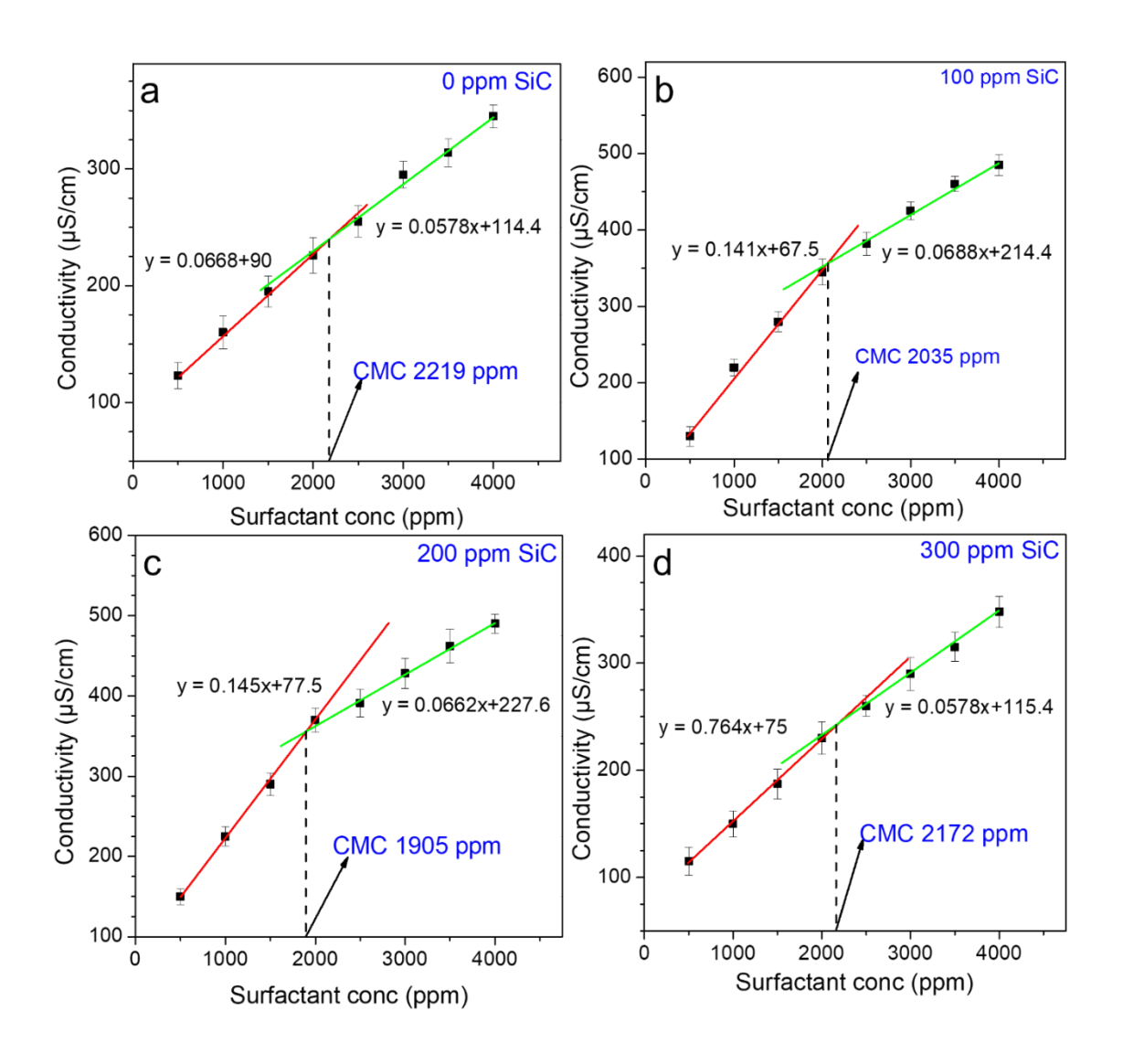


Figure 3. 2: Determination of the CMC using conductivity method

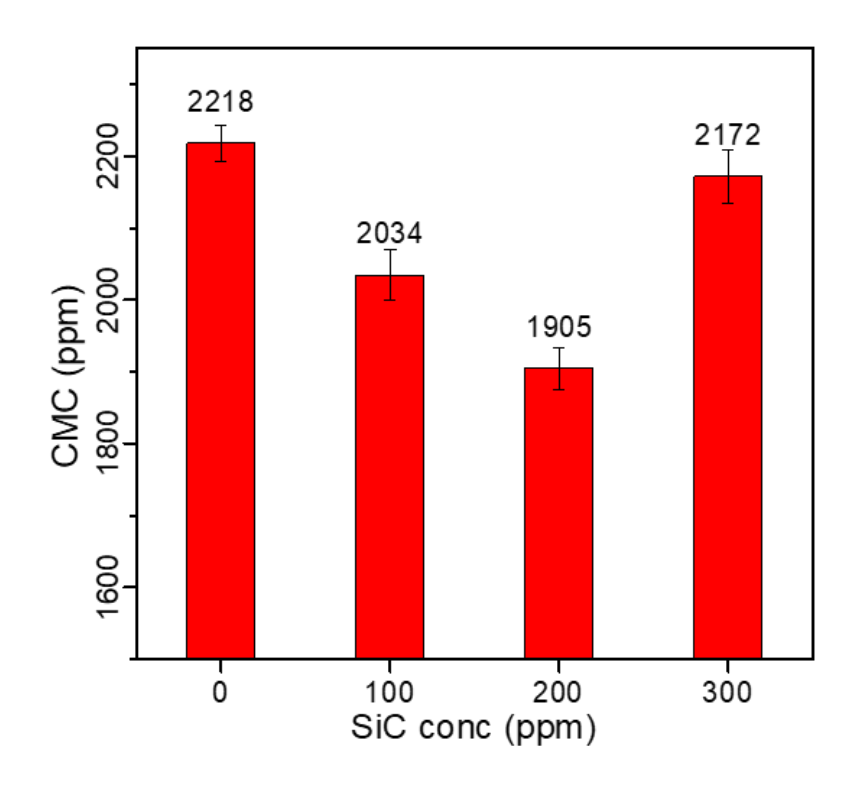


Figure 3. 3: Variation of CMC with the concentration of SCN

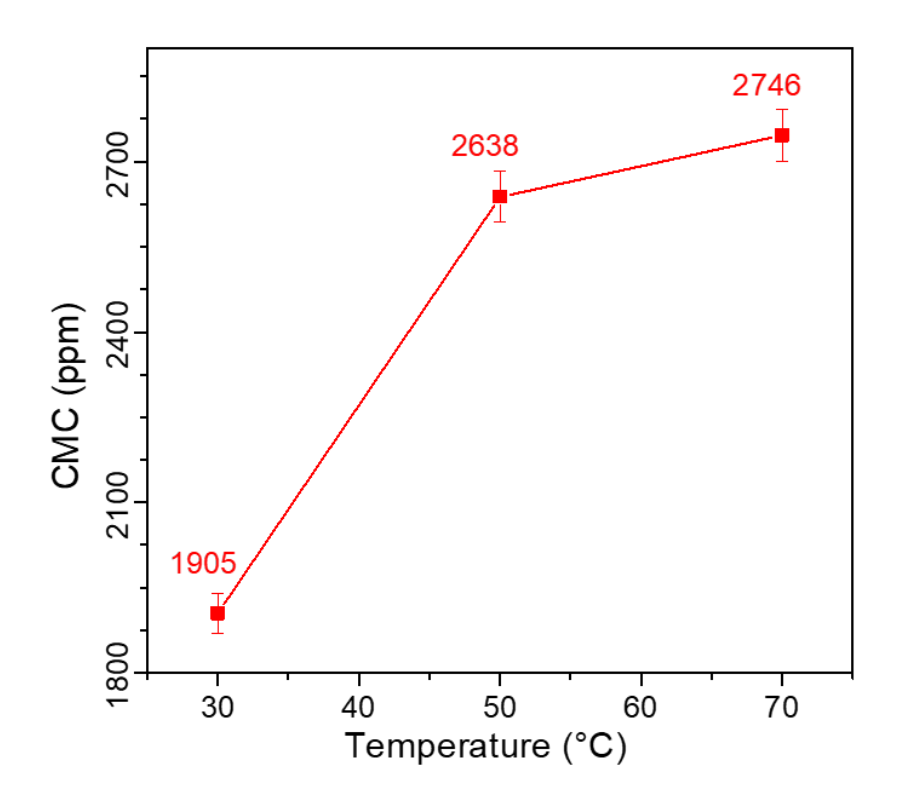


Figure 3. 4: Effect of temperature on the CMC of surfactant in the presence of 200 ppm SCN

3.3.3 Influence of surfactant concentration on the extent of adsorption

Some researchers discussed the surfactant concentration's impact on the anionic surfactant's adsorption onto reservoir rocks. According to the rock type, some rock surfaces are negatively charged, like sandstone, and some are positively charged, like carbonate. There are several mechanisms regarding surfactant adsorption on the sand particles, i.e., ion exchange, ion association, hydrophobic bonding, adsorption by the polarization of π electrons, and adsorption by dispersion forces [71]–[73]. The surfactant adsorption on the sand surface above a specific limit is an unfavourable phenomenon in oil recovery. It is governed by the difference in thermodynamic stability between surface-liquid and surface-water interactions [61]. The surfactant's tendency to escape an aqueous solution, known as the hydrophobic effect, plays a vital role in its adsorption process. The results (Figure 3.5(a)) illustrate that the surfactant loss rose with an increase in the surfactant concentration from 0.86 (mg/g) to 3 (mg/g) at 500 ppm to 6 (mg/g) to 19 (mg/g) at 4000 ppm from a period of day 1 to day 5. However, a plateau was reached after the CMC of surfactant. As the surfactant concentration increases, more surfactant molecules are available in the bulk phase, which enhances the likelihood of interactions between the surfactant molecules and the sand surface. And, at CMC, agglomeration begins, and keeping the surfactant in the solution no longer reduces the system's free energy.

3.3.4 Impact of time on surfactant adsorption

Adsorption of an adsorbate over a surface is a time-dependent phenomenon. The extent of adsorption (surfactant over sand particles) was studied over five days at intervals of 24 hours. Figure 3.5(c) shows that surfactant loss increased with the contact time. The increase from 5 mg/g to 11 mg/g was linear in our study period. However, it

is known that the rate of adsorption declines after a certain period. This decline is because of the steric repulsion from existing surfactant molecules adsorbed on the sand's surface [73].

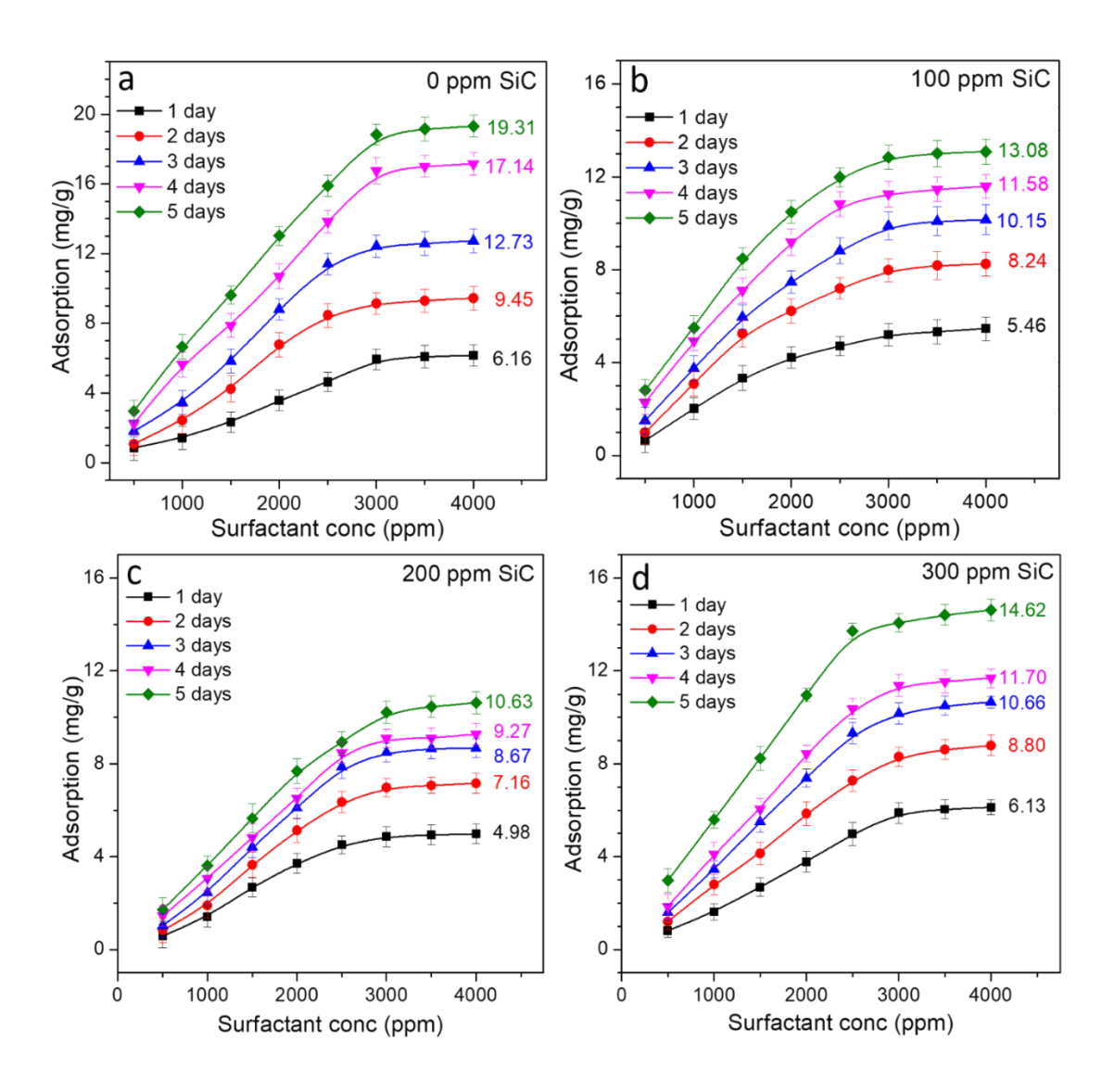


Figure 3. 5: Surfactant adsorption variation with different parameters (Time, Surfactant Concentration, SCN Concentration) at 30° C.

3.3.5 Effect of SCN on surfactant adsorption

As shown by Figure 3.6, for SDS near the CMC, the adsorption at the end of the five days was 16 mg/g. The results of introducing 100 ppm SCN to the solution demonstrate that surfactant adsorption at the end of 5 days was reduced to 12 mg/g.

Increasing the SCN concentration to 200 ppm resulted in the surfactant loss, which further plunged to 9 mg/g (44% reduction). The results are better than most reported literature using silica-based nanoparticles of similar applications. The silicon dioxide nanoparticles have more hydrogen bonding than SCN nanoparticles with the surfactant molecules and the sand surface due to the presence of oxygen atoms. This hydrogen bonding is the primary reason for reducing the surfactants' adsorption on the SCN surface [74], [75]. A lower dosage of SCN means that it has a massive edge over Silica nanoparticles in terms of economic viability for the same purpose. As the experiments were extended to test the effect of 300 ppm SCN, adsorption rose to 15 mg/g. The initial decrease in the adsorption of up to 200 ppm SCN is because of surfactant adherence on the nanoparticles. The surfactant adsorption on the nanoparticle in place of the sand surface enables the surfactant molecules to stay in the solution and participate in the EOR process. It is known that nanoparticles tend to agglomerate at higher concentrations [15], [68]. This aggregation is the reason behind the change in the experimental trends at 300 ppm or above. Thus, 200 ppm of SCN was deemed the ideal concentration to minimize the adsorption of surfactants. The mechanism for this reduction in surfactant adsorption is preferential surfactant adsorption on the SCN surface. Since the SCN nanoparticles remain mobile and suspended in the solution, loss of surfactant does not occur. This is not the case when high surfactant adsorption occurs on the sand surface. Singh et al. showed that SCN possesses a net negative charge in environments with a pH over 4.9 [76]. Hence, electrostatic repulsion between the SCN (negatively charged) and anionic surfactant particles is vital in altering adsorption.

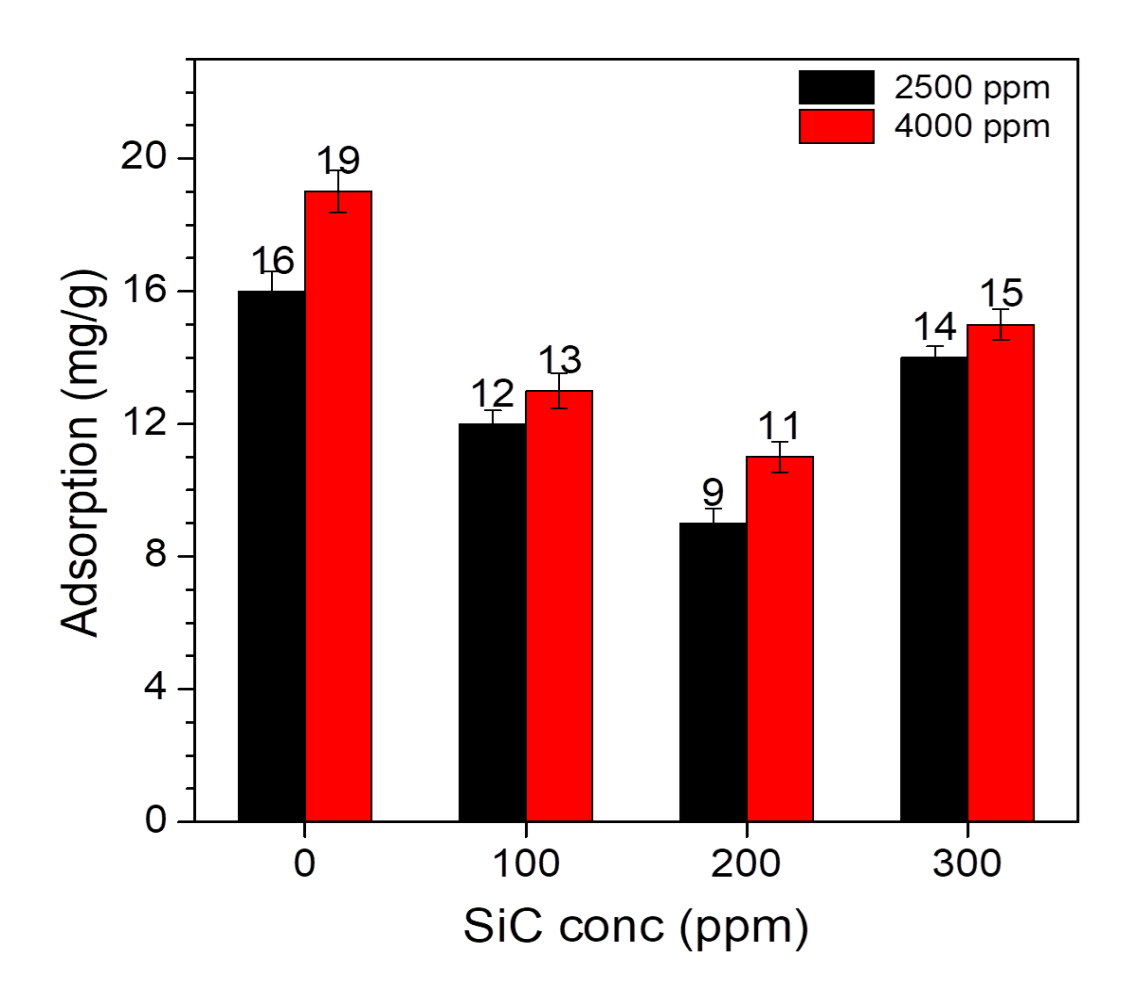


Figure 3. 6: Effect of SCN concentration on surfactant adsorption

3.3.6 Effect of temperature on surfactant adsorption

Since oil reservoirs are often found at high temperatures, it is crucial to understand the impact of temperature variation on surfactant loss. The optimum concentration of SCN was 200 ppm, and thus, solutions containing 200 ppm of SCN were used as subjects for studying the effects of temperature. For five days, the surfactant adsorption for a solution containing 2500 ppm and 4000 ppm SDS and 200 ppm SCN was studied at three different temperatures: 25°C, 50°C, and 70°C. Figure 3.7 illustrates that adsorption decreased with increased temperature, which aligns with previous studies [77], [78].

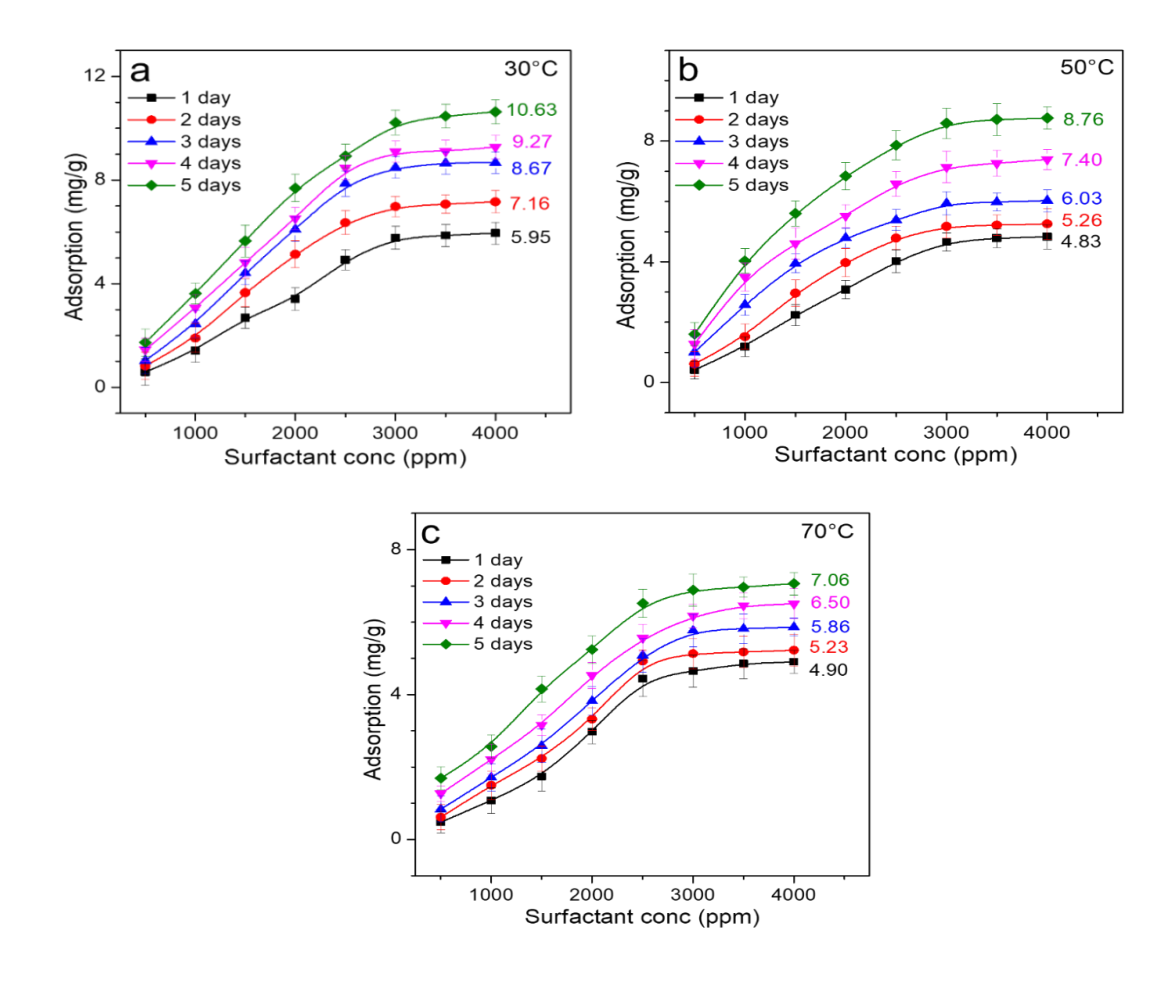


Figure 3. 7: Effect of temperature on adsorption of 200 ppm SCN with anionic surfactant solutions at (a). 30° C temperature, (b). 50° C temperature, and (c). 70° C temperature.

3.3.7 Study of adsorption isotherm models

To comprehend the mechanisms or characteristics of the adsorption, the adsorption data was fitted into the most widely used adsorption models, namely Langmuir, Temkin, and Freundlich.

3.3.7.1 Langmuir Adsorption Isotherm

The Langmuir adsorption isotherm assumes a limited number of adsorption sites and a lack of interaction between adsorbed surfactant molecules. It also considers adsorption a monolayer phenomenon and allows only one surfactant molecule to adsorb on a specific adsorption site [79]. Langmuir adsorption assumes all adsorption sites to

be identical and energetically equivalent. There is no interaction between neighboring adsorbed atoms [80]. Equations 3.2 and 3.3 are used to plot the Langmuir isotherm model.

$$q_e = \frac{q_{\text{max}} C_e K_L}{1 + K_L C_e} \tag{3.2}$$

Or

$$\frac{1}{q_e} = \left(\frac{1}{K_L q_{\text{max}}}\right) \frac{1}{C_e} + \frac{1}{q_{\text{max}}}$$

$$(3.3)$$

Where q_e represents equilibrium adsorption, q_{max} adsorption capacity, C_{eq} is the adsorbate concentration at equilibrium, and K_L is the Langmuir constant related to adsorption capacity. The adsorption capacity depends on the surface area and pore volume, implying a greater surface area and pore volume increase.

Table 3.2 shows the correlation coefficients of the data with the Langmuir isotherm. The extremely high values of the correlation coefficients indicate surfactant adsorption on the clean sand, which follows the Langmuir model. Interestingly, the highest correlation coefficient was obtained when the SCN concentration was 200 ppm, at which the lowest surfactant loss was obtained. This observation confirms the selection of 200 SCN as an optimized system. Figure 3.8 illustrates the fit between the actual data and the Langmuir isotherm.

3.3.7.2 Freundlich Adsorption Isotherm

This isotherm does not stick to the assumption of monolayer adsorption. It states that the sum of adsorption in the different adsorption layers gives the amount of material adsorbed. The Freundlich isotherm model is known to explain particle adsorption on

the heterogeneous surface. Freundlich isotherm characterizes dynamic sites' surface heterogeneity and distribution and their energies [81]. The linearized and nonlinearized Freundlich isotherm is mathematically demonstrated by equations 3.4 and 3.5 [7];

$$q_e = K_f \left(C_e \right)^{1/n} \tag{3.4}$$

Or

$$q_e = \log K_f + (1/n)\log C_e$$
 (3.5)

Where given constants K_f and 1/n are the Freundlich constant, which provides adsorption capacity and intensity information.

For deciding the most extreme adsorption capacity, it is essential to work with constant initial concentration C_i and variable weight of adsorbent; accordingly, $ln(q_m)$ is the extrapolated value of $ln(q_e)$ for $C = C_i$. According to Halsey, equation 3.6 can be used to determine the value of q_m . [82].

$$K_f = \frac{q_m}{C_i^{1/n}} \tag{3.6}$$

where C_i is the initial concentration of the solute in the bulk solution (mgL⁻¹). q_m is the Freundlich maximum adsorption capacity (mg/g). Table 3.3 represents the observations of the data fitted into the Freundlich model. The Freundlich parameters 1/n and Kf relate to the adsorption intensity and adsorption strength, respectively. The value of n greater than one demonstrates good adsorption [83]. The adsorption intensity measures the heterogeneity of adsorption sites [81]. The correlation coefficients indicate that the

Freundlich isotherm does not describe the adsorption being studied as accurately as the Langmuir isotherm.

Table 3. 2. Langmuir adsorption parameters

SCN Conc. (ppm)	Correlation	K _L (L/mg)	q _{max} (mg/g)	\mathbb{R}^2
0	$1/q_e = 500.668 \ / C_e + 0.0027$	5.273E-06	378.789	0.9734
100	$1/q_e = 662.661/C_e + 0.0228$	3.430E-05	43.995	0.9941
200	$1/q_e = 712.091/C_e + 0.0822$	0.0001155	12.166	0.9983
300	$1/q_e = 451.563/C_e + 0.1859$	0.0004117	5.381	0.9780

Table 3. 3. Freundlich adsorption parameters

SCN Conc.(ppm)	Correlation	K _f (L/mg)	1/n	\mathbb{R}^2
0	$q_e = 0.00291(C_e)^{0.9533}$	0.00291	0.9533	0.93749
100	$q_e = 0.00825(C_e)^{0.8220}$	0.00825	0.8220	0.92134
200	$q_e = 0.00239(C_e)^{0.9813}$	0.00239	0.9813	0.94895
300	$q_e = 0.00235(C_e)^{1.0122}$	0.00235	1.0122	0.91753

3.3.7.3 Temkin Adsorption Isotherm

This isotherm assumes that as adsorption occurs and the surface continues to get covered, the heat of adsorption of the adsorbate molecules decreases linearly. The Temkin Adsorption isotherm model is legitimate for an intermediary range of ion concentrations [84]. The mathematical expression of Temkin isotherm is given by equation 3.7 [7], [81]

$$q_e = B_T \ln K_T + B_T \ln C_e \tag{3.7}$$

Where the above constants K_T and B_T are the Temkin constants. Table 3.4 shows the Temkin constants, and the correlation coefficients of the experimental data fitted into the Temkin adsorption isotherm. K_T and B_T are Temkin Constants relating to the equilibrium binding constant and the heat of adsorption, respectively. As can be seen, the values of R^2 are not as high as they were for the Langmuir Isotherm. Thus, the Temkin isotherm fails to describe the surfactant adsorption onto the sand as well as the Langmuir isotherm does.

Table 3. 4. Temkin adsorption parameters

SCN Conc. (ppm)	Correlation	K _T (L/mg)	B _T (J/mol)	\mathbb{R}^2
0	$q_e = 2.94149 \ln (C_e) -17.755$	0.002391	2.94149	0.8883
100	$q_e = 2.49755 ln (C_e) -14.371$	0.003169	2.49755	0.9632
200	$q_e = 3.01146 ln (C_e) -18.338$	0.002267	3.01146	0.9334
300	$q_e = 3.65746 \ln{(C_e)} -22.151$	0.002343	3.65746	0.8863

3.4. Conclusion

A comprehensive study of the adsorption of SDS surfactant enriched with silicon carbide nanoparticles (SCN) onto the sand surfaces was done. The addition of SCN resulted in a 44% reduction in surfactant adsorption. The nanoparticles reduce the surface area of sand for adsorption by preferentially adsorbing the surfactant on its surface. Preferential adsorption on the nanoparticle surface allows the surfactant to remain in the solution instead of getting lost on the rock surface. Above the pH of 4.9, SCN is known to possess a slight negative charge in aqueous solutions. An increase in the electrostatic forces of repulsion in the system also plays a role. This reduction intensifies with increasing concentration of SCN till it reaches a value of 200 ppm.

Above 200 ppm, aggregation of the SCN nanoparticles begins. SCN can lower SDS adsorption by a greater degree than previously used nanoparticles at dramatically lower concentrations. Only 200 ppm SCN reduces the surfactant adsorption by a higher percentage than 5000 ppm Silica nanoparticles do. The introduction of 200 ppm SCN also reduced the anionic surfactant's CMC by over 14%, making it practical and economical.

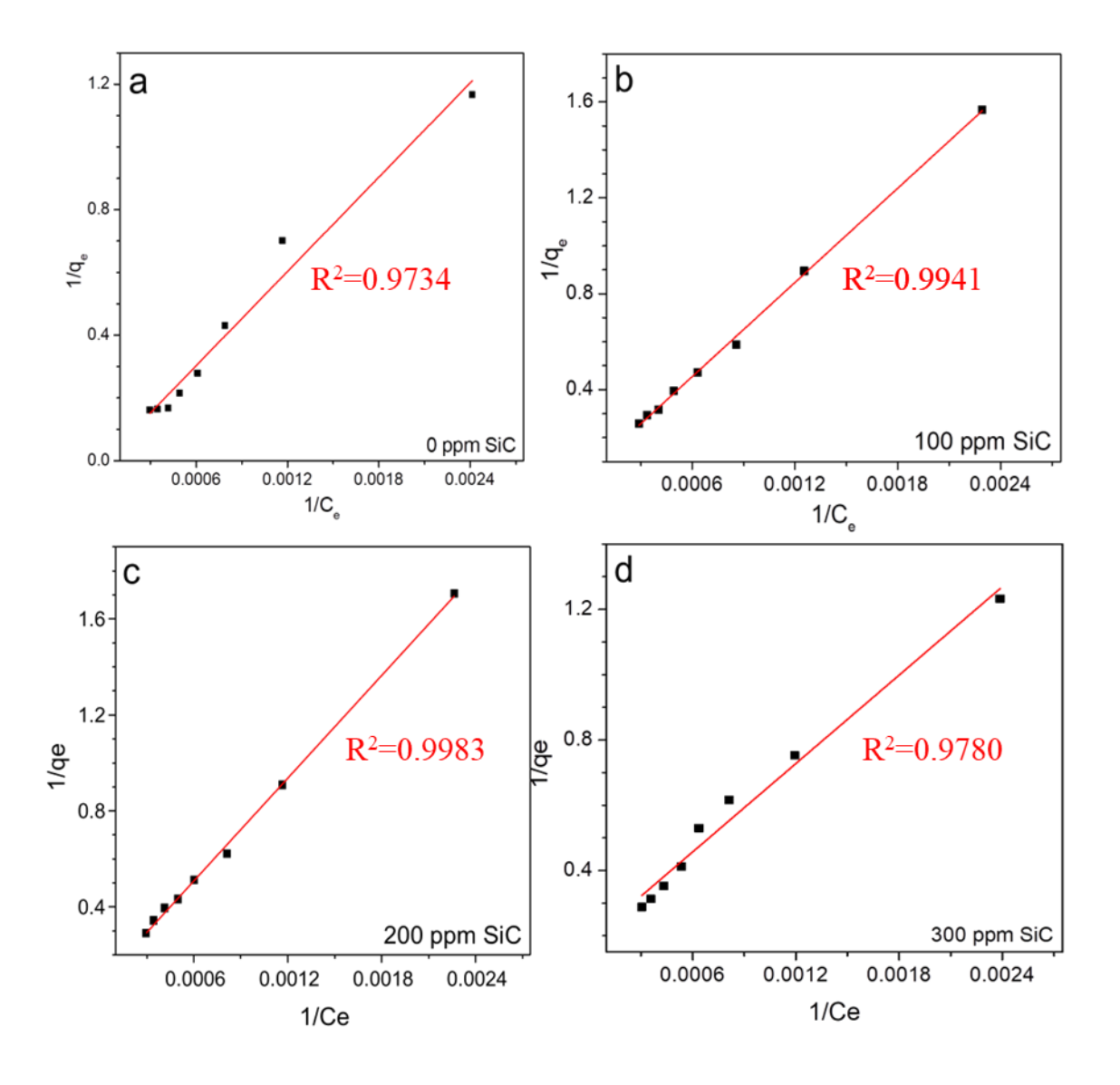


Figure 3. 8: The best-fit model (Langmuir Isotherm Model) for adsorption isotherm study.

Chapter: 4

Advanced multi-wall carbon nanotube-optimized surfactant-polymer flooding for enhanced oil recovery

Abstract

In this captivating study, we explored the fascinating potential of carbon nanotube-based nanofluids in improving oil recovery efficiency and transforming interfacial tension. To accomplish this, we acquired high-purity multi-walled carbon nanotubes from Plasma Chem Gmbh, ensuring a purity level exceeding 95%, which underwent additional functionalization and experimentation to explore their impact. The Functionalization of multi-wall carbon nanotubes with ammonium hydroxide and hydrogen peroxide generated diverse surface groups, reduced van der Waals interactions, and increased carbon nanotube dispersibility through enhanced interactions with polymers or solvents. The modified multi-wall carbon nanotubes were characterized using Raman analysis, HRTEM, and zeta potential. Varying concentrations of modified multi-wall carbon nanotube-based fluids were prepared to study their impact on surface tension using a Surface tensiometer.

Additionally, conducted adsorption studies to minimize surfactant loss and performed contact angle experiments using a Goniometer to alter the wetting characteristics of the rock surface. Finally, a core flooding experiment was carried out using two pore volumes of the nanofluid with the optimal concentration of mMWCNT with SDS and 1000 ppm of polymer, and the oil recovery factor was calculated. The

study's findings revealed that the modified multi-wall carbon nanotubes significantly reduced surface and interfacial tension by approximately 59% and 56%, respectively, at the optimum concentration. Moreover, the nanotubes successfully minimized surfactant loss by approximately 49.3%. The contact angle experiments demonstrated that the modified nanotubes transformed the rock surface from oil-wet to water-wet, as evidenced by a substantial reduction of roughly 54% in the contact angle value. In conclusion, the core flooding experiment, employing a chemical slug composed of SDS at CMC, modified multi-wall carbon nanotubes, and industrial-grade polymer, yielded a remarkable oil recovery factor of approximately 70% of the original oil in place.

4.1. Introduction

Primary oil recovery extracts oil using natural or artificial lift devices, bringing hydrocarbons to the surface. The primary methods have limitations in extracting oil, as they focus on pay zones with good oil saturation. The conventional recovery method can only extract about 30% of the oil reserves. Various enhanced oil recovery (EOR) approaches are employed to recover the remaining oil after primary methods. The EOR procedures comprise thermal recovery, gas injection, and chemical injection. Chemical infusion is a frequently used EOR method that mobilizes the oil trapped in the microporous structure. This mobilization occurs due to lowering surface tension (ST), enhancing water-flooding efficiency [85]–[88]. Chemical EOR involves mixing several chemicals into the infused water. Different chemical-based EOR approaches involve polymer flooding, alkaline flooding, surfactant flooding, foam flooding, and a grouping of alkaline, surfactant, and polymer flooding. The efficiency and techno-economic viability have made it a widely accepted technique throughout the industry. Nanoparticle (NPs) uniqueness and exciting features have recently aroused much

interest in EOR applications [1], [89]. Nanoparticles tend to reduce surfactant adsorption on solid surfaces and improve oil recovery. They improve the EOR process's overall efficiency when used in synergy with the surfactant. Surfactants are substances that contain hydrophilic and hydrophobic parts. Including surfactants lowers the interfacial tension (IFT) among the infused aqueous solutions and oil and alters the wettability of the rock surface. Also, an increasing amount of attention is being given to anionic and cationic surfactants as they are now widely recognized for their ability to alter the surface of biochar. This modification aims to enhance the biochar's capacity to adsorb pollutants [90]. Besides surfactants, chemical slug-displacing oil contains highly viscous fluids known as polymers. Polymers boost the viscosity of injected water [91], [92]. Hence, it controls water mobility and improves sweep efficiency. Mobility is the relationship between the competence of a fluid to flow [93] via a porous medium and its resistance to deformation or flow, also known as apparent viscosity. In other words, mobility refers to how easily a fluid can move through a substance of its thickness or resistance to flow. Reduced mobility of water leads to improved sweep efficiency. The sweep efficiency is the ratio between the flood pattern in contact with the displacing fluid and the total flood pattern [55], [94]. The surfactant utilized in EOR applications modifies the interactions between the reservoir's liquid and solid phases [52]. When surfactants are ionized, they tend to stick to the charged surfaces of rocks found in reservoirs. This phenomenon happens because the point where the liquid and solid meet often offers greater thermodynamic stability than the larger body of the liquid phase. In other words, the favorable energy conditions at the liquid-solid interface compared with the bulk liquid phase lead to the adsorption of ionized surfactants onto charged surfaces of rocks in reservoirs [7]. Surfactants with identical

surface charges decrease surfactant adsorption [10], [55], [95], [96]. Other properties like pH and salt concentration also impact surfactant adsorption [53], [97]. The impact of the flood on recovery reduces due to a decrease in the effective surfactant concentration [52]. In addition, surfactants' poor natural degradability raises an urgent concern about the pollution of the subterranean environment [94].

Research has been conducted to lessen the surfactant's propensity to adsorb on the surface [10], [54], [55], [96]. Al Hashim's study investigates the efficacy of the ASP technique in recovering oil from carbonate reserves. At lower surfactant concentrations (1% by wt.), it was discovered that the combined effect of NaHCO3 and Na2CO3 considerably lowered the loss of surfactant on carbonate rock. The effect is desirable for creating a practical ASP slug [54]. To decrease surfactant adsorption in carbonate reservoirs, Wang et al. experimented with polymers. Polymers were discovered to form a coating on the rocks' surface, reducing active adsorption sites [55]. Alkali can be utilized to minimize surfactant loss, according to Seethepalli et al. [96]. Saxena et al. experimented to explore the impact of various factors, including minerals, alkalinity, salinity, and NPs, on the loss of surfactants. Their findings indicated that silica NPs were more efficacious than alkali in promoting surfactant adsorption [10]. Ma et al. explored the characteristics of interfacial tension with negatively charged hydrophilic silica nanoparticles in various surfactant solutions. They reported that including nanoparticles enhances sodium dodecyl sulfate (SDS) molecule performance [98]. Ahmadi and the group utilized the nanoparticles on carbonate and sandstone rock samples, noticing reduced surfactant loss and improved oil recovery. Chemical slugs for EOR are designed using them because they decrease adsorption and interfacial tension, making them a preferred option [8], [99], [100].

On the other hand, some studies have yielded contradictory results regarding the ability of polymers and alkalis to achieve the intended objective, suggesting that they may not be effective [55]. Therefore, the current focus is on nanoparticles and their potential influence on the adsorption of surfactants. Research focusing on nanoparticles like SiO₂, TiO₂, Graphene, Silica carbide nanoparticles, etc., has acquired an interest in oil and gas recovery [48], [58], [59]. Nanotechnology encompasses various disciplines, including science, engineering, and technology. The utilization of nanotechnology in applied science and engineering is extensive and includes a vast array of applications [88]. The study of nanoparticles has been a prominent area of research that has boosted oil recovery throughout the past several years [88]. A carbon nanotube is a cylinder with a nanoscale diameter created by coiling a graphene nanosheet. MWCNTs (multiwalled carbon nanotubes) are a group of concentric SWCNTs (single-walled carbon nanotubes) [101], [102]. It is produced using concentrically layered sheets of cylindrically rolled graphene [103]. Carbon nanotubes have a variety of advantageous and distinctive qualities, including better mechanical strength, good thermal conductivity, and high surface-to-volume ratios (length/diameter = 1000) [104]. They tend to diminish the interfacial tension and modify the surface wettability [105]. Carbon nanotubes (MWCNTs) unique quality of interfacial activity has demonstrated a comparatively strong ability to boost sweep efficiency among nanoparticles [15], [58], [64].

This leaves a research gap between the nanoparticles synthesized (MWCNT) in the lab and their application and behavioral patterns regarding how they will suit the oil displacement. This motivated the authors to investigate this NP for its application in the EOR by performing various studies such as IFT, ST, CA, and oil recovery as a goal of

the current study. The current research subjected a modified multiwall carbon nanotube (mMWCNT) solution to surface/interfacial forces, contact angle, and loss of surfactant studies. The impact of carbon nanotubes (mMWCNTs) on an SP solution's ST/IFT and wettability is studied using surface tensiometer and contact angle experiments. These tests are executed to establish the CMC of the surfactant and to conclude the optimal concentration of mMWCNT for improving oil recovery. The influence of the mMWCNT concentrations on surfactant loss on the sandstone surface in the SP solution was examined at various concentrations. Reviewing prior studies on the application of NPs in SP flooding reveals that the impact of mMWCNT has yet to be studied, implying that no research has been reported on determining the effect of mMWCNT on SP solution.

4.2. Methodology

4.2.1 Materials

This investigation utilized sodium dodecyl sulfate (SDS), an anionic surfactant procured from Rankem Chemicals with a purity of >94% and a molecular weight of \sim 289 g/mol. The MWCNT purchased from Plasma Chem Gmbh with >95% purity was used for further functionalization and experimentation. Deionized (DI) water has been employed for sample formulation and cleaning, with a resistivity measurement of 18.2 M Ω -m. The sand pellets utilized in the CA investigation have been created by taking ordinary beach sand, washing it, and then drying it in an oven at 385 Kelvin to remove any moisture content.

4.2.2 Methods

This section outlines the procedures utilized to optimize surfactant formulations that can be employed for enhanced oil recovery. Figure 4.1 provides a succinct illustration of these techniques for the EOR application.

4.2.3 Modification of MWCNT

The MWCNT purchased from Plasma Chem Gmbh with >95% purity was used for further functionalization and experimentation. The MWCNT purchased were further activated by using ammonium hydroxide and hydrogen peroxide. The MWCNT was mixed thoroughly with NH₄OH+H₂O₂ in the ratio 1:1 and ultrasonicated for 6 hours. Then, they were vacuum filtered and dried under vacuum for 12 hours. The functionalized MWCNT exhibited different groups on the surface, a reduced long-range van der Waals interaction, and increased interaction between carbon nanotube and polymer or solvent [106]. This functionalization further helps in increasing the solubility of the carbon nanotube. This modified MWCNT (mMWCNT) was characterized by Raman analysis, HRTEM, and zeta potential. The 0.005 g of modified MWCNT was dispersed in 50 ml toluene and was characterized by RENISHAW Micro Raman Spectrometer. The excitation was carried out at 785 nm with an Argon laser. The TecnaiTM G220 high-resolution electron microscope (HRTEM) was utilized for imaging modified carbon nanotubes. The Malvern Zetasizer Nano ZS was employed to evaluate the zeta potential of the modified MWCNT.

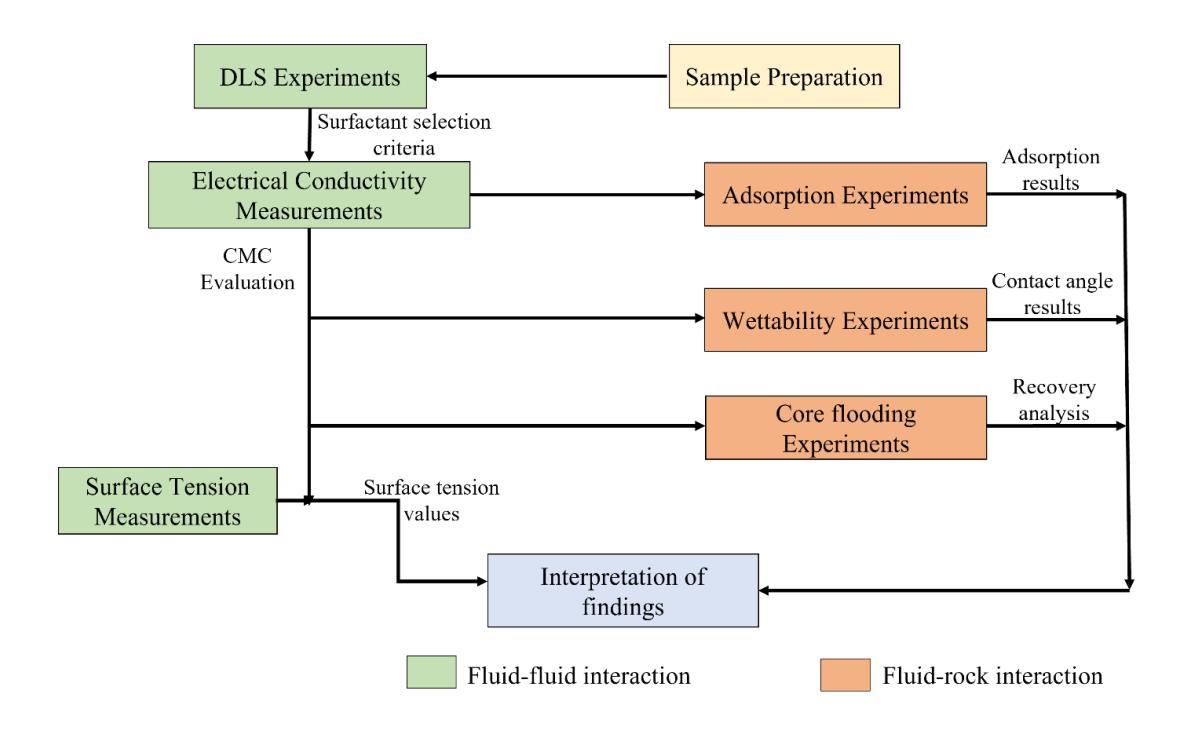


Figure 4. 1: Flow chart for experimental methodology.

4.2.4 Dynamic light scattering (DLS) studies

The distribution of particle sizes for mMWCNT was examined using DLS tests, while the stability of the nanofluid was assessed by measuring its zeta potential. The Malvern Zetasizer Nano-ZS instrument evaluated the average diameter and zeta potential of the NPs dispersed in water [7]. About 1.5 mL of the batch of mMWCNTs were placed into the cuvette to measure particle size, and a 30 °C was maintained throughout the experimentation. The samples are irradiated to a laser beam with a wavelength of 635 nm for analysing the movement of particles undergoing Brownian motion in a liquid phase. The particle sizes are determined using the Stokes-Einstein equation. The zeta potential and particle size of the mMWCNTs with and without surfactants were determined using dynamic light scattering. The cuvette was cleansed twice, utilizing methanol after every test to eliminate impurities. Additionally, the instrument's equilibrium period was set to 120 seconds to ensure a suitable temperature

for the measurement. The average particle size and zeta potential findings reveal the dispersed nanofluids' average hydrodynamic size and stability.

4.2.5 Critical micelle concentration measurement

The conductivity of the surfactant solution at differing concentrations helps identify the surfactant's critical micelle concentration (CMC) [64]. During conductivity measurement, the ions in the bulk solution dissociate, causing the surfactant's electrical conductivity to increase until the concentration reaches the CMC value. After reaching the CMC value, micelle formation starts, causing a reduction in the conductivity. A surfactant solution was prepared in deionized water with and without mMWCNT by stirring the mixture utilizing a magnetic stirrer at 700 rpm for one hour and sonicating the prepared samples for 30 minutes. A total of ten solutions were formulated, with differing concentrations ranging from 500 ppm to 5000 ppm. A LABMAN Multiparameter LMMP-30 has been utilized to evaluate the conductivity of the samples. The equipment was calibrated using a provided solution before measuring the surfactant solution's conductivity. Following each measurement, the instrument's probe was cleansed thoroughly using DI water and then gently dried using Kim-wipes tissue paper. The conductivity of the subsequent sample was estimated after the conductivity of deionized water, ensuring no surfactant adsorption on the probe. The investigations were executed at 30°C temperature and atmospheric pressure [7]. The CMC findings of the dispersed nanofluid solution tell us about the minimum concentration at which the values are obtained.

4.2.6 Loss of surfactant experiment

The researchers used the same approach as earlier studies to evaluate how the surfactant adheres to the rock's surface. [64], [107]. The surfactant was mixed in 30 mL of solutions at 500 to 5000 ppm concentrations. The conductivity meter precisely measured the conductivity of each solution. The prepared solution was supplemented with 3 grams of 400 µm sand particles and left undisturbed for 24 hours. After 24 hours, the electrical conductivity of each sample was examined again after removing the sand grains from the sample with the centrifuge. After removing the sand particles, the surfactant left in the solution phase was determined by comparing the conductivity data to a standard conductivity curve. This procedure aids in estimating the discrepancy between the initial and final amounts of surfactant. The electrical conductivity of the 250-ppm surfactant solution determines the conductivity reduction compared to 500 ppm of solution. The trials were operated at room (30°C) temperature and atmospheric pressure, and the mass of the sand grains introduced within the surfactant solution was kept constant for each concentration. The surfactant molecules that adhered to the sand surface were isolated from the solution via centrifugation. The quantity of surfactant in the solution has been reduced because of the surfactant being adsorbed onto the surface (sand particles). Surfactant loss has been calculated via equation 4.1. [7]

$$A = \frac{\left[(c_i - c_f) \times \frac{M_S}{M_T} \right]}{1000} \tag{4.1}$$

The amount of surfactant that will be absorbed in the presence of mMWCNTs is calculated using Equation 4.1 (Rahimi and Adibifard 2015). In this equation, the variables represent the following: M_s is the weight of the solution in grams, M_r is the weight of the sand particles combined with the surfactant solution in grams, surfactant's

initial amount in the solution is C_i , and its ultimate amount in the solution is C_f (in parts per million), and A is the quantity of surfactant loss (in milligrams/gram). The present work also examines the effect of mMWCNT on surfactant loss due to adsorption. Ten samples of surfactant solution with 500 to 5000 ppm concentrations were made, and concentrations of mMWCNTs varied from 0 to 500 ppm. Before utilizing the solutions, the conductivity was assessed before and after sand particles were added and removed to examine the variations in conductivity.

4.2.7 Effects of Time on the Loss of Surfactant

The conductivity of solutions with distinct surfactant concentrations was determined after regular intervals. A standard conductivity versus concentration curve assessed the surfactant concentration left in the solution after the removal of sand particles via centrifugation. The amount of surfactant loss has been assessed after 1, 2, and 3 days. The surfactant loss data was incorporated into the Langmuir, Freundlich, and Temkin adsorption models to understand the mechanisms or properties of adsorption. Both duration and surfactant concentration variations were used to measure the surfactant's adsorption. The data was plotted between $1/q_{eq}$ and $1/C_{eqi}$, where C_{eqi} is the equilibrium concentration, and q_{eq} is the equilibrium adsorption. The correlation factor was determined to establish the best-fitting model for adsorption data.

4.2.8 Surface Tension Experiment

The cohesive nature of water molecules results in the surface tension (ST) property, which enables a liquid's surface to withstand an exterior force. Surface forces were investigated with the help of a surface tensiometer using the Du Nouy ring technique. The technique involves applying a controlled force to an object with a specific shape on the surface of the liquid and measuring the resulting force required to

pull it away, thereby determining the surface tension. The KYOWA DY-500 tensiometer utilizes Du Nouy's ring system to determine the surface forces of different samples. The ring technique employed a platinum ring owing to its excessive heat conductivity, which instantaneously wipes all the moisture from its surface when heated. The experiment's repeatability was ensured by performing each experiment thrice. The amount of force denoted as F_c , which is needed to lift the ring off the surface of the liquid, is determined, and this measurement connects to the surface tension σ_s of the liquid and the weight of the ring, W_{ring} . The tensiometer measures this pull force F_c , which is calculated by equation 4.2.

$$F_c = W_{ring} + 4\pi (r_i + r_o)\sigma_s \tag{4.2}$$

The difference in the size and shape of the inner & outer surfaces of the ring requires a meniscus correction factor for correct measurement. In this experiment, surface tension acts on the inward and exterior of the ring, so both radii are considered [108], [109]. The SDS's ST value ensures the anionic surfactant's CMC (SDS). The ST value of varied concentrations of mMWCNTs (ranging from 100 ppm to 500 ppm) was evaluated in the presence of SDS at its critical micelle concentration (CMC). The surface tension results gave information regarding the surface activity of the prepared nanofluids.

4.2.9 Analysis of Wetting Behavior

The goniometer setup, shown in Figure 2.2, provided by Apex Instruments, India (Acam–NSC series), measures the contact angle in an evacuated chamber to determine any changes in the wetting behavior of the rock surface [7]. The setup has a flat stage, a light source, and a high-speed camera to record the photos of the drops.

The range of the goniometer setup is from 0° to 180° along with a precision of ± 0.05°. The liquid under examination was added to the syringe and infused at a flow rate of (~0.0012 mL/min) onto a surface placed in a chamber. The liquid emerged from the needle as a pendant drop and attached to the surface, which was recorded by the camera. An imaging instrument (camera) takes continuous photos of the liquid as it forms a sessile drop on the surface. An oil-soaked glass slide was the surface, treated to determine the contact angle. The glass slides were submerged in crude oil for one week to test their ability to moisten surfaces. All measurements were made at a pressure of 14.7 psi and 25 °C. The sample was made using deionized water mixed with various mMWCNT concentrations of anionic surfactant at the CMC. The flow lines underwent two rounds of cleaning procedures using deionized water, and the pendent drop of the DI water confirmed that there were no traces of impurities left behind. The experiments were performed three times to ensure the apparatus's consistency.

4.2.10 Viscometry measurements

The rheological parameters of the chemical slug were identified by viscometry analysis utilizing an Anton Paar rheometer cup and bob geometry. The outside radius of the cup is 32.00 mm, the bob's length is 60.00 mm for the bob & cup assembly, the external dimension of the bob is 35.120 mm, and the internal dimension is 32.800 mm. The shear rate was changed from 1 to 1000 s⁻¹ to comprehend the fluid's shear-dependent characteristics better. The investigations were implemented at 30°C, 60°C, and 90°C. After the temperature reached the appropriate level, a 3-minute stabilization period was allowed for the samples before viscosity measurement. Viscosity fluctuation with shear rate comprehends the chemical slug behavior and how temperature and shear rate affect its deformation. The range of ambiguity for three experimental

measurements was around \pm 0.8 and 8% of the reported value. Before and after every examination, the equipment's components were all thoroughly cleaned with deionized water and dried. The various mMWCNT concentrations, ranging from 100 to 500 ppm, were added to a 1000 ppm polymer at intervals of 100 ppm to formulate the chemical slug.

4.2.11 Core Flooding Experimentations

Core flooding studies determined the efficacy of surfactant polymer flooding for chemical-enhanced oil recovery (CEOR) in the presence of mMWCNT nanoparticles (NPs). An extensive set of core displacement tests has been performed under ambient temperature & pressure to measure the efficacy of the slugs (surfactant, nanotube/surfactant) in increasing the recovery rate under reservoir circumstances. The core used during the flooding experiments had dimensions of 7.7 cm long and 3.8 cm in diameter. The helium porosity meter estimates the core sample's porosity and the core sample's pore volume. The operational configuration (Figure 4.3) comprises two transfer accumulators, one for oil and the other for the nanofluid and a core holder. The core holder also housed an HPLC constant rate syringe pump for high-pressure injection of water or nanofluid. A back-pressure regulator (BPR) maintains the system's pressure at the core's output. A differential pressure transducer (DPT) measured the pressure drop throughout the core. The core was primarily saturated by water and again by light oil at a minimal flow rate (0.5 ml/m). This process continued until the connate water saturation was achieved under the reservoir conditions. D-CAM Engineering India provided the syringe pump and core flooding setup shown in Fig. 2.4.

4.3. Results and Discussion

4.3.1 Characterization of modified MWCNT (mMWCNT)

The HRTEM image of the modified MWCNT in Figure 4.2 validates the presence of multiwalled carbon nanotubes after modification. It shows that the modified carbon nanotubes entangle with each other. It can be noted from Figure 4.2 (a) that the diameter of the tubes is around 0.34 nm. The image in Figure 4.2 (b) also confirms the presence of a few aggregates.

The zeta (ζ) potential was evaluated for both the pure and modified MWCNT by Malvern Zetasizer Nano ZS at room temperature. The zeta potential for pristine MWCNT is -8.34 mV, and that for modified MWCNT (mMWCNT) is -21.2 mV [106]. The zeta potential is symptomatic of the stabilization of the colloidal system. It was noted that zeta potential changes with the attachment of the functional group on the surface of the MWCNT. Thus, the modification enhances the stability property of the MWCNT, which leads to better dispersibility. Various variations in ionic mechanisms in the surface properties also led to changes in zeta potential and stability.

The modified MWCNT was analyzed with Raman spectroscopy, RENISHAW Micro Raman Spectrometer, and the excitation was produced by a 785 nm Argon laser. For pure MWCNT, the Raman allowed a G band corresponding to the stretching mode of the graphitic plane, which was noted to be around 1582 cm⁻¹ [110]. However, this band is highly affected by strain or modification. Thus, it can be seen that there is a shift due to surface modification leading to a blue shift with the G band at 1564 cm⁻¹ [110]. The second-order dispersive Raman feature, the G' or 2D band, is observed for pristine and modified MWCNT at around 2600 cm⁻¹ [110]. The D-band, the defectactivated Raman mode, is around 1350 cm⁻¹ [110] and is found in both cases, as

observed in Figure 4.3. The other bands corresponding to D+D' corresponding to the disorder were observed in pristine and modified MWCNT [106]. The higher intensities in the case of modified MWCNT (mMWCNT) confirm the presence of modifications and attachment of functional groups on the surface of MWCNT. Carbon nanotubes (CNTs) have a crystalline structure, according to X-ray diffraction (XRD) examinations. From the attached Figure 4.4, it can be observed that mMWCNT displays the characteristic peak at 2θ approximately 26.09° and 43.13°, correspondingly, which corresponds to the regular structure of graphite (002) and (100) reflections (Joint Committee for Powder Diffraction Studies (JCPDS) No. 01-0646)[101], [111], [112]. Similar outcomes were reported by Oh et al.[113], Gupta et al.[114], Chen et al.[115] and Chen & Oh [116].

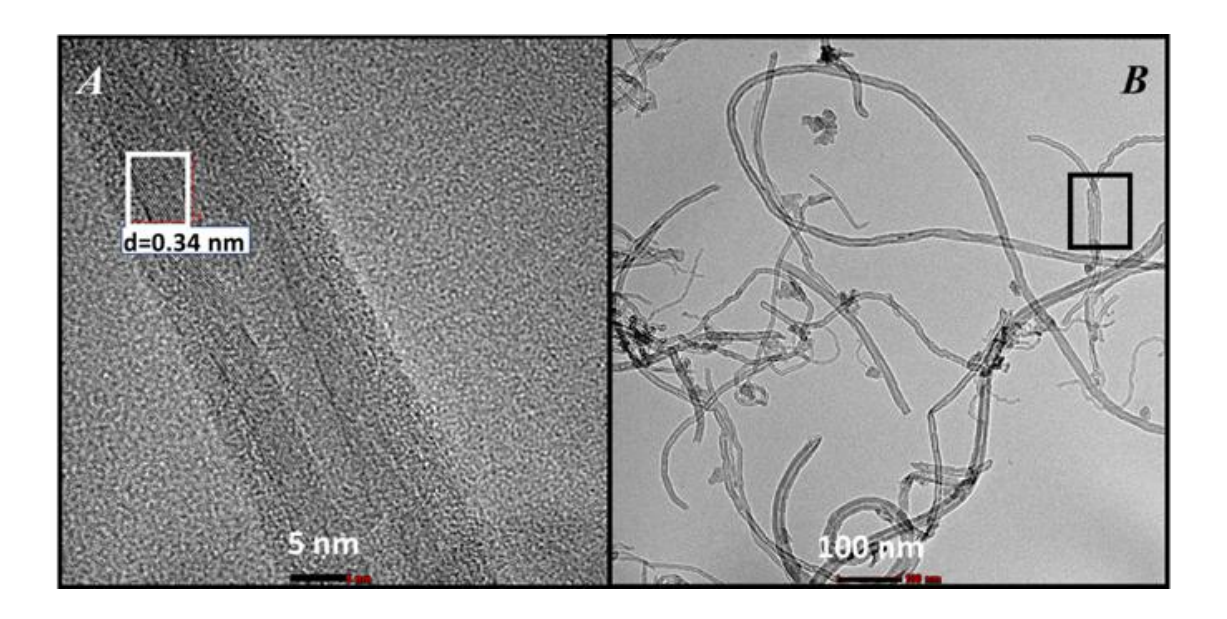


Figure 4. 2: HRTEM images of modified MWCNT (mMWCNT)

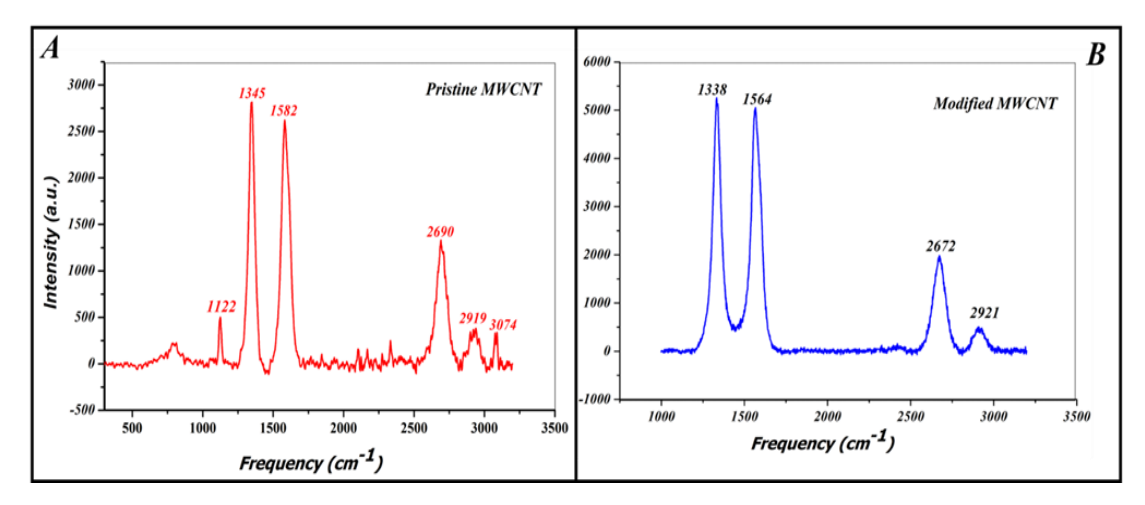


Figure 4. 3: Raman Spectroscopy of (A) Pristine CNT (B) Modified MWCNT (mMWCNT)

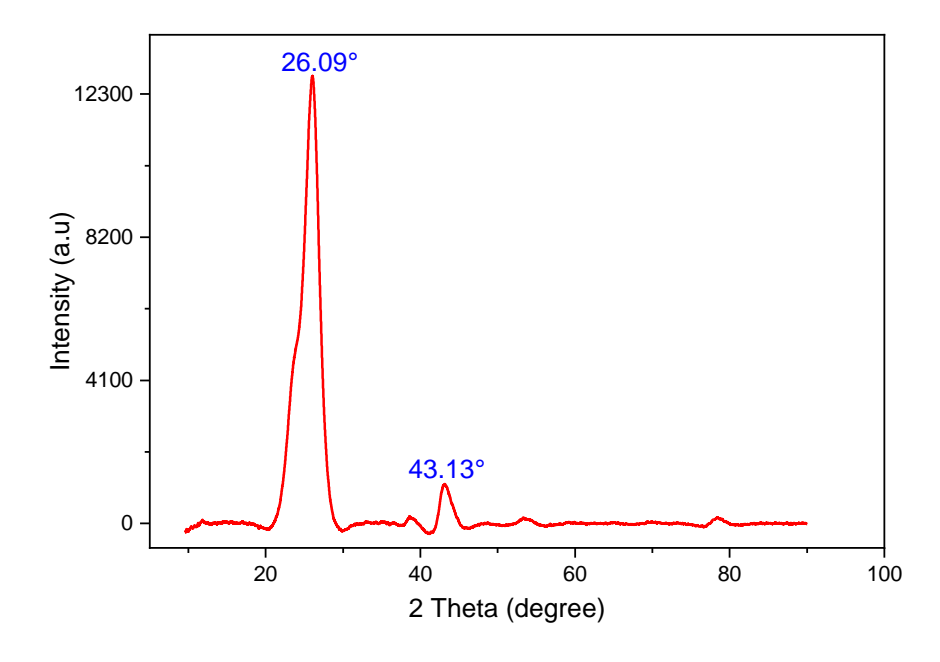


Figure 4. 4: XRD analysis of mMWCNT

4.3.2 Particle size and ζ-potential of mMWCNT

Investigating the size distribution of the mMWCNT introduced to the chemical slug is critical because the particle size considerably influences the interfacial characteristics that affect oil recovery. The mMWCNT's average hydrodynamic diameter was 139.8 nm without an anionic surfactant, and it was 228 nm with an anionic surfactant, as shown in Figure 4.5. According to Wang et al. (2018), the surfactant sodium bis(2-Ethylhexyl) sulfosuccinate (AOT) boosted the ζ -potential and the

electrostatic potential between silica nanoparticles, which stabilized the nanofluid. Al-Anssari et al. (2017) assessed the impacts of SDS and CTAB surfactants on stabilising silica nanofluids in salty environments (NaCl, up to 5 wt%). They concluded that SDS provided more stability than CTAB.

Consequently, applying an appropriate anionic surfactant may restore the unstable nanofluid's stability [117]. One main characteristic of estimating a colloidal dispersion's stability is its ζ -potential. Ultimately, stability is indicated by a stronger electrostatic repulsion. The colloidal dispersion will be stable if the particles have a repulsion coefficient that is high enough to prevent flocculation. In contrast, flocculation or coagulation will eventually occur without the repulsion mechanism [67]. For colloidal dispersions to be stable, the ζ -potential must be equal to or greater than ± 30 mV [117], [118]. The zeta potential of the prepared mMWCNT dispersion in DI water was obtained to be -21.2 mV without surfactant. However, adding an anionic surfactant (Figure 4.5) increased the potential to -39.4 mV, making the dispersion solution more stable.

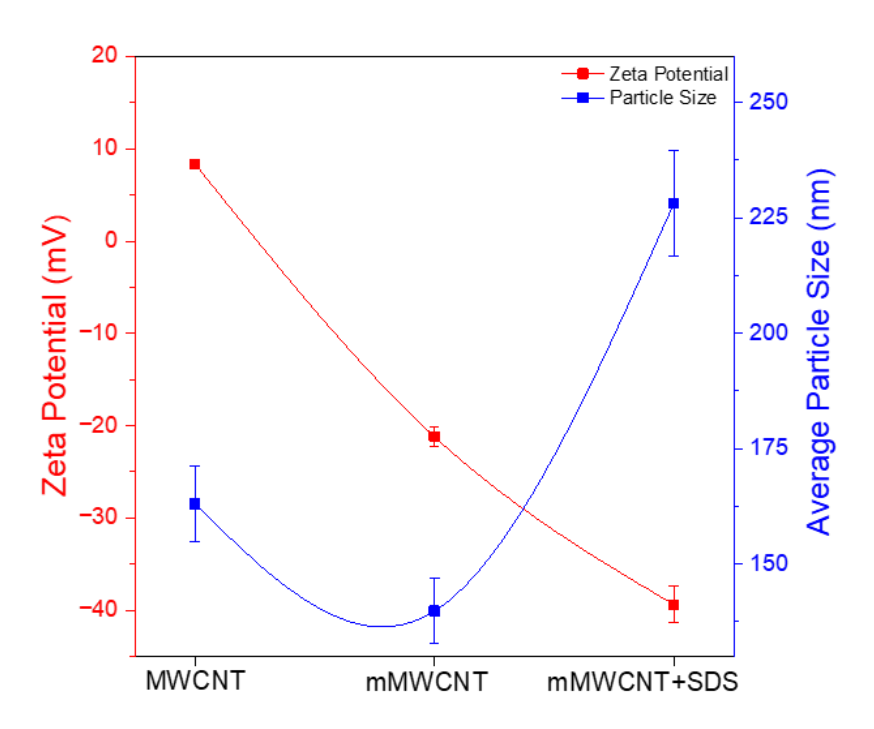


Figure 4. 5: Particle and zeta size of the mMWCNT with anionic surfactants.

4.3.3 Effect of mMWCNT on CMC

Critical micelle concentration is a fundamental characteristic of surfactants. The surfactant concentration above which the micelles spontaneously developed is called CMC [119], [120]. Surfactants are dispersed in the bulk liquid phase and separated on the interface. This separation lessens the free energy of the bulk phase via diminishing surface tension / interfacial tension and reducing hydrophobic components of the surfactant from water contact. The surfactants aggregate into micelles as the surfactant molecule concentration at the surface increases. This phenomenon reduces the surface free energy (surface tension) by decreasing the contact area of the hydrophobic sections of the surfactant with water. Any additional surfactant additions will only increase the number of micelles once the CMC is reached [121]. Figure 4.6 (b) represents mMWCNT's impact on the anionic surfactant's CMC value. As mentioned in Fig. 4.6, the anionic surfactant's CMC was observed to be 2337 ppm at 0 ppm mMWCNT

concentration via the conductivity method, whereas using a tensiometer, it would be found to be 2500 ppm.

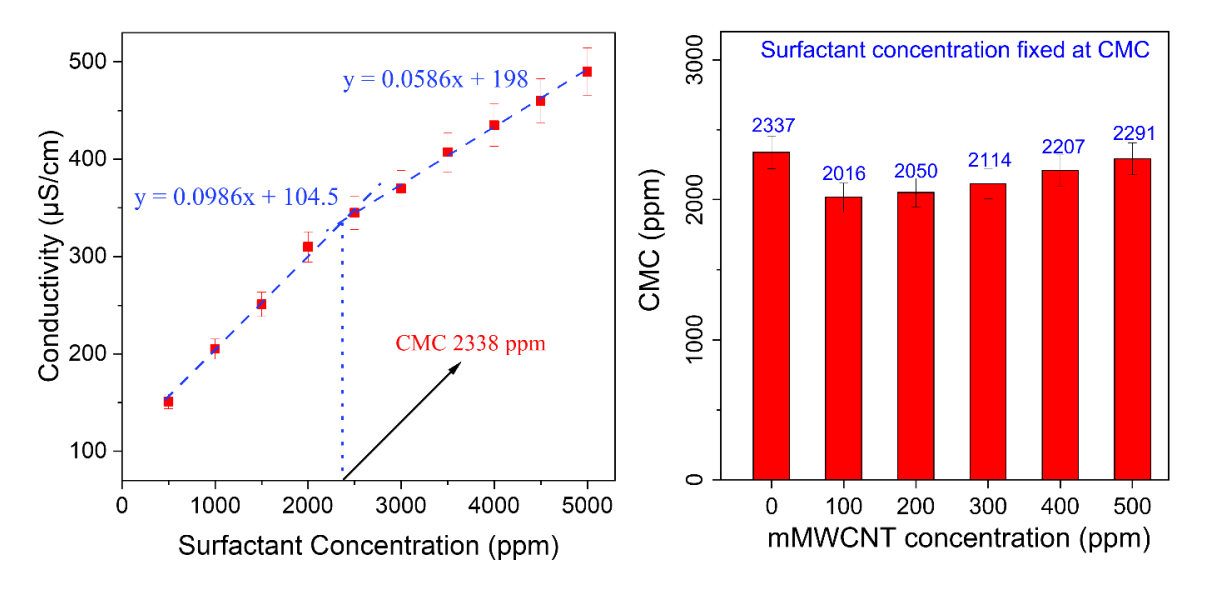


Figure 4. 6: (a) CMC determination of SDS through conductivity measurement (b) Effect of mMWCNT concentration on the CMC of the surfactant.

4.3.4 Impact of mMWCNT on ST

The surface tension (ST) of surfactants determines their capacity to reduce the disparity in the forces playing at the air/liquid interface. Surface active compounds or nanoparticles can be added to a liquid to lower its surface tension [122], [123]. By adsorbing at the liquid surface, surfactants tend to stabilize the forces at the interface. Surface tension is another crucial attribute when evaluating the effectiveness of a thermal system. The surface tension of fluids has an extensive range of applications, like improved boiling heat transfer, oil recovery efficiency, and the ability to clean up oil spills [123]. Vafaei et al. examined the ST value of the Bi₂Te₃/water nanofluids and observed that the ST value reduced as particle concentration rose in the prepared solution. Surface tension decreased up to surfactant CMC. However, after CMC, increasing the particle concentrations in the bulk solution, surface tension rose again, but the slope of the trend was not more prominent [124]. The addition of nanoparticles

rises along with the volume fractions, which causes the ST of the nanofluids to rise. The increasing nanoparticle concentration renders more nanoparticles actively dispersed and interacting with each other. The present molecule in the dispersed solution imposes a cohesive force that increases the ST of the dispersed nanofluids [125]. In addition, the mean distance between molecules and nanoparticles decreases with increasing concentration. The electrostatic repulsion force among the molecules is replaced by an attractive Van der Waals attraction, increasing the nanofluid's surface tension [125]. Fig. 4.7 represents the surface tension behavior with surfactant and mMWCNT concentrations. The water's surface tension value was measured at 70.83 millinewtons per meter (mN/m). However, it decreased to 33.98 mN/m when 2500 parts per million (ppm) of SDS (sodium dodecyl sulfate) was added to the deionized (DI) water. The surface tension further reduces to 29.23 mN/m after adding 100 ppm mMWCNT to the surfactant solution, illustrated in Figure 4.7. The prepared surfactant solution reduced the ST value by ~52%, Whereas after introducing 100 ppm mMWCNT in the surfactant solution, the ST value was reduced by ~59%. Further raising the mMWCNT concentration to 200 ppm in the SDS solution, the ST value lessens by $\sim 50\%$, represented in Fig. 4.7 (a, b).

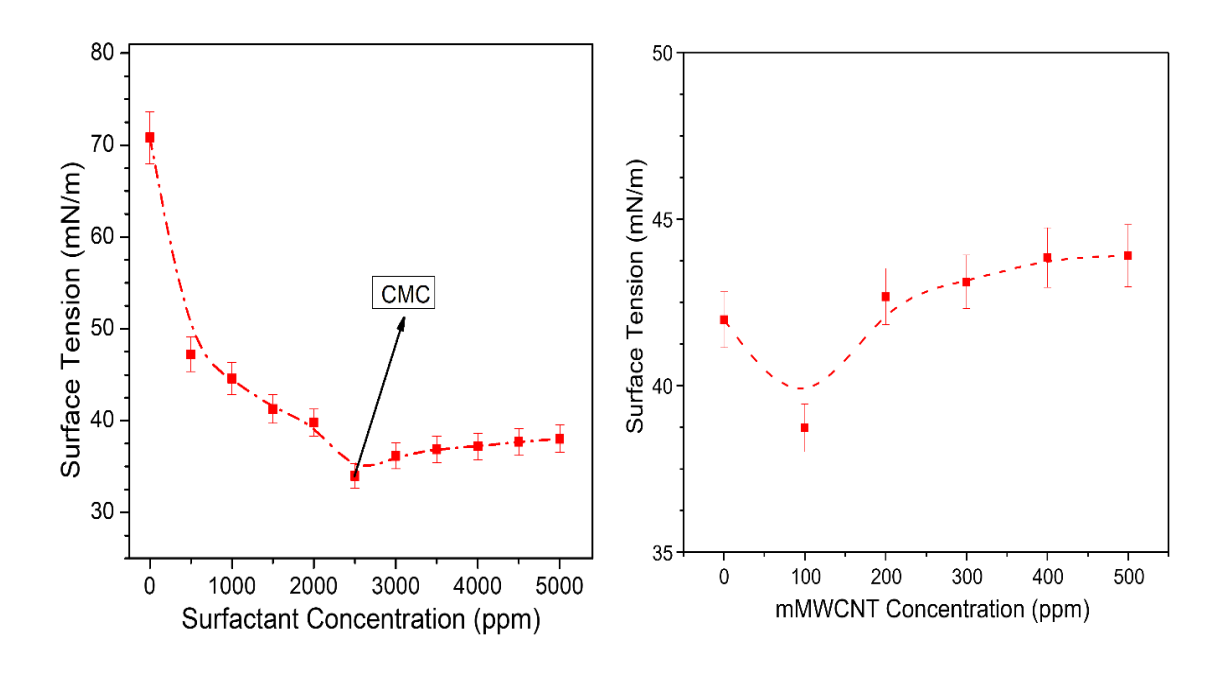


Figure 4. 7: (a) Surface tension vs varied surfactant concentration (SDS), (b) the effect of surface tension using mMWCNT with SDS surfactants (CMC).

4.3.5 Impact of mMWCNT on IFT

One of the critical functions of chemical EOR in the oil industry is to diminish the interfacial tension (IFT) between the oil phase and the aqueous phase [52], [68], [126], [127]. The capillary number (CN) is a dimensionless parameter that describes the ratio of viscous forces to capillary forces. Usually, the CN value for water flooding is around 10⁻⁷. When the CN value is higher, ranging from 10⁻⁴ to 10⁻², a less significant volume of residual oil saturation remains in the reservoir [128]. To reach such a large figure, it is necessary to reduce the IFT to an extremely low value of 10⁻³ mN/m [53]. Therefore, the IFT among crude oil and mMWCNT were measured in the presence and absence of SDS surfactant to investigate how the mMWCNTs can affect and potentially further decrease the IFT. The decrease in interfacial tension (IFT) usually happens when both SDS and NPs are absorbed at the interface between two fluids [129], [130]. Figure 4.8 shows the process of IFT with or without the SDS (sodium dodecyl sulfate) solution

and the oil phase while using mMWCNT (modified MWCNT) at various concentrations. Figure 4.8 (b) indicates that when the concentration of mMWCNT added to the SDS solution was raised, the IFT among the SDS solution and oil phase decreased significantly. Specifically, when 100 ppm mMWCNT was introduced to the solution containing 2500 ppm SDS, the IFT decreased by 55%. The primary explanation for the considerable decrease in IFT in the presence of nanoparticles (NPs) is their capability to transport surfactant molecules to the interfacial region through Brownian motion [131]. If additional surfactant molecules are present at the interface between two liquids, then IFT between those two liquids will decrease. The data shown in Figure 4.8 (b) show no further decrease in IFT beyond the concentration of 100 ppm of mMWCNT. One possible explanation for this observation is that at concentrations higher than 100 ppm, the nanoparticles (NPs) start to aggregate, which hinders their ability to act as carriers of surfactant molecules. This, in turn, could lead to no further improvement in interfacial tension (IFT) reduction [132]. Thus, from ST and IFT results, it was found that 100 ppm concentration is the optimum concentration.

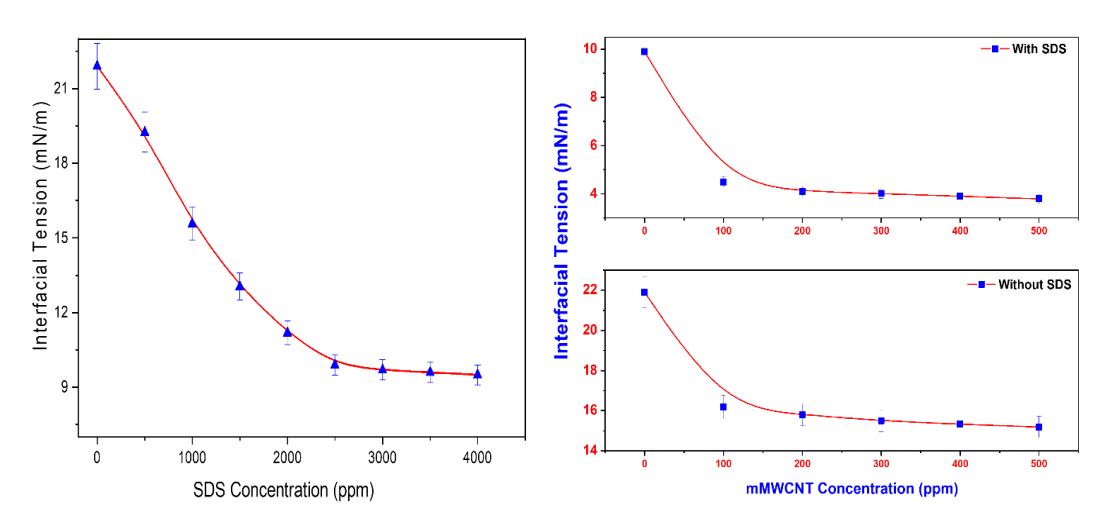


Figure 4. 8: (a) Interfacial tension of varying SDS concentration, (b) effect of interfacial tension with and without SDS (at CMC).

4.3.6 Impact of the SDS on the Degree of Adsorption

The phenomenon of loss of surfactants involves the accumulation of surfactant molecules from the bulk liquid solution on a reservoir rock surface [133]. The loss of surfactant at the solid-liquid interface is vital in various industrial and scientific applications, which has adverse technical and financial effects. Consequently, surfactant retention is a fundamental concern in surfactant-based chemical EOR procedures, surfactant flooding, surfactant polymer flooding, and alkaline/surfactant/polymer (ASP) flooding [134]. Adsorption, phase entrapment, and precipitation lead to the retention of surfactants throughout the chemical EOR procedure. The migration of surfactants into microemulsions or the oil phase causes phase entrapment. Phase trapping is mainly due to high salinity, temperature, and the presence of highly divalent ions. The process of reaching ultralow IFT is hampered by this collective action, resulting in surfactant loss [135].

Several authors have investigated how surfactant loss onto reservoir rocks affects surfactant concentration. Sandstone surfaces are charged negatively, whereas carbonate rocks have a positive charge at their surface, depending on the kind of rock. Ion exchange, ion association, hydrophobic bonds, adsorption by electron polarization, and adsorption by dispersion forces are a few of the processes involved in surfactant adsorption on sand particles [61], [71], [72], [120], [136]. The solid substrate, solvent, type of surfactant, and the nature of its polar head groups and tail part all play a distinct role in the adsorption [137]. Beyond a specific limit, surfactant loss on the sand grain damages oil recovery, which is controlled by the disparity in thermodynamic stability among interactions between surfaces of liquid and water [61]. The hydrophobic effect describes a substance's propensity to elude an aqueous solution, which is crucial to

adsorption. The result (Figure 4.10) shows that the surfactant (SDS, anionic) adsorption increased with increasing concentration from 0.93 to 3.73 (mg/g) at 500 ppm to 7.9 to 12.6 (mg/g) at 5000 ppm from day one to day three. The increase in surfactant adsorption with rising surfactant concentration is attributed to the higher availability of surfactant molecules in the bulk phase, which enhances the likelihood of interactions between the surfactant molecules and the sand surface. However, when surfactant adsorption reached its saturation point, a maximum adsorption plateau was attained, indicating that adding more surfactant would have no further impact on adsorption [65], [133]. SDS molecules were free and readily adsorbed when the SDS concentration was below CMC because they were negatively charged.

Consequently, the adsorption rose as the surfactant concentrations rose above 2500 ppm. As the concentration of SDS increased beyond 2500 ppm, the individual surfactant molecules began to aggregate into micelles with other SDS molecules. This prevented them from adhering to the sand particles and explained why there was no discernible change in the SDS adsorption values beyond 2500 ppm. According to this, the loss of surfactants is only impacted via the surfactant-free molecules available in the aqueous phase [68].

4.3.7 Time effect on adsorption

For the static adsorption experiment, the impact of surfactant loss over time on adsorption density was examined beforehand to certify symmetry throughout the studies. The experiments were performed for three days at 24-hour intervals to ensure surfactant adsorption. The plot represents the impact of time from 24 h to 72 h over the adsorption, as shown in Figure 4.9. The graph illustrates that surfactant loss increased

with contact time. The steric repulsion of surfactant molecules already adsorbed on the surface of the sand accounts for this drop. However, it is well known that the adsorption rate slows down after a while [53] because most of the sites are occupied early, leading to a plateau in adsorption curve.

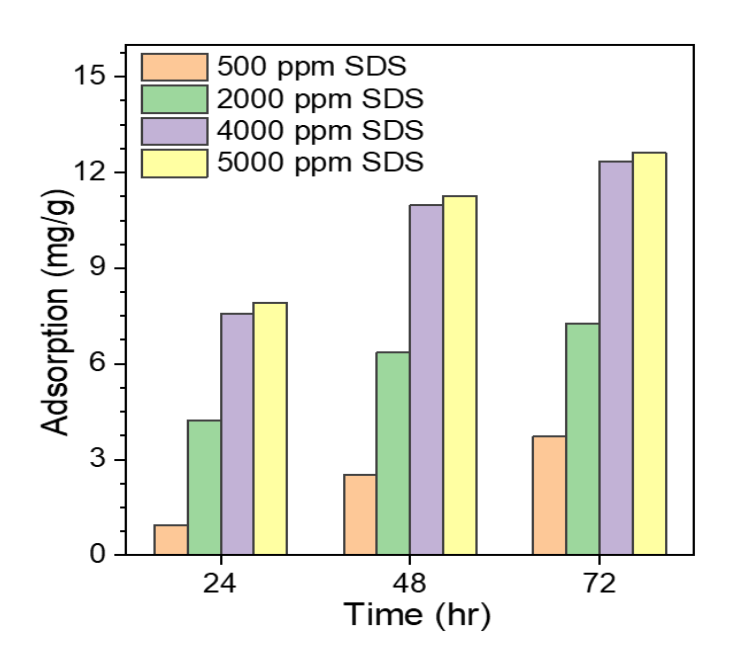


Figure 4. 9: Impact of the duration of ageing on the process of surfactant adsorption

4.3.8 Impact of mMWCNT on surfactant loss

The approach to computing the surfactant loss on the rock's grain was the same as earlier studies [50], [61], [64], [68], [120]. Figure 4.10. illustrates that after three days, the adsorption for SDS at the CMC was 8.74 mg/g. The results show that after 3 days, the surfactant adsorption decreases to 4.77 mg/g by adding 100 ppm mMWCNT to the prepared sample. The surfactant loss minimizes ~46% on introducing 100 ppm mMWCNT to the sample, which is better than the significant studies employing silicabased nanoparticles for comparable treatments. While the loss of surfactant diminishes as the solution's mMWCNT concentration rises, this reduction is not as impressive as the 100 ppm mMWCNT solution. Many possible reasons could explain the lessening

surfactant loss with nanoparticles, nanotubes, and nanosheets. The primary methods surfactants bind to rock surfaces are typically through electrostatic and van der Waals interactions. These interactions involve the attraction of oppositely charged particles and the attractive forces between molecules. Conversely, the process of surfactant loss onto the surface is complex and influenced by a range of factors, including surfactant properties and environmental conditions such as temperature and pH [50], [61], [68], [120]. Therefore, altering the adsorption process depends on electrostatic repulsion among the negatively charged mMWCNT particles and the SDS [15], [138], [139]. Preferential SDS adsorption on the mMWCNT surface decreases SDS adsorption on the rock surface. SDS loss reduces as the mMWCNT stays movable and suspended in the solution. After adding 100 ppm mMWCNT, the surfactant loss decreased to 4.77 mg/g at the CMC of SDS; however, when 200, 300, 400, and 500 ppm mMWCNT were introduced to the bulk solution, the SDS loss was minimized but increased in comparison to the 100 ppm mMWCNT solution. The sudden increment in adsorption is responsible for the desorption mechanism. After introducing 100 ppm mMWCNT into the prepared surfactant solution at CMC, the loss of surfactant was minimized ~ 49.3% after 3 days. Minimizing surfactant loss ensures that less surfactant is needed for Enhanced Oil Recovery (EOR) operations, effectively reducing interfacial tension (IFT) and altering the rock surface's wetting characteristics. This optimization significantly lowers EOR operational costs while maximizing the recovery factor. Additionally, it minimizes the amount of residual surfactant left in the subsurface, thereby reducing the ecological impact.

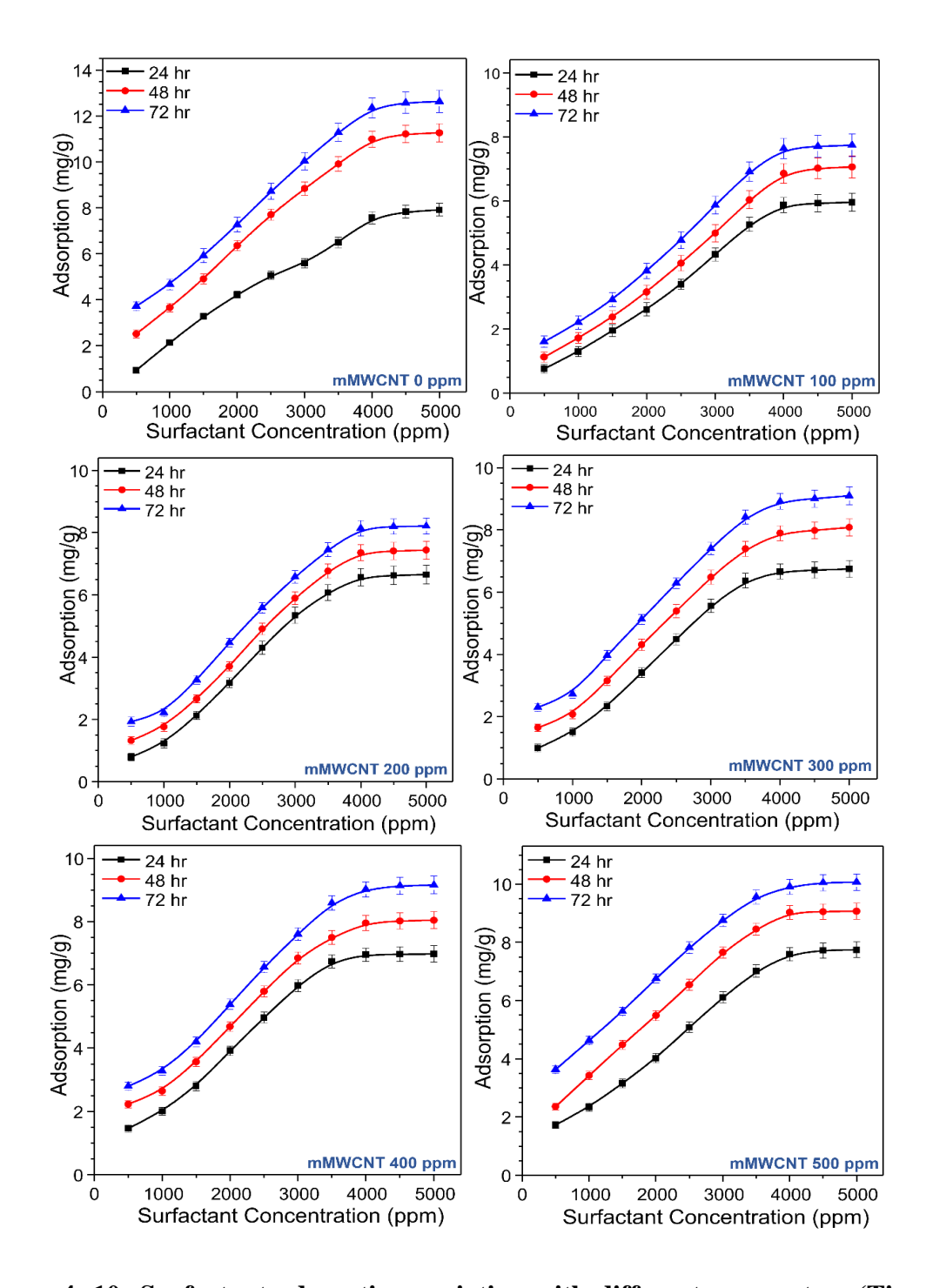


Figure 4. 10: Surfactant adsorption variation with different parameters (Time, Surfactant Concentration, mMWCNT Concentration) at 30°C.

4.3.9 Adsorption isotherm model

Surfactant loss is a surface phenomenon where particles (adsorbate) get adsorbed on a solid surface (adsorbent). The solid particle gets attached to the adsorption sites on the adsorbent due to electrostatic attraction between the charged adsorbent and adsorbate. Three primary adsorption models help to understand the mechanisms or characteristics of the adsorption data, namely, the Langmuir, Temkin, and Freundlich adsorption isotherm model [57,58]. Adsorption isotherm models offer data on the adsorption process mechanism crucial for adsorption system design. The adsorption equilibrium data modelling, the adsorbent's characterization before and after adsorption, and other methods have been used to examine the adsorption mechanisms. Additionally, the adsorption isotherm models offer data on the maximal adsorption capacity, which is essential in assessing the adsorbent's efficacy.

As per the Langmuir adsorption isotherm, the surfactant loss process occurs linearly at low densities of adsorbate and eventually reaches a maximum surface coverage as the concentration of adsorbate increases. It is a widely used model for calculating the extent of adsorbate on an adsorbent as a function of partial pressure or concentration at a specific temperature. The Langmuir adsorption isotherm model postulates that a finite number of adsorption sites are available, and it does not consider any interaction among the surfactant molecules that are already adsorbed. It also believes that adsorption is a single-layer process, and only one surfactant molecule can be adsorbed at a time on a particular site. The Langmuir adsorption model proposes that all adsorption sites are alike and have the same energy. According to this model, neighboring adsorbed atoms do not affect each other in any way. It describes how

chemisorption works. Langmuir adsorption isotherm (equation 4.3) provides better quantitative explanations; hence, it is the most widely used adsorption model [140].

$$\frac{1}{q_{eq}} = \left(\frac{1}{K_{lang}} q_m\right) \frac{1}{C_{eqi}} + \frac{1}{q_m} \tag{4.3}$$

Where q_{eq} represents equilibrium adsorption, q_m is the maximum capacity of adsorption. C_{eqi} is the equilibrium concentration of adsorbate. K_{lang} is the Langmuir constant, that is associated with the capacity of adsorption. The parameters are mentioned in below Table 4.1.

Table 4. 1. Model parameters of Langmuir isotherm model.

(a) Langmuir mathematical parameters							
mMWCNT Conc. (ppm)	Linear relation	$K_{lang}(L/mg)$	q _m (mg/g)	\mathbb{R}^2			
0	$1/q_{eq} = 522.56 / C_{eqi} - 0.0066$	-1.26E-05	-152.21	0.9912			
100	$1/q_{eq} = 663.17 / C_{eqi} + 0.032$	4.83E-05	31.26	0.9905			
200	$1/q_{eq} = 662.39/Ceqi + 0.002$	3.05E-06	500	0.9725			
300	$1/q_{eq} = 508.87 / C_{eqi} + 0.0415$	8.18E-05	24.09	0.9711			
400	$1/q_{eq} = 324.79/C_{eqi} + 0.0839$	2.58E-04	11.94	0.9411			
500	$1/q_{eq} = 182.45/C_{eqi} + 0.0785$	4.30E-04	12.74	0.9863			

The Freundlich adsorption is a model that depicts how the amount of gas that is adsorbed by a specific amount of solid adsorbent varies with changes in the pressure of the system at a constant temperature. It is related to multi-molecular layer adsorption and assumes that the surface of the solid adsorbent is heterogeneous for this purpose. The adsorbent's surface is not uniform. Certain limitations to this model make it undesirable. This model fails to explain chemisorption. The Freundlich adsorption

isotherm does not provide a quantitative explanation. It gives a comparatively less satisfactory explanation of the gas adsorption on solids [141], [142]. Freundlich adsorption model is given by equation 4.4.

$$q_{eq} = K_{frad} \left(C_{eqi} \right)^{1/n} \tag{4.4}$$

 K_{frad} & 1/n is the constant, providing info about adsorption intensity and capacity, which is represented in equation 4. When n is larger than 1, this indicates effective adsorption [120]. The adsorption intensity determines the degree of heterogeneity present at the adsorption sites [81]. Table 4.2 contains the constants for the Freundlich adsorption isotherm as well as the correlation coefficients.

Table 4. 2. Parameters of Freundlich isotherm model.

(b) Freundlich model parameters						
mMWCNT	Mathematical relation	K _{frad} (L/mg)	1/n	\mathbb{R}^2		
Conc.(ppm)						
0	$q_{eq} = 0.098234(C_{eqi})^{0.907}$	0.098234	0.907	0.9774		
100	$q_{eq} = 0.054573(C_{eqi})^{1.030}$	0.054573	1.030	0.9889		
200	$q_{eq} = 0.057509(C_{eqi})^{1.035}$	0.057509	1.035	0.9662		
300	$q_{eq} = 0.089117(C_{eqi})^{0.914}$	0.089117	0.914	0.9653		
400	$q_{eq} = 0.179281(C_{eqi})^{0.721}$	0.179281	0.721	0.9587		
500	$q_{eq} = 0.223398(C_{eqi})^{0.667}$	0.223398	0.667	0.9681		

Temkin isotherm is a modification of Langmuir that considers adsorbate-adsorbate interaction and changes in adsorption enthalpy. This statement suggests that the heat of adsorption for all molecules in the layer reduces linearly as the coverage increases. The decrease in heat is attributed to synergies among adsorbent and adsorbate [81]. The Temkin model is linearly represented as an equation and usually applied in the form given in equation 4.5.

$$q_{eq} = B_{tem} \ln K_{tem} + B_{tem} \ln C_{eqi}$$

$$\tag{4.5}$$

Where the constants mentioned above K_{tem} & B_{tem} are the Temkin constants. K_{tem} and B_{tem} relate the equipoise binding constant and the heat of adsorption, respectively. Table 3 contains the Temkin adsorption isotherm constants and the empirical observations' correlation coefficients. The coefficients of R^2 in the Freundlich and Temkin models are not as impressive as they are for the Langmuir isotherm, as shown in Tables 4.1, 4.2 and 4.3. As a result, the Langmuir isotherm better captures the surfactant loss onto the sand than the Freundlich and Temkin isotherm, which is illustrated in Figure 4.11.

Table 4. 3. Temkin model parameters

(c) Temkin mathematical parameters						
mMWCNT Concentration (ppm)	Linear correlation	K _{tem} (L/mg)	B _{tem} (J/mol)	\mathbb{R}^2		
0	$q_{eq} = 7.44 \ln (C_{eqi}) - 19.15$	0.076167	7.44	0.9683		
100	$q_{eq} = 6.13 \ln (C_{eqi}) - 16.44$	0.068287	6.13	0.9151		
200	$q_{eq} = 6.99 \ln (C_{eqi}) - 18.67$	0.069362	6.99	0.9179		
300	$q_{eq} = 6.73 \ln (C_{eqi}) - 17.56$	0.073582	6.73	0.9163		
400	$q_{eq} = 7.44 \ln (C_{eqi}) - 19.15$	0.084531	6.18	0.9135		
500	$q_{eq} = 7.44 \ln (C_{eqi}) - 19.15$	0.088295	6.38	0.9042		

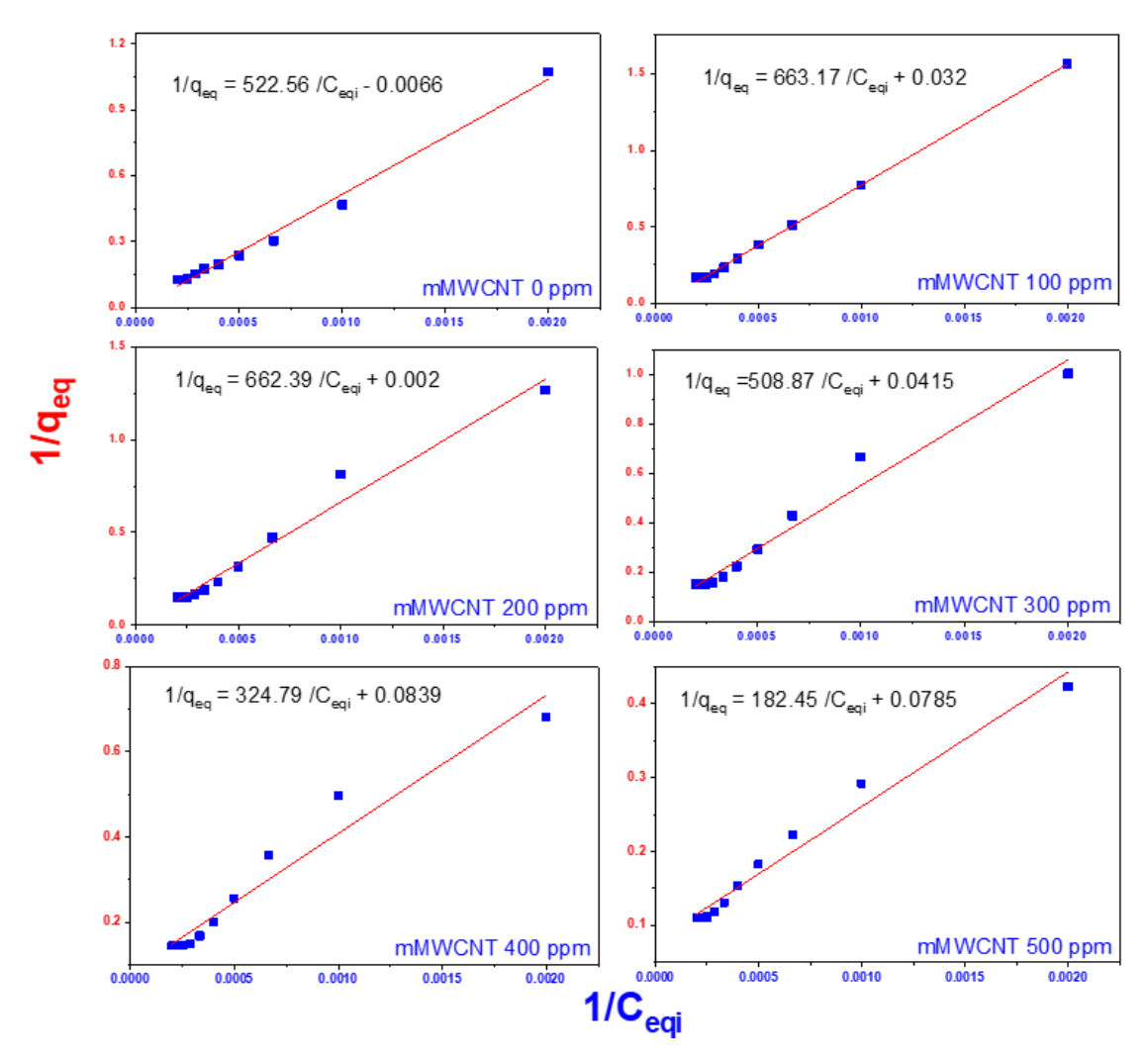


Figure 4. 11: Langmuir adsorption isotherm model fit in mMWCNT data at ambient pressure and temperature.

4.3.10 Contact Angle Analysis

The purpose of the contact angle (CA) experiments is to assess the wetness characteristics of the surface and gain an understanding of its surface properties. The composition and type of the rocks, crude oil, and mineral composition influence the rock surface wetting characteristics. Several physiochemical processes, including multi-ionic exchange, salting, fine migration, electric double-layer expansion, mineral dissolving, and pH variation govern wettability alteration. Several theories apply to sandstone, while others correspond to carbonate reservoirs [133], [143], [144]. Nanoparticles are used as potential agents to modify the wetness behavior of rocks. The

wettability modification is influenced by nanoparticle concentration, size, and salinity. Researchers have observed the CA between crude oil and a solution containing nanoparticles at various concentrations on silica pellets. They concluded that amplifying the NPs concentration in the fluid enhances the hydrophilic nature of rocks. Roustaei and Bagherzadeh examined the impact of SiO₂ (Silicon dioxide) nanoparticles on the wetness attributes of a carbonate reservoir rock, showing that SiO₂ nanoparticles are prone to change the wetting characteristics of carbonate reservoir rock [145]. According to Hendraningrat et al., dispersing Al₂O₃ solution can modify the wetting characteristics of sandstone rocks from strongly oil wet (above 90°) to strongly waterwet (below 75°) [146]. The CA investigation was performed at 2500 ppm surfactant concentration with varying mMWCNT concentrations (100, 200, 300, 400, and 500 ppm). This observation shows that the CA values were demoted to more water-wet after increasing mMWCNT concentration. Because adsorption is a time-dependent phenomenon, thus the frequency of the adsorption process accelerates with contact time. Over time, contact angles between the polar surfactant component and the nonpolar crude oil part decrease [126], [147]. Because NPs are smaller and have higher surface free energy, they tend to attach to the surface. After rising NPs concentrations, the contact angles become smaller, which is explained by disjoining pressure. The nanoparticles form a self-assembled film with a wedge-like shape that comes into contact with the base using the crude oil phase [125], [148], [149]. As the concentration of NPs in the solution rises, more NPs aggregate at the wedge film, improving the disjoining pressure that causes the angle to decrease. A similar trend in the CA was found subsequently augmenting NPs in the DI water, implying that nanoparticles tend to alter the wetness behavior of the oil-wet sand pellet. The adsorption of NPs on the

rock forms a nanotextured surface, which changes the rock's morphology to semi-homogeneous. Thus, a fine layer of the NPs formed on the rock surface leads to a modification in the wetting characteristics of the surface to strong water-wet from oil-wet, resulting in an improvement in oil production. Figure 4.12 & 4.13. illustrates that the CA of the SDS was 57° on the oil-wet surface, which reduced to 53° after introducing 100 ppm mMWCNT in the bulk phase. When the mMWCNT concentration increases to 200, 300, 400, and 500 ppm, the wettability reduces to 50°, 46°, 41°, and 36°. This change indicates that the wetness characteristic of an oil-wet surface would change to that of a water-wet surface. Modified MWCNTs (mMWCNTs), being highly hydrophobic with a large surface area, strongly interact with both surfactants like SDS and the rock surface. They act as carriers for surfactants, enhancing their distribution and effectively converting oil-wet or mixed-wet rock surfaces to water-wet, thereby improving water displacement efficiency and oil mobility.

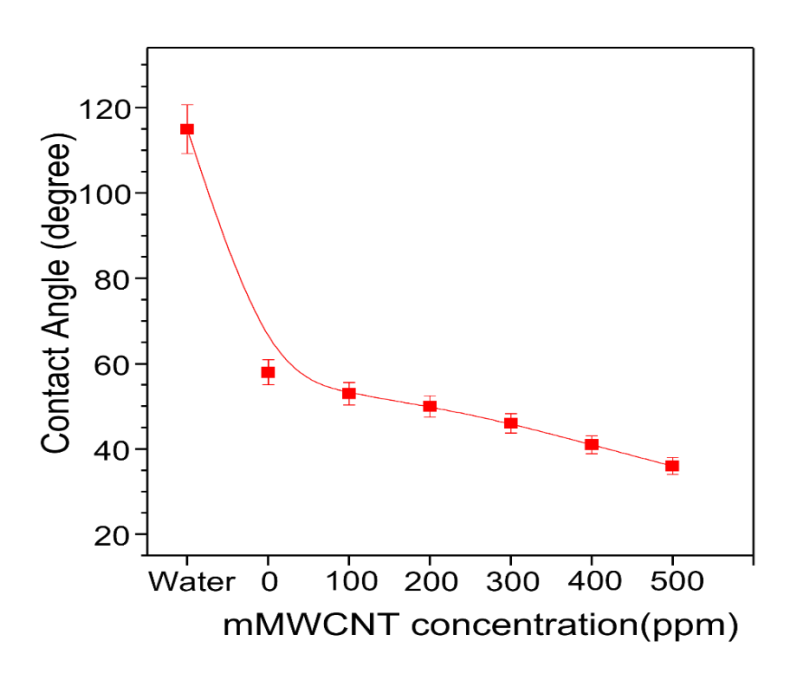


Figure 4. 12: Contact angle measurement using various mMWCNT concentration in the presence of anionic surfactants at CMC and polymer.

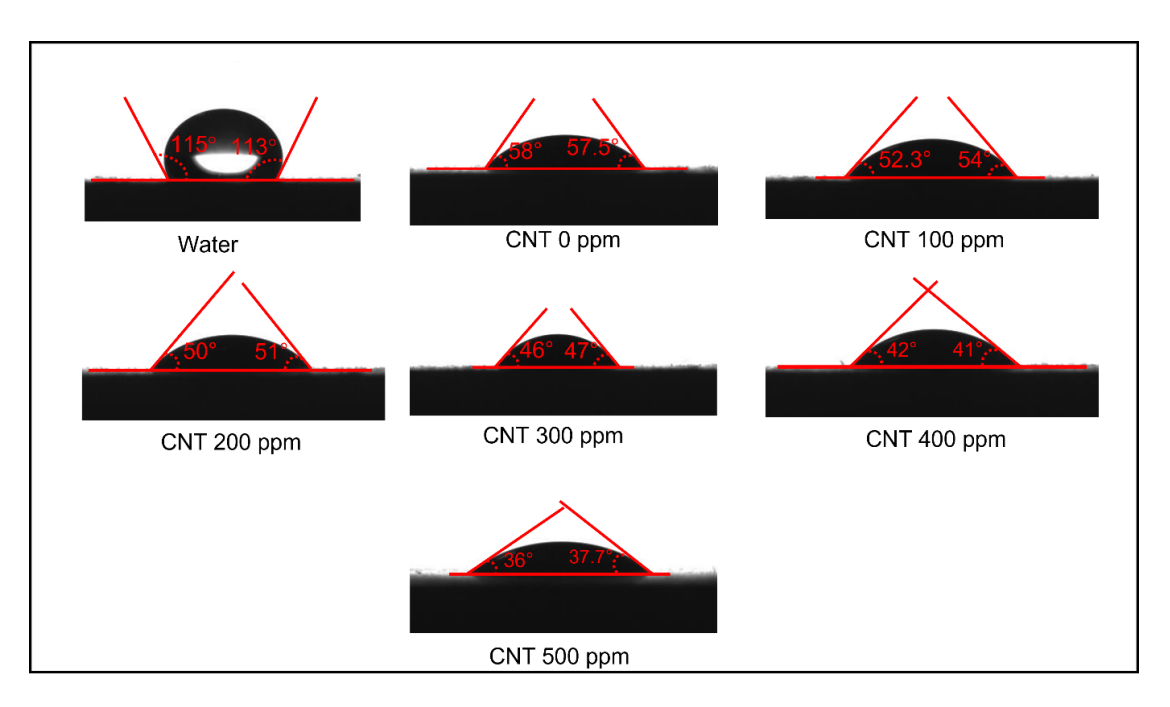


Figure 4. 13: Contact angle measurement by goniometer.

4.3.11 Viscometry Analysis

The rheological examination for viscosity measurements was performed to support the analysis of nanofluid stability. The measurement aids in understanding the nanofluid's flow properties during operation [94], [118], [150]. Nanoparticles, nanotubes, and nanosheets affect the solution's flow characteristics, including the surfactant and polymer. The fluid's rheology is influenced by nanoparticle size, shape, and concentration [50], [67], [68], [131]. Figure 4.14 (a) shows that the rheological investigations quantify the nanofluids' viscosity at various shear rates between 1 and 1000 s⁻¹. The rheological properties of a slug with a fixed amount of 1000 ppm of polymer and varying mMWCNT concentrations (100 ppm, 200 ppm, 300 ppm, 400, and 500 ppm) were determined using a rheometer. When the shear rate was changed from 4.2 to 1000 s⁻¹, it was observed that the viscosity of the fluid with 2500 ppm of the surfactant and 1000 ppm of PAM decreased from 298.75 mPa s to a value of 3.1 mPa s. This demonstrated the fluid's shear-thinning characteristic, which Meyer et al.

had reported in their earlier investigations [151]. When mMWCNTs were added to the chemical slug, viscosity improved. At a shear rate of 4.2 s⁻¹, the addition of mMWCNT raised the fluid's viscosity from 298.75 mPa s (0 ppm) to 348 mPa s (100 ppm), 435.12 mPa s (200 ppm), 470 mPa s (300 ppm), 500 mPa s (400 ppm), and 540 mPa s (500); The outcomes are compatible with the results of Mahbubul et al., [152]. Because of the reduced mobility ratio and viscous fingering caused by the increased viscosity, more oil would be swept, increasing the volumetric sweep efficiency [48], [68]. Table 4.4 represents the rheological analysis of the prepared chemical slug.

Table 4. 4. Rheological analysis of chemical slug

S. N	Shear Rate (s ⁻¹)	Viscosity (m Pa.sec)						
		0 ppm	100 ppm	200 ppm	300 ppm	400 ppm	500 ppm	- (°C)
1	4.2	298.75	348.10	435.12	470	499.96	539.35	26.8
2	20.8	73.37	92.58	115.72	162	198	223.63	27.1
3	102	15.28	24.90	29.29	35.38	40.56	47.11	27.3
4	347	4.79	7.41	8.38	8.57	9.28	9.9	27.2
5	653	3.99	4.21	4.68	4.75	4.82	5.16	27.5
6	1000	3.10	3.38	3.55	3.60	3.68	3.77	27.4

It is crucial to investigate the viscosity of the slug at higher temperatures because the reservoir's temperature is high. When the temperature rises, the viscosity of the polymer in the slug tends to diminish; therefore, it is essential to study its behavior under these conditions. The slug was composed of a polymer (1000 ppm), surfactant (2500 ppm) and mMWCNT (100 ppm) and was studied at varying temperatures. At a shear rate of 1000 s⁻¹, the slug's viscosity decreased from 3.373 to 2.698 and then to

2.294 mPa·s as the temperature rose from 30 to 60 and 90 °C, subsequently (Figure 4.14 (b)). This drop in viscosity could be attributed to the degradation of the polymer chains at higher temperatures, resulting in a reduction in viscosity. The findings of previous studies support these results.

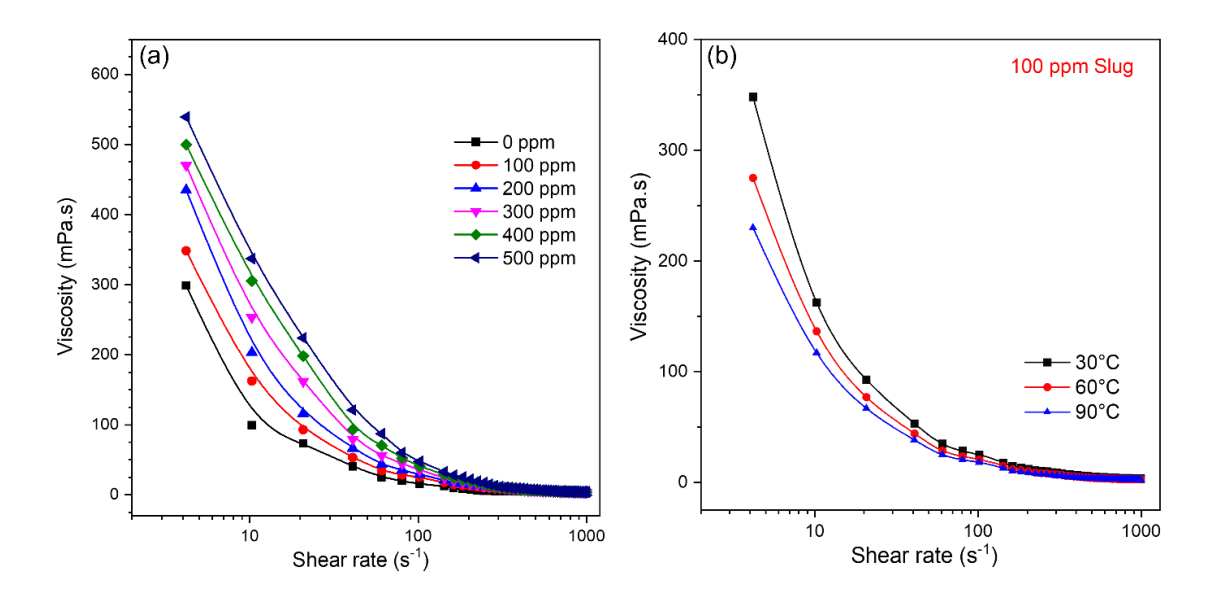


Figure 4. 14: (a) Rheological trends of the chemical slug at various concentrations. (b) Temperature effect at optimized slug concentration (100 ppm mMWCNT+SDS+PAM).

4.3.12 Dimensional measurement of core

The porosity of the core was assessed using the Helium porosity meter. Bulk volume, matrix volume, and pore volume are required to evaluate the porosity of the core sample. A parametric (dimensional) study of the core was performed to assess the porosity of the core, and the findings are illustrated below in Table 4.5. The porosity of the core sample can be evaluated via the below-mentioned mathematical equations 4.6 and 4.7.

$$\varphi = \frac{V_{pore}}{V_{bulk}} \tag{4.6}$$

Or
$$\varphi = \frac{V_{bulk} - V_{mat}}{V_{bulk}}$$
 (4.7)

Where ϕ is the porosity, V_{bulk} , V_{pore} , and V_{mat} are the bulk, pore, and matrix volumes of the core sample, respectively.

Table 4. 5. Parameters of the core

Parameter of the core					
Diameter	Length	Dry weight	Bulk volume		
3.80 cm	7.70 cm	185.40 gm	87.362 ml		
Matrix Volume	Pore volume	Porosity	Gran density		
71.299 ml	16.062 ml	18.39 %	2.60 g/ml		

4.3.13 Core Flooding Analysis

The surfactant and polymer activities cannot be seen as two distinct processes occurring concurrently in the reservoir. The synergy of both chemicals influences the recovery factor. So far, the movement of one of these chemicals affects the other to varying degrees and vice versa. Several researchers have shown this compatibility in computational models and experimental studies [5], [153]–[156]. The polymer serves as a "sacrificial agent" to avoid utmost adsorption or promote conformity if injected before the surfactant.

On the other hand, if the injection approach is reversed, the surfactant slug is spared from the water-fingering phenomena. Both chemicals may not be infused simultaneously, but dispersion and diffusion processes will lead them to interact during the sweeping process; therefore, this interplay must always be considered in porous media [157]. Core flooding experiments were carried out,

as well as oil recovery tests. The efficacy of PAM + SDS + mMWCNT for CEOR was evaluated and compared with SDS and water flooding by implementing three flooding tests. Figure 4.15 illustrates the percentage of ultimate oil recovery and pressure drop with the injected fluid volume, which includes water, SDS solution, and PAM + SDS + mMWCNT nanofluid. In the flooding test, consistent values were used for specific parameters, such as the amount of fluid injected and the rate at which it flowed. The same volume of fluid, equivalent to ~2 pore volumes (PV), was infused into the core for all flooding processes. According to Figure 4.15, the water flooding process resulted in the most significant amount of oil recovery when 1.3 pore volumes (PV) of fluid were infused into the core. However, there was no further improvement in oil recovery beyond ~34% of the original oil in place (OOIP) after this amount of fluid injection. Subsequently, the core was flooded with a solution containing 2500 ppm SDS and PAM + mMWCNT nanofluids with an optimal concentration. The outcomes of these procedures are displayed in Figure 4.15. Comparing the results of different flooding tests, it was found that using mMWCNT nanotubes in SDS + polymer solution led to higher recovery of oil compared to other methods. More specifically, when utilizing the SDS solution without mMWCNT, only 46% of the oil was recovered, but the addition of mMWCNT in the SDS + polymer solution caused almost 70% of the oil to be recovered. The reason for the superior performance of the PAM + SDS + mMWCNT nanofluid is that nanoparticles can significantly limit the loss of surfactants onto the rock formation. Additionally, the friction generated through the nanoparticles on the adsorbent removes the adsorbed molecules

from the surface of the rock, which ultimately decreases the adsorption of surfactants [15]. In addition, NPs increase the effectiveness of reducing IFT, which significantly improves the efficiency of chemical flooding. In Figure 4. 15, the graph illustrates the variation in pressure drop throughout the injection process. Water injection increases the pressure, reaching a peak at approximately 1.4 to 1.5 pore volumes (PV) of injection. Subsequently, the pressure drop starts to decline, indicating the occurrence of brine breakthrough in the core sample. The high breakthrough PVs suggest the displacement procedure is stable [158]. When emulsion droplets are much smaller than the pore-throat width, there is a negligible increase in pressure drop. However, as surfactant flooding continues, some emulsion droplets adhere to the pore-throat walls, reducing the effective width.

Consequently, the emulsion droplets become blocked, causing them to merge into larger droplets and resulting in a higher pressure drop. Nevertheless, the larger droplet size also means a decrease in the total number of droplets since the overall oil content in the core system remains constant. As a result, pressure drop decreases after reaching its peak value, occurring once the emulsion droplet size surpasses a specific diameter [155], [158], [159].

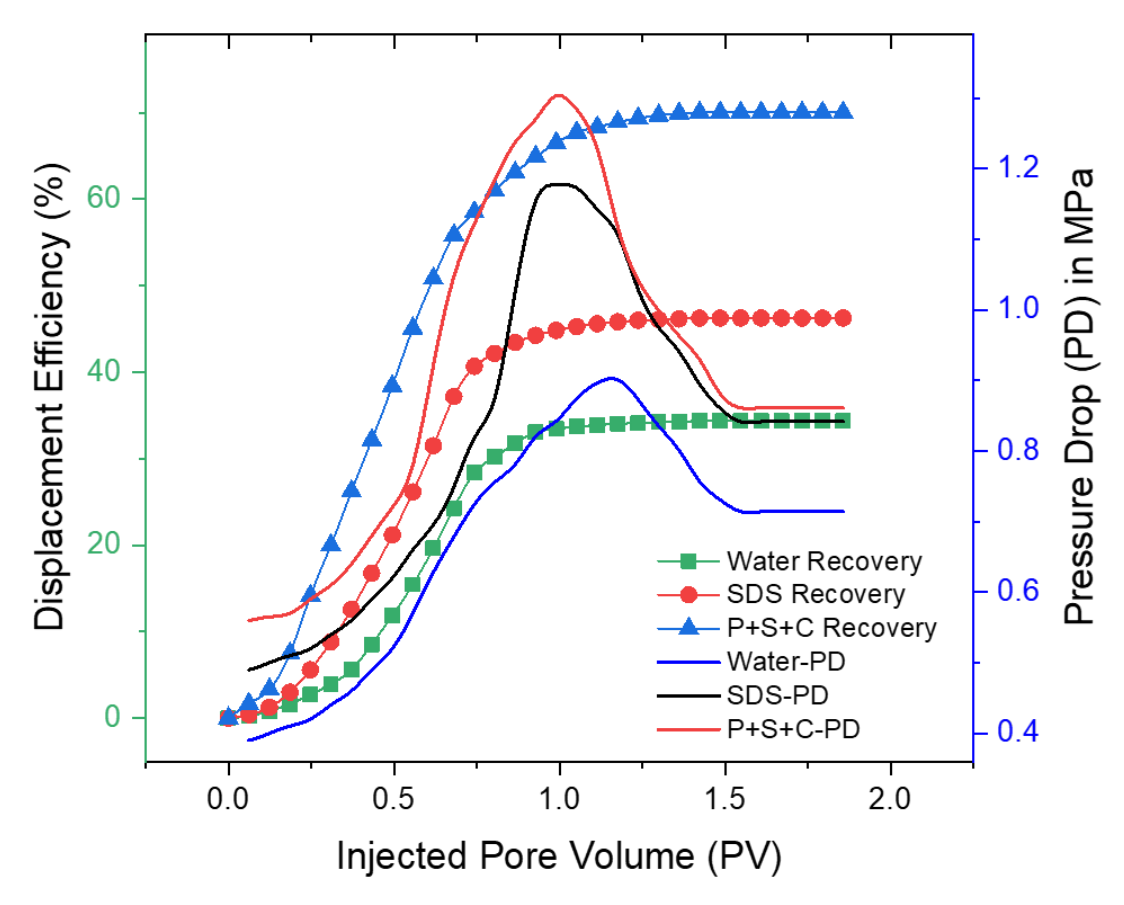


Figure 4. 15: Displacement efficiency and pressure drop of water, SDS and PAM+SDS+ mMWCNT (P+S+C), where P stands for polymer, S for SDS and C for mMWCNT.

4.4. Conclusion

This study aimed to explore the effectiveness of mMWCNT in enhancing the efficiency of surfactants. Before conducting flooding experiments, the study examined how mMWCNT affects surfactant properties such as Surface tension (ST) /interfacial tension (IFT) and adsorption behavior on sand grains. The findings show that the inclusion of mMWCNT in a solution of SDS (sodium dodecyl sulfate) causes an abrupt decline in the IFT between the prepared solution and oil. The mMWCNT minimizes the IFT up to 56% at 100 ppm concentration. The mMWCNT also reduces surfactant loss, which was assessed through adsorption experiments, and alters the wetness characteristics of the rock surface from oil wet to water wet, which helps achieve better

recovery. The improved oil recovery tests were done using core flooding experiments that recovered ~ 70% cumulative oil via surfactant polymer flooding using mMWCNT particles.

Waste Plastic Derived Reduced Graphene Oxide as A Potential

Additive for the Surfactant Polymer Flooding: A Sustainable

Solution

Abstract

The twenty-first century's major problems are the demand for sustainable green energy and the eco-friendly upcycling of plastic waste. The solutions to these problems should have an alluring, cost-effective industrial synergy. Tackling these issues addresses the concerns of clean energy generation and the long-term preservation of the economy and environment from plastic waste. This study focuses on upcycling waste plastics into reduced graphene oxide (RGO) and their application in enhanced oil recovery. Raman and TEM analysis confirmed the successful synthesis of RGOs. In addition, FTIR helps study the presence of functional groups and TGA for thermal stability analysis.

The RGO improves the oil recovery by altering wettability, reducing surface tension / interfacial tension, and minimizing surfactant loss. The surface / interfacial property and wetting attributes of the RGO-based prepared solution were examined by surface tension and contact angle measurement. The surface tension and contact angle reduction using RGO were ~25% and ~20% without surfactant. Whereas with surfactant (anionic, cationic, and nonionic) and RGO, the reduction in surface tension

was ~55%, ~57%, and ~57%, respectively. Also, the reduction in contact angle with surfactant was ~83%, ~46%, and ~80% for anionic, cationic, and nonionic surfactant with RGO particles. The chemical slug's viscosity was then examined at elevated temperatures. The viscosity results follow the power law model to comprehend fluid flow behavior. Finally, the chemical slug consisting of a surfactant mixture, RGO particles, and an industrial-grade polymer was used in the sand pack flooding studies, recovering ~71% of the original oil in place.

5.1. Introduction

Worldwide hydrocarbon production from functional reservoirs is on the decline. The increasing reservoir energy depletion restricts the oil recovery to around 50% of the original oil in place (OOIP) [158], [160]. The oil majors are doing their best to maximize the recovery of OOIP by utilizing different enhanced oil recovery (EOR) techniques [161]. Thus, EOR techniques help recover the non-producible oil from the reservoirs. The EOR techniques include gas injection, chemical flooding, surfactant flooding, low-salinity water injection, thermal methods, and many more [162]. EOR involves various mechanisms, including interfacial tension (IFT) reduction, wettability alteration, mobility control, and gravity drainage [161]–[165]. These mechanisms govern oil mobilization using chemical, thermal, and gas injection methods for oil recovery. The chemical flooding process, categorized under the EOR technique, requires the addition of one or more chemicals to an injecting fluid to reduce IFT (interfacial tension)/ surface tension (ST) or amplify the volumetric sweep efficiency of the injecting fluids. Surfactant, polymer, and their individual and combined injections help extract oil from a reservoir via chemical processes. Surfactant flooding, a chemical flooding process, decreases the IFT/Surface tension and alters the wetness

to increase oil recovery. Surfactants weaken the surface or interfacial forces when it adsorbs on the surface. Surfactants have a hydrophobic hydrocarbon chain or nonpolar group (tail) and a polar hydrophilic group (head). This structure makes them readily soluble in water and organic solvents [133]. Significant challenges associated with surfactant flooding include surfactant loss due to absorption, which reduces efficacy. The development of novel approaches to improve oil recovery is expanding along with the demand for oil production in the global energy market.

Nanoparticles (NPs) are the most effective and widely utilized chemicals for extracting residual oil from reservoirs [148], [166]–[168]. However, the chemicals are expensive and can lead to possible formation damages and chemical loss during the chemical injection [11]. For example, during the gas injection process, injection gas often instantly invades reservoirs from injection to producing wells because of the high mobility ratio of injected gas and oil, leaving a large amount of oil untouched [125]. Thus, techno economically viable and environment-friendly traditional EOR techniques are desirable. Pore plugging is one of the most challenging problems to solve throughout the chemical injection process [11], [125]. Also, trapping injected chemicals in porous media increases the skin factor (reduction in formation permeability), resulting in lower oil recovery and increasing the injection cost [149]. Nanoparticles with an average particle size smaller than the pore throat radius can be employed to reduce formation permeability, aiding oil recovery. The nanoparticles also improve well drilling by modifying fluid characteristics and boosting trapped oil mobility [162], [167]. NPs have piqued attention in the application of thermal and chemical EOR. As additives or nanofluid flooding processes, NPs have the potential to augment traditional recovery techniques [149], [169]. Nanoparticles are also beneficial in EOR applications. The wetting behavior of the rock surface changes by NPs addition to the injected fluid [170]. Micro and nanospheres lower the capillary force and relative permeability of injection fluid. These alterations change the fluid injection path, helping to recover the immobile oil [171]. In the last decade, several researchers have studied the impact of nanoparticles on EOR processes [65], [162], [168]. In addition to NPs, some researchers are investigating the effect of the surfactant on oil recovery in harsh reservoir conditions. NPs have unique properties with sizes ranging from 1–100 nm. Due to the smaller particle sizes, NPs have a higher surface-to-volume ratio. NPs influence drilling operations, production evolution, limiting formation damage, improving oil recovery, and improving heat transfer [162]. They have been investigated from various perspectives to tackle the current issues regarding pore plugging and formation damage in the oil and gas industry [172].

Another critical parameter in the EOR process is the mobility ratio (MR), which should always be kept to a minimum to enhance the recovery process. Injected fluids such as water, CO₂, and chemicals have a lower viscosity than oil. Hence, the MR of the displacing phase is high. An elevated MR causes viscous fingering, poor conformance, and poor sweep efficiency. The MR reduces by lowering the oil phase viscosity or increasing the injected fluid viscosity. To overcome the abovementioned issues, NPs can be added to conventional fluids to enhance the effective viscosity of injection fluids, which can help alleviate the problems [95], [120], [149], [173]. Many researchers have used nanoparticles in their studies and stated that introducing NPs lowers IFT and surface tension while altering wettability. Surfactant adsorption on the sand surface decreases by adding nanoparticles [15], [57], [68]. Many studies have demonstrated wettability changes with nanoparticles from oil-wet to highly water-wet

by injecting nanofluids. The contact angle experiments on even surfaces by injecting nanofluids validate the above claims [148]. Anderson (1986) defined wettability as "the ability of a liquid to spread or hold fast to the rock surface within sight of another immiscible liquid" [174]. Several factors influence reservoir rock's original wettability, including oil composition, temperature, mineral surface, pH, brine chemistry, initial water saturation, and pressure. Several researchers stated that crude oil composition is critical in controlling the rock surface's wettability alteration [175]. The crude oil polar component adsorbs on the rock's surface, causing wettability reduction. These surface-active agents have functional groups containing oxygen, nitrogen, and sulfur.

Moreover, acid and base were the most active compounds of components with charged groups [176]. At pH below 9.5, the negatively charged acidic compounds get adsorbed on the positively charged carbonate rocks due to electrostatic attraction. Many researchers believed that wettability modification towards oil wet increased due to an increment in crude oil acidic components [177], and some literature reviews mentioned this in Table 5.1.

In this paper, reduced graphene oxide synthesized using waste plastic as a precursor (carbon source) has aided the EOR process. Graphene (2-dimensional, one atom thick single layer of sp2 hybridized carbon atoms) and its derivatives like graphene oxide and reduced graphene oxide, have wonderful electrical, mechanical, and thermal properties. Graphene oxide (GO) is produced by the oxidation of graphene, containing abundant oxygen-functional carbonyl, epoxide, hydroxyl and carboxyl groups. At the same time, thermal or chemical reduction leads to the formation of RGO.

The presence of these oxygenated functional groups is less in RGO. RGO has sheetlike structure and high surface area, providing more interacting sites for the reactions.

Table 5. 1. Review of different literature outcomes demonstrating NP (with/without surfactant) effect on wettability modification, IFT reduction, and EOR.

Base Fluids	Oil Type	Surface Type	Affected Properties	Studied the effect of NPs	Measurement Technique	Ref
SiO ₂ /brine	Light Oil	Sandstone	Wettability Alteration	NP size	Amott Test, Contact angle measurement	[146]
ZrO ₂ + Surfactants/ distilled water	Heavy Oil	Carbonate	Wettability Alteration	Type of non ionic surfactants, Effect of time	Amott Test, Contact angle measurement	[178]
SiO ₂ /brine	Light Oil	Glass	Wettability Alteration	NPs concentration	Contact angle measurement	[179]
PAM 1000 ppm	Medium Oil	Sandstone	IFT Reduction and Wettability Alteration	NPs concentration & SDS concentration	Contact angle method & Pendant drop technique	[131]
HPAM 3150 ppm	Heavy Oil	Sandstone	Mobility Control	NPs & surfactant concentration	Viscosity measurement	[25]
SiO ₂ - biomaterial/water	Heavy Oil	Shale	Wettability Alteration	NPs concentration	Contact angle measurement	[180]

The synthesized nanosheets (graphene) exhibit more surface area than conventional metal oxide nanoparticles, providing higher surface activity for the nanosheets. Usually, other synthesis methods for graphene nanosheets are complex and involve using toxic chemicals. However, this study involves the use of waste plastic material as the sole raw material for the synthesis of reduced graphene oxide. Waste plastic is a universal problem affecting our environment and human health indices worldwide and has harmful consequences on the ecosystem [181]–[183]. The astounding expansion of the global economy and productivity are the leading causes of solid plastic waste overproduction. The growth of the human population is directly proportional to the demand for plastic production. Out of the various plastic waste, single-use plastic covers a significant portion of the plastic waste. These factors raised

the requirement for waste plastic management. Converting solid waste into precious carbon-based nanomaterials (CNMs), like CNT, graphene, and carbon quantum dots (CQDs), is a moral option to improve solid waste management [184]–[187].

5.2. Methodology

5.2.1 Materials

Cationic surfactants Cetyl trimethyl ammonium bromide (CTAB) [(C₁₆H₃₃) N(CH₃)₃ Br] of analytical grade purity > 99% were acquired from Molychem Chemicals. In liquid form, nonionic Surfactant Triton X-100 (extra pure for scintillation), $C_{14}H_{22}O(C_2H_4O)_n$ ethanol. Sodium dodecyl ſ sulfate, [CH₃(CH₂)₁₁OSO₃Na] also known as SDS, having a purity >94%, was obtained from Rankem Chemicals. Sodium hydroxide (NaOH) and hydrochloric acid (HCl) have been utilized to study the variation in pH obtained from SD Fine-Chem limited and Merck Life Science Private Limited, respectively. Deionized (DI) water was used for sample preparation and cleaning purposes, having a resistivity value of 18.2 M Ω -m. Reduced graphene oxide used in this study was synthesized in the lab, and the synthesis part has been reported in our earlier work [181]. Experimental methodology of this chapter shown in Figure 5.1.

5.2.2 Synthesis of graphene oxide from waste plastic

Reduced graphene nanosheets (RGO) were produced according to our previously reported method [181]. The waste plastics were purchased from the flea markets and the local municipalities. The gathered waste plastic was chopped in the cutting chamber and washed in the washing unit to remove the dirt and other impurities. Further, this material was dried in a drying unit and placed in a mixing chamber where bentonite nano clay was added as a degradation agent. In this chamber, the waste plastic

and nano clay are mixed. A stainless-steel pyrolysis chamber with a horizontal hollow cylindrical shape was then used to contain this mixture. Slow pyrolysis with a heating rate of 5 °C/min was done in an inert nitrogen gas environment at 400°C. The slow pyrolysis at this temperature resulted in the nucleation of an amorphous, porous, and lustrous black charred residue. The amorphous black charred residue is obtained in the initial stage and added to the ball mill unit to get the ultrafine powder to boost its productivity. This powder was placed inside the secondary vertical cylindrical reactor at 750 °C with a heating rate of 10 °C/min in an inert nitrogen gas environment. The final black-coloured RGO obtained in the second reactor was cleaned with 5% HCl and distilled water, improving the graphene oxide's purity.

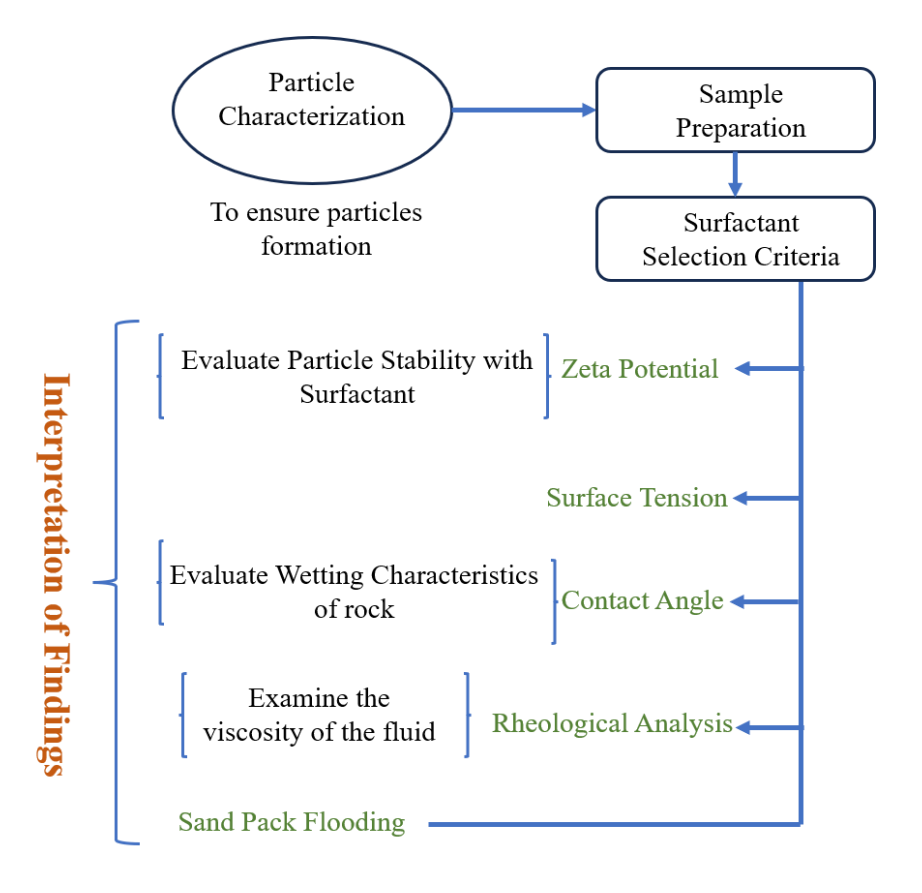


Figure 5. 1: Experimental methodology

5.2.3 Dynamic Light Scattering (DLS)

Dynamic light scattering is the technique to measure the precise value of the particle size and zeta potential in the suspension and emulsions. It depends on the Brownian movement of the particles, which states that the smaller particles tend to move faster, while the bigger ones move slowly in the liquids [188]. The light beam from the suspended particles contains diffusion speed and size distribution information. DLS analysis has a particle size range from 0.3 to 10000 nm, and this technique is best suited for the analysis and characterization of the nanoparticles dispersed in a solution. DLS experiments aim to study various surfactants like anionic, cationic, and nonionic with and without RGO dispersed in DI water by the Malvern Zetasizer of model Nano-ZS instruments. The cuvette was washed twice with methanol to eliminate any contaminants, and the instrument's equilibrium duration of 120 seconds was adjusted to stabilize the temperature for the experiment. The Stokes-Einstein relation, shown in equation 5.1, computes the particle size [68].

$$D_c = \frac{kT}{3\pi\eta d} \tag{5.1}$$

Dc is the diffusion coefficients, T is the temperature, k is the Boltzmann constant, viscosity, and d is the hydrodynamic diameter.

5.2.4 Surface tension measurement

Surface tension (ST) is the distinctive property of the fluid to oppose the external forces acting at the liquid surface [49], [136]. The tensiometer model KYOWA DY-500 measures the ST of the different samples using the Du-Nouy ring system. The ST of different surfactants was measured before and after adding RGO nanosheets (100-1000 ppm). The mixture was sonicated before ST measurement using a probe

sonicator for better dispersion. In the supporting information of methodology section 1.1, the experimental technique of the surface tension must be covered in more detail in Figure 5.2.

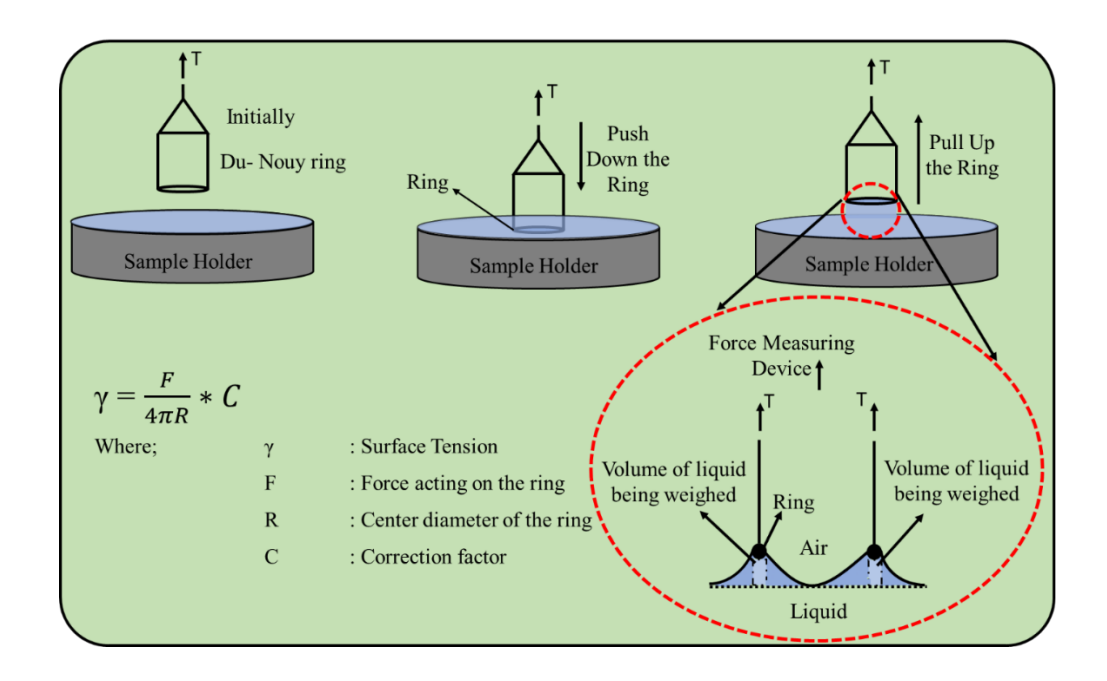


Figure 5. 2: The Surface tension measurement with the help of Du-Nouy ring.

5.2.5 Contact Angle Experiments

The contact angle (CA) test characterizes the wettability modification. The experiments were conducted using an Acam-NSC series goniometer provided by Apex Instruments, India Figure 5.3. The equipment is composed of a flat stage with a light source at the back, a needle or a pipette to dispense the solution, and a recording device to obtain the image of the drops. The sessile drop technique determines the contact angle. The range of the contact angle of the instruments is from 0° to 180° with an accuracy of $\pm 0.05^{\circ}$. The surfactant samples were prepared at CMC using deionized water with the subsequent addition of RGO nanosheets. After every measurement, the syringe attached to the equipment was cleaned with deionized water. The experiments were repeated thrice to ensure their repeatability.

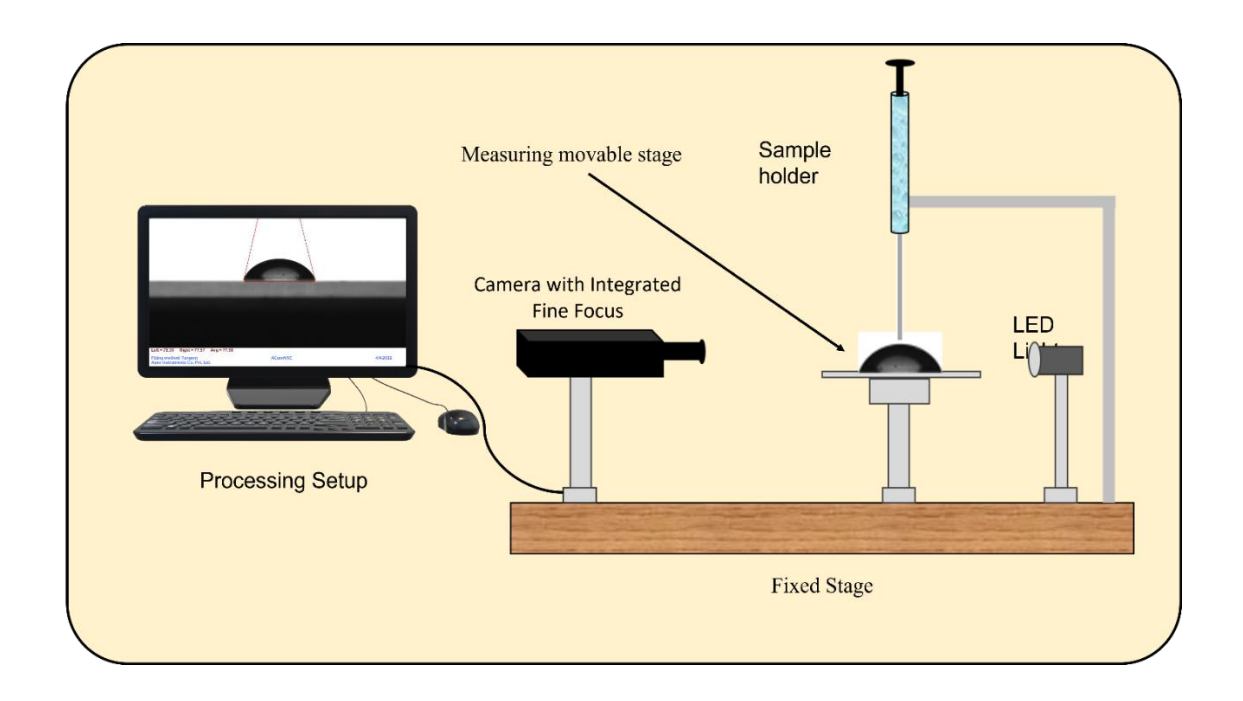


Figure 5. 3: Measurement setup of the goniometer instruments.

5.2.6 Viscosity Measurement

Rheology analysis studies a sample's flow behavior and deformation considering the shear rate and temperatures under the applied force [48]. Viscosity was measured with the help of Anton Par's modular compact rheometer (MCR-52). The rheological properties of the slug, which had different concentrations of polymer and nanoparticles, were found utilizing the rheometer's bob and cup assemblage system. After each measurement, the instrument components were washed and dried using DI water and the dryer. The slug was prepared using a 1000 ppm polymer and differing concentrations of RGO ranging from 100 to 1000 ppm. The rheological studies were performed on the prepared chemical slug at ambient and elevated temperatures to study the slug's degradation.

5.2.7 Flooding Experiments

Flooding tests were conducted using a sand pack flooding assembly. D-CAM Engineers, Ahmedabad, manufactured the sand pack flooding equipment to study the

displacement test. The instrument contains a sand pack holder and four accumulator cells holding the chemicals, crude oil, water, and toluene for flooding experiments. Previously, many researchers had used a similar setup for sand pack flooding [53], [189]. The chemical slug included a combination of 1000 ppm of polymer. Different concentrations of RGO nanosheets from 100, 250, 500, and 1000 ppm and anionic surfactant at CMC values were used during the experiments. After water flooding, half the pore volume of the ASP slug was injected into the porous media through the flow lines at the same flow rate of 2 ml/min. Additionally, chase water was infused through the flow lines into the porous media till no oil drop eluded from the sand pack. The sand pack flooding experiments were performed at 60 °C temperature, and the flooding setup is shown in Figure 2.3.

5.3. Results and Discussion

5.3.1 Characterization of RGO

Raman spectroscopy determines the number, layer orientation, defects, and material quality, as represented in Figure 5.4. The C-C bond stretching gives the E2g vibrational mode, providing the graphite peak (G Band). The A1g vibrational mode provides the disorder peak (D-band). The Raman spectra of the synthesized graphene show the D band at 1360 cm⁻¹ and the G bands at 1577.8 cm⁻¹. Also, the 2D peak shows few layers in the material. The intensity ratio of the D and G bands, i.e. (ID/IG ratio) estimates the structural defects of graphene-based samples. The higher ratio ensures more defects in graphene-based materials. SP²-bonded carbon atoms in-plane vibration generates the G Band. However, the out-of-plane vibration generates the D Band, responsible for structural defects. Scanning electron microscopy (SEM) and transition electron microscopy (TEM) evaluate the morphology of plastic-derived RGO. SEM

and TEM images illustrate the sheet-like morphology of the RGO, shown in Figure 5.5. Fourier transformation infrared spectroscopy (FT-IR) helps identify the functional group's presence on RGO, which is represented in Figure 5.6 (a). FT-IR Spectra showed peaks at 1029 cm⁻¹, 1421 cm⁻¹, 1560 cm⁻¹, 3294 cm⁻¹, 2916 cm⁻¹, 2092 cm⁻¹, 2304 cm⁻¹ corresponding to carbon-oxygen, C-O stretching vibration, carbon-carbon double bond, hydroxyl group respectively [190], [191]. The peak at 1575 cm⁻¹ shows that the carbon-carbon double bond (aromatic) supports the graphene structure. The carbon-oxygen exhibits partial oxidation of the graphene nanosheets during the purification process. Further Thermogravimetric analysis (TGA) evaluates the groups containing oxygen and the graphitic nature of RGO, as shown in Figure 5.6 (b). The first stage of weight loss in the temperature range of 50°C to 100°C was due to moisture and chemically adsorbed water on RGO [181], [182], [185]. In the second stage, significant weight loss in the temperature range between 400°C and 580°C results from removing oxygen-associated functional groups in the RGO.

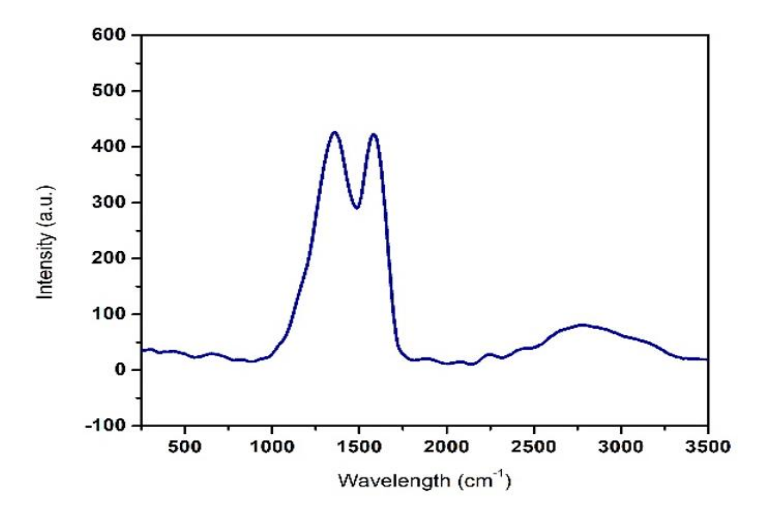


Figure 5. 4: Characterization of RGO using Raman spectroscopy.

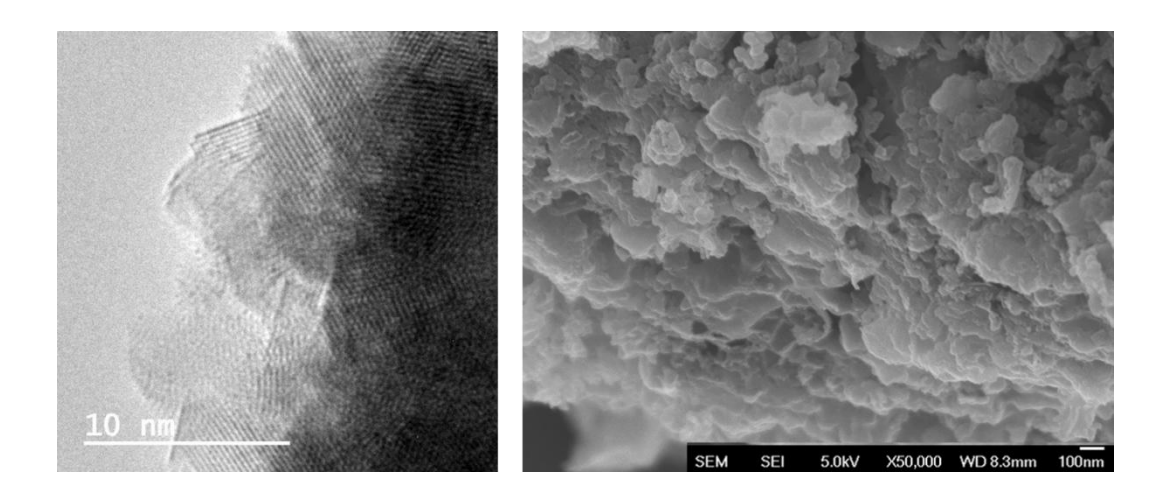


Figure 5. 5: TEM and SEM analysis of the reduced graphene oxide.

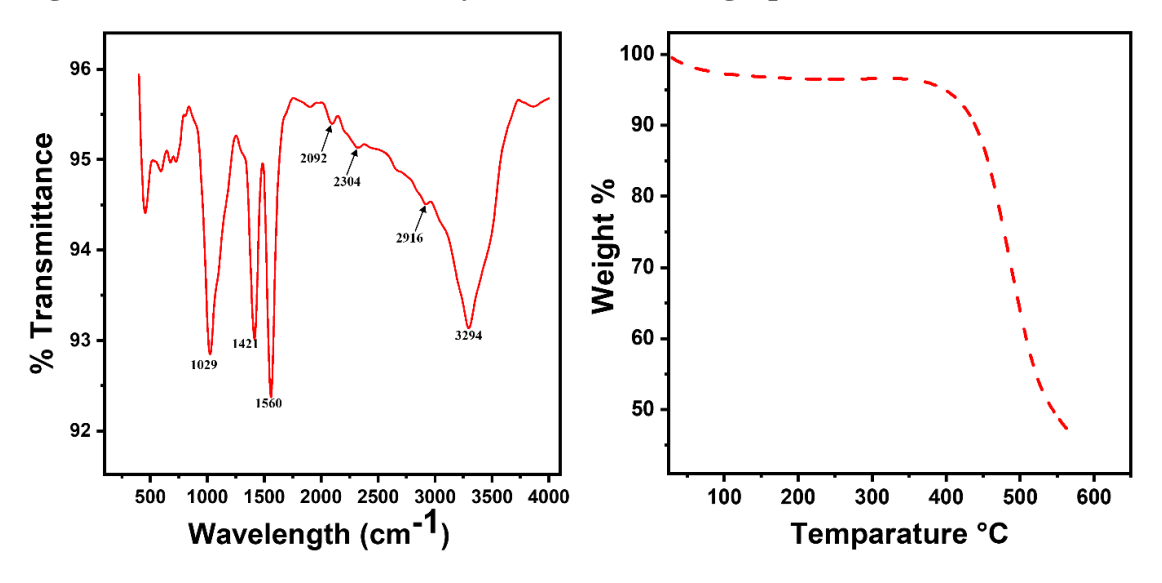


Figure 5. 6: (a) FTIR analysis of reduced graphene oxide, (b) TGA analysis of reduced graphene oxide.

5.3.2 Particle size and Zeta potential

The nanoscale range particles are chemical slug additives that change the surface's wettability and aid oil production. The RGO exhibit an average particle size of 295 nm in deionized water. The smaller-size NPs easily penetrated the pore throat of the rock. The NPs get adsorbed onto the water-oil interface, reducing the IFT of the fluids. This effect helps in improving the oil recovery from the formation.

Further, this study examines the particle size of the nano-assisted surfactant solution.

According to Figure 5.7, the RGO particle size approaches 390 nm in nonionic surfactant, 375 nm in cationic surfactant, and 380 nm in anionic surfactant. Due to their small sizes, NPs agglomerate and block the path of least resistance. This obstruction allows the slug to move through the oil-filled pores by altering its wetting behavior and sweeping out the trapped oil via a disjoining pressure mechanism [7], [62], [192]. The ζ -potentials of the RGO on adding anionic, cationic, and nonionic surfactants were also measured, as shown below in Figure 5.7. The ζ -potential of RGO dispersed in DI water ensured the stability of the nanofluids [67]. The ζ -potential of the RGO was -24 mV, indicating the electrophoretic stability of RGO [67], [96].

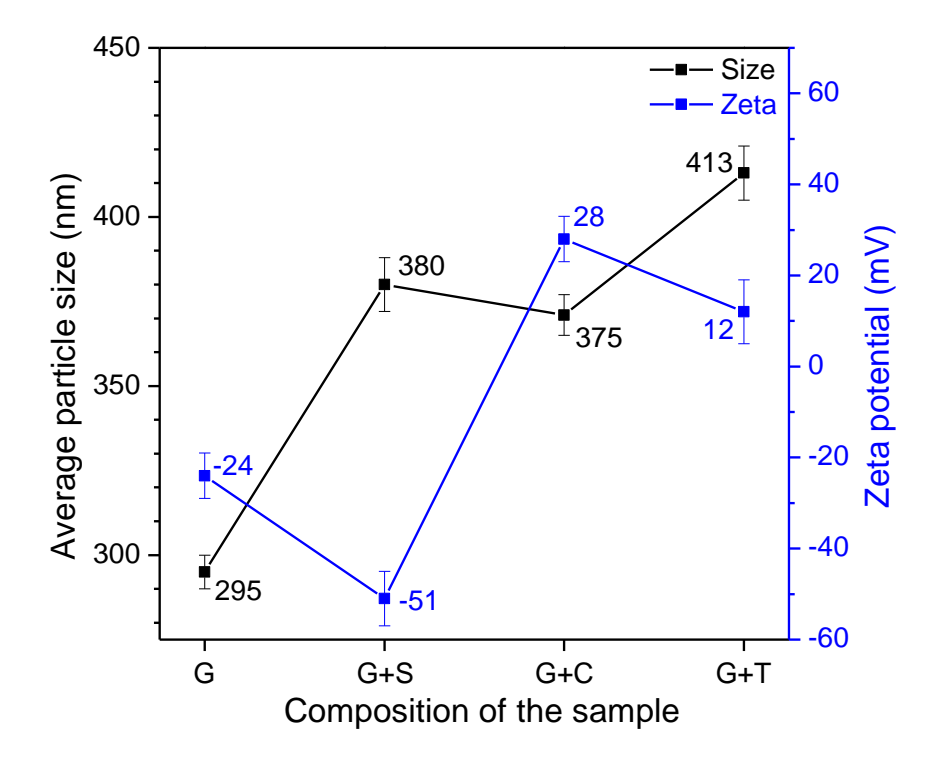


Figure 5. 7: Particle size and zeta potential of the RGO.

5.3.3 Surface Tension

The ST significantly influences residual oil mobilization. Surfactants get attached to form micelles into the solutions up to their critical micelle concentration (CMC) [119]. Beyond CMC, the surface tension remains constant irrespective of the

increase in concentration. The adsorption of surfactants at the liquid-air interface produces the balancing force at the interface, causing lower surface tension [45–48]. Initially, the tensiometer measured the ST of DI water to be 71.2–71.5 mN/m at ambient conditions. The surfactant introduction into the DI water resulted in a sudden reduction in the ST. The surface tension of the DI water decreased when a surfactant solution containing nanoparticles was added. This is because an electrostatic repulsive force between the nanoparticles would be reduced by an ionic surfactant's adsorption on the nanoparticles' surface [193]. Now, a higher number of surfactants and nanoparticles would be adsorbed at the liquid-gas interface, and therefore, a lower surface tension value of the nanofluid would be observed [133], [194]. Further, the influence of RGO on the ST for differing concentrations of the nanoparticles (100 ppm, 250 ppm, 500 ppm, and 1000 ppm) in DI water was studied. The addition of RGO to DI water reduces surface tension. The surface tension for DI water was reduced from 61 mN/m at 100 ppm of RGO to 53.5 mN/m at 250 ppm RGO. Further addition of 500 ppm RGO to the deionized water increased the ST values. The sudden increment in ST value is due to an increment in the surface free energy, which increases the kinetic energy of the particles. Thus, the particle is not retained in the stationary phase and will move into the bulk phase through desorption. After introducing 1000 ppm RGO, the surface tension values further increase. The rise in ST with increasing NPs concentration is due to the increasing nanofluids particle size, resulting in a reduction in surface area and surface free energy [9], [63], [125]. Therefore, the above results illustrate that the surface tension reduction was most prominent at 250 ppm RGO. Thus, the optimized concentration of the RGO is up to 250 ppm, and increasing the RGO concentration above 250 ppm was not favored. The study of the surface-acting forces using RGO is shown in Figure 5.8.

5.3.3.1 Impact of Surfactant on the ST

The ST studies of surfactants optimized the surfactant concentration. The ST reduces the addition of surfactants into the DI water. ST values reduce up to CMC of surfactant, beyond which it does not exhibit any appreciable change in its properties [55], [62]. The ST studies helped estimate the CMC of anionic, cationic, and nonionic surfactants. The ST of deionized water was measured initially, and subsequently, surfactants were added to the DI water. The CMC for cationic, anionic, and nonionic surfactants was 300 ppm, 2500 ppm, and 170 ppm, respectively. RGO was added to the emulsion after measuring the surface tension of the surfactant solution. The nanoassisted surfactant solution diminished ST more prominently than the surfactant solution. ST of the surfactant solutions are demonstrated in Figure 5.8. The experimental results suggest that the ST of the nanofluid decreases at lower particle concentrations. The ST increases at higher nanoparticle concentrations. The observed trend is due to modifying the liquid air ST in the presence of NPs. This modification also affects the surface energy of the liquid-air interface [124].

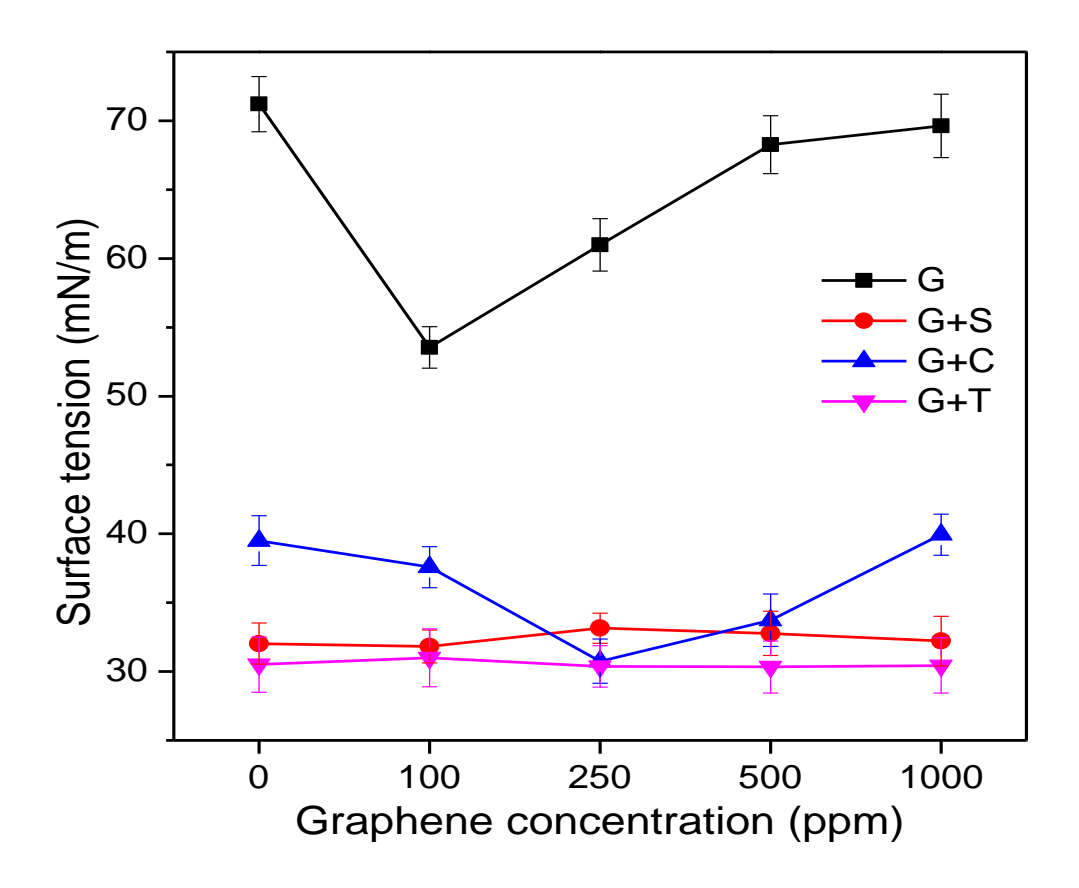


Figure 5. 8: Effect of RGO concentration with surfactant on Surface Tension whereas G is graphene nanosheets, S is SDS, C is CTAB, and T-is Triton X100.

5.3.3.2 Impact of pH on the Surface Tension

The surface-acting force of the prepared solution mainly depends on the surface charge. The pH influences the surface-acting forces of the prepared solution. The rising hydroxyl ion (OH-) increases the pH value, making the solution basic. The increasing hydrogen ions (H+) in a solution reduces the pH, making the solution acidic. ST of the solutions is affected by the imparity in charge of the solutions. Thus, it is essential to investigate the impact of pH on nano-assisted solutions [195]–[197]. The influence of pH on surface tension was studied at the optimized concentration of the RGO. The ST reduced from 54.95 mN/m to 34.41 mN/m as the pH of the nano-assisted solution decreased from 7 to 2 towards acidic at 250 ppm of RGO, illustrated in Figure 5.9. A

similar trend was observed when the pH of the solution rose from 7 to 12.

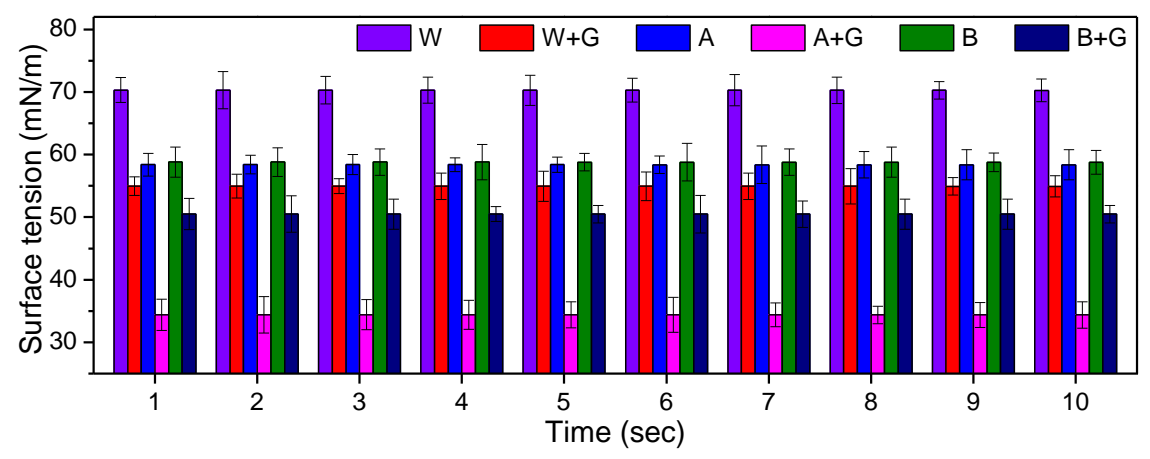


Figure 5. 9: Effect of pH on the ST at optimized RGO concentration (100 ppm), whereas W stands for water, G is RGO, A is acid, and B is base.

5.3.4 Study of the wetting behavior

The contact angle (CA) measurement assessed the surface's wetting behavior, helping to understand surface properties. Rock compositions and their nature, crude oil composition, and mineralogy govern the wetting behavior of the rock surfaces [50], [51]. Wetting behavior plays an essential role in understanding surface properties. The physiochemical mechanisms supporting wettability reduction are the multi-ions exchange, salting, fine migration, electric double-layer expansion, mineral dissolution, and pH fluctuation [144], [174]. Some mechanisms are valid in sandstone and others in carbonate reservoirs [143], [144], [174]. The CA experiments using the sessile drop method were performed at the CMC of the various surfactants. Dynamic contact angles were measured for up to 300 seconds to study the wetting nature of the rock surface. The wetting nature of the rock categorizes them as water-wet (0 –75°), intermediate-wet (75 - 105°), and oil-wet (105 - 180°) [158], [198]. Nanoparticles are promising wettability-altering agents [148]. NP concentration, size, and saltiness influence the modification of wettability. Researchers determined the contact angle of crude oil

alongside nanoparticle solution with differing concentrations of the nanoparticles on silica pellets. They also deduced that increasing the nanoparticle concentration in the solution amplifies the hydrophilic character of rocks [149], [199]. As the size of the nanoparticles decreases, the aqueous phase's contact angle also reduces. The reduction in contact angle is due to a significant amount of nanoparticles in the solution. The nanoparticle's electrostatic repulsion force is inversely proportional to its size [62], [69], [73]. This study uses RGO to perform the contact angle experiments at 100 ppm, 250 ppm, 500 ppm, and 1000 ppm. The variation in the contact angle value of different RGO concentrations is illustrated in Figure 5.10.

5.3.4.1 Impact of Surfactant type on Wetting behavior

The contact angle tests (CA) were carried out at different surfactant concentrations to study the impact of the wetting characteristics of the surface. The CA and surfactant concentrations exhibit an inverse relationship. On the water-wet surface, the CA of the DI water was ~51°, which reduced to ~21° at the CMC of the SDS (anionic) surfactant. In comparison, CA dropped to ~49° at the CMC of the CTAB (cationic) surfactants and up to 25° at the CMC of the nonionic surfactants. The rate of the adsorption process increases with contact duration because adsorption is a time-dependent phenomenon. Thus, the interaction possibilities between the polar part of the surfactants and the nonpolar parts of the crude oil increase with time, diminishing the contact angles with time [126], [147]. NPs get adsorbed onto the surface due to their smaller size and more considerable surface-free energy. The contact angles reduce after increasing NP concentrations, easily explained by disjoining pressure. The NPs form the self-assembled wedge-shaped film touching base using the crude oil phase [4,9,10,51,67]. Increasing the NPs concentration in the solution causes more significant

NP aggregation at the wedge film, leading to an improved disjoining pressure that reduces the contact angle. A comparable shift in the contact angle occurred after adding nanoparticles into the deionized water, suggesting that NPs tend to change the wetting phase of the oil-wet sand pellet. The NPs adsorption onto the rock surfaces leads to the formation of a nanotextured surface, which changes the rock's morphology to semi-homogeneous [79], [148]. Therefore, a thin layer of the NPs is created on the rock surface, leading to a change in the wetting behavior of the surface to strong water-wet from oil-wet and an increment in oil production.

The synergistic effect of varying surfactant concentrations (anionic, cationic, and nonionic) at CMC and distinct NPs concentrations was studied. The CA measurement for various surfactants and RGO concentrations illustrates the favourable result for anionic surfactants and RGO combinations. The contact angle of the anionic surfactant reduced from 21° to 15° after introducing 100 ppm NPs into the anionic surfactant solution. The CA values reduce to 13° after adding 250 ppm RGO into the solution. Increasing the RGO concentration to 500 ppm resulted in a further reduction in CA values up to 10°.

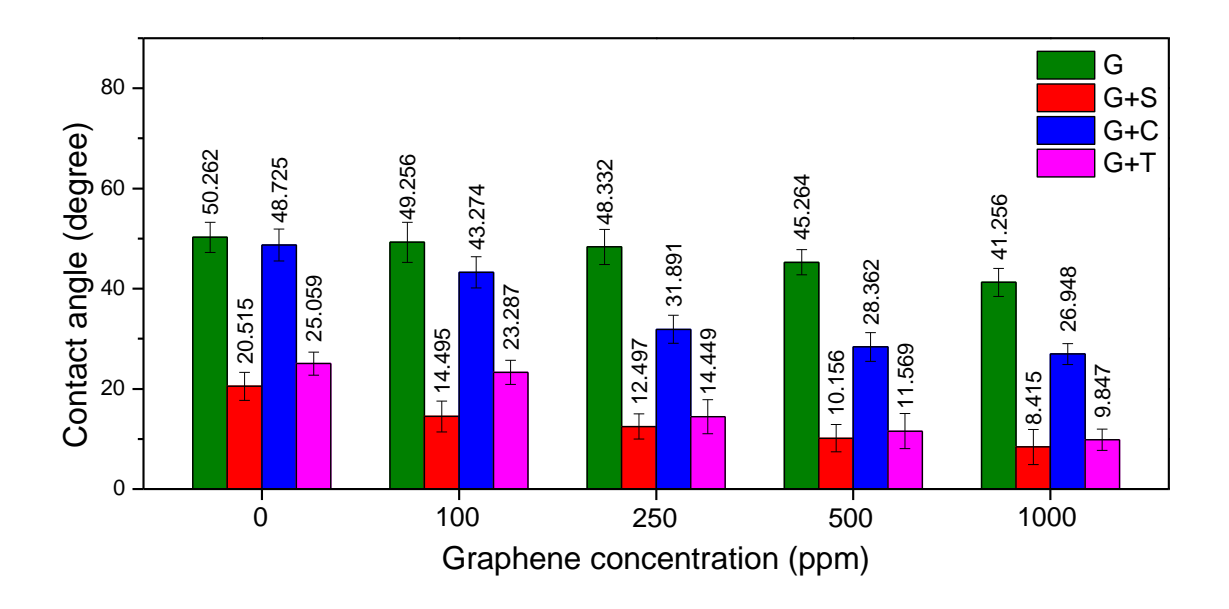


Figure 5. 10: Wetting characteristics of RGO using contact angle measurements, G is reduced graphene oxide nanosheets, S is SDS, C is CTAB, T is Triton X100.

In contrast, the same for 1000 ppm was found to be 8.5°, as shown in Figure 5.10. Similar decreasing trends of the CA occurred for cationic and nonionic surfactants. Roustaei and Bagherzadeh studied the effect of SiO₂ NPs on the wetting characteristics of a carbonate reservoir rock. The findings revealed that SiO₂ NPs act as wetness modifiers in carbonate rocks [145]. Hendraningrat, et al. observed that diffusing Al₂O₃ nanofluids can modify the wetting behavior of the sandstone rock surface from a strongly oil-wet to a strongly water-wet [146]. A similar result of the wetting behavior has been found using RGO particles, which modified the wettability from oil-wet to water-wet. The combination of the RGO and various surfactants changed the wetness of the surface from oil-wet to strong water-wet, favoring better conditions for the movement of the oil from pore spaces.

5.3.4.2 Synergistic effect of RGO concentration and different surfactants on the dynamic contact angle of the mixture

Dynamic CA measurements determined the contact angle while spreading the

drop over time. Water drops were placed on sand surfaces, and the drop shape was monitored with time to determine the contact angle of the prepared solution with time. The loss of chemicals onto the sand surfaces modified the drop's shape and size, reducing wettability with increasing time [200]. The reduction in contact angle confirms the wetting modification of the oil-soaked sand pellet. The sessile drop techniques performed the contact angle measurement. The technique accurately measures the contact angle from the shape of a water droplet. The contact angle experiments were conducted for 300 sec to observe the wetting behavior with time dependency shown in Figure 5.11. The time-dependent CA experiments were performed for various surfactants with or without differing RGO concentrations.

5.3.4.3 Impact of pH on wetting behavior

Wettability is one of the imperative studies for formulating any chemical slug to be applicable for residual oil mobilization. Conventionally the CA experiments characterize the wetting nature of a surface. The contact angle formed on a solid surface by a liquid drop (sessile drop method) was used in this study. The angle thus formed on the surface is highly dependent on the net charge of the system. The presence of minerals on the solid surface or the ionic concentration of the liquid solution governs the system's charge [201]. In this study, the effect of hydronium and hydroxyl ion was explored for the same graphene concentration (100 ppm) on the water Figure 5.12. The graph illustrates that the contact angle for the deionized water reduced from ~51° to ~12° and ~23°, corresponding to the system of hydronium ions (pH~2) and hydroxyl ion (pH~12), respectively. The significant reduction in the contact angle with increasing ions contributes to strong electrostatic interactions between the solid surface and the liquid phase [202]. The interaction of H+ ions with the negatively charged quartz

surface results in lower contact angles. The lowering of the CA for higher pH results from the interaction between the quartz's silica and the liquid phase's hydroxyl ion [68]. These interactions would lead to the adsorption of the few ions on the solid surface, leading to a lower contact angle.

The addition of RGO to deionized water slightly reduces the contact angle from 51° to 48° due to the hydrophobic nature of the graphene. Reduced graphene nanosheets that are hydrophobic get adhered to the solid surface, leading to slightly lower CA values. Conversely, it is worth mentioning that reduced graphene oxides in the acidic or basic solution led to a significant increase in the contact angle compared to the respective solution without reduced graphene oxides. The contact angle increased to 28° and 45°, corresponding to the acidic and basic solutions. The interaction between the ions and graphene illustrates the change in the contact angle. Without RGOs nanosheets, ions (H+ and OH-) only had a solid surface as available adsorption sites for the interaction. Our hypothesis proposes that this interaction can be slightly hindered by the presence of graphene nanosheets in the liquid phase. This diminishes the interaction between the ions and the quartz surface, providing a relatively higher contact angle.

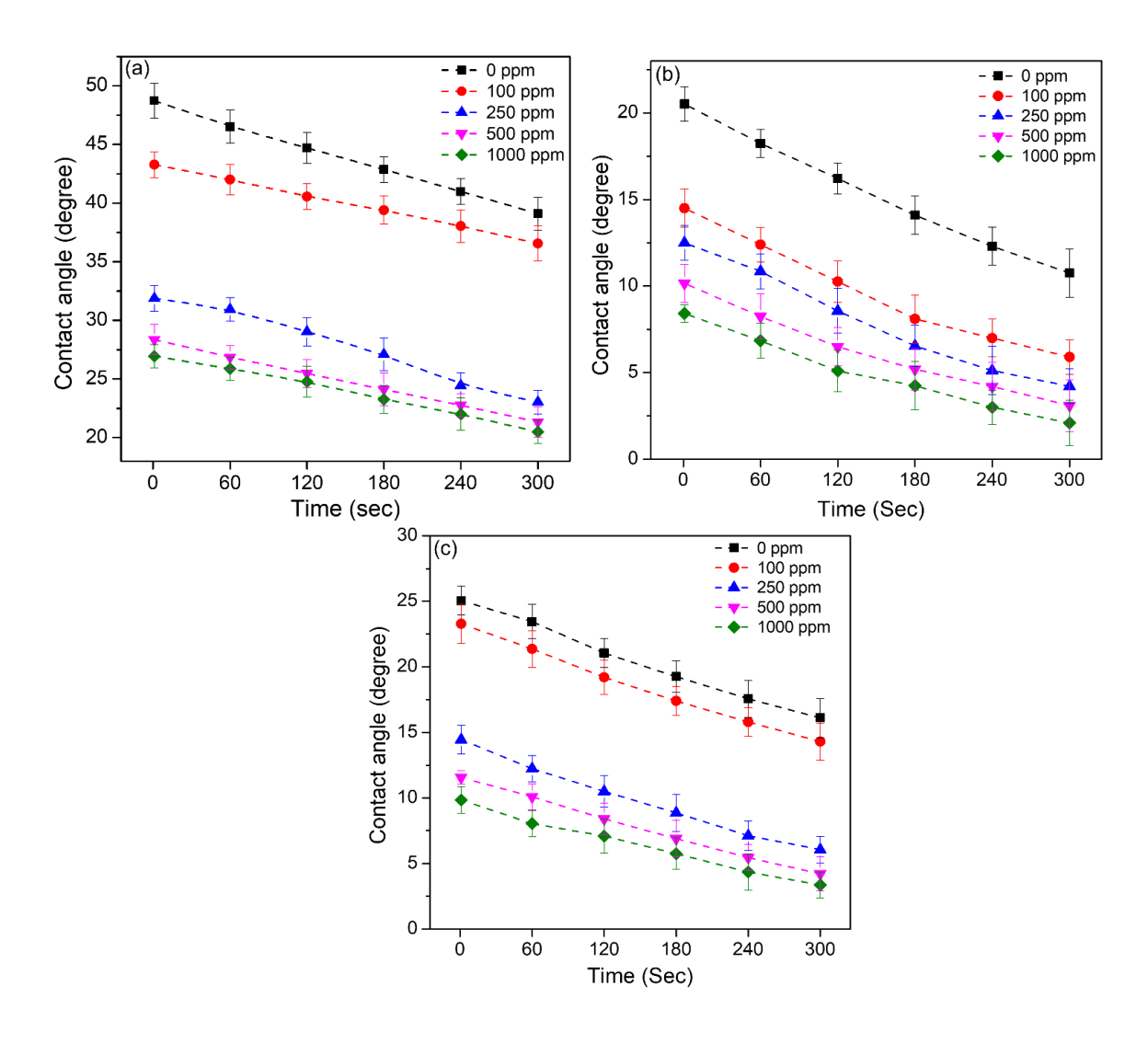


Figure 5. 11: Study of the wetting behavior of varying RGO concentration of (a) Cationic surfactant (CTAB), (b) Anionic surfactant (SDS), and (c) Nonionic surfactant (Triton X-100) versus time.

5.3.5 Rheological analysis

Viscosity measurement is a part of the rheological investigation that validates the study of nanofluid stability. The measurement helps understand the flow behavior of the nanofluids in many aspects of industrial applications [150], [168], [203]. The rheological studies measure the viscosity of the nanofluids at varying shear rates of 1-1000 s⁻¹, shown in Figure 5.13(a). The combination of the NPs and a PAM changes the viscosity of the prepared solution. The viscosity analysis of the prepared solution is affected by the type of NPs, shape, and size of the nanoparticles[53], [117], [118]. Using

a rheometer, we measured the viscosity of a slug with a fixed 1000 ppm of polymer and different RGO concentrations (100 ppm, 250 ppm, 500 ppm, and 1000 ppm) with the shear rate. The measured viscosity of the slug at a shear rate of 10.5 s⁻¹ increased from 50.78 mPa.s to 58.29 mPa.s, 66.54 mPa.s, 80.56 mPa.s, and 95.67 mPa.s after introducing 100 ppm, 250 ppm, 500 ppm, and 1000 ppm of the NPs with the polymer. The increasing viscosity trend of the solution is due to the presence of solid particles in the slug, leading to more friction among long polymeric chains [12], [152], [204]. The NPs increase the viscosity of the injecting fluids, reducing MR and preventing viscous fingering during the flooding process, increasing the displacement efficiency. The decreasing trend of the viscosity with the shear rate up to certain values is explained by the shear-thinning properties of the non-Newtonian fluids. The viscosity of the prepared slug having 250 ppm NPs concentration as well as 1000 ppm polymer was reduced from 49.13 mPa.s to 10.86 mPa.s, 6.03 mPa.s, and 2.09 mPa.s with an increasing shear rate from 16.6 s⁻¹ to 68.2 s⁻¹, 120 s⁻¹, and 993 s⁻¹ respectively.

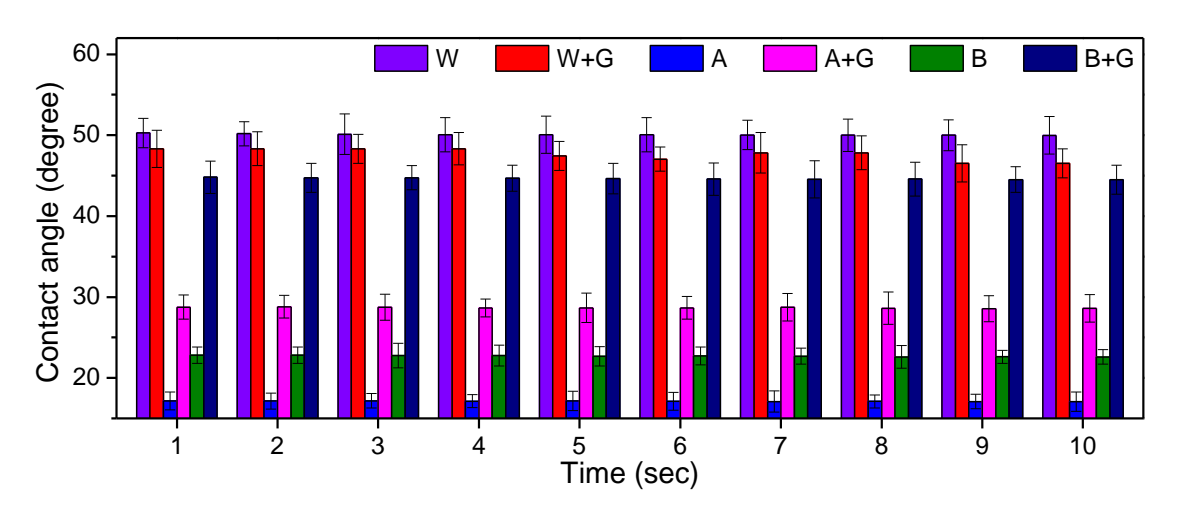


Figure 5. 12: Study of pH on optimized RGO concentration (100 ppm), although legend W stands for water, G is RGO, A is acid, and B stands for the base.

The viscosity reduces because the temperature of the slug rises from 30 °C to 60 °C, as shown in Figure 5.13(b). The decrease in viscosity with increasing temperature is due to the degradation of the polymeric chain. When the temperature increases, the molecules get excited, and the kinetic energy amplifies, leading to bond breakage and reduction in viscosity [53].

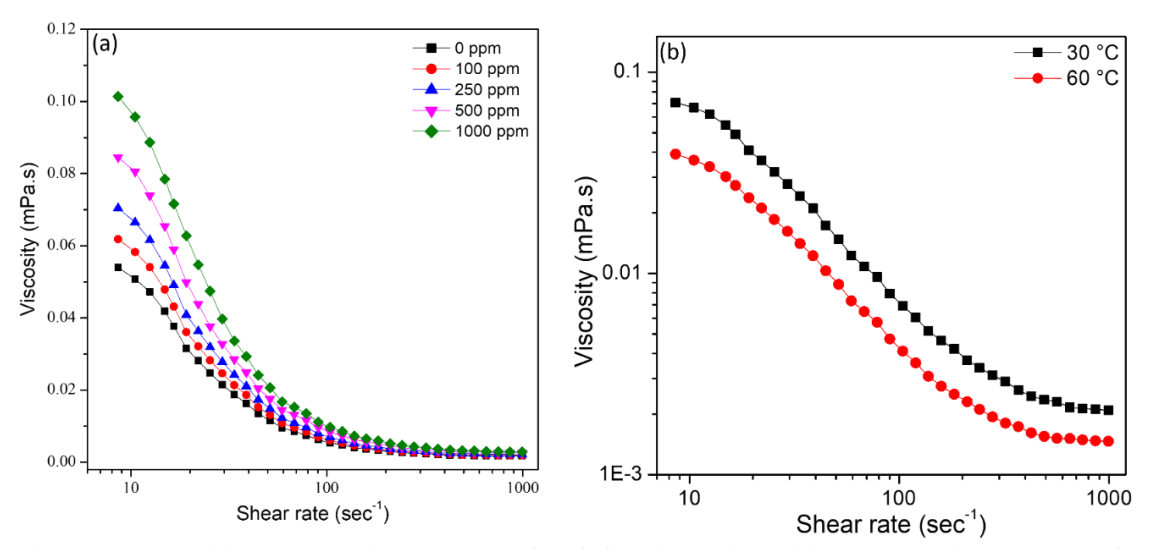


Figure 5. 13: (a). Rheological study of RGO with PAM (b). Rheological study of RGO at elevated temperature.

5.3.6 Flooding Results

4.3.6.1 Pressure Drop Studies

Sand pack flooding experiments help study the oil displacement from the sand pack holder using a polymer slug with RGO. The sand pack was porous and permeable, so the fluids easily flowed from the sand pack without becoming trapped in the medium. The pressure difference between the inlet and outlet of the sand pack during the flooding process reflects the fluid flow inside the accumulator. The pressure difference helps calculate the absolute permeability of the sand pack using Darcy's equation, shown below in Equation 5.2.

$$Q = -\frac{k \cdot A \cdot \Delta p}{\mu \cdot l} \tag{5.2}$$

Or
$$Q = \frac{0.001127kA\Delta p}{\mu \times l}$$
 (5.3)

Where Q is the total discharge (m³/s), k is the permeability (m²), Δp is the differential pressure (Pa), μ is the dynamic viscosity (Pa. s), A is the cross-sectional area (m²), and l is the length of the sample (m). Where Darcy law in FPS unit in Equation 5.3, in which Q is in bbl/day, k is in mD, A in ft², Δp is in psi, μ in cP and, l is in ft.

Initially, the water flooding was initiated with a pressure drop of ~1.27 psi, while the pressure drop reached ~18.3 psi after injecting the slug through the sand pack. Differential pressure during the flooding experiments increases as the viscosity of the injecting fluid rises. The viscous slug is more resistant to flow and maintains a steady flow rate to increase pressure. The pressure drop increased during the chemical slug injection, then progressively decreased upon injecting the chase water into the sand pack. Infusing displacing (highly viscous) fluid into the sand pack triggered a pressure drop, providing more oil recovery. Again, the pressure drop declines and stabilizes at ~2.05 psi due to the viscosity of the injection fluid after chase water injection. The pressure drop versus various pore volumes of the injected fluids is illustrated in Figure 5.14 (a). The pressure drop changes the chemical composition of the slug. The pressure drops increase after increasing the RGO concentrations in the prepared chemical slug. The pressure drops of a 0ppm chemical slug were 18.3 psi, while it was 20.6 psi after raising the RGO concentration to 1000 ppm.

4.3.6.2 Oil Recovery studies

Oil recovery was investigated for water and different RGO concentrations, shown in Figure 5.14 (b). NPs affect surfactant characteristics and increase their

influence on the oil recovery process. The NPs presence at the interfacial layer changes the IFT between the oil and water [11], [17]. At lower NPs concentrations, a considerable IFT reduction occurs. The IFT reduction occurs because the NPs get adsorbed onto the liquid surface. However, increasing NPs concentration removes the surfactant from the bulk aqueous phase, minimizing free surfactants' availability in the aqueous phase [18]. Surfactant adsorption reduces by generating a layer with a charge similar to micelles, which repels SDS micelles and leads them to move forward, decreasing crude oil IFT. Thus, nanoparticle addition reduces surfactant adsorption and increases oil recovery in sandstone media. Also, the rock wetness alters from more oilwet to more water-wet by using NPs with anionic surfactants, ultimately enhancing the oil recovery [44]. Several researchers have examined the rheological properties that also change with using NPs, which increases viscosity and impacts oil recovery from surfactant flooding [17], [18]. NPs additions modify IFT/ST, encourage spontaneous emulsion formation, reduce wetting behavior reduction, and modify flow characteristics, which helps in oil recovery.

The nano-assisted surfactant solution efficiently controls the mobility ratio during the surfactant flooding. The flooding experiments help in optimizing the chemical slug composition. The flooding experiments were performed at optimized surfactant concentration, selected from previous studies [50], [53], [117], [149]. The flooding experiments were conducted at 60°C, and the heating jackets temperated the sand pack holder and the crude oil accumulator. The SDS surfactant and polymer concentration were fixed at 2500 ppm and 1000 ppm during the flooding process, and the RGO concentration in the slug was 100 ppm, 250 ppm, 500 ppm, and 1000 ppm used during the flooding experiments. The oil recovered from the secondary recovery process with

water flooding during the experiment was ~ 34 to 39%. After secondary recovery, the surfactant polymer (SP) chemical slug with RGO was injected into the sand pack to recover the residual oil left behind in the sand pack. Additional oil recovered from the sand pack without RGO concentration in the SP chemical slug was ~64%. The oil recovery increases after adding RGO concentration to the prepared SP slug. When 100, 250, 500, and 1000 ppm RGO particles were added to the 2500 ppm anionic surfactant and 1000 ppm polymer solution, oil recovery increased by 65.93, 67.63, 69.69, and 71%, as shown in Figure 5.14 (b).

4.3.6.3 Water cut studies

The water volume fraction turns out from cumulative fluid represented by water cut. The produced water volume was constantly monitored during the experiment to estimate the water cut. The percentage of water cut versus pore volume (PV) was noted and represented in Figure 5.14 (c). Initially, during the water flooding experiments, a lower % water cut value of 55 % was achieved, indicating the presence of connate water, as represented in Figure 5.14 (c). Furthermore, excessive connate water can dilute the infused polymer mixture. This dilution creates a mobility imbalance between the polymer and oil [117], [149]. The increment in water cut was observed constantly with the pore volume (PV) till the values reached 100%.

The SP slug of 0.5 PV was introduced after 1.5 PV of water flooding, and the reduction in water cut occurred. The delayed reduction in water cut depends on the duration of slug displacement from the sand pack injection end to the production end. The sudden reduction in the water increases the oil recovery at the production end, as indicated in Figure 5.14 (b). Following the injection of 0.5 PV slugs, water flooding resumes,

revealing a delayed increase in the water cut, as shown in Figure 5.14 (c). The chemical slug's movement would mobilize the remaining oil, building an oil bank ahead of the chemical slug's front. As this oil bank approached the sand pack's production end, the oil recovery performance improved, and the water cut declined. The water cut increased again, terminating the flooding as the water level stabilized at 100%. The water-cut graphs showed the same pattern when the chemical slug composition changed during the experiments.

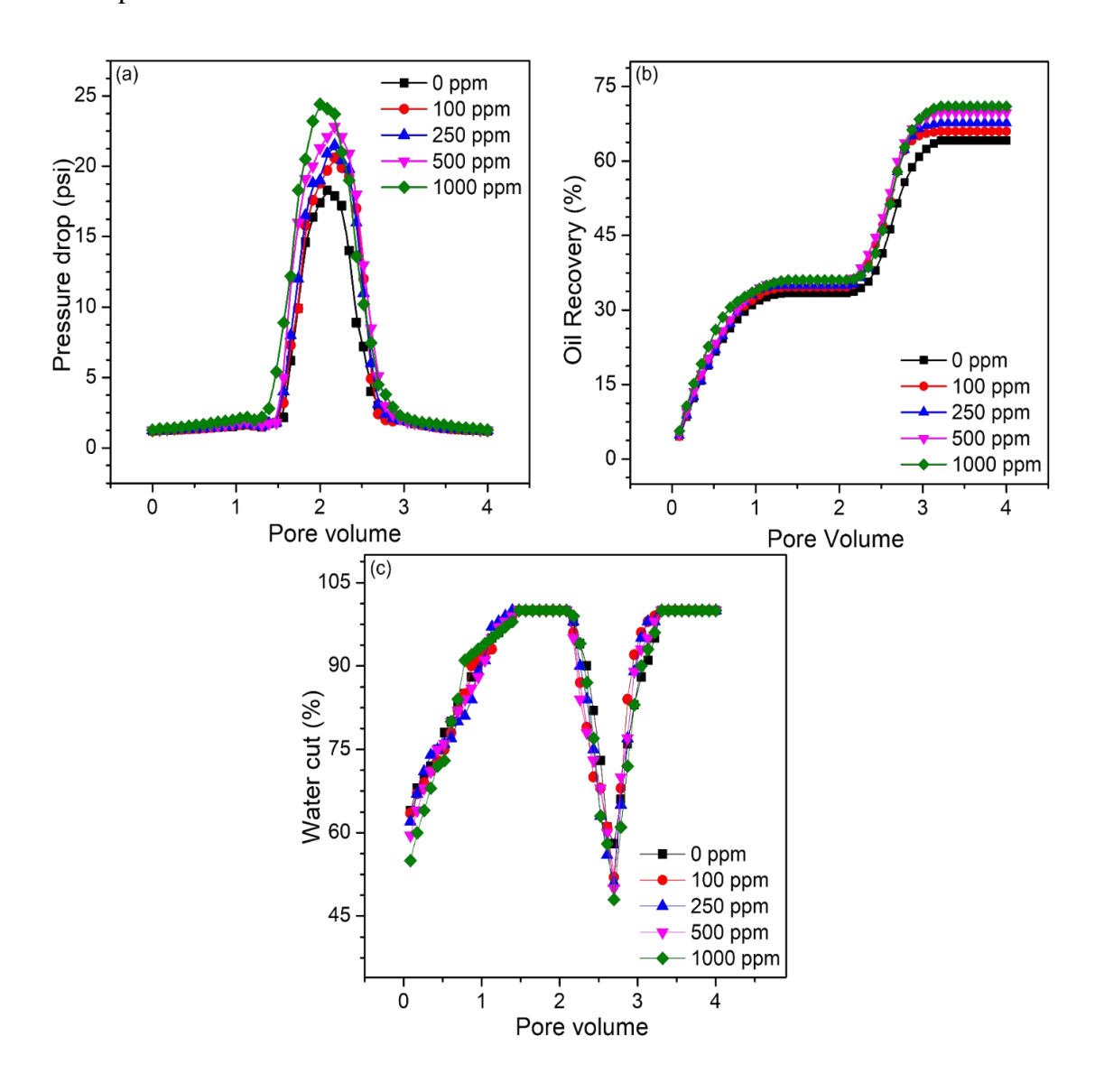


Figure 5. 14: Sand pack flooding experiment result. (a) Pressure drops, (b) Oil recovery, & (c) Water cut.

5.4. Conclusion

The feasible environmental conservation from plastic waste was accomplished by its conversion through upcycling processes rather than the conventional recycling processes, offering better economic and ecological benefits. This is the first research to employ waste plastic-derived reduced graphene oxide in the field of improved oil recovery for surfactant polymer flooding. The major problem remains techno-economic viability. The process described in this paper allows waste plastic to be converted into reduced graphene oxide nanosheets (RGO), with its application in enhancing oil recovery. FT-IR and EDX confirm the synthesis of RGO, and Raman spectroscopy establishes the layered structure of RGO. The thermogravimetric analysis assesses groups containing oxygen and the graphitic nature of RGO. The RGO effectively decreased the surface tension and contact angle by ~ 25% and ~ 20%, respectively, which was further reduced up to ~ 55% and ~ 83%, correspondingly using surfactants with RGO. The oil mobilization potential of the RGO was explored by carrying out flooding experiments, which recovered ~71% cumulative oil through the ASP slug with the help of RGO particles.

Chapter: 6

Sustainable potassium-doped graphene oxide from oak fruit agricultural waste for a synergistically improved nanofluidsurfactant slug for enhancing oil recovery

Abstract

This study presents an eco-friendly solvothermal method for synthesizing potassium-doped graphene oxide (K-GO) from agricultural waste, specifically oak fruit. Various spectrographic analyses, including XRD, FTIR, Raman, and UV-Vis, confirmed the successful synthesis of graphene oxide. The synthesized K-GO was then combined with different surfactants to create nanofluids to enhance oil recovery. Anionic sodium dodecyl sulfate (SDS) demonstrated the best performance among the surfactants tested. When 250 ppm of K-GO was added to a 2500 ppm SDS solution, the surface tension was reduced by over 10%. The study of zeta potential experiments validated that the K-GO-SDS nanofluid is compatible with sandstone reservoirs. Furthermore, the interfacial tension between the K-GO-SDS nanofluid and crude oil decreased by approximately 40%. Batch adsorption studies showed that the combination of SDS and K-GO significantly reduced surfactant loss to reservoir surfaces, reducing up to 32%. Additionally, incorporating K-GO resulted in a notable improvement in wettability alteration, with contact angle measurements showing an

improvement of over 20°. The sustainable synthesis of potassium-doped graphene oxide (K-GO) facilitates synergistic interactions with sodium dodecyl sulfate (SDS), thereby optimizing the formulation of nanofluids for enhanced oil recovery applications. This combination demonstrates superior efficacy in accessing trapped oil compared to using surfactants alone, highlighting the significant potential of K-GO-SDS nanofluids in advancing oil recovery techniques.

6.1. Introduction

Worldwide energy demand is rising due to population growth and economic development. The International Energy Agency (IEA) projects a 30% increase in global energy requirements by 2040, driven by developing nations in Asia, Africa, and the Middle East. Meeting higher demand necessitates significant investments in energy infrastructure and technology, improved efficiency, and reduced emissions [205]. Fossil fuels remain the planet's most reliable energy source, though few new hydrocarbon reserves have been discovered recently. Surfactant flooding, an enhanced oil recovery (EOR) technique, helps address the gap between energy consumption and production by improving recovery from existing reserves. Surfactants injected into reservoirs adhere at the oil-water interface, reducing interfacial tension among pore fluids and altering solid substrate wettability from hydrophobic to hydrophilic states. It also lowers the capillary forces trapping oil, which mobilize and displace residual oil, significantly increasing overall recovery [133], [205]–[208]. Surfactant adsorption deficits on solid substrates are prevalent when charges are incompatible with reservoir minerals, escalating costs to mobilize trapped oil through flooding. Moreover, field implementation of surfactant flooding has proven less effective than expected based on laboratory findings, chiefly attributable to the inability of conventional surfactants to

withstand downhole environmental extremes of high temperature and salinity. Mitigating these limitations necessitates customized formulations with optimized compatibility with reservoir conditions, thereby achieving cost-effective enhancement of oil recovery [85].

There has been growing research focusing on using nanoparticles to enhance the stability and efficacy of surfactants in subsurface conditions [209]. Nanoparticles exhibit greater resilience and stability when exposed to high temperatures and in brine formation. The small size of nanoparticles results in a larger surface area, which can effectively control their wettability. This property enables greater versatility and improved macroscopic and microscopic sweep efficiency during fluid flooding that combines nanoparticles and surfactants. Prior research has examined the potential use of nanotechnology in enhancing oil recovery (EOR) methods, which included investigating the use of nanofluids, synthesizing and producing nanoemulsions using nanoparticles and surfactants, and utilizing active metals as nanocatalysts to improve heavy oil recovery in situ. According to Yang et al. [210], modifying the surface of titania nanoparticles with oleic acid improved the ability of the nanoparticles to enhance the hydrocarbon recovery from the low permeability reservoirs. Additionally, this modification led to a reduction in injection pressure. In general, nanomaterials refer to materials that have outer dimensions or internal frameworks that are 100 nanometres or less in size. Nanomaterials can be classified into three main categories: nano clays, nano emulsions, and nanoparticles. They can also have different structures, such as spherical, tubular, irregular, or cylindrical, and can be classified as organic or inorganic. Examples of inorganic nanomaterials include nano silica (which consists of SiO₂ nanoparticles) and nano alumina (which consists of Al₂O₃ nanoparticles), while carbon nanotubes are

an example of an organic nanomaterial [211]. Surfactants tend to be unstable under reservoir conditions, while nanoparticles are not as surface-active as surfactant molecules. As a result, nanoparticles cannot reduce contact angles or the interfacial forces among the oil and water to the same ultralow levels that can be achieved with surfactants [212]. The combination of NPs and surfactants is recognized as an efficient method for attaining optimal hydrocarbon recovery. Surfactants decrease interfacial tension (IFT) between oil and water and alter the wetting properties of the rock. NPs reinforce surfactant performance and withstand high salinity and temperatures, enabling effectiveness despite harsh subsurface conditions. The synergies between NPs and surfactants optimize interfacial properties and wettability for improved oil recovery [213]. Previous research has shown that the combination of typical surfactants, including sodium dodecyl sulfate (SDS) and sodium dodecyl benzene sulfonate (SDBS), with NPs such as SiO₂ and Al₂O₃, has a more significant potential for enhanced oil recovery (EOR) than surfactant solutions or nanofluids alone [132], [214], [215]. SiO₂ nanoparticles are commonly employed for enhanced oil recovery (EOR) in sandstone reservoirs, while Al₂O₃ nanoparticles are advantageous for EOR in carbonate reservoirs. SiO₂ carries a negative charge similar to sandstone, while Al₂O₃ has a positive charge similar to carbonates. The charge match between nanoparticles and reservoir rocks allows the injected nanofluids to target the trapped oil rather than adsorb onto the rock surfaces [216], [217]. Prior studies have indicated that the presence of SiO₂ and Al₂O₃ nanoparticles reduces the surfactant loss on the rock surfaces. The surfactant molecules compete with the nanoparticle surfaces for adsorption, reducing the surfactant molecule's loss onto the rock surfaces [119], [122], [217], [218]. Lower surfactant concentrations are needed for nanoparticle (NP) flooding as SiO₂ and Al₂O₃

NPs reduce surfactant loss to rock surfaces. NP shape affects EOR effectiveness - cylindrical multiwalled carbon nanotubes (MWCNTs) differ from near-spherical SiO₂ and Al₂O₃ NPs. Beyond NP size and concentration, shape and geometry impact adsorption and orientation at liquid-liquid and solid-liquid interfaces [219]–[221].

The article describes the synthesis of environmentally safe potassiumdoped graphene oxide (K-GO) particles using oak fruit waste from the lesser Himalayas. This raw material, considered waste, significantly reduces initial material costs and can provide cost savings through waste disposal credits. Oak fruit waste was selected due to its abundance, availability, cost-effectiveness, and ease of access. Utilizing this biocompatible and biodegradable waste minimizes environmental pollution and promotes the valorisation of agricultural by-products, aligning with green chemistry principles by reducing reliance on synthetic chemicals. Unlike previous EOR methods that used hazardous commercially procured or synthesized nanomaterials, the eco-friendly K-GO nanomaterials are derived from agricultural waste. Following the synthesis of K-GO, experiments were performed to determine the critical micelle concentration with the help of the surface tension technique. Zeta potential was measured to evaluate the stability of particles treated with various surfactants. After selecting a surfactant that met specific criteria, interfacial tension measurements were conducted, followed by analysing the loss of surfactant through adsorption experiments. Furthermore, alterations in the wetting characteristics of rock surfaces were investigated through the measurement of contact angles. The study also examined the viscosity of slugs using rheological experiments and performed core flooding experiments to improve recovery efficiency. The use of KGO derived from oak fruit waste for EOR demonstrates strong economic feasibility due to the negative valuation

of the raw material, efficient and eco-friendly synthesis, significant performance improvements, and reduced environmental and operational expenses. This combination offers a cost-effective and sustainable solution for enhancing oil recovery.

6.2. Methodology

6.2.1 Materials

CTAB, a cationic surfactant with a purity exceeding 99%, was procured from Molychem Chemicals. Triton X-100, a nonionic surfactant in liquid form, was obtained in extra pure quality for scintillation purposes. Sodium dodecyl sulfate (SDS), with a purity exceeding 95%, was sourced from Rankem Chemicals. Sodium hydroxide (NaOH) and hydrochloric acid (HCl) were employed for pH variations and were purchased by SD Fine-Chem Limited and Merck Life Science Private Limited, respectively. Deionized (DI) water, with a resistivity of 18.2 M-m, was employed for sample preparation and cleaning procedures. Quercus Ilex (oak fruits) was gathered from Nainital, Uttarakhand, India. Ethanol and nylon filter papers (pore size 0.2µm) are purchased from Sigma Aldrich. The experimental methodology is schematically represented in Figure 6.1.

6.2.2 Synthesis of GO from agricultural waste

The graphene oxide (GO) synthesis from oak fruit was carried out using a solvothermal procedure employing ethanol solvent and double distilled water, which proved both environmentally friendly and economically efficient [185], [186], [222], [223]. Oak fruits have been extracted from Nainital, India, and washed to remove contaminants. The cupule and pericarp (outer layer) were separated, leaving the white inner fruit component. Fifty grams of this was pulverized into a paste using a mortar and pestle. The paste was mixed with equal 200mL volumes of ethanol and double-

distilled water. Heating this suspension at 120°C in a vacuum oven formed a brown solid residue. This residue was pulverized, suspended in 100mL deionized water, and stirred for 30 minutes. Centrifuging the reaction mixture for 15 minutes at 7000 rpm removed larger particles. The resultant reddish-brown supernatant was filtered through 0.2µm nylon. The filtrate was dried at 100 °C in a vacuum oven, yielding 4.32g of brownish graphene oxide, or K-GO, produced from the oak fruit agricultural waste.

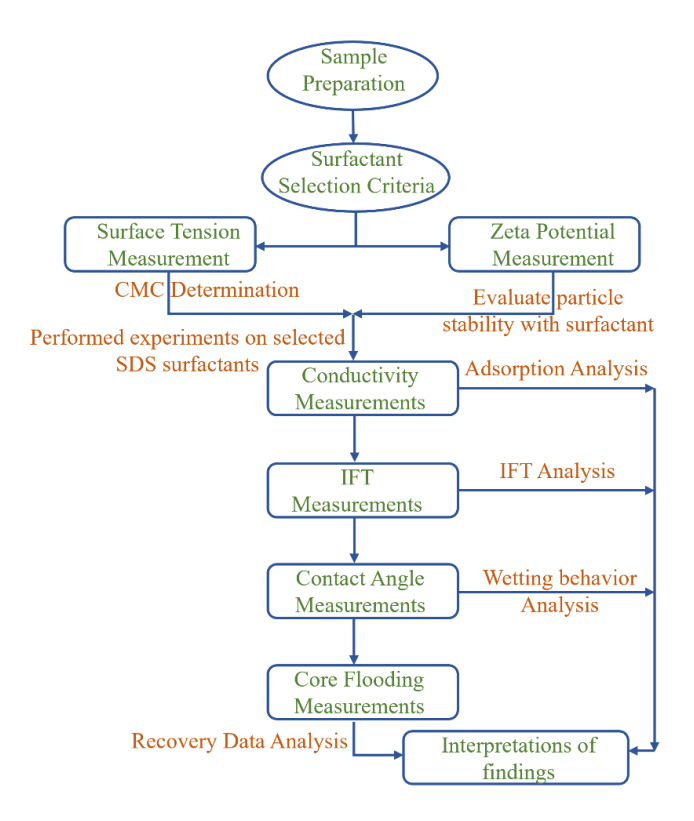


Figure 6. 1: Experimental methodology.

6.2.3 Characterization

The Fourier Transform Infrared (FT-IR) spectra were analyzed with a resolution of 4 cm⁻¹, employing an average of 16 scans. The spectra encompassed a range of wavenumbers from roughly 400 cm⁻¹ to 4000 cm⁻¹. The investigation was performed using a PerkinElmer Instrument, namely the Spectrum Two model, which employed the Attenuated Total Reflectance (ATR) approach. X-ray diffraction (XRD, Rigaku)

spectroscopy was utilized to assess the crystalline or amorphous nature of K-GO. The analysis was conducted utilizing a high-resolution X-ray diffractometer (Rigaku Smart Lab) equipped with Cu Ka radiation, which has a wavelength of 0.154 nm. The experimental parameters were configured to a voltage of 45 kilovolts and a current of 200 milliamperes. Data acquisition was performed throughout a scanning range spanning from 10 degrees to 80 degrees, with a scanning rate of 4 degrees per minute. The structure and characteristics of K-GO were analysed using Raman spectroscopy, explicitly employing the Horiba Japan Xplora Plus instrument at a wavelength of 514 nm. The UV-visible spectra of the K-GO were acquired using a twin-beam UV-visible spectrophotometer produced by Esico International (Model 3375).

6.2.4 Hydrodynamic Size and Stability Analysis

Dynamic light scattering (DLS) analysed the particle size range of K-GO nanofluid and zeta potential and evaluated stability. Using a Malvern Zetasizer, the mean hydrodynamic diameter and zeta potential of K-GO nanoparticles dispersed in distilled water were measured. Approximately 1.5ml of the K-GO solution at 30°C was added to a cuvette for the DLS size distribution analysis. DLS measures size by studying the Brownian motion of particles in liquid to obtain hydrodynamic diameter via the Stokes-Einstein equation. Knowing temperature and viscosity is necessary to evaluate results accurately. Overall, DLS non-invasively and non-destructively analyses nanoparticle size distributions. As per the Stokes-Einstein relationship, there is an inverse relationship between particles' diffusion coefficients (Dc) and their size (h_d, hydrodynamic diameter). In simpler terms, the larger the particle size, the lower the diffusion coefficient, and vice versa, illustrated in Equation 6.1.

$$D_c = \frac{KT}{3\pi \nu h_d} \tag{6.1}$$

In equation 6.1, D_c is the diffusion coefficients of particles, h_d is the hydrodynamic diameter, K is the Boltzmann constant, T is the temperature, and υ is the viscosity. To accurately determine the particle size, one must know the precise values of the liquid's temperature (T) and viscosity (υ) parameters. The zeta potential and particle size of the prepared cationic, anionic, and nonionic surfactant with K-GO were evaluated to examine the prepared nanofluids' stability and hydrodynamic size.

6.2.5 Surface tension measurement

The surface tension of the formulated surfactant mixture in aqueous solution was assessed using the KYOWA DY-500 tensiometer to compute the critical micelle concentration (CMC). Initially, surface tension values of the individual cationic, anionic, and nonionic surfactants were measured to investigate their CMCs. Surfactant solutions of differing concentrations (40mL) were formulated in DI water to study how surface tension changes. Surface tension was computed using the Du'Nouy ring (diameter 14.5mm, thickness 0.4mm) technique. The ring was heated before each test to prevent contamination. Each surface tension measurement was performed thrice, ensuring repeatability. Solvents like acetone, hexane, and DI water were tested to validate equipment accuracy. The evaluation of CMC involved creating a graph that illustrates the reduction in surface tension as the concentration of the surfactant mixture increases. The ST values of the surfactant were measured using the below-mentioned Equation 6.2.

$$S_{tension} = \frac{F_{acting}}{4\pi R} * c \tag{6.2}$$

Where surface tension is denoted as $S_{tension}$, F_{acting} is referred to as the acting force on the ring, the diameter of the ring is R, and c is the correction factor, which depends upon the ring size and the density of the sample. Also, the surface tension of the K-GO at differing concentrations, i.e., 100, 250, 500, and 1000 ppm, were measured with or without surfactant at their respective CMC value.

6.2.6 Interfacial tension study

KYOWA DY 500 tensiometer measured the interfacial tension between the K-GO-based solution and crude oil at ambient pressure and room temperature. IFT experiments utilized the platinum Du-Nouy ring with a precision of 0.02 mN/m. After every experiment, the sample holder was cleaned with the help of toluene to eliminate the remaining crude oil and further washed with acetone to remove the surfactant remnants and then dry the sample holder. Similarly, the ring was cleaned via burner to eliminate the remnants of crude oil or surfactant traces from the ring diameter. Also, it examined the variation of the IFT with K-GO at varying pH with or without surfactant at their respective CMC values.

6.2.7 Adsorption studies

This experiment uses a batch technique to evaluate the adsorption of surfactants and nanofluids onto sand particles [53], [64], [119], [120]. Initially, the conductivity of the solutions was measured to determine the suitable calibration curves for each set of aqueous solutions [53], [132]. A Labman Scientific LMMP-30 Multiparameter measured solution conductivity to assess surfactant loss. 1g of 400-500µm sand particles was added to 40 mL of each surfactant and nanofluid solution. Initial conductivities were measured in triplicate for reliability, cleaning the probe between

solutions. 4g of sand was mixed into each 40 mL solution to examine surfactant adsorption over 12 hours. The nanofluids combined 100-1000ppm K-GO and 500-3000 ppm anionic surfactant. Every 12 hours, the fluids and sands were separated by centrifuging at 4000 rpm for 20 minutes. The conductivity of the remaining solutions was measured to plot calibration curves assessing surfactant loss over time. This comprehensive approach evaluated the ability of K-GO nanoparticles to reduce surfactant adsorption across varying concentrations with ageing. Equation 6.3 estimates the surfactant's adsorption density if the surfactant's preliminary concentration and equilibrium concentration are known.

$$A_{adsorption} = \frac{\left[\left(C_{initial} - C_{final} \right) * \frac{M_{sol}}{M_{sand}} \right]}{1000}$$
(6.3)

In the equation mentioned above, the $A_{adsoption}$ is the adsorption density of the surfactant (mg/g), M_{sol} and M_{sand} are the mass of solution and sand grains (grams), and $C_{initial}$ and C_{final} are the initial and final concentrations.

6.2.8 Measurement of contact angle

The contact angle (CA) test assesses changes in wettability. The tests were carried out with the help of a high-pressure and high-temperature (HPHT) goniometer offered by D-CAM Engineers, India. The HPHT goniometer measures the contact angle of the prepared sample onto the sandstone substrate in the evacuated chamber to assess any modification in the wetting characteristics of the substrate. The equipment consists of a stable stage with a lamp source at the back, a needle, a pipette to dispense the sample, and a recorder to retrieve a picture of the drops. The closed chamber, connected to the instruments, housed the surface where the CA values were measured. The sessile

drop technique evaluates the contact angle. The instruments used have a contact angle range of 0° to 180° , and they provide measurements with a precision of \pm 0.052°. Surfactant solutions were prepared in DI water at the critical micelle concentration (CMC), and K-GO nanoparticles were added to the system. After each experiment, the needle connected to the equipment was rinsed using DI water. Each experiment was performed three times to evaluate the repeatability of the instruments.

6.2.9 Rheological analysis

Viscometry analysis is a scientific method used to examine a sample's flow behavior and deformation in response to applied forces, considering factors such as shear rate and temperature. It involves studying how materials respond and change their shape under different levels of force or stress. Rheology analysis provides insights into the sample's viscoelastic properties and flow characteristics by measuring and analyzing the relationship between the applied force and resulting deformation. The viscosity of the samples was determined using a modular rheometer (MCR-302e) manufactured by Anton Paar. The rheological characteristics of the slug, with varying concentrations of the polymer and nanoparticles, were examined using the rheometer's bob and cup assembly system. Following each experiment, the instrument apparatuses were cleansed with DI water and dried using a dryer. The chemical slug was formulated by combining a 1000 ppm polymer with varying concentrations of K-GO, ranging from 100 to 1000 ppm, as shown in Figure 6.2. Rheological investigations were conducted on the formulated chemical slug at room temperature to examine its degradation behavior.

6.2.10 Core flooding experiments

The flooding evaluates the effectiveness of the surfactant polymer flooding for enhanced oil recovery with K-GO particles. The experiments were performed on the two sets of cores, and their properties are mentioned in Table 6.1. The helium porosity meter calculated the porosity of the core. In contrast, the gas permeability was estimated with the help of a gas permeability meter, which was procured from D-CAM Engineering India. The core flooding setup contains the HPLC constant rate syringe pump, core holder, and two transfer accumulators, one for oil and another for the slugs. Also, the back pressure regulator (BPR) maintains the system's pressure at the output end. Initially, the core was saturated with the help of water. After the water saturation had been completed, the core was again saturated with oil until the connate water saturation was attained under the reservoir conditions. The flow rate of ~0.5 ml/m was fixed during the whole experimentation.

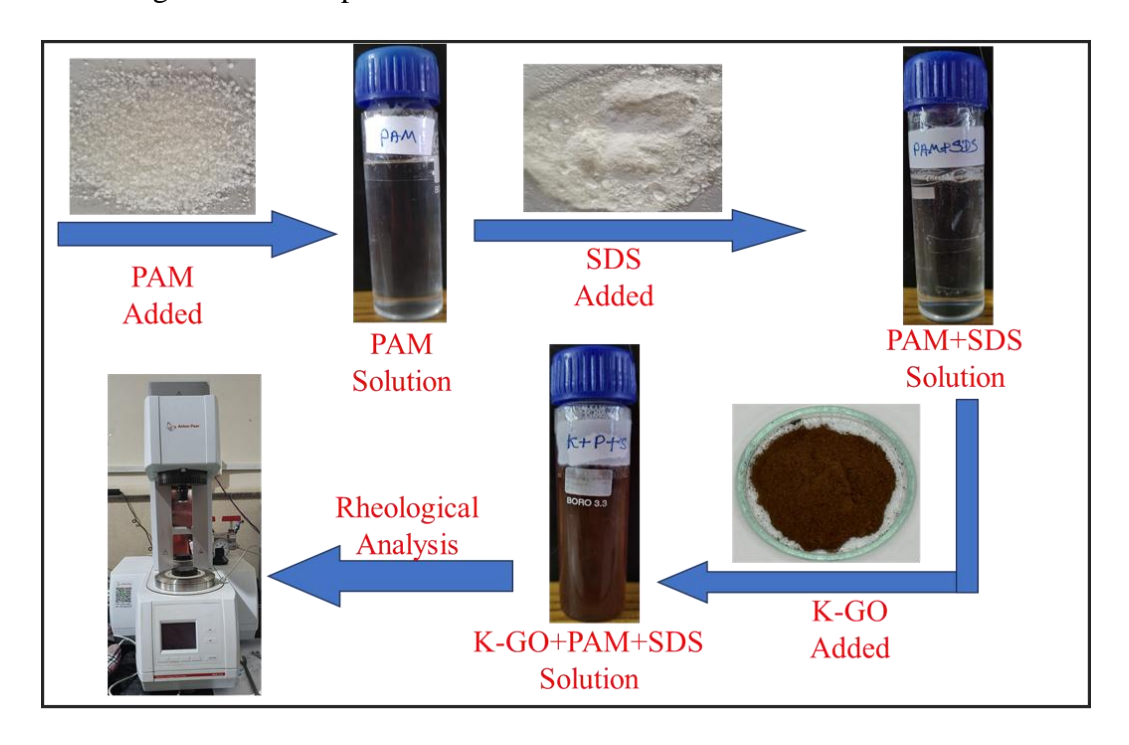


Figure 6. 2: Graphical representation of sample preparation for Rheological analysis.

Table 6. 1. Properties of the Core

Petrophysical analysis of the core			
S. N	Properties	Core ID-1	Core ID-2
1	Diameter (cm)	3.7	3.72
2	Length (cm)	7.7	8.7
3	Pore Volume (ml)	12.50	18.2
4	Bulk Volume (ml)	85.14	70.54
5	Average Grain density (g/cc)	2.61	2.64
6	Porosity (%)	14.68	25.80
7	Gas Permeability (mD)	1149.23	3237.48

6.3. Results and Discussion

6.3.1 Characterization of synthesized K-GO

As shown in Figure 6.3 (a), the XRD technique was utilized to investigate the structural nature of K-GO. This XRD pattern demonstrates the amorphous nature of the prepared material. The integrity of the synthesized K-GO is confirmed by the presence of a broad XRD peak at 20 =25.62 (002) and an interlayer spacing of 3.47 A°. Using Scherrer's and Bragg's equations, the sample's thickness and number of layers were determined. The layer count of the sample was calculated by dividing the crystal size (C) by the interlayer distance (d), followed by adding one. The estimated crystal size (C) of K-GO was measured to be 14.48 A°, which corresponds to the diffraction peak at 20 =25.62, whereas the interlayer distance (d) between graphene layers was measured to be 3.47 A°. Consequently, the calculated particle size (C) and layer distance (d) using XRD data [183], [184], [223] indicated the presence of 4-5 layers of the GO originating from oak fruit. In addition, FTIR was performed to determine the nature of functional groups on the material. The different functional groups on the K-GO surface were identified by analyzing the FT-IR spectra. The Fourier Transform Infrared (FTIR) spectrum of K-GO exhibits distinct peaks at certain wavenumbers, indicating the

existence of several functional groups. These peaks include a strong band at 2895 cm⁻¹ corresponding to C-H stretching, a peak at 1687 cm⁻¹ associated with C=O stretching, another peak at 1609 cm⁻¹ indicating C=C stretching, a peak at 1191 cm⁻¹ representing C-O-C stretching, a peak at 1032 cm⁻¹ indicating C-O stretching. Peaks at 3207 cm⁻¹ and 1326 cm⁻¹ show hydroxyl group deformation, shown in Figure 6.3 (b). Consequently, the aforementioned characteristic peaks provide evidence for the presence of epoxy, carbonyl, and hydroxyl groups on K-GO nanosheets [183], [222], [224]. Raman spectroscopy is also helpful in confirming GO formation and evaluating synthesized K-GO's integrity, especially in samples containing double and conjugated carbon-carbon bonds. Figure 6.4 (a) depicts the Raman spectra of K-GO, revealing the presence of the D band at 1338 cm⁻¹. This band is a consequence of the disorder within the graphene nanosheet and can be attributed to unreacted oxygenic sites and edge defects. It represents the elongation of the sp³ hybridized carbon lattice in the GO and indicates local defects resulting from structural irregularities. In contrast, the G-band is the most prominent component of the Raman spectrum of graphene-based materials. The G band, located at 1569 cm⁻¹, is attributed to the sp²-hybridized carbon network present in the GO. The authors Tewari et al. [185], [186], [225] described the synthesis of K-GO from agricultural waste. They identified two prominent Raman bands, D and G, at 1312cm⁻¹ and 1531cm⁻¹, respectively, similar to the observed G and D bands. Moreover, it is believed that the sp³ hybridized carbon atoms in the oak seed cellulose transformed into sp² hybridized carbon atoms during the solvothermal process [223]. According to some reports, this conversion process, known as dehydrogenative aromatization, enables a carbon atom to achieve its utmost stability [226], [227]. Consequently, the G band intensity in K-GO was increased relative to the D band intensity. The existence of the D and G bands demonstrates that K-GO was effectively synthesized. Results were consistent with previously reported GO levels in agricultural waste. Somanathan et al. [228] reported the synthesis of GO from sugarcane bagasse and demonstrated that its spectrum contains D and G peaks at 1358cm^{-1} and 1550cm^{-1} , respectively. The UV spectra of K-GO, as seen in Figure 6.4 (b), have a distinct peak at 230nm. This peak arises from the π - π * transitions of the aromatic sp² hybridized carbon atoms (C=C) in K-GO, as stated in reference [185], [186]. The SEM (FE-SEM, Nova Nano SEM 450, FEI, USA) images in Figure 6.5 vividly depict the discernible layered structure of K-GO. The images depict the sheet-like shape of K-GO.

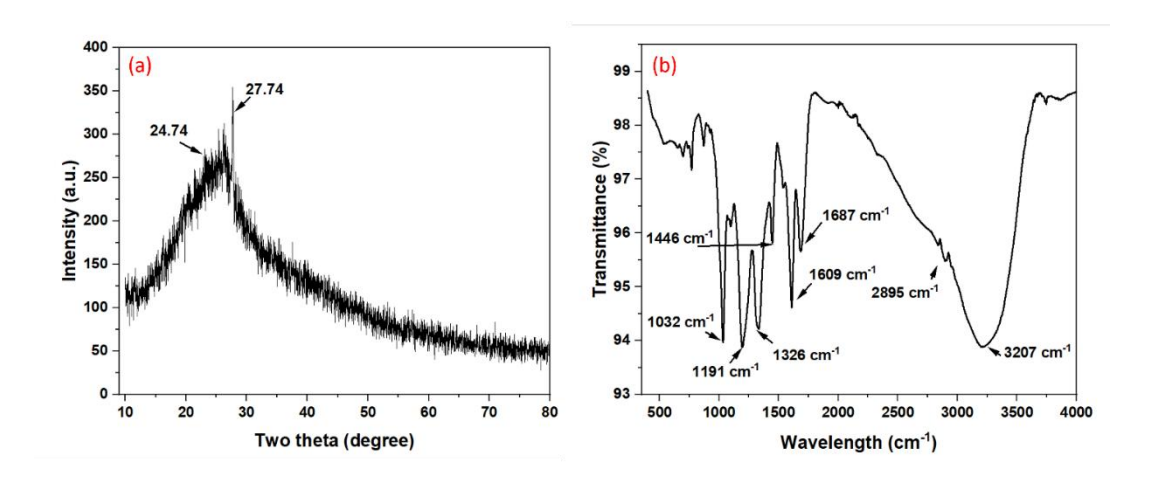


Figure 6. 3: (a) XRD analysis of K-GO, and (b) FTIR analysis of K-GO 6.3.2 Particle Size and Zeta Potential

Examining the size distribution of the K-GO within the chemical slug is crucial as the particle size significantly impacts the interfacial properties that play a significant role in oil recovery [46]. Dynamic light scattering showed the average hydrodynamic size of K-GO to be 87 nm in distilled water. This small particle size enables effective navigation through pore throats during oil recovery without the risk of entrapment. Absorption of the nanoparticles at the oil-water interface contributed to the observed

interfacial tension (IFT) reduction. Figure 6.6 reports the interactions between K-GO and surfactants affected particle size, with mean diameters of approximately 161 nm for anionic, 205 nm for cationic, and 360 nm for nonionic surfactants.

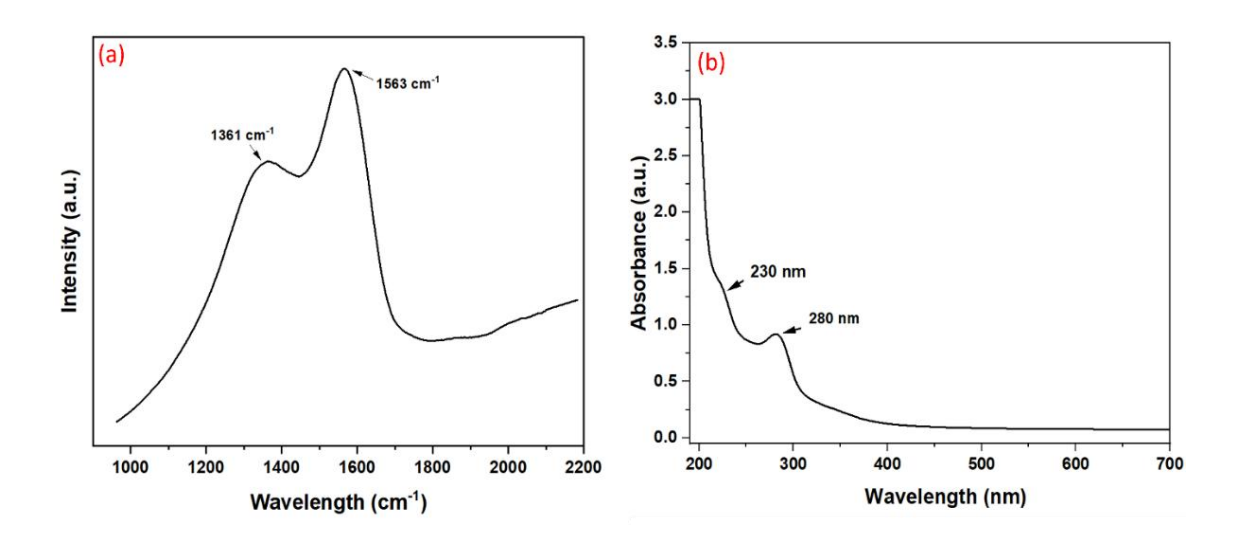


Figure 6. 4: (a) Characterization of K-GO by Raman spectroscopy, and (b) UV spectra of K-GO

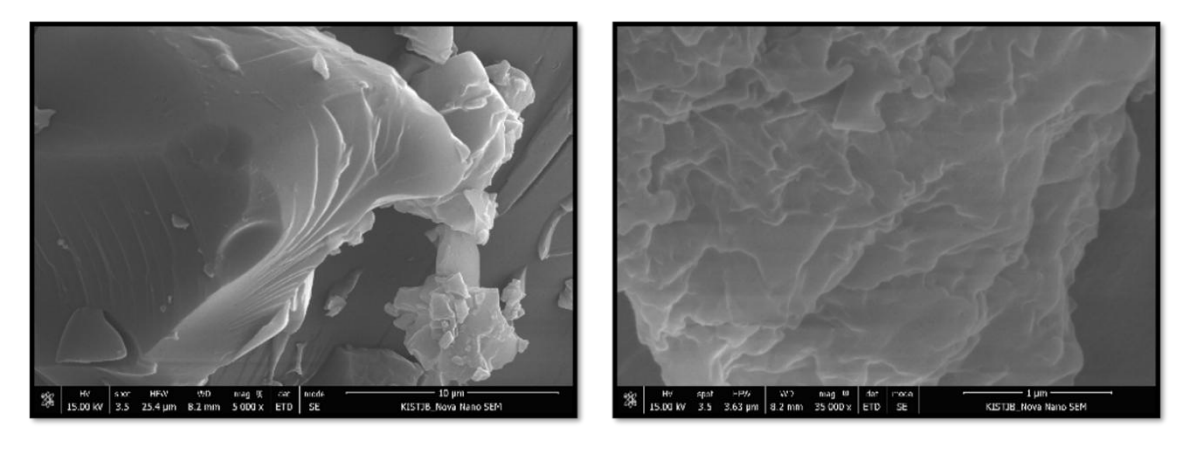


Figure 6. 5: SEM analysis of K-GO.

The significantly larger size with nonionic surfactants suggests less favorable interactions. Overall, the nanoscale size of K-GO combined with anionic and cationic surfactant compatibility allows it to access trapped oil in porous reservoirs for enhanced recovery. The zeta potential of natural rock surfaces is significant as it governs ionic interactions with charged aqueous species. The measured zeta potential of K-GO

particles was ~-10 mV. When combined with surfactants, values were approximately -28 mV (anionic), 6 mV (cationic), and 19.5 mV (nonionic), as shown in Figure 6.6. Zeta potential evaluates colloidal dispersion stability; high repulsion between particles prevents agglomeration and indicates stability. K-GO's negative charge suits sandstone reservoirs. The further decreased, the more negative the zeta potential with added anionic surfactant contributes to additional stability. Cationic surfactant inverted the charge, reducing repulsion between nanoparticles. Nonionic surfactant produced a positive zeta potential, likely making the nanofluid incompatible with sandstone. By evaluating zeta potential changes with surfactant addition, the nanofluid can be optimized for maximum stability and oil recovery efficiency [67]. Al-Anssari et al. (2017) investigated the effects of SDS and CTAB surfactants and highlighted SDS's effectiveness in stabilizing silica nanofluids within high-salinity conditions (up to 5 wt% NaCl). Therefore, a suitable anionic surfactant could potentially reinstate stability to an otherwise unstable nanofluid [229], [230].

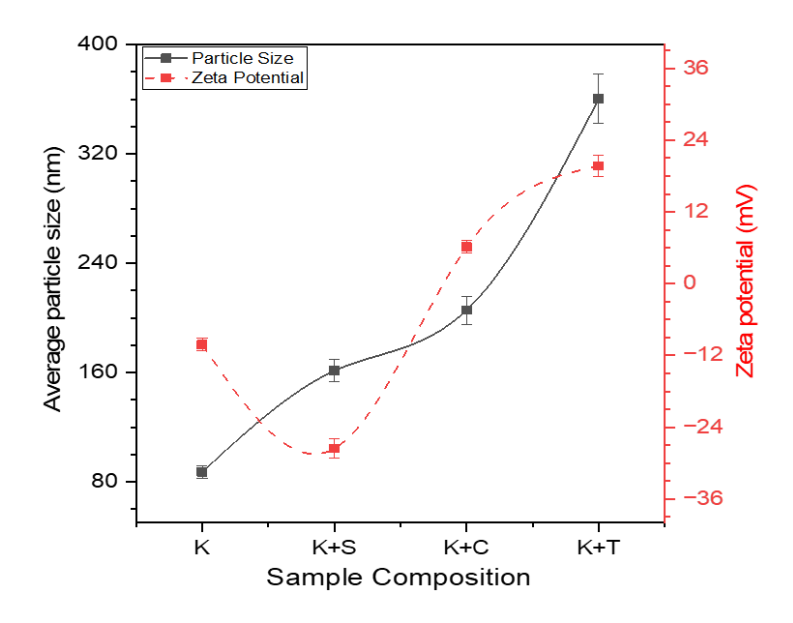


Figure 6. 6: Particle size and Zeta potential of samples in which K stands for K-GO, S for SDS, C for CTAB, and T for Triton X100.

6.3.3 Studies of Surface Tension

Surface tension (ST) represents critical fluid characteristics influencing oil extraction from reservoir pore spaces [231]. These properties are closely linked to capillary pressure, which retains residual oil within the reservoir. Therefore, decreasing these properties enables crude oil to surpass capillary pressure, enhancing the potential for increased recovery. Injecting a surfactant solution into the reservoir lowers the interfacial tension between crude oil and the displacing fluid, elevating the capillary number and displacement efficiency [232]. The plotted surface tension values at various surfactant concentrations (Figure 6.7) indicate a decreasing trend with rising surfactant concentration, reaching a minimum value at critical micelle concentration (CMC). For instance, the SDS surfactant exhibited a minimum surface tension of 29.8 mN/m at its CMC of 2500 ppm, while CTAB and Triton X100 showed minimum values at 300 and 200 ppm, respectively, which is approximately 33.42 mN/m and 32.53 mN/m respectively. The reduction in surface tension can be attributed to surfactant particles adsorbing with their heads in the liquid phase and hydrophobic tails facing outward. This arrangement balances the interfacial forces between immiscible fluids. However, beyond the surfactant's CMC, the surface tension of the solution remains unchanged. This is likely due to the surfactant's micellization, where free monomers start forming micelles, ceasing further impact on interfacial forces. According to the Figure 6.7, the ST value shows a greater reduction with the assistance of SDS. Additionally, analysis of the zeta potential indicates that the colloidal suspension of SDS remains more stable in the presence of K-GO compared to CTAB and Triton X100. Consequently, the subsequent investigation focused solely on the anionic surfactant (SDS).

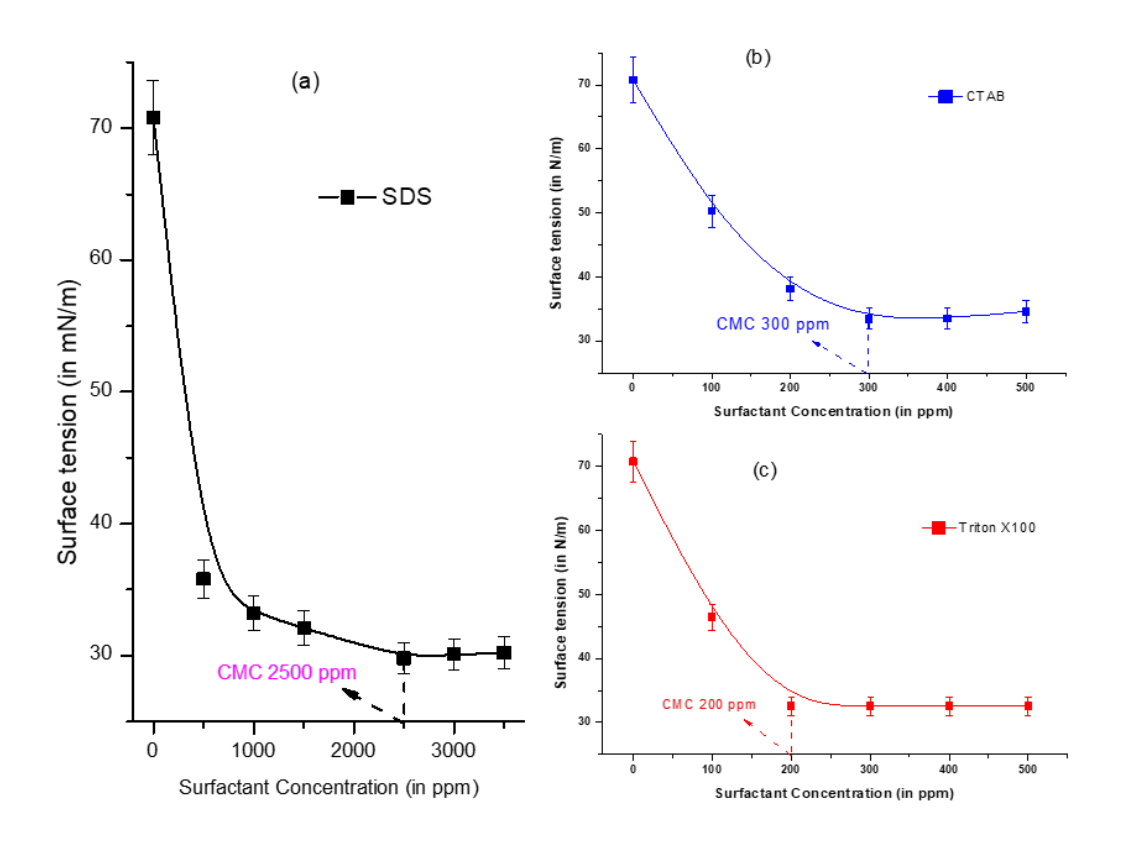


Figure 6. 7: Impact of surfactant concentrations on the surface tension, (a) for anionic surfactant (SDS), (b) for cationic surfactant (CTAB), and (c) for nonionic surfactant (Triton X100).

6.3.4 Impact of nanoparticles on the surface tension

Nanoparticles can lower surfactant solution surface tension and improve nanofluid stability by providing increased surface area for surfactant adherence. The enhanced surface coverage of nanoparticles by surfactant molecules creates a more significant steric hindrance between the nanoparticles. This steric repulsion reinforces the electrostatic repulsion measured through zeta potential, promoting a more resistant dispersion less prone to aggregation. The synergistic interaction between nanoparticles and surfactants at fluid interfaces underlies application performance benefits. [50], [233]. Nanoparticle-surfactant interactions depend on nanoparticle properties, surface charge, dispersion medium, and surfactant type. Opposite charges promote stronger coupling, with Coulombic attraction dominating to reduce interparticle repulsion at

fluid interfaces. Combinations of anionic surfactants and nanoparticles effectively reduce surface tension, suggesting factors beyond charge governing their synergy. The observation that charges repulsion does not prohibit performance aligns with other studies. Overall, attractions between properly matched nanoparticles and surfactants enable stable dispersions to access trapped oil, but the complex relationship between nanofluid components necessitates case-by-case optimization. [46], [98], [119], [234], [235]. Figure 6.8 (a) illustrates the consistent decline in surface tension values upon introducing nanoparticles into anionic surfactant (SDS) solutions. The decrease in surface tension values is attributed to nanoparticles adhering to the interface between the liquid and air, subsequently causing a further reduction in surface tension [43]. Adding 250ppm K-GO to a 2500ppm anionic surfactant (SDS) solution decreased surface tension from 29.8 mN/m to 26.9 mN/m. Without surfactant, 100ppm K-GO reduced surface tension from 70.8 to 52.27 mN/m, as shown in Figure 6.8 (a). The high surface charge density of the nano-scaled K-GO can enable increased interaction with liquid molecules, enhancing their surface adsorption, which reduces surface tension. Smaller nanoparticles with greater surface charge disproportionately impact this effect. The synergy of K-GO with SDS demonstrates that anionic surfactants effectively stabilize the nanofluid while accessing additional interfaces. Combining 250ppm K-GO with 2500ppm SDS produced optimal surface tension reduction, establishing it as an efficient formulation for enhanced oil recovery applications. [125], [236].

6.3.5 Effect of pH on the Surface Tension

Surface charge influences the Surface tension, which significantly depends on the solution pH. Increasing pH raises hydroxyl ion (OH⁻) concentration, making the solution more alkaline. Decreasing pH increases hydrogen ion (H⁺) concentration,

making it more acidic. This pH-mediated change in ion content impacts surface charge density and, thus, surface tension. Evaluating pH effects on surfactant solution surface tension is key before reservoir injection to mobilize residual oil. Imbalances in charge concentration with pH drastically alter surface tension. Therefore, investigating nanofluid pH sensitivity tied to surface charge density is critical for enhanced oil recovery applications [122], [195], [197], [237]. The impact of pH on surface tension was examined using the optimized concentration of K-GO. As the pH of the nanoassisted solution decreased from 7 to 3, becoming more acidic at 250 ppm of K-GO, the ST decreased from 26.9 mN/m to 26.2 mN/m, as shown in Figure 6.8 (b). A similar reduction in surface tension was observed when the solution pH was increased from 7 to 11 or decreased to more acidic values. This reduction can be due to enhanced electrostatic interaction between surfactant molecules adsorbed at the liquid-air interface under non-neutral pH conditions. At pH 7, minimal hydrogen and hydroxyl ions increase repulsive forces between surfactant particles, resulting in higher surface tension. However, introducing counterions at lower or higher pH levels encourages surfactant particle adsorption and stabilizes interfacial forces. Acidic pH saturates the solution with hydrogen ions that counter the anionic surfactants, reducing repulsion between adsorbed particles. This phenomenon allows more surfactant accumulation at the interface, lowering surface tension. Similarly, the increased hydroxyl ions counter the cationic surfactants under an alkaline environment. By mitigating like-charge repulsive forces, pH-controlled ion concentrations directly impact surfactant interface stability and surface tension [195], [237]–[239].

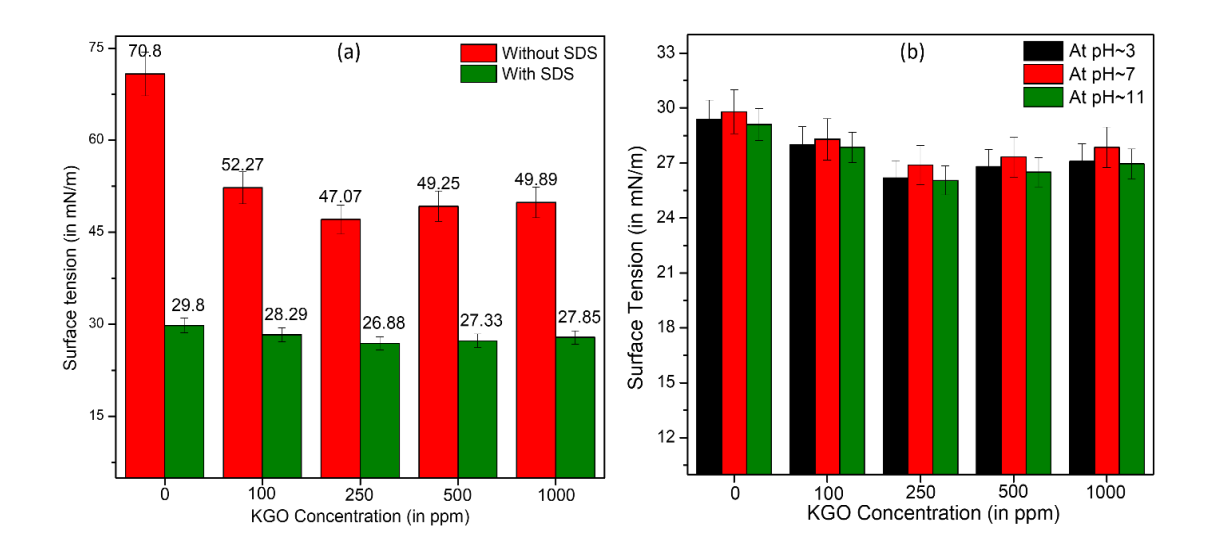


Figure 6. 8: (a) Impact of K-GO on the surface tension with and without surfactant. (b) Role of pH on the surface tension with surfactant at CMC (2500 ppm).

6.3.6 Analysis of Interfacial Tension

Several industrial operations, specifically those involving enhanced oil recovery (EOR) applications, focus on the interfacial tension (IFT) between immiscible solutions. While interfacial tension (IFT) can be demonstrated in various immiscible phases, it describes the forces present at the interface between two liquid phases in liquid-liquid systems [98], [195], [212]. The IFT between liquids having various affinities for water, such as hydrophilic and hydrophobic liquids, plays vital roles in industrial applications in petroleum and chemical engineering. Some of the well-known techniques in this area include stabilization of emulsions, liquid-liquid extraction, water flooding, two-phase liquid displacement, and EOR. The IFT alteration is crucial in enhancing the capillary number in EOR operations, aiming to extract the trapped oil from reservoirs. The Du'Nouy ring was employed to gauge the interfacial tension between the oil and the prepared nanofluid. K-GO concentration in water was adjusted in steps of 250 ppm, ranging from 0-1000 ppm. By adding different concentrations of K-GO to the solution while keeping the concentration of SDS constant at CMC, better

outcomes were seen, as mentioned in Figure 6.9 (b). Whereas without anionic surfactant, the IFT has been observed at ~23.45 mN/m between distilled water and oil. After introducing 100 ppm K-GO, the reduction in IFT has been observed from 23.45 to ~14.24 mN/m, shown in Figure 6.9 (a).

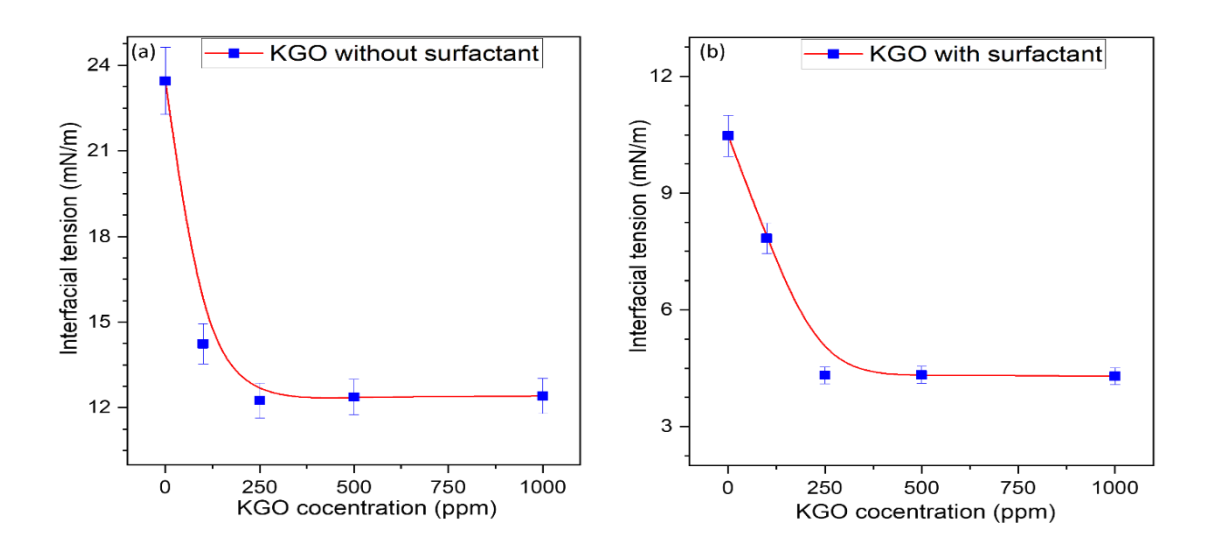


Figure 6. 9: Effect of K-GO on Interfacial tension (a) without anionic surfactant (SDS), (b) with anionic surfactant (SDS).

6.3.7 Impact of K-GO on Interfacial Tension

One of the most critical processes in the enhanced oil recovery (EOR) technique is lowering IFT among water and oil in the reservoirs. It significantly affects the permeability, fluid flow properties, and capillary pressure in porous media. The measured interfacial tension (IFT) between distilled water and crude oil was originally 23.45 mN/m. Adding the anionic surfactant SDS at its critical micelle concentration (CMC) of 2500ppm reduced IFT to 10.47 mN/m due to enhanced surfactant adsorption at oil-water interfaces. 100 ppm of the K-GO nanoparticle decreased IFT to 14.24 mN/m through similar interfacial activity, increasing aqueous phase surface coverage. The IFT decreased to 12.26 mN/m after adding 250 ppm, as mentioned in Figure 6.9 (b). Combining varying concentrations from 0-1000 ppm K-GO with a fixed 2500 ppm

SDS concentration further reduced IFT due to synergistic interactions, reaching an IFT of 7.84 mN/m at 100 ppm K-GO and 4.32 mN/m at optimal 250 ppm K-GO surfactant nanofluid combination as shown in Figure 6.9 (b). Greater interfacial coverage and accumulation of surfactant and nanoparticles are responsible for considerable IFT reductions. Lowering the trapping capillary pressure from decreased IFT facilitates oil droplet release from narrow pores. This nanofluid blend leverages cooperative SDS-K-GO interfacial interactions to recover additional crude oil effectively.

6.3.8 Impact pH on Interfacial Tension

The pH of the aqueous phases was evaluated using the LMMP-30 multiparameter before conducting the interfacial tension experiments. Sodium hydroxide and hydrochloric acid were employed to modify and regulate the pH level of the solution. The experiment was performed at pH values 3, 7, and 11. Hoeiland et al. (2001) noted that a reduction in interfacial tension (IFT) was achievable solely at elevated pH levels when acidic elements were present within the crude oil [238]. The reduction in interfacial tension (IFT) curves occurs uniformly as the pH rises within the alkaline range of the aqueous phase. This observation aligns with the anticipated findings documented in the literature (Cratin, 1993; Danielli, 1937; Hartridge and Peters, 1922) [240]–[242]. This trend is attributed to the heightened surface activity of acids resulting from their dissociation, explaining the observed phenomenon. Both acidic and alkaline components play a role at the interfaces between crude oil and brine, resulting in the highest IFT observed around a neutral pH. As the pH moves away from neutrality, either rising or falling, the IFT reduces, as Buckley (1996) and Reisberg with Doscher (1956) noted. The same trend followed during the experimentation, as shown in Figure 6.10. Initially, interfacial tension (IFT) between distilled water and the oil was 23.45 mN/m at a pH of 7. This value decreased to 15.1 mN/m and 18.6 mN/m at pH levels 3 and 11, respectively. Incorporating 100 ppm K-GO without surfactant led to a maximum IFT reduction of approximately 27% at pH 3, as in Figure 6.10 (a). However, when 100 ppm K-GO was combined with the surfactant in the solution, the IFT reduction was notably higher, around 40%. The same trend persisted when 100 ppm K-GO was introduced into the solution while adjusting the pH to 11, as shown in Figure 6.10 (b).

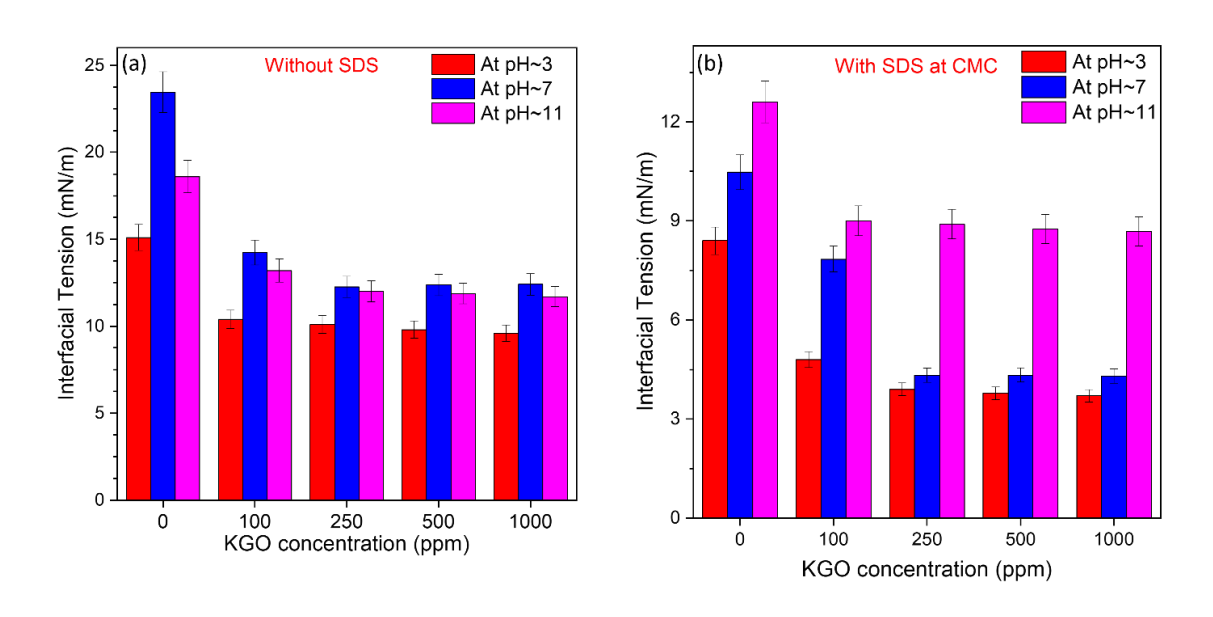


Figure 6. 10: Role of pH with varying K-GO concentrations on Interfacial tension, (a) Without anionic surfactant (SDS), (b) With anionic surfactant (SDS).

6.3.9 Analysis of Adsorption behavior

The activity of surfactant loss involves gathering surfactant molecules from the bulk liquid sample onto the surface of a reservoir rock [133]. This loss at the interface between solids and liquids is essential in several industrial and scientific realms, leading to adverse technological and financial repercussions. Therefore, retaining surfactants becomes a critical concern in procedures reliant on surfactant-based chemical EOR, such as surfactant flooding, surfactant polymer flooding, and

alkaline/surfactant/polymer (ASP) flooding [134]. Surfactant retention occurs primarily due to adsorption, phase entrapment, and precipitation, which persist during the chemical EOR process. The movement of surfactants into microemulsions or the oil phase contributes to phase entrapment. The phase entrapment is due to elevated salinity, temperature, and highly charged divalent ions. This combined action impedes the achievement of extremely low interfacial tension (IFT), consequently leading to surfactant loss. Various researchers have explored the impact of surfactant concentration on its loss due to surfactants becoming attached to reservoir rocks, which possess distinct surface charges based on their nature. For instance, sandstone surfaces exhibit a negative charge, while carbonate surfaces exhibit a positive charge. Surfactant adsorption onto sand particles involves ion exchange, ion association, hydrophobic bonds, electron polarization, and dispersion forces [61], [71], [120], [243], [244]. The type of solid substrate, solvent, surfactant type, and the characteristics of its polar head groups and tail parts all influence the adsorption process [137]. Surpassing a specific threshold, loss of surfactant on sand grains can compromise oil recovery, governed by the differences in thermodynamic stability between interactions among liquid surfaces and water [61]. The hydrophobic effect, which determines a substance's tendency to avoid aqueous solutions, significantly affects adsorption. The findings (Figure 6.11(a)) illustrate that the adsorption of SDS (anionic surfactant) increased as its concentration rose, reaching 1.45 to 2.20 (mg/g) at 1000 ppm and 4.97 to 5.94 (mg/g) at 3000 ppm from 12 hours to 60 hours. However, once surfactant adsorption reaches saturation, a maximum adsorption plateau indicates that further surfactant additions would not impact adsorption [65]. Due to their negative charge, SDS molecules were readily adsorbed when the concentration remained below the critical micelle concentration

(CMC). Subsequently, as surfactant concentrations surpassed 2500 ppm, the loss of surfactant increased because the molecules began to aggregate into micelles with other SDS molecules. This micellization hindered their adhesion to sand particles, explaining the lack of noticeable change in SDS adsorption values beyond 2500 ppm. This phenomenon emphasizes the influence of surfactant-free molecules on surfactant loss in the aqueous phase [68].

Before conducting the static adsorption test, the impact of adsorption time on adsorption density was examined to ensure experimental equilibrium. Different concentrations of SDS were studied concerning their adsorption density over a range of 12 to 60 hours. Figure 6.11 (a) depicts the relationship between SDS adsorption and time. Initially, SDS adsorption increased until it reached 36 hours of ageing time. Subsequently, there was a consistent plateau for 24 hours, indicating that the adsorption of SDS onto sand grains achieved equilibrium after 36 hours. The study investigated how different concentrations of SDS solutions interacted with sandstone rock in the presence of K-GO. Figure 6.11 (b) illustrates a substantial decrease in adsorption density at the same SDS solution concentration when introducing K-GO. For instance, the adsorption of 1000 ppm SDS dropped from 1.45 mg/g without K-GO to 0.97 mg/g (a 32% reduction) with the addition of 250 ppm K-GO. Similarly, the adsorption value decreased from 4.42 to 3.01 mg/g at the CMC in the presence of 250 ppm K-GO. This observation suggests that surfactant molecules prefer adsorption onto NPs rather than sand grains. Moreover, the retained NPs might act as a shield on the sand surface, leading to a significant decrease in surfactant adsorption. Additionally, it is noteworthy that beyond a concentration of 250 ppm, the impact of K-GO nanoparticles on limiting

SDS adsorption becomes insignificant. This behavior is due to the formation of aggregates at concentrations exceeding 250 ppm. [136]

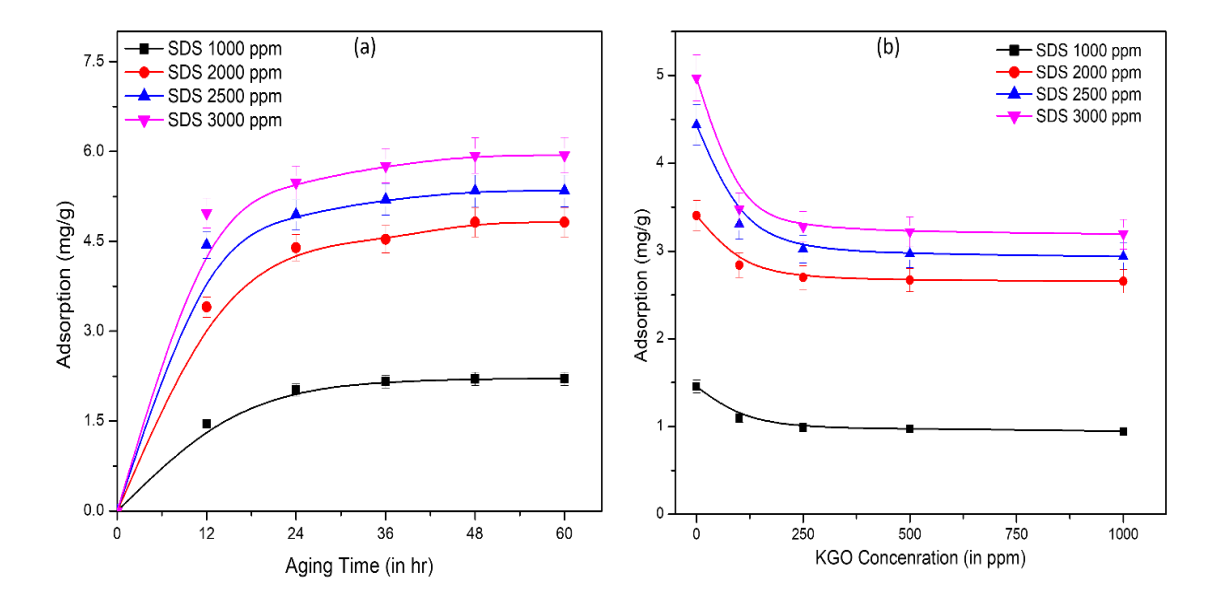


Figure 6. 11: Role of varying K-GO concentrations on the extent of adsorption, (a) at aging time, and (b) at varying K-GO concentrations at varying surfactant concentration.

6.3.10 Adsorption isotherm model of SDS on Sand surface

The data obtained from the adsorption process was analyzed using four commonly used adsorption models (Langmuir, Temkin, Freundlich, and Redlich-Peterson) to help understand the mechanisms and behavior of adsorption. [50], [53], [119], [120], [136]:. The Langmuir and Freundlich adsorption isotherm models are frequently employed to describe the equilibrium adsorption isotherm.

The Langmuir equation, formulated by Irving Langmuir in 1916 [61], establishes a relationship between the quantity of adsorbate that is adsorbed on a solid (q_{eq}) and the equilibrium concentration (C_{eq}) of the liquid at a specific temperature. The Langmuir adsorption model assumes that adsorption occurs as a monolayer phenomenon, where only one surfactant molecule can be adsorbed on each site [79]. It further assumes that all adsorption sites are identical and possess equal energy.

According to the Langmuir model, there is no interaction between adjacent adsorbed atoms [80]. The nonlinear form of the Langmuir model is represented below in equation (6.4).

$$q_{eq} = \frac{q_m C_{eq} k_l}{1 + k_l C_{eq}} \tag{6.4}$$

Where q_{eq} is the amount of absorbate adsorbed, q_m corresponds to the maximum amount adsorbed, k_l is the Langmuir constant, and C_{eq} is the equilibrium fluid concentration. The Langmuir isotherm model includes a significant parameter called R_l , a dimensionless constant known as the separation factor or equilibrium parameter [7], [61]. It can be expressed using the following equation (6.5).

$$R_{l} = \frac{1}{1 + k_{l}C_{i}} \tag{6.5}$$

Where C_i corresponds to the initial adsorbate concentration in the solution, the R_l parameter provides valuable indications regarding the compatibility of adsorption for a given adsorbant-adsorbate combination. There are four potential scenarios based on the value of R_l . When the R_l value is between 0 and 1, adsorption is advantageous. Meanwhile, adsorption is unfavorable if the R_l value is greater than 1. Subsequently, when the R_l value is equal to 1, it suggests a linear relationship in adsorption. On the other hand, if R_l equals 0, it implies that adsorption is irreversible. The mathematically fitted model of the Langmuir isotherm is shown in Figure 6.12 (a).

The Freundlich isotherms assume that the equilibrium concentration of the solute (C_{eq}) is raised to the power of 1/n to the amount of solute adsorbed (q_{eq}). This assumption considers the constant (K_f) to remain consistent at a given temperature [7], [10], [71], [79]. The equation (6.6) expressing this relationship is nonlinear.

$$q_{eq} = K_f C_{eq}^{-1/n} (6.6)$$

The Freundlich adsorption model involves two constants: K_f, which represents the sorption capacity, and n, which signifies the sorption intensity. The Freundlich isotherm is established based on the assumption of an exponentially decreasing distribution of sorption site energy. It further assumes that the adsorption of the surfactant takes place on a heterogeneous surface through multilayer sorption. The Freundlich constant (1/n) is associated with the adsorption intensity of the adsorbent. When the value of 1/n is between 0.1 and 0.5, it indicates favorable adsorption. If the value of 1/n is between 0.5 and 1, it suggests easy adsorption. On the other hand, if the value of 1/n is greater than 1, it indicates difficulty in adsorption [7], [61], [142], [245]. The fitted model of Freundlich isotherm is represented in Figure 6.12 (b)

The Temkin isotherm model, introduced by Tempkin and Pyzhev in 1940, describes the impact of the interaction between the adsorbate and adsorbing molecules. According to this model, the heat of adsorption for the surfactant molecules decreases linearly as the surface coverage area of the adsorbent increases. The model also suggests that adsorption involves gradually distributing binding energies among the molecules, reaching a maximum binding energy [246]. The Temkin isotherm model, expressed by the below-mentioned equation (6.7), was utilized to evaluate and interpret the adsorption data.

$$q_{eq} = \frac{RT}{h} \ln k_{t} + \frac{RT}{h} \ln C_{eq}$$
 (6.7)

In equation 6.7, b is the Temkin constant associated with the heat of sorption (J/mol), k_t is the equilibrium binding constant, which relates to the maximum binding energy (L/g). R signifies the gas constant with a value of 8.314 J/mol K, and T

represents the temperature in Kelvin (K). Figure 6.12 (c) demonstrates the application of the Temkin model for fitting adsorption data.

The Redlich-Peterson (R-P) isotherm is a mathematical model incorporating elements from the Langmuir and Freundlich isotherm models. It integrates essential ideas from both models and is defined by three parameters [10], [247], [248]. The adsorption mechanism is unique and does not adhere to the assumption of ideal monolayer adsorption. The experimental data gathered from an adsorption study of surfactant solutions at distinct concentrations were examined using the Redlich-Peterson model, as shown in Figure 6.12 (d). The mathematical expression of the R-P isotherm is illustrated in the equation (6.8) below.

$$q_{eq} = \frac{k_R C_{eq}}{1 + \alpha C_{eq}^{\beta}} \tag{6.8}$$

The linear form of the equation,

$$\ln(k_R \frac{C_{eq}}{q_{eq}} - 1) = \beta \ln C_{eq} + \ln \alpha$$
 (6.9)

In the Redlich-Peterson isotherm equation (6.8), k_R (L/mg) and α [(L/mg) $^{\beta}$] are the constants. The exponential constant β , which falls between 0 and 1, helps describe the behavior of the adsorption isotherm model. When β equals 1, the equation simplifies to the Langmuir model, while β equaling 0 reduces the equation to the linear isotherm model. Through the examination of various models in this article, it was noted that the Freundlich isotherm model displayed an excellent fit. The R^2 value and linear equation for all models are detailed in the provided Table 6.2.

Table 6. 2. The fitting parameters of the isotherm model

S. N	Isotherm Model & Parameters							
	Langmuir	Freundlich	Temkin	Redlich-Peterson				
1	$R^2 = 0.985$	$R^2 = 0.993$	$R^2 = 0.966$	$R^2 = 0.975$				
2	$K_1 = 729*10^{-6}$	$K_f = 2.547*10^{-3}$	$K_t = 2.07*10^{-3}$	$k_R = 0.00139$				
3	$Q_{m} = 6.41$	1/n = 0.93	$B_t=2.062$	$\alpha = 1.78*10^2$				

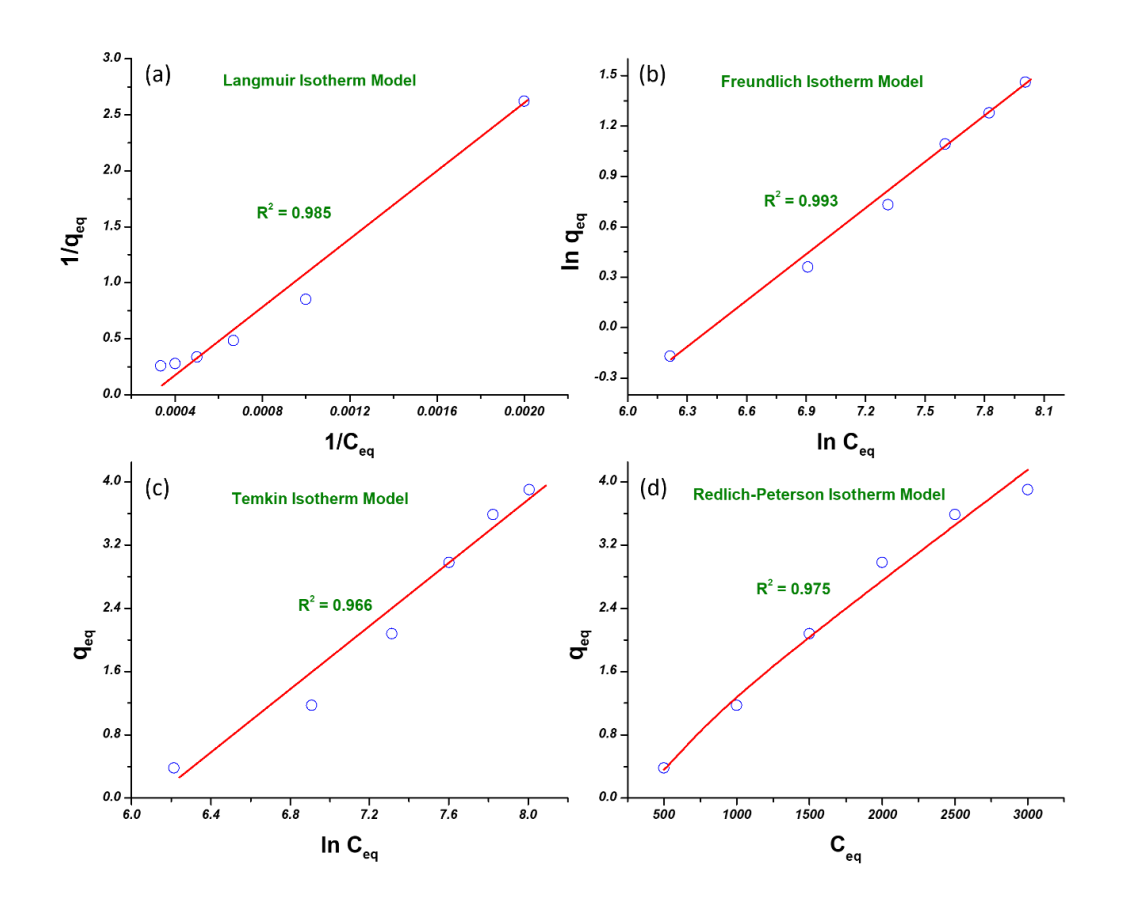


Figure 6. 12: Fitting curve of, (a) Langmuir, (b) Freundlich, (c) Temkin, and (d) Redlich-Peterson isotherm model.

6.3.11 Adsorption kinetics model

Adsorption, a physicochemical activity, includes the transfer of adsorbate from a liquid phase to the surface of an adsorbent. It is valuable to examine adsorption's kinetics to assess this process's effectiveness, which provides insights into the

underlying mechanism [10], [61]. The performed adsorption studies data of surfactants on sand particles was studied using two distinct models: the pseudo-first-order (pFO) kinetic Equation and the pseudo-second-order (pSO) equations (6.10 and 6.11).

The pFO kinetic model can be stated as [61], [137], [248], [249]:

$$\frac{dq_t}{dt} = K_{pFO}(q_e - q_t) \tag{6.10}$$

Simplified the above-mentioned equation after applying boundary conditions t=0 to t=1 t and $q_t=1$ to $q_t=1$, which gives:

$$-\ln(q_e - q_t) = \ln q_e + K_{pFO}t$$
 (6.11)

The provided equation describes the amount of surfactant adsorption on sand particles under two specific conditions. The parameter q_e signifies the degree of surfactant adsorption when the system reaches equilibrium. At the same time, q_t represents the amount of surfactant adsorption at any given time t, even during non-equilibrium states. K_{pFO} is the first-order rate constant; from the experimental data, the -ln $(q_e - q_t)$ values are computed and plotted against time (t), and the slope of this plot yields the value of K_{pFO} [137].

The pSO (pseudo-second order) kinetic model can be stated as [10], [137], [249]:

$$\frac{dq_t}{dt} = K_{pSO}(q_e - q_t)^2 \tag{6.12}$$

To simplify equation (6.12), implement boundary conditions t=0 to t=t and $q_t=0$ to $q_t=q_e$.

$$\frac{t}{q_t} = \frac{1}{K_{pSO}q_e^2} + \frac{t}{q_e} \tag{6.13}$$

Figure 6.13 illustrates the relationship between time (t) and the quantity t/q_t . K_{pSO} and q_e are estimated from the intercept and slope of the plot of t/q_t with t. Table

6.3 shows that the pSO kinetic model corresponds well to this study of surfactant adsorption at sand surfaces. The plot of the best fit is mentioned in Figure 6.13.

Table 6. 3. The SDS surfactant adsorption kinetics parameters on sand surfaces.

S.	Adsorption	Model Parameter	Surfactant Concentration +250 ppm K-GO					
N	Kinetics		1000 ppm 2000 ppi		2500 ppm	3000 ppm		
	model							
1	pFO	K_{pFO} (min $^{-1}$)	$2.4 * 10^{-3}$	$2.0 * 10^{-3}$	$2.3 * 10^{-3}$	$2.2 * 10^{-3}$		
	(Lagergren first	q_e (mg. g $^{-1}$)	0.4791	0.5352	0.5818	0.6034		
	order)	\mathbb{R}^2	0.923	0.928	0.931	0.918		
		APE (%)	1.720	2.047	2.104	2.064		
2	pSO	K_{pSO} (g.mg $^{-1}$.min $^{-1}$) q_e (mg. g $^{-1}$) R^2 APE (%)	8.12 *10 ⁻² 0.7384 0.996 0.799	9.94 *10 ⁻² 0.7639 0.998 0.649	7.90 *10 ⁻² 0.8611 0.995 0.627	7.77 *10 ⁻² 0.8903 0.992 0.683		

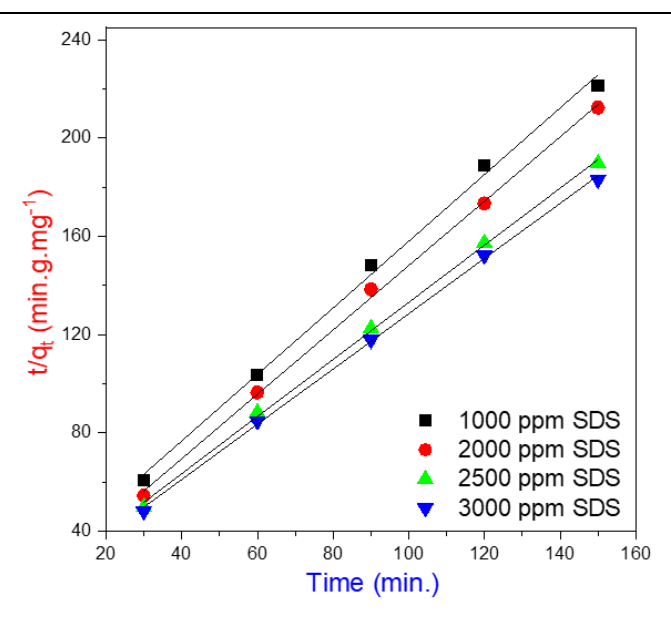


Figure 6. 13: The study of anionic surfactant adsorption (SDS) on sandstone revealed a pseudo-second order kinetics profile i.e., the best fit model.

6.3.12 Wettability modification

Wettability is the potential of a fluid to either spread over or adhere to a solid substrate when another immiscible fluid is present. Wettability is crucial in multi-phase flow and impacts reservoir factors like capillary pressure, relative permeability, and oil recovery efficiency [63]. Furthermore, wettability controls fluid movement, remaining oil saturation, and rock distribution [250]. Academic and industrial interests drive the ongoing and evolving area of research in wettability modification through chemical actions [251]. Therefore, changing the wettability is crucial for enhancing oil recovery from either oil-wet or intermediate-wet reservoirs. To understand the wetting attributes of the sand pallet surface were evaluated through the contact angle experiment. The wetting characteristics of the reservoir rock substantially influence the efficiency of pore-scale displacement in oil recovery. The evaluation of the wetting characteristics of rock-fluid interactions can be accomplished through the measurement of contact angles (CA). Various factors, such as the pH of the reservoir, the charge of the rock surface, salinity, the concentration of NPs (nanoparticles), the attachment of NPs to the rock surface, and the density of charge on the NP surface, all influence the condition of wettability [46], [122]. The wettability modification using surfactants occurs by creating ion pairs and their subsequent adsorption at the interface between oil, water, and rock. Conversely, disjoining pressure has been suggested as a potential explanation for transforming wettability from oil-wet to water-wet when exposed to a nanofluid. According to the disjoining pressure hypothesis, nanoparticles can alter wettability by causing a shift in the wetting properties when a wedge-like film develops at the boundary of oil, water, and rock surfaces [252]. The electrostatic, Van der Waals and structural forces between the nanoparticles in the wedge layer formed more structured arrangements than what was observed in the larger solution volume. The disjoining pressure increases with high nanoparticle concentrations and smaller sizes, resulting in a more potent effect. The organization of nanoparticles contributes to an overall dispersion where increased entropy enables the free movement of nanoparticles within

the liquid's bulk [252]. The contact angle of distilled water was initially found to be 113°, which was reduced to 99.8° when the contact time was extended from 0 seconds to 500 seconds, represented in Figure 6.14 (a). An observable reduction in the contact angle was noticed with an increase in surfactant concentration, dropping to 48° at a concentration of 2500 ppm. However, as the surfactant concentration continued to rise beyond this point, there was no significant alteration in the contact angle. This phenomenon can be elucidated by considering the saturation of the rock surface with surfactant [53], [253]. Upon the addition of K-GO to the solution's bulk phase containing an anionic surfactant concentration of 2500 ppm, a subsequent decrease in the observed contact angle was noted on the identical substrate. As the concentration of K-GO raised from 0 to 100, 250, 500, and 1000 ppm in a 2500 ppm SDS solution, the CA value on the sandstone surface progressively decreased from 48° to 44.1°, 40°, 38°, and 35° respectively, as indicated in Table 5.4. This decrement can be described through the adsorption of nanoparticles at the interface between solid and liquid phases [51], [254]. Similarly, varying results were observed with different surfaces. Specifically, on the positively charged carbonate surface, the contact angle diminished progressively from 55° to 49°, 45°, 43°, and 42° as the concentration of K-GO in the 2500 ppm surfactant solution increased from 0 ppm to 100, 250, 500, and 1000 ppm, respectively. Conversely, for the dolomite surface, the contact angles measured were 60°, 54°, 51°, 48°, and 45° at the corresponding concentrations, which is represented in Figure 6.14 (b).

Table 6. 4. Contact angle data for the different substrates with varying K-GO concentration

S. No	Surfactant concentration	Substrate	KGO concentration	Contact angle (degrees)		
	(ppm)		(ppm)	0 sec	500 sec	
1			0	48	41	
2		Sandstone	100	44.1	38	
3			250	40	35	
4			500	38	32	
5			1000	35	28	
6			0	55	48	
7		Carbonate	100	49	44	
8	2500		250	45	41	
9			500	43	37	
10			1000	42	35	
11			0	60	53	
12			100	54	49	
13		Dolomite	250	51	45	
14			500	48	42	
15			1000	45	38	

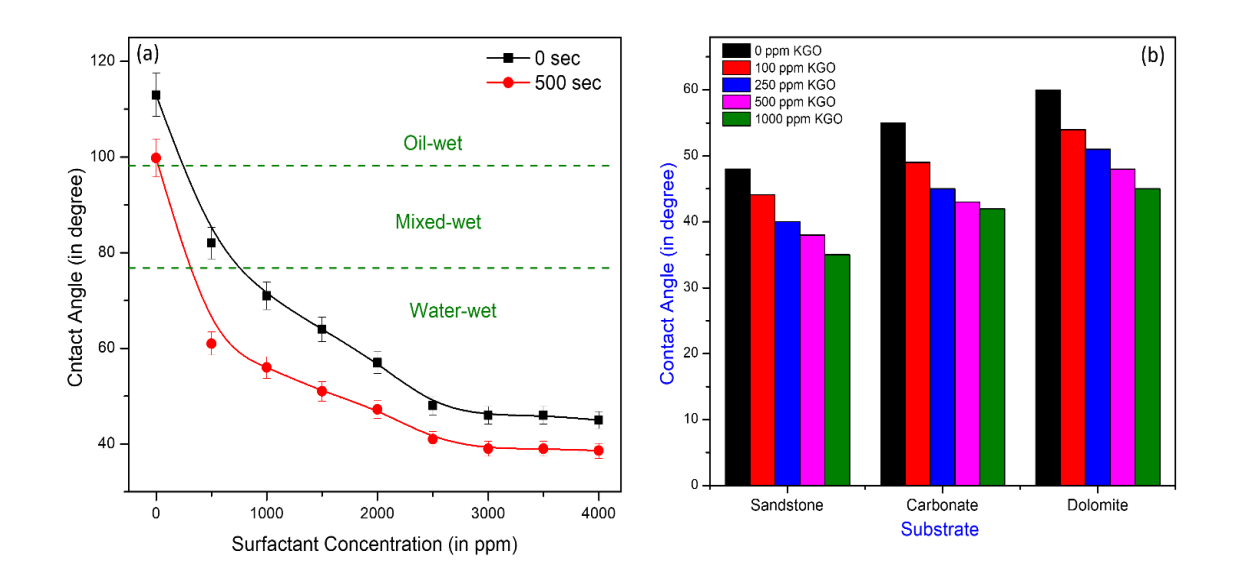


Figure 6. 14: Contact angle, (a) varying anionic surfactant concentration (SDS), and (b) varying K-GO concentration at CMC of anionic surfactant concentration at different surface.

6.3.13 Rheological Analysis

Rheology deals with how an applied external force alters fluid flow characteristics. Key rheological parameters are shear rate (γ) , indicating the rate of

shear strain change over time, shear stress (τ) as the tangential force per unit area, and viscosity (η) from their relationship. Fluids are Newtonian or non-Newtonian based on their response to shear force. Newtonian fluids demonstrate a linear shear stress and shear rate relationship, giving uniform viscosity independent of shear rate. Non-Newtonian fluids have variable shear stress and shear rate, causing their viscosity to change with the shear rate. Mathematical models like the power law (equation 6.14), Bingham plastic, Carreau (equation 6.15), Herschel–Buckley, and Casson models describe rheological behaviors. Appropriate model selection depends on parameter number, ease of use, and computational time to fit different fluids. Power law index values classify fluid types: n<1 indicates shear thinning, n>1 is Newtonian, and n=1 shows shear thickening. Evaluating these rheological properties is vital to predicting and controlling nanofluid flow through porous oil reservoirs.

$$\eta = k \gamma^{n-1} \tag{6.14}$$

$$\eta = \eta_o (1 + \alpha \gamma)^2)^{\frac{n-1}{2}}$$
(6.15)

The relationship between apparent viscosity (η), shear rate (γ), zero shear viscosity (η_0), relaxation time (α), consistency index (k), and power law index (n) define various fluid rheological behaviors seen in the oil and gas sector. Figure 6.16 demonstrates these different behaviors visually. The study investigated the rheological behavior of a chemical slug with a constant polymer and surfactant combination at shear rates between 0.01 and 1300 sec⁻¹. The flow characteristics of a solution can be influenced by the presence of nanoparticles, nanotubes, and nanosheets, which surfactants and polymers may influence. The nanoparticle's concentration, dimensions, and

morphology can affect the fluid's rheological behavior. The rheometer assessed the viscosity of the slurry, which had a consistent 1000 ppm polymer (PAM) and SDS at its CMC while having differing concentrations of K-GO. The slug's viscosity at a shear rate of 2 s⁻¹ rose from 45.49 mPa.s to 61.25 mPa.s when 100 ppm of K-GO was added, then further increased to 145.35 mPa.s, 200.5 mPa.s, and 240.1 mPa.s with the introduction of 250 ppm, 500 ppm, and 1000 ppm of K-GO, respectively, along with PAM (1000 ppm) and SDS (2500 ppm). The increasing trend in viscosity of the bulk solution with varying K-GO concentrations occurs because of solid particles within the slug, which causes greater friction between extended polymeric chains [12], [48], [68], [255]. Viscosity is crucial in the recovery process as it directly impacts the mobility ratio: higher viscosity reduces the mobility ratio, curbing viscous fingering and thereby boosting displacement efficiency [256]–[259]. As the shear rate escalated from 2 to 15.7, 166, and 400 s⁻¹, the viscosity of the solution decreased from 145.35 Pa.s to 47.93, 14.073, and 9.424 mPa.s, as shown in Figure 6.15. The viscosity data was mathematically analyzed to confirm the shear thinning characteristics. Figure 6.16 illustrates the results of this analysis, while Table 6.5 presents the corresponding parameter values obtained from the fitting process.

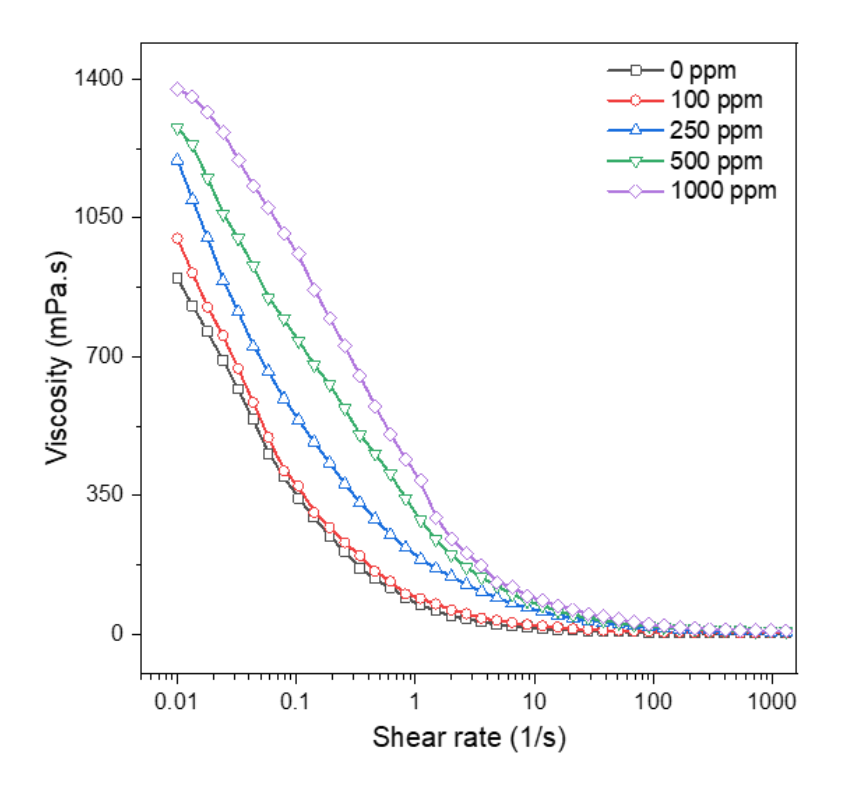


Figure 6. 15: The viscometry analysis of the K-GO with PAM (1000 ppm) and SDS (at 2500 ppm).

Table 6. 5. Mathematical model fitting of viscosity data

Surfactant	Polymer Conc. (ppm)	K- GO	Mathematical model						
Conc. (ppm)		Conc. (ppm)	Carreau Fitting				Power Law Fitting		
		11 /	η_0	α	n	\mathbb{R}^2	k	n	\mathbb{R}^2
	1000	0	953.7	55.65	0.406	0.991	111.6	0.528	0.989
		100	1090.3	67.58	0.438	0.993	122.7	0.529	0.992
2500		250	1339.1	92.60	0.582	0.998	212.8	0.615	0.995
		500	1247.8	34.57	0.588	0.992	312.5	0.671	0.978
		1000	1314.6	15.42	0.529	0.994	398.8	0.695	0.957

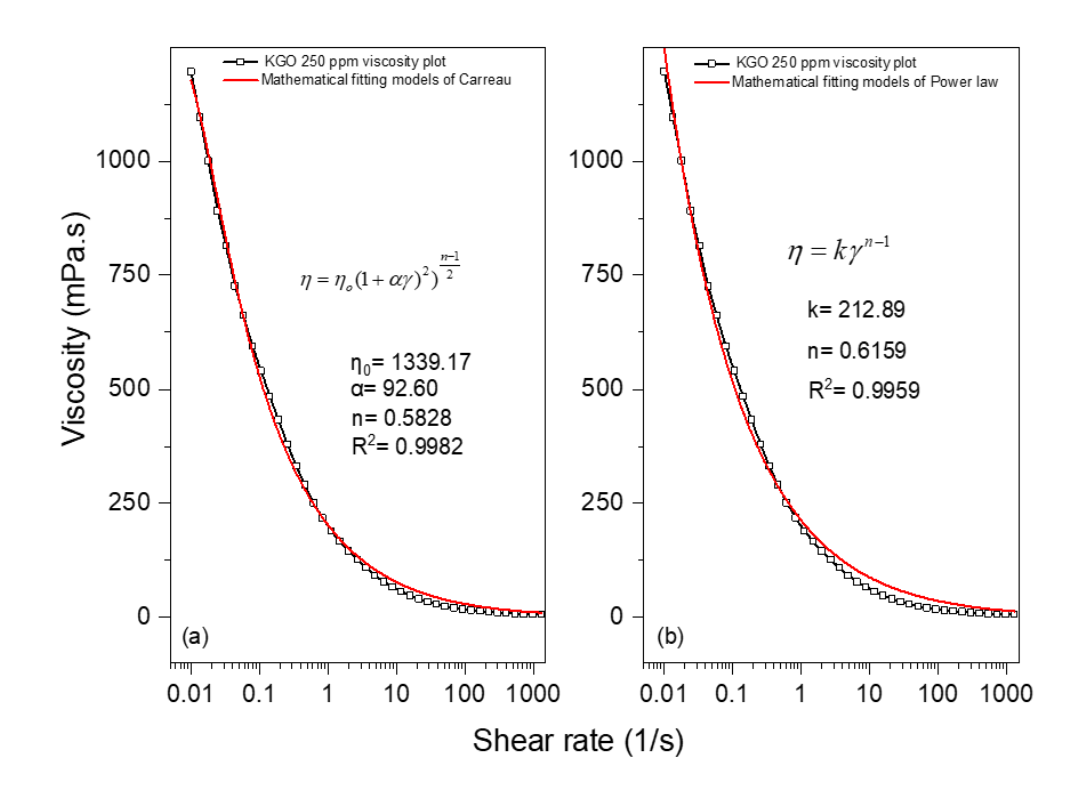


Figure 6. 16: The mathematical fitting of rheological data, (a) Carreau Model, (b) Power law model.

6.3.14 Recovery test

Oil displacement experiments utilized two core sets with varying porosity and gas permeability, as shown in Table 6.1. Six recovery trials were conducted, employing water, anionic surfactant, and a nanofluid blend (K+P+S). The selection of surfactant and nanofluid solutions, namely SDS for surfactant and K-GO + SDS + PAM for surfactant-polymer-assisted nanofluids, was based on prior investigations into adsorption, interfacial tension (IFT), and contact angle studies. The simultaneous actions of surfactants and polymers in the reservoir are interconnected, influencing the recovery factor together. Their activities interact, each impacting the other to different extents, creating a synergy that affects overall effectiveness. Multiple studies conducted by researchers have demonstrated the alignment between computational models and experimental investigations regarding this compatibility [5], [46], [95], [147], [260],

[261]. The experimental results of both sets of cores are shown in Figure 6.17, which shows how the percentage of total oil recovery varies with the volume of injected fluids, including water, SDS solution, and PAM + SDS + K-GO nanofluid. Uniform parameters such as injected fluid volume and flow rate were maintained in the flooding experiments. Approximately 1.8 fluid pore volumes (PV) were consistently injected into the core for all flooding tests. At first, water was injected into core ID-1, producing oil at another end of the core holder. In the early stages, there was a noticeable rise in oil production. However, after injecting 1.25 pore volumes (PV) of water, the increment in oil production became less significant. The recovery reached a maximum of ~ 28.2% after injecting water. A recovery of approximately 41% was attained through the core on injecting the SDS solution. However, introducing a solution having K-GO, SDS, and PAM resulted in a higher recovery of about 59% of the original oil in place (OOIP). In the case of core ID-2, oil recovery reached approximately 37.4% through water injection and about 50% through SDS injection alone. After injecting K-GO along with SDS and PAM, the oil retrieval reached approximately 67%, as shown in Figure 6.17, because the higher permeability of core ID-2 compared to core ID-1 led to superior recovery in the core ID-2. The enhanced effectiveness of the PAM + SDS + K-GO nanofluid is credited to the nanoparticles ability to reduce the surfactants' adsorption onto the rock formation notably.

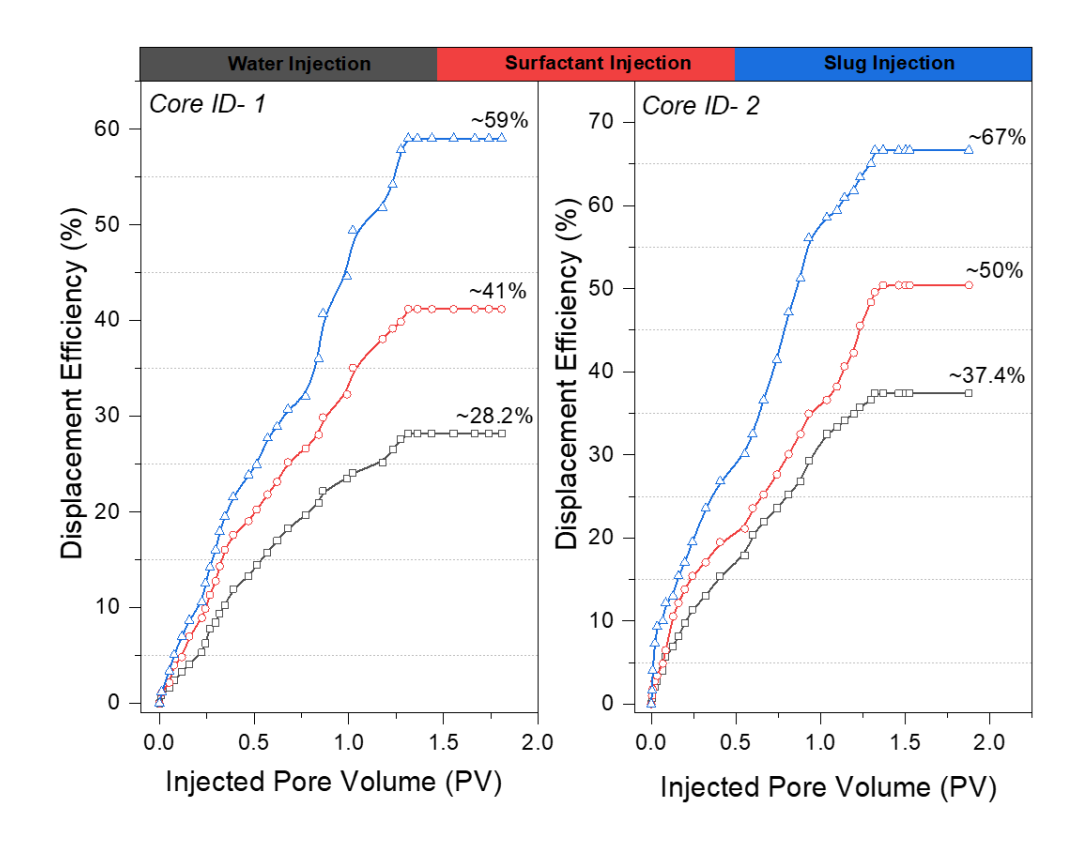


Figure 6. 17: The ultimate oil recovery using water, SDS and Nanofluid (K+S+P) injection for core ID-1&2.

6.4. Conclusion

This study presents an eco-friendly method to synthesize potassium-doped graphene oxide (K-GO) from agricultural waste biomass. The synthesized K-GO was successfully combined with surfactants to produce nanofluids with tunable surface activity. The optimal nanofluid, containing K-GO and anionic SDS surfactant, exhibited significant reductions in surface tension, interfacial tension with crude oil (up to 40%), and surfactant adsorption loss (up to 32%), as well as improved wettability alteration. The synergistic interactions between K-GO and surfactants provide mechanistic insights and enable enhanced oil recovery performance that is unachievable with surfactants alone.

7.1. Conclusions

This chapter presents a detailed conclusion of the extensive experiments conducted to complete various manuscripts throughout the project. The specific findings and conclusions of this research program are presented as follows:

- ❖ The issue of surfactant loss in the EOR process was significantly mitigated with the introduction of silicon carbide nanoparticles (SCN). Initially, surfactant adsorption was approximately 19.31 mg/g onto the sand surface. However, incorporating 200 ppm SCN into the solution reduced this adsorption to around 10.63 mg/g, resulting in a 44% decrease in surfactant loss at 30°C. When the temperature was increased to 50°C and 70°C, the reduction in surfactant loss also improved by ~17% and 33% compared to the 30°C baseline, respectively. Additionally, adding 200 ppm SCN to the surfactant solution decreased the anionic surfactant's critical micelle concentration (CMC) by 14%.
- ❖ Next, the study investigated using modified multi-walled carbon nanotubes (mMWCNT) in EOR. These mMWCNTs were tested both with and without an anionic surfactant, which helps to lower surface tension and IFT and alters the wetting properties of the rock surface. At the optimal concentration, mMWCNTs reduced surface tension by approximately 59% and decreased IFT by about 55% (using 100 ppm

mMWCNT combined with the CMC of the anionic surfactant). Additionally, mMWCNTs decreased surfactant loss by roughly 49% and changed the rock surface's wettability, facilitating oil mobilization from the reservoir. The optimum concentration (100 ppm) of mMWCNTs was combined with SDS at its CMC and 1000 ppm of polyacrylamide (PAM) to form a slug used for oil recovery. This combination resulted in a 70% oil recovery.

Next, the application of waste plastic-derived reduced graphene oxide (RGO) nanosheet was investigated. RGO synthesized from plastic waste was a potential additive for the surfactant-polymer (SP) chemical slug. The addition of **RGO** not only lowered the CMC of the surfactant but also reduced the surface tension of the solution. The effect of **RGO** was studied with different types of surfactants and varying concentrations. Initially, adding **RGO** alone led to a 25% reduction in surface tension and a 20% decrease in contact angle. When combined with surfactants (anionic, cationic, and nonionic), RGO resulted in approximately 55%, 57%, and 57% reductions in surface tension, respectively. Additionally, the reduction in contact angle with **RGO** and surfactants (anionic, cationic, and nonionic) was around 83%, 46%, and 80%, respectively. Finally, oil recovery tests were conducted using the best-performing combination of anionic surfactant and RGO in the presence of polymer, achieving approximately 71% oil recovery through sand pack flooding procedures.

❖ Finally, K-GO were synthesized from agricultural waste to be used as an additive for the SP chemical slug. These K-GO were produced in the lab and characterized through FTIR, XRD, Raman, and UV techniques. When combined with the surfactant solution, K-GO reduced the IFT by approximately 40%. The synergy between K-GO and surfactant molecules was also evident in wettability analysis and surfactant adsorption studies. Incorporating K-GO with the surfactant polymer slug resulted in the recovery of approximately 59% and 67% from core id-1 and core id-2, respectively, indicating that the use of K-GO with surfactants in enhanced oil recovery (EOR) can be further explored.

Incorporating nanoparticles such as SCN, mMWCNT, RGO, and K-GO into surfactant-polymer slugs significantly reduces surfactant loss, enhances oil mobilization, and improves oil recovery. These materials exhibit considerable potential for improving the efficiency of EOR processes, especially when combined with surfactants and polymers.

7.2. Potential Areas for Future Study

The research was carried out entirely through laboratory experiments, utilizing additives synthesized on a small scale in the lab with analytical-grade chemicals. This method of synthesis is not cost-effective. Before these additives can be widely applied, it is crucial to conduct molecular simulation studies to gain a comprehensive understanding of their behavior at the molecular level under conditions that closely resemble the actual subsurface environment. Such simulations are essential because they allow researchers to predict the interactions of additives with various fluid and solid phases in the reservoir, including their adsorption, diffusion, and potential

reactivity with reservoir minerals or hydrocarbons. These studies can also provide insights into the efficiency of additives in enhancing oil recovery or improving the mobility of injected fluids, which are critical for optimizing field applications. Furthermore, a significant limitation in current research is the frequent use of homogeneous and uniform porous media for laboratory experiments, which fail to accurately reflect the complex and heterogeneous nature of real reservoir formations. Field conditions often involve variable porosity, permeability, and wettability, with the presence of fractures, clay content, and mineral heterogeneity, all of which influence the flow and distribution of fluids. Therefore, it is essential to extend studies beyond simplified laboratory setups and employ more representative porous media models to evaluate the true potential and limitations of these additives under realistic conditions. This would lead to a more reliable prediction of their performance in field applications and help in designing more effective reservoir management strategies. To better understand the effects of different lithologies, it is recommended that porous media composed of particles of varying sizes and types be investigated. Future studies should also consider using reservoir core samples to better mimic actual reservoir conditions.

Moreover, the chemicals synthesized in this study were produced on a lab scale, which is not economical. For broader applications, developing a cost-effective synthesis process using commercial-grade chemicals is necessary. This approach will help explore the broader applicability of this study.

References

- [1] S. M. Farouq Ali and S. Thomas, "The promise and problems of enhanced oil recovery methods," *J. Can. Pet. Technol.*, vol. 35, no. 7, pp. 57–63, 1996, doi: 10.2118/96-07-07.
- [2] H. Schott, "Hydrophilic-Lipophilic Balance, Solubility Parameter, and Oil-Water Partition Coefficient as Universal Parameters of Nonionic Surfactants," pp. 1215–1222, 1995.
- [3] Yuji Yamashita and Kazutami Sakamoto, "Hydrophilic–lipophilic balance (hlb): classical indexation and novel indexation of surfactant," vol. 1, pp. 570–574, 2016.
- [4] Abillon. O, Binks. P. B, Otero. C, "Wlnsor Microemulsions with Cationic Surfactants: Structure 0.," no. 3, pp. 4411–4416, 1988.
- [5] E. D. Goddard, "Polymer/surfactant interaction: Interfacial aspects," *J. Colloid Interface Sci.*, vol. 256, no. 1, pp. 228–235, 2002, doi: 10.1006/jcis.2001.8066.
- [6] G. Klein, "Principles of adsorption and adsorption processes," *Reactive Polymers, Ion Exchangers, Sorbents*, vol. 4, no. 1. p. 62, 1985, doi: 10.1016/0167-6989(85)90037-6.
- [7] M. A. Ahmadi and S. R. Shadizadeh, "Adsorption of Novel Nonionic Surfactant and Particles Mixture in Carbonates: Enhanced Oil Recovery Implication," 2012.
- [8] M. A. Ahmadi and S. R. Shadizadeh, "Induced effect of adding nano silica on adsorption of a natural surfactant onto sandstone rock: Experimental and

- theoretical study," *J. Pet. Sci. Eng.*, vol. 112, pp. 239–247, 2013, doi: 10.1016/j.petrol.2013.11.010.
- [9] M. Zargartalebi, N. Barati, and R. Kharrat, "Influences of hydrophilic and hydrophobic silica nanoparticles on anionic surfactant properties: Interfacial and adsorption behaviors," *J. Pet. Sci. Eng.*, vol. 119, pp. 36–43, 2014, doi: 10.1016/j.petrol.2014.04.010.
- [10] N. Saxena, A. Kumar, and A. Mandal, "Adsorption analysis of natural anionic surfactant for enhanced oil recovery: The role of mineralogy, salinity, alkalinity and nanoparticles," *J. Pet. Sci. Eng.*, vol. 173, pp. 1264–1283, 2019, doi: 10.1016/j.petrol.2018.11.002.
- [11] M. Y. Rezk and N. K. Allam, "Impact of Nanotechnology on Enhanced Oil Recovery: A Mini- Review," 2019, doi: 10.1021/acs.iecr.9b03693.
- [12] H. Rezvani, M. Riazi, M. Tabaei, Y. Kazemzadeh, and M. Sharifi, "Experimental Investigation of Interfacial Properties in the EOR Mechanisms by the Novel Synthesized Fe3O4@Chitosan Nanocomposites Authors:," *Colloids Surfaces A Physicochem. Eng. Asp.*, 2018, doi: 10.1016/j.colsurfa.2018.02.012.
- [13] H. Ehtesabi, M. M. Ahadian, and V. Taghikhani, "Enhanced Heavy Oil Recovery Using TiO 2 Nanoparticles: Investigation of Deposition during Transport in Core Plug," 2015, doi: 10.1021/ef5015605.
- [14] J. Cesar, C. Venancio, R. Sandra, V. Nascimento, and A. Pérez-gramatges, "Colloidal stability and dynamic adsorption behavior of nano fl uids containing

- alkyl-modi fi ed silica nanoparticles and anionic surfactant," vol. 308, 2020, doi: 10.1016/j.molliq.2020.113079.
- [15] Y. Wu *et al.*, "Reducing surfactant adsorption on rock by silica nanoparticles for enhanced oil recovery," *J. Pet. Sci. Eng.*, vol. 153, pp. 283–287, 2017, doi: 10.1016/j.petrol.2017.04.015.
- [16] N. Yekeen, E. Padmanabhan, and A. Kamal, "Journal of Petroleum Science and Engineering Synergistic e ff ects of nanoparticles and surfactants on n-decane-water interfacial tension and bulk foam stability at high temperature," *J. Pet. Sci. Eng.*, vol. 179, no. May, pp. 814–830, 2019, doi: 10.1016/j.petrol.2019.04.109.
- [17] A. M. Munshi *et al.*, "Effect of nanoparticle size on sessile droplet contact angle Effect of nanoparticle size on sessile droplet contact angle," vol. 084315, no. 2008, pp. 10–15, 2014, doi: 10.1063/1.2912464.
- [18] F. Ravera, E. Santini, G. Loglio, M. Ferrari, and L. Liggieri, "Effect of Nanoparticles on the Interfacial Properties of Liquid / Liquid and Liquid / Air Surface Layers," pp. 19543–19551, 2006.
- [19] B. A. Suleimanov, F. S. Ismailov, and E. F. Veliyev, "Journal of Petroleum Science and Engineering Nano fl uid for enhanced oil recovery," vol. 78, pp. 431–437, 2011, doi: 10.1016/j.petrol.2011.06.014.
- [20] R. Ponnapati, O. Karazincir, E. Dao, R. Ng, K. K. Mohanty, and R. Krishnamoorti, "Polymer-Functionalized Nanoparticles for Improving Waterflood Sweep Efficiency: Characterization and Transport Properties," pp.

- 13030-13036, 2011.
- [21] W. Pu *et al.*, "Water-Soluble Core Shell Hyperbranched Polymers for Enhanced Oil Recovery," 2015, doi: 10.1021/ie5039693.
- [22] N. K. Maurya, P. Kushwaha, and A. Mandal, "Studies on interfacial and rheological properties of water soluble polymer grafted nanoparticle for application in enhanced oil recovery," *J. Taiwan Inst. Chem. Eng.*, vol. 70, pp. 319–330, 2016, doi: 10.1016/j.jtice.2016.10.021.
- [23] Y. Cheng, M. Zhao, C. Zheng, S. Guo, X. Li, and Z. Zhang, "Water-Dispersible Reactive Nanosilica and Poly (2-acrylamido-2- methyl-1-propanesulfonic acid sodium) Nanohybrid as Potential Oil Displacement Agent for Enhanced Oil Recovery," 2017, doi: 10.1021/acs.energyfuels.7b00743.
- [24] C. Zheng, Y. Cheng, Q. Wei, X. Li, and Z. Zhang, "Suspension of surface-modi fi ed nano-SiO 2 in partially hydrolyzed aqueous solution of polyacrylamide for enhanced oil recovery," *Colloids Surfaces A*, vol. 524, no. February, pp. 169–177, 2017, doi: 10.1016/j.colsurfa.2017.04.026.
- [25] H. Yousefvand and A. Jafari, "Enhanced Oil Recovery Using Polymer/nanosilica," *Procedia Mater. Sci.*, vol. 11, no. 2010, pp. 565–570, 2015, doi: 10.1016/j.mspro.2015.11.068.
- [26] A. Maghzi, A. Mohebbi, and R. Kharrat, "Pore-Scale Monitoring of Wettability Alteration by Silica Nanoparticles During Polymer Flooding to Heavy Oil in a Five-Spot Glass Micromodel," pp. 653–664, 2011, doi: 10.1007/s11242-010-

9696-3.

- [27] Z. F. Nanjun Lai, Wu Tao, Ye Zhongbin, Zhang Yan, Zhou Nng, "Hybr i d Hyperbranched Po I ymer Based on Mod ifi ed Nano-S i O 2 f or Enhanced O il Recovery," pp. 1189–1191, 2016, doi: 10.1246/cl.160554.
- [28] K. Yang-chuan, W. Guang-yao, and W. Yi, "Preparation, morphology and properties of nanocomposites of polyacrylamide copolymers with monodisperse silica," vol. 44, pp. 2448–2457, 2008, doi: 10.1016/j.eurpolymj.2008.06.007.
- [29] Z. Ye, X. Qin, N. Lai, Q. Peng, X. Li, and C. Li, "Synthesis and Performance of an Acrylamide Copolymer Containing Nano-SiO 2 as Enhanced Oil Recovery Chemical," vol. 2013, 2013.
- [30] R. Liu, W. Pu, and D. Du, "Synthesis and characterization of core-shell associative polymer that prepared by oilfield formation water for chemical flooding," *J. Ind. Eng. Chem.*, 2016, doi: 10.1016/j.jiec.2016.10.018.
- [31] R. Liu, W. Pu, J. J. Sheng, and D. Du, "Star-like hydrophobically associative polyacrylamide for enhanced oil recovery: Comprehensive properties in harsh reservoir conditions," *J. Taiwan Inst. Chem. Eng.*, vol. 0, pp. 1–11, 2017, doi: 10.1016/j.jtice.2017.08.043.
- [32] A. Behzadi and A. Mohammadi, "Environmentally responsive surface-modified silica nanoparticles for enhanced oil recovery," *J. Nanoparticle Res.*, vol. 18, no. 9, p. 266, 2016, doi: 10.1007/s11051-016-3580-1.
- [33] G. Cheraghian, "Effect of nano titanium dioxide on heavy oil recovery during

- polymer flooding," *Pet. Sci. Technol.*, vol. 34, no. 7, pp. 633–641, 2016, doi: 10.1080/10916466.2016.1156125.
- [34] A. Rezaei, M. Abdi, A. Mohebbi, A. Tatar, and A. H. Mohammadi, "Using surface modified clay nanoparticles to improve rheological behavior of Hydrolyzed Polyacrylamide (HPAM) solution for enhanced oil recovery with polymer flooding," *J. Mol. Liq.*, 2016, doi: 10.1016/j.molliq.2016.08.004.
- [35] Y. Assef, P. Pourafshary, and H. Hejazi, "Controlling Interactions of Colloidal Particles and Porous Media During Low Salinity Water Flooding and Alkaline Flooding By MgO Nanoparticles," 2016.
- [36] S. Li and O. Torsæter, "The Impact of Nanoparticles Adsorption and Transport on Wettability Alteration of Water Wet Berea Sandstone Adsorption and Transport of Nanoparticles inside Porous Medium," pp. 1–11, 2015.
- [37] M. Y. Rezk and N. K. Allam, "Unveiling the Synergistic Effect of ZnO Nanoparticles and Surfactant Colloids for Enhanced Oil Recovery," *Colloids Interface Sci. Commun.*, vol. 29, no. December 2018, pp. 33–39, 2019, doi: 10.1016/j.colcom.2019.01.004.
- [38] T. T. Huang, B. Hughes, D. E. Clark, and C. Nrg, "Enhancing Oil Recovery With Specialized Nanoparticles by Controlling Formation- Fines Migration at Their Sources in Waterflooding Reservoirs," no. August, pp. 743–746, 2015.
- [39] Y. Kazemzadeh, M. R. Malayeri, M. Riazi, and R. Parsaei, "Journal of Natural Gas Science and Engineering Impact of Fe 3 O 4 nanoparticles on asphaltene precipitation during CO 2 injection," *J. Nat. Gas Sci. Eng.*, vol. 22, pp. 227–

- 234, 2015, doi: 10.1016/j.jngse.2014.11.033.
- [40] J. H. Greff and T. Babadagli, "SPE 146604 Catalytic Effects of Nano-Size Metal Ions in Breaking Asphaltene Molecules During Thermal Recovery of Heavy-Oil," 2011.
- [41] J. T. Cie, Ğ. Ĕ, and K. Krygier, "IN WATER-Al2O3, WATER-TiO2 AND WATER-Cu NANOFLUIDS," vol. 01012, pp. 1–9, 2014.
- [42] M. Zhao et al., Study on the synergy between silica nanoparticles and surfactants for enhanced oil recovery during spontaneous imbibition, no. 2017. Elsevier B.V, 2018.
- [43] B. A. Suleimanov, F. S. Ismailov, and E. F. Veliyev, "Nanofluid for enhanced oil recovery," *J. Pet. Sci. Eng.*, vol. 78, no. 2, pp. 431–437, 2011, doi: 10.1016/j.petrol.2011.06.014.
- [44] J. Giraldo, P. Benjumea, S. Lopera, F. B. Corte, and M. A. Ruiz, "Wettability Alteration of Sandstone Cores by Alumina-Based Nano fl uids," 2013.
- [45] M. Mohajeri and M. Hemmati, "An experimental study on using a nanosurfactant in an EOR process of heavy oil in a fractured micromodel," *J. Pet. Sci. Eng.*, vol. 126, pp. 162–173, 2015, doi: 10.1016/j.petrol.2014.11.012.
- [46] A. Pandey, S. Feraz, S. Das, S. Basu, and H. Kesarwani, "Advanced multi-wall carbon nanotube-optimized surfactant-polymer flooding for enhanced oil recovery," *Fuel*, vol. 355, no. August 2023, p. 129463, 2024, doi: 10.1016/j.fuel.2023.129463.
- [47] W. B. Cox, "an Analysis of Co2 Injection At Citronelle Oil Field," *Dep. Chem.*

- Biol. Eng. Grad. Sch. Univ. Alabama TUSCALOOSA, vol. 53, no. 9, pp. 1689–1699, 2019.
- [48] H. Kesarwani, V. Srivastava, A. Mandal, S. Sharma, and A. Choubey Kumar, "Application of α-MnO2 nanoparticles for residual oil mobilization through surfactant polymer flooding," *Environ. Sci. Pollut. Res.*, 2022, doi: 10.1007/s11356-022-19009-0.
- [49] H. Kesarwani, F. Khan, A. Tandon, R. Azin, S. Osfouri, and S. Sharma, "Performance Improvement of the Surfactant Polymer Flooding Using Bio Synthesized Calcium Carbonate Nanoparticles: An Experimental Approach," *Arab. J. Sci. Eng.*, pp. 1–18, Jan. 2022, doi: 10.1007/S13369-022-06571-5.
- [50] H. Kesarwani, A. Saxena, A. Mandal, and S. Sharma, "Anionic/nonionic surfactant mixture for enhanced oil recovery through the investigation of adsorption, interfacial, rheological, and rock wetting characteristics," *Energy and Fuels*, vol. 35, no. 4, pp. 3065–3078, 2021, doi: 10.1021/acs.energyfuels.0c03767.
- [51] A. Gupta, A. Pandey, H. Kesarwani, S. Sharma, and A. Saxena, "Automated determination of interfacial tension and contact angle using computer vision for oil field applications," *J. Pet. Explor. Prod. Technol.*, no. 0123456789, 2021, doi: 10.1007/s13202-021-01398-6.
- [52] P. Druetta and F. Picchioni, "Surfactant flooding: The influence of the physical properties on the recovery efficiency," *Petroleum*, vol. 6, no. 2, pp. 149–162, 2020, doi: 10.1016/j.petlm.2019.07.001.

- [53] H. Kesarwani, A. Saxena, N. Saxena, and S. Sharma, "Oil Mobilization Potential of a Novel Anionic Karanj Oil Surfactant: Interfacial, Wetting Characteristic, Adsorption, and Oil Recovery Studies," *Energy and Fuels*, vol. 35, no. 13, pp. 10597–10610, 2021, doi: 10.1021/acs.energyfuels.1c01327.
- [54] H. S. Al-Hashim, V. Obiora, H. Y. Al-Yousef, F. Fernandez, and W. Nofal, "Alkaline surfactant polymer formulation for carbonate reservoirs," *Pet. Sci. Technol.*, vol. 23, no. 5–6, pp. 723–746, 2005, doi: 10.1081/LFT-200033098.
- [55] J. Wang, M. Han, A. B. Fuseni, and D. Cao, "Surfactant adsorption in Surfactant-Polymer flooding for carbonate reservoirs," SPE Middle East Oil Gas Show Conf. MEOS, Proc., vol. 2015-Janua, pp. 1736–1746, 2015, doi: 10.2118/172700-ms.
- [56] P. Lorenz, D. P.-O. and G. Journal; (USA), and undefined 1989, "Guidelines help select reservoirs for NaHCO/sub 3/EOR," *osti.gov*, Accessed: Sep. 14, 2021. [Online]. Available: https://www.osti.gov/biblio/5459473.
- [57] R. Suresh, O. Kuznetsov, D. Agrawal, Q. Darugar, and V. Khabashesku, "Reduction of surfactant adsorption in porous media using silica nanoparticles," *Proc. Annu. Offshore Technol. Conf.*, vol. 2, pp. 984–992, 2018, doi: 10.4043/28879-ms.
- [58] M. Beg, H. Kesarwani, and S. Sharma, "Effect of CuO and ZnO nanoparticles on efficacy of poly 4-styrenesulfonic acid-co-maleic acid sodium salt for controlling HPHT filtration," in *Society of Petroleum Engineers Abu Dhabi International Petroleum Exhibition and Conference 2019*, ADIPEC 2019, 2019, pp. 1–11, doi: 10.2118/197703-ms.

- [59] M. Beg, H. Kesarwani, S. Sharma, and A. Saxena, "Impact of low-molecular-weight poly(4-styrenesulfonic acid-co-maleic acid) sodium salt on filtration and rheological parameters of nanoparticles-enhanced drilling fluid," *J. Vinyl Addit. Technol.*, vol. 28, pp. 125–139, 2022, doi: 10.1002/vnl.21873.
- [60] R. A. Andrievski, "Synthesis, structure and properties of nanosized silicon carbide," *Rev. Adv. Mater. Sci.*, vol. 22, no. 1–2, pp. 1–20, 2009.
- [61] A. Bera, T. Kumar, K. Ojha, and A. Mandal, "Adsorption of surfactants on sand surface in enhanced oil recovery: Isotherms, kinetics and thermodynamic studies," *Appl. Surf. Sci.*, vol. 284, pp. 87–99, 2013, doi: 10.1016/j.apsusc.2013.07.029.
- [62] A. B. Fuseni, B. H. Al-Zahrani, and A. M. AlSofi, "Critical micelle concentration of different classes of EOR surfactants under representative field conditions," *Soc. Pet. Eng. SPE Kingdom Saudi Arab. Annu. Tech. Symp. Exhib.* 2017, pp. 404–411, 2017, doi: 10.2118/188011-ms.
- [63] M. Almahfood and B. Bai, "The synergistic effects of nanoparticle-surfactant nanofluids in EOR applications," *J. Pet. Sci. Eng.*, vol. 171, no. March, pp. 196–210, 2018, doi: 10.1016/j.petrol.2018.07.030.
- [64] M. A. Ahmadi and J. Sheng, "Performance improvement of ionic surfactant flooding in carbonate rock samples by use of nanoparticles," *Pet. Sci.*, vol. 13, no. 4, pp. 725–736, 2016, doi: 10.1007/s12182-016-0109-2.
- [65] K. Rahimi and M. Adibifard, "Experimental study of the nanoparticles effect on surfactant absorption and oil recovery in one of the Iranian oil reservoirs,"

- *Pet. Sci. Technol.*, vol. 33, no. 1, pp. 79–85, 2015, doi: 10.1080/10916466.2014.950382.
- [66] I. Khan, K. Saeed, and I. Khan, "Nanoparticles: Properties, applications and toxicities," *Arab. J. Chem.*, vol. 12, no. 7, pp. 908–931, 2019, doi: 10.1016/j.arabjc.2017.05.011.
- [67] M. Larsson, A. Hill, and J. Duffy, "Suspension stability: Why particle size, zeta potential and rheology are important Product Technical Specialists Rheometry Products Malvern Instruments Limited," *Annu. Trans. Nord. Rheol. Soc.*, no. 1988, p. 1999, 2012.
- [68] H. Kesarwani, S. Sharma, and A. Mandal, "Application of Novel Colloidal Silica Nanoparticles in the Reduction of Adsorption of Surfactant and Improvement of Oil Recovery Using Surfactant Polymer Flooding," ACS Omega, vol. 6, no. 17, pp. 11327–11339, 2021, doi: 10.1021/acsomega.1c00296.
- [69] M. Eftekhari, K. Schwarzenberger, A. Javadi, and K. Eckert, "The influence of negatively charged silica nanoparticles on the surface properties of anionic surfactants: Electrostatic repulsion or the effect of ionic strength?," *Phys. Chem. Chem. Phys.*, vol. 22, no. 4, pp. 2238–2248, 2020, doi: 10.1039/c9cp05475h.
- [70] L. Tennouga, A. Mansri, K. Medjahed, A. Chetouani, and I. Warad, "The micelle formation of cationic and anionic surfactants in aqueous medium: Determination of CMC and thermodynamic parameters at different temperatures," *J. Mater. Environ. Sci.*, vol. 6, no. 10, pp. 2711–2716, 2015.

- [71] C. T. Q. Dang, Z. Chen, N. T. B. Nguyen, W. Bae, and T. H. Phung, "Development of isotherm polymer/surfactant adsorption models in chemical flooding," *Soc. Pet. Eng. SPE Asia Pacific Oil Gas Conf. Exhib. 2011*, vol. 2, pp. 1562–1571, 2011, doi: 10.2118/147872-ms.
- [72] S. Paria and K. C. Khilar, "A review on experimental studies of surfactant adsorption at the hydrophilic solid-water interface," *Adv. Colloid Interface Sci.*, vol. 110, no. 3, pp. 75–95, 2004, doi: 10.1016/j.cis.2004.03.001.
- [73] P. Somasundaran and L. Huang, "Adsorption/aggregation of surfactants and their mixtures at solid-liquid interfaces," *Adv. Colloid Interface Sci.*, vol. 88, no. 1–2, pp. 179–208, 2000, doi: 10.1016/S0001-8686(00)00044-0.
- [74] X. Wu, E. Sacher, and M. Meunier, "The effects of hydrogen bonds on the adhesion of inorganic oxide particles on hydrophilic silicon surfaces," *J. Appl. Phys.*, vol. 86, no. 3, pp. 1744–1748, 1999, doi: 10.1063/1.370956.
- [75] B. Bharti, J. Meissner, U. Gasser, and G. H. Findenegg, "Surfactant adsorption and aggregate structure at silica nanoparticles: Effects of particle size and surface modification," *Soft Matter*, vol. 8, no. 24, pp. 6573–6581, 2012, doi: 10.1039/c2sm25648g.
- [76] B. P. Singh, J. Jena, L. Besra, and S. Bhattacharjee, "Dispersion of nano-silicon carbide (SiC) powder in aqueous suspensions," *J. Nanoparticle Res.*, vol. 9, no. 5, pp. 797–806, 2007, doi: 10.1007/s11051-006-9121-6.
- [77] A. F. Belhaj, K. A. Elraies, S. M. Mahmood, N. N. Zulkifli, S. Akbari, and O.S. E. Hussien, "The effect of surfactant concentration, salinity, temperature,

- and pH on surfactant adsorption for chemical enhanced oil recovery: a review," *J. Pet. Explor. Prod. Technol.*, vol. 10, no. 1, pp. 125–137, 2020, doi: 10.1007/s13202-019-0685-y.
- [78] V. M. Ziegler and L. L. Handy, "Effect of temperature on Surfactant Adsorption in Porous Media," *Soc. Pet. Eng. J.*, vol. 21, no. 02, pp. 218–228, 1981, doi: 10.2118/8264-PA.
- [79] J. Wang and X. Guo, "Adsorption isotherm models: Classification, physical meaning, application and solving method," *Chemosphere*, vol. 258, p. 127279, 2020, doi: 10.1016/j.chemosphere.2020.127279.
- [80] K. Y. Foo and B. H. Hameed, "Insights into the modeling of adsorption isotherm systems," *Chem. Eng. J.*, vol. 156, no. 1, pp. 2–10, 2010, doi: 10.1016/j.cej.2009.09.013.
- [81] N. Ayawei, A. N. Ebelegi, and D. Wankasi, "Modelling and Interpretation of Adsorption Isotherms," *J. Chem.*, vol. 2017, 2017, doi: 10.1155/2017/3039817.
- [82] G. D. Halsey, "The Role of Surface Heterogeneity in Adsorption GEORGE," *Adv. Catal.*, vol. 4, pp. 259–269, 1952, doi: https://doi.org/10.1016/S0360-0564(08)60616-1.
- [83] N. A. A. Salim *et al.*, "Interpretation of isotherm models for adsorption of ammonium onto granular activated carbon," *Biointerface Res. Appl. Chem.*, vol. 11, no. 2, pp. 9227–9241, 2021, doi: 10.33263/BRIAC112.92279241.
- [84] H. Shahbeig, N. Bagheri, S. A. Ghorbanian, A. Hallajisani, and S. Poorkarimi, "A new adsorption isotherm model of aqueous solutions on granular activated

- carbon," World J. Model. Simul., vol. 9, no. 4, pp. 243–254, 2013.
- [85] A. O. Gbadamosi, R. Junin, M. A. Manan, A. Agi, and A. S. Yusuff, *An overview of chemical enhanced oil recovery: recent advances and prospects*, vol. 9, no. 3. Springer Berlin Heidelberg, 2019.
- [86] M. Ambaliya and A. Bera, "A Perspective Review on the Current Status and Development of Polymer Flooding in Enhanced Oil Recovery Using Polymeric Nanofluids," *Ind. Eng. Chem. Res.*, vol. 62, no. 6, pp. 2444–2459, 2023, doi: 10.1021/acs.iecr.2c04582.
- [87] J. Mariyate and A. Bera, "Recent progresses of microemulsions-based nanofluids as a potential tool for enhanced oil recovery," *Fuel*, vol. 306, no. August, p. 121640, 2021, doi: 10.1016/j.fuel.2021.121640.
- [88] A. Bera and H. Belhaj, "Application of nanotechnology by means of nanoparticles and nanodispersions in oil recovery A comprehensive review," *J. Nat. Gas Sci. Eng.*, vol. 34, pp. 1284–1309, 2016, doi: 10.1016/j.jngse.2016.08.023.
- [89] A. Sircar, K. Rayavarapu, N. Bist, K. Yadav, and S. Singh, "Applications of nanoparticles in enhanced oil recovery," *Pet. Res.*, no. xxxx, 2021, doi: 10.1016/j.ptlrs.2021.08.004.
- [90] F. S. Nworie, N. Mgbemena, A. C. Ike-Amadi, and J. Ebunoha, "Functionalized Biochars for Enhanced Removal of Heavy Metals from Aqueous Solutions: Mechanism and Future Industrial Prospects," *J. Human*, *Earth, Futur.*, vol. 3, no. 3, pp. 377–395, 2022, doi: 10.28991/HEF-2022-03-

03-09.

- [91] H. Shamsijazeyi, C. A. Miller, M. S. Wong, J. M. Tour, and R. Verduzco, "Polymer-coated nanoparticles for enhanced oil recovery," *J. Appl. Polym. Sci.*, vol. 131, no. 15, pp. 1–13, 2014, doi: 10.1002/app.40576.
- [92] A. Aitkulov and K. K. Mohanty, "Investigation of alkaline-surfactant-polymer flooding in a quarter five-spot sandpack for viscous oil recovery," *J. Pet. Sci. Eng.*, vol. 175, pp. 706–718, 2019, doi: 10.1016/j.petrol.2019.01.018.
- [93] T. O. Oni, "CFD Study of Behavior of Transition Flow in Distinct Tubes of Miscellaneous Tape Insertions," *HighTech Innov. J.*, vol. 3, no. 2, pp. 130–139, 2022, doi: 10.28991/HIJ-2022-03-02-02.
- [94] S. Kumar and A. Mandal, "Rheological properties and performance evaluation of synthesized anionic polymeric surfactant for its application in enhanced oil recovery," *Polymer (Guildf)*., vol. 120, pp. 30–42, 2017, doi: 10.1016/j.polymer.2017.05.051.
- [95] A. Pandey, H. Kesarwani, A. Saxena, R. Azin, and S. Sharma, "Effect of heterogeneity and injection rates on the recovery of oil from conventional sand packs: A simulation approach," *Pet. Res.*, no. xxxx, pp. 0–6, 2022, doi: 10.1016/j.ptlrs.2022.05.005.
- [96] A. Seethepalli, B. Adibhatla, and K. K. Mohanty, "Physicochemical interactions during surfactant flooding of fractured carbonate reservoirs," *SPE J.*, vol. 9, no. 4, pp. 411–418, 2004, doi: 10.2118/89423-PA.
- [97] A. B. D. Nematov, K. Kholurodov, M. Husenzoda, A. Lyubchyk, "Molecular

- Adsorption of H2O on TiO2 and TiO2:Y Surfaces D.," *Chem. Lett.*, vol. 3, no. 5, 2022, doi: 10. 28991/HEF-2022-03-02-07.
- [98] H. Ma, M. Luo, and L. L. Dai, "Influences of surfactant and nanoparticle assembly on effective interfacial tensions w z," pp. 2207–2213, 2008, doi: 10.1039/b718427c.
- [99] M. A. Ahmadi and S. R. Shadizadeh, "Nano-surfactant flooding in carbonate reservoirs: A mechanistic study," *Eur. Phys. J. Plus*, vol. 132, no. 6, 2017, doi: 10.1140/epjp/i2017-11488-6.
- [100] M. A. Ahmadi, "Use of nanoparticles to improve the performance of sodium dodecyl sulfate flooding in a sandstone reservoir," *Eur. Phys. J. Plus*, vol. 131, no. 12, 2016, doi: 10.1140/epjp/i2016-16435-5.
- [101] H. Soleimani *et al.*, "Impact of carbon nanotubes based nanofluid on oil recovery efficiency using core flooding," *Results Phys.*, vol. 9, pp. 39–48, 2018, doi: 10.1016/j.rinp.2018.01.072.
- [102] J. Bernholc, D. Brenner, M. Buongiorno Nardelli, V. Meunier, and C. Roland, "Mechanical and electrical properties of nanotubes," *Annu. Rev. Mater. Sci.*, vol. 32, pp. 347–375, 2002, doi: 10.1146/annurev.matsci.32.112601.134925.
- [103] N. Yahya, Advanced structured materials: carbon and oxide nanostructures, vol. 5. 2010.
- [104] A. Salar Elahi and M. Ghoranneviss, "Growth and characterization of carbon nanotubes and zinc oxide nanocomposite with the PECVD technique," *Results Phys.*, vol. 7, pp. 1006–1009, 2017, doi: 10.1016/j.rinp.2017.02.001.

- [105] S. H, "Synthesis of Carbon Nanotubes for Oil-water Interfacial Tension Reduction," *Oil Gas Res.*, vol. 1, no. 1, pp. 1–5, 2015, doi: 10.4172/2472-0518.1000104.
- [106] A. Tomova *et al.*, "Functionalization and characterization of MWCNT produced by different methods," *Acta Phys. Pol. A*, vol. 129, no. 3, pp. 405–408, 2016, doi: 10.12693/APhysPolA.129.405.
- [107] Y. Bai, D. Lin, F. Wu, Z. Wang, and B. Xing, "Adsorption of Triton X-series surfactants and its role in stabilizing multi-walled carbon nanotube suspensions," *Chemosphere*, vol. 79, no. 4, pp. 362–367, 2010, doi: 10.1016/j.chemosphere.2010.02.023.
- [108] S. Ebnesajjad and A. H. Landrock, "Surface Tension and Its Measurement," *Adhes. Technol. Handb.*, pp. 19–34, 2015, doi: 10.1016/b978-0-323-35595-7.00002-4.
- [109] H. W. Fox and C. H. Chrisman, "The ring method of measuring surface tension for liquids of high density and low surface tension," *J. Phys. Chem.*, vol. 56, no. 2, pp. 284–287, 1952, doi: 10.1021/j150494a031.
- [110] M. Szybowicz, A. B. Nowicka, and A. Dychalska, "Characterization of carbon nanomaterials by raman spectroscopy," *Charact. Nanomater. Adv. Key Technol.*, vol. 26, no. 2, pp. 1–36, 2018, doi: 10.1016/B978-0-08-101973-3.00001-8.
- [111] M. Moazzen *et al.*, "Multi-walled carbon nanotubes modified with iron oxide and silver nanoparticles (MWCNT-Fe 3 O 4 /Ag) as a novel adsorbent for

- determining PAEs in carbonated soft drinks using magnetic SPE-GC/MS method," *Arab. J. Chem.*, vol. 12, no. 4, pp. 476–488, 2019, doi: 10.1016/j.arabjc.2018.03.003.
- [112] N. T. Abdel-Ghani, G. A. El-Chaghaby, and F. S. Helal, "Individual and competitive adsorption of phenol and nickel onto multiwalled carbon nanotubes," *J. Adv. Res.*, vol. 6, no. 3, pp. 405–415, 2015, doi: 10.1016/j.jare.2014.06.001.
- [113] W. C. Oh, F. J. Zhang, and M. L. Chen, "Characterization and photodegradation characteristics of organic dye for Pt-titania combined multi-walled carbon nanotube composite catalysts," *J. Ind. Eng. Chem.*, vol. 16, no. 2, pp. 321–326, 2010, doi: 10.1016/j.jiec.2010.01.032.
- [114] V. K. Gupta, S. Agarwal, and T. A. Saleh, "Synthesis and characterization of alumina-coated carbon nanotubes and their application for lead removal," *J. Hazard. Mater.*, vol. 185, no. 1, pp. 17–23, 2011, doi: 10.1016/j.jhazmat.2010.08.053.
- [115] C. Chen, J. Hu, D. Shao, J. Li, and X. Wang, "Adsorption behavior of multiwall carbon nanotube/iron oxide magnetic composites for Ni(II) and Sr(II)," *J. Hazard. Mater.*, vol. 164, no. 2–3, pp. 923–928, 2009, doi: 10.1016/j.jhazmat.2008.08.089.
- [116] M. L. Chen and W. C. Oh, "Synthesis and highly visible-induced photocatalytic activity of CNT-CdSe composite for methylene blue solution," *Nanoscale Res. Lett.*, vol. 6, pp. 1–8, 2011, doi: 10.1186/1556-276X-6-398.

- [117] T. Sharma, "Impact of anionic surfactant on stability, viscoelastic moduli, and oil recovery of silica nanofluid in saline environment," *J. Pet. Sci. Eng.*, p. 107634, 2020, doi: 10.1016/j.petrol.2020.107634.
- [118] R. S. Kumar, R. Goswami, K. R. Chaturvedi, and T. Sharma, "Effect of nanoparticle on rheological properties of surfactant-based nanofluid for effective carbon utilization: capturing and storage prospects," 2021.
- [119] H. Kesarwani, A. Mandal, and S. Sharma, "Enhanced Oil Recovery from the Methyl Ester Sulfonate Derived from Flaxseed Oil: Interfacial, Adsorption and Rock Wetting Characteristics," *ChemistrySelect*, vol. 7, no. 13, 2022, doi: 10.1002/slct.202104593.
- [120] A. Pandey, V. Roy, H. Kesarwani, S. Sharma, and A. Saxena, "Evaluation of Silicon Carbide Nanoparticles as an Additive to Minimize Surfactant Loss during Chemical Flooding," *ChemistrySelect*, vol. 7, no. 22, 2022, doi: 10.1002/slct.202104294.
- [121] James J. Sheng, Modern Chemical Enhanced Oil Recovery. 2011.
- [122] A. Pandey, H. Kesarwani, C. Tewari, A. Saxena, S. Sharma, and N. G. Sahoo, "Waste plastic derived reduced graphene oxide as a potential additive for the surfactant polymer flooding: A sustainable solution," *J. Environ. Chem. Eng.*, vol. 11, no. 3, p. 109661, 2023, doi: 10.1016/j.jece.2023.109661.
- [123] S. S. Khaleduzzaman, I. M. Mahbubul, I. M. Shahrul, and R. Saidur, "Effect of particle concentration, temperature and surfactant on surface tension of nano fl uids ☆," *Int. Commun. Heat Mass Transf.*, vol. 49, pp. 110–114, 2013, doi:

- 10.1016/j.icheatmasstransfer.2013.10.010.
- [124] S. Vafaei, A. Purkayastha, A. Jain, G. Ramanath, and T. Borca-Tasciuc, "The effect of nanoparticles on the liquid-gas surface tension of Bi 2Te3 nanofluids," *Nanotechnology*, vol. 20, no. 18, 2009, doi: 10.1088/0957-4484/20/18/185702.
- [125] M. H. U. Bhuiyan, R. Saidur, M. A. Amalina, R. M. Mostafizur, and A. K. M. S. Islam, "Effect of nanoparticles concentration and their sizes on surface tension of nanofluids," *Procedia Eng.*, vol. 105, no. Icte 2014, pp. 431–437, 2015, doi: 10.1016/j.proeng.2015.05.030.
- [126] P. Pillai and A. Mandal, "A comprehensive micro scale study of poly-ionic liquid for application in enhanced oil recovery: Synthesis, characterization and evaluation of physicochemical properties," *J. Mol. Liq.*, p. 112553, 2020, doi: 10.1016/j.molliq.2020.112553.
- [127] A. Bera, A. Mandal, and B. B. Guha, "Synergistic E ff ect of Surfactant and Salt Mixture on Interfacial Tension Reduction between Crude Oil and Water in Enhanced Oil Recovery," 2014.
- [128] M. S. Kamal, I. A. Hussein, and A. S. Sultan, "Review on Surfactant Flooding: Phase Behavior, Retention, IFT, and Field Applications," *Energy and Fuels*, vol. 31, no. 8, pp. 7701–7720, 2017, doi: 10.1021/acs.energyfuels.7b00353.
- [129] S. Vats, F. Khan, D. Prajapati, A. Pandey, S. Sharma, and A. Saxena, "Synthesis and Evaluation of Mesoporous Silica Nanoparticle and its Application in Chemical Enhanced oil Recovery," *ChemistrySelect*, vol. 8, no. 12, 2023, doi: 10.1002/slct.202204206.

- [130] J. A. Ali, K. Kolo, A. K. Manshad, and K. D. Stephen, "Potential application of low-salinity polymeric-nanofluid in carbonate oil reservoirs: IFT reduction, wettability alteration, rheology and emulsification characteristics," *J. Mol. Liq.*, vol. 284, pp. 735–747, 2019, doi: 10.1016/j.molliq.2019.04.053.
- [131] T. Sharma, S. Iglauer, and J. S. Sangwai, "Silica Nanofluids in an Oilfield Polymer Polyacrylamide: Interfacial Properties, Wettability Alteration, and Applications for Chemical Enhanced Oil Recovery," *Ind. Eng. Chem. Res.*, vol. 55, no. 48, pp. 12387–12397, 2016, doi: 10.1021/acs.iecr.6b03299.
- [132] O. Tavakkoli, H. Kamyab, R. Junin, V. Ashokkumar, A. Shariati, and A. M. Mohamed, "SDS-Aluminum Oxide Nanofluid for Enhanced Oil Recovery: IFT, Adsorption, and Oil Displacement Efficiency," ACS Omega, vol. 7, no. 16, pp. 14022–14030, 2022, doi: 10.1021/acsomega.2c00567.
- [133] S. Chowdhury, S. Shrivastava, A. Kakati, and J. S. Sangwai, "Comprehensive Review on the Role of Surfactants in the Chemical Enhanced Oil Recovery Process," *Ind. Eng. Chem. Res.*, vol. 61, no. 1, pp. 21–64, 2022, doi: 10.1021/acs.iecr.1c03301.
- [134] F. Applications, M. S. Kamal, I. A. Hussein, and A. S. Sultan, "Review on Surfactant Flooding: Phase Review on Surfactant Flooding: Phase Behavior, Retention, IFT and Field Applications," 2017, doi: 10.1021/acs.energyfuels.7b00353.
- [135] S. Pal, M. Mushtaq, F. Banat, and A. M. Al Sumaiti, "Review of surfactant-assisted chemical enhanced oil recovery for carbonate reservoirs: challenges and future perspectives," *Pet. Sci.*, vol. 15, no. 1, pp. 77–102, 2018, doi:

- 10.1007/s12182-017-0198-6.
- [136] A. P. Pandey, V. Roy, H. Kesarwani, G. Mittal, S. Sharma, and A. Saxena, "OTC-31439-MS Effect of Silicon Carbide on the Surface Tension and Adsorption of SDS on the Sandstone Formation," 2022, doi: 10.4043/31439-MS.
- [137] S. C. Biswas and D. K. Chattoraj, "Kinetics of Adsorption of Cationic Surfactants at Charcoal-Water Interface," *J. Surf. Sci. Technol.*, vol. 14, no. 1--4, pp. 78–92, 1998, doi: 10.18311/jsst/1998/2101.
- [138] D. T. Grow and J. A. Shaeiwitz, "Surfactant adsorption dynamics," *J. Colloid Interface Sci.*, vol. 86, no. 1, pp. 239–253, 1982, doi: 10.1016/0021-9797(82)90062-5.
- [139] D. J. Groenendijk and J. N. M. Van Wunnik, "The Impact of Micelle Formation on Surfactant Adsorption-Desorption," *ACS Omega*, vol. 6, no. 3, pp. 2248–2254, 2021, doi: 10.1021/acsomega.0c05532.
- [140] T. W. Weber and R. K. Chakravorti, "Pore and solid diffusion models for fixed-bed adsorbers," *AIChE J.*, vol. 20, no. 2, pp. 228–238, 1974, doi: 10.1002/aic.690200204.
- [141] "Freundlich, H.M.F. (1906) Over the Adsorption in Solution. The Journal of Physical Chemistry, 57, 385-471. - References - Scientific Research Publishing."
 - https://www.scirp.org/(S(351jmbntvnsjt1aadkposzje))/reference/ReferencesPapers.aspx?ReferenceID=1530539 (accessed Sep. 29, 2021).

- [142] D. A.O, "Langmuir, Freundlich, Temkin and Dubinin–Radushkevich Isotherms Studies of Equilibrium Sorption of Zn 2+ Unto Phosphoric Acid Modified Rice Husk," *IOSR J. Appl. Chem.*, vol. 3, no. 1, pp. 38–45, 2012, doi: 10.9790/5736-0313845.
- [143] A. Sari, Q. Xie, Y. Chen, A. Saeedi, and E. Pooryousefy, "Drivers of Low Salinity E ff ect in Carbonate Reservoirs," 2017, doi: 10.1021/acs.energyfuels.7b00966.
- [144] R. A. Nasralla, H. A. Nasr-el-din, and A. Texas, "SPE 154334 Double-Layer Expansion: Is It A Primary Mechanism of Improved Oil Recovery by Low-Salinity Waterflooding?," no. 2008, 2012.
- [145] A. Roustaei and H. Bagherzadeh, "Experimental investigation of SiO 2 nanoparticles on enhanced oil recovery of carbonate reservoirs," pp. 27–33, 2015, doi: 10.1007/s13202-014-0120-3.
- [146] L. Hendraningrat and O. Torsæter, "Understanding Fluid-Fluid and Fluid-Rock Interactions in the Presence of Hydrophilic Nanoparticles at Various Conditions," no. 2011, 2014.
- [147] P. Pillai, A. Kumar, and A. Mandal, "Mechanistic Studies of Enhanced Oil Recovery by Imidazolium-based Ionic Liquids as Novel Surfactants

 ACCEPTE," J. Ind. Eng. Chem., 2018, doi: 10.1016/j.jiec.2018.02.024.
- [148] H. Eltoum, Y. L. Yang, and J. R. Hou, "The effect of nanoparticles on reservoir wettability alteration: a critical review," *Pet. Sci.*, vol. 18, no. 1, pp. 136–153, 2021, doi: 10.1007/s12182-020-00496-0.

- [149] X. Sun, Y. Zhang, G. Chen, and Z. Gai, "Application of nanoparticles in enhanced oil recovery: A critical review of recent progress," *Energies*, vol. 10, no. 3, 2017, doi: 10.3390/en10030345.
- [150] M. Kamibayashi, H. Ogura, and Y. Otsubo, "Rheological Behavior of Suspensions of Silica Nanoparticles in Associating Polymer Solutions," pp. 6899–6905, 2006.
- [151] J. P. Meyer, S. A. Adio, M. Sharifpur, and P. N. Nwosu, "The Viscosity of Nanofluids: A Review of the Theoretical, Empirical, and Numerical Models," *Heat Transf. Eng.*, vol. 37, no. 5, pp. 387–421, 2016, doi: 10.1080/01457632.2015.1057447.
- [152] I. M. Mahbubul, R. Saidur, and M. A. Amalina, "International Journal of Heat and Mass Transfer Latest developments on the viscosity of nanofluids," *Int. J. Heat Mass Transf.*, vol. 55, no. 4, pp. 874–885, 2012, doi: 10.1016/j.ijheatmasstransfer.2011.10.021.
- [153] Y. Alzahid, P. Mostaghimi, M. E. Warkiani, R. T. Armstrong, V. Joekar-Niasar, and N. Karadimitriou, "Alkaline surfactant polymer flooding: What happens at the pore scale?," *Soc. Pet. Eng. SPE Eur. Featur. 79th EAGE Conf. Exhib.*, pp. 386–402, 2017, doi: 10.2118/185832-ms.
- [154] S. Panmai, R. K. Prud'homme, D. G. Peiffer, S. Jockusch, and N. J. Turro, "Interactions between hydrophobically modified polymers and surfactants: A fluorescence study," *Langmuir*, vol. 18, no. 10, pp. 3860–3864, 2002, doi: 10.1021/la020165g.

- [155] C. Marliere, N. Wartenberg, M. Fleury, R. Tabary, C. Dalmazzone, and E. Delamaide, "Oil Recovery in Low Permeability Sandstone Reservoirs Using Surfactant-Polymer Flooding," 2015, doi: 10.2118/177072-ms.
- [156] Y. Ji, D. Wang, X. Cao, L. Guo, and Y. Zhu, "Both-branch amphiphilic polymer oil displacing system: Molecular weight, surfactant interactions and enhanced oil recovery performance," *Colloids Surfaces A Physicochem. Eng. Asp.*, vol. 509, pp. 440–448, 2016, doi: 10.1016/j.colsurfa.2016.09.031.
- [157] P. Druetta and F. Picchioni, "Surfactant-Polymer Flooding: Influence of the Injection Scheme," *Energy and Fuels*, vol. 32, no. 12, pp. 12231–12346, 2018, doi: 10.1021/acs.energyfuels.8b02900.
- [158] O. Massarweh and A. S. Abushaikha, "Application of surfactants in enhancing oil recovery from tight carbonates: Physicochemical properties and core flooding experiments," *Geoenergy Sci. Eng.*, vol. 221, no. August 2022, p. 211400, 2023, doi: 10.1016/j.geoen.2022.211400.
- [159] A. Rezaei, Z. Derikvand, R. Parsaei, and M. Imanivarnosfaderani, "1 P re of,"
 J. Mol. Liq., p. 115091, 2020, doi: 10.1016/j.molliq.2020.115091.
- [160] R. Abhishek, G. S. Kumar, and R. K. Sapru, "Wettability alteration in carbonate reservoirs using nanofluids," *Pet. Sci. Technol.*, vol. 33, no. 7, pp. 794–801, 2015, doi: 10.1080/10916466.2015.1014967.
- [161] Z. Fan *et al.*, "Oil sorption and recovery by using vertically aligned carbon nanotubes," *Carbon N. Y.*, vol. 48, no. 14, pp. 4197–4200, 2010, doi: 10.1016/j.carbon.2010.07.001.

- [162] G. Cheraghian and L. Hendraningrat, "A review on applications of nanotechnology in the enhanced oil recovery part A: effects of nanoparticles on interfacial tension," *Int. Nano Lett.*, vol. 6, no. 2, pp. 129–138, 2016, doi: 10.1007/s40089-015-0173-4.
- [163] M. C. F. S. Lima *et al.*, "Aqueous suspensions of carbon black with ethylenediamine and polyacrylamide-modified surfaces: Applications for chemically enhanced oil recovery," *Carbon N. Y.*, vol. 109, pp. 290–299, 2016, doi: 10.1016/j.carbon.2016.08.021.
- [164] M. Inagaki, A. Kawahara, and H. Konno, "Sorption and recovery of heavy oils using carbonized fir fibers and recycling," *Carbon N. Y.*, vol. 40, no. 1, pp. 105–111, 2002, doi: 10.1016/S0008-6223(01)00083-5.
- [165] M. S. Kamal, A. A. Adewunmi, A. S. Sultan, M. F. Al-hamad, and U. Mehmood, "Recent Advances in Nanoparticles Enhanced Oil Recovery: Rheology, Interfacial Tension, Oil Recovery, and Wettability Alteration," vol. 2017, 2017.
- [166] K. R. Chaturvedi and T. Sharma, "Evaluation of Polymer-Assisted Carbonated Water Injection in Sandstone Reservoir: Absorption Kinetics, Rheology, and Oil Recovery Results," 2019, doi: 10.1021/acs.energyfuels.9b00894.
- [167] O. A. Alomair, K. M. Matar, and Y. H. Alsaeed, "Nanofluids Application for Heavy Oil Recovery," no. October, pp. 14–16, 2014, doi: https://doi.org/10.2118/171539-MS.
- [168] B. Wei, Q. Li, F. Jin, H. Li, and C. Wang, "The Potential of a Novel Nano fl

- uid in Enhancing Oil Recovery," 2016, doi: 10.1021/acs.energyfuels.6b00244.
- [169] B. Peng, L. Zhang, J. Luo, P. Wang, and B. Ding, "A review of nanomaterials for nano fl uid enhanced," pp. 32246–32254, 2017, doi: 10.1039/C7RA05592G.
- [170] G. Cheraghian and S. Rostami, "Nanotechnology in Enhanced Oil Recovery," pp. 1–17, 2020.
- [171] Y. Tian, L. Wang, Y. Tang, C. Liu, C. Ma, and T. Wang, "Research and application of nano polymer microspheres diversion technique of deep fluid," *Soc. Pet. Eng. SPE Int. Oilf. Nanotechnol. Conf. 2012*, vol. 2, pp. 261–266, 2012, doi: 10.2118/156999-ms.
- [172] S. Ayatollahi, P. Engineering, and M. M. Zerafat, "SPE 157106094 Nanotechnology-Assisted EOR Techniques: New Solutions to Old Challenges," no. c, 2012.
- [173] D. Rusheet and A. Fairbanks, "Application of Nanoparticle Saturated Injectant Gases for EOR of Heavy Oils," no. August 2003, pp. 4–7, 2009.
- [174] P. Purswani, M. S. Taw, and Z. T. Karpyn, "Factors and Mechanisms

 Governing Wettability Alteration by Chemically Tuned Water fl ooding: A

 Review," 2017, doi: 10.1021/acs.energyfuels.7b01067.
- [175] I. K. Shaik, J. Song, S. L. Biswal, G. J. Hirasaki, P. K. Bikkina, and C. P. Aichele, "Journal of Petroleum Science and Engineering Effect of brine type and ionic strength on the wettability alteration of naphthenic-acid-adsorbed calcite surfaces," *J. Pet. Sci. Eng.*, no. May, p. 106567, 2019, doi:

- 10.1016/j.petrol.2019.106567.
- [176] S. Al-araimi, M. Karimi, and R. S. Al-maamari, "Experimental Investigation of the E ff ect of Acid and Base on Wettability Alteration of a Calcite Surface," 2021, doi: 10.1021/acs.energyfuels.1c01167.
- [177] T. Puntervold, S. Strand, and T. Austad, "Water Flooding of Carbonate Reservoirs: Effects of a Model Base and Natural Crude Oil Bases on Chalk Wettability," vol. 28, no. 5, pp. 1606–1616, 2007.
- [178] A. Karimi *et al.*, "Wettability alteration in carbonates using zirconium oxide nanofluids: EOR implications," *Energy and Fuels*, vol. 26, no. 2, pp. 1028–1036, 2012, doi: 10.1021/ef201475u.
- [179] S. Li, M. Genys, K. Wang, and O. Torsæter, "Experimental Study of Wettability Alteration during Nanofluid Enhanced Oil," 2015.
- [180] M. Mohebbifar, M. H. Ghazanfari, and M. Vossoughi, "Experimental Investigation of Nano-Biomaterial Applications for Heavy Oil Recovery in Shaly Porous Models: A Pore-Level Study," *J. Energy Resour. Technol.*, vol. 137, no. 1, pp. 1–9, 2015, doi: 10.1115/1.4028270.
- [181] S. Pandey *et al.*, "Bulk synthesis of graphene nanosheets from plastic waste:

 An invincible method of solid waste management for better tomorrow," *Waste Manag.*, vol. 88, pp. 48–55, Apr. 2019, doi: 10.1016/j.wasman.2019.03.023.
- [182] G. Tatrari *et al.*, "Waste plastic derived graphene sheets as nanofillers to enhance mechanical strength of concrete mixture: An inventive approach to deal with universal plastic waste," *Clean. Eng. Technol.*, vol. 5, p. 100275,

- Dec. 2021, doi: 10.1016/j.clet.2021.100275.
- [183] S. Kumar, C. Tewari, N. G. Sahoo, and L. Philip, "Mechanistic insights into carbo-catalyzed persulfate treatment for simultaneous degradation of cationic and anionic dye in multicomponent mixture using plastic waste–derived carbon," *J. Hazard. Mater.*, vol. 435, p. 128956, Aug. 2022, doi: 10.1016/j.jhazmat.2022.128956.
- [184] C. Tewari *et al.*, "Green and cost-effective synthesis of 2D and 3D graphene-based nanomaterials from Drepanostachyum falcatum for bio-imaging and water purification applications," *Chem. Eng. J. Adv.*, vol. 10, p. 100265, May 2022, doi: 10.1016/j.ceja.2022.100265.
- [185] C. Tewari *et al.*, "A simple, eco-friendly and green approach to synthesis of blue photoluminescent potassium-doped graphene oxide from agriculture waste for bio-imaging applications," *Mater. Sci. Eng. C*, vol. 104, p. 109970, Nov. 2019, doi: 10.1016/j.msec.2019.109970.
- [186] C. Tewari, B. SanthiBhushan, A. Srivastava, and N. G. Sahoo, "Metal doped graphene oxide derived from Quercus ilex fruits for selective and visual detection of iron(III) in water: Experiment and theory," *Sustain. Chem. Pharm.*, vol. 21, p. 100436, Jun. 2021, doi: 10.1016/j.scp.2021.100436.
- [187] S. Stankovich *et al.*, "Synthesis of graphene-based nanosheets via chemical reduction of exfoliated graphite oxide," *Carbon N. Y.*, vol. 45, no. 7, pp. 1558–1565, 2007, doi: 10.1016/j.carbon.2007.02.034.
- [188] W. I. Goldburg, "Dynamic light scattering," Am. J. Phys., vol. 67, no. 12, pp.

- 1152–1160, 1999, doi: 10.1119/1.19101.
- [189] M. Mohammad, P. Omidvar, and F. Naeimi, "Salinity of injection water and its impact on oil recovery absolute permeability, residual oil saturation, interfacial tension and capillary pressure," *Egypt. J. Pet.*, 2016, doi: 10.1016/j.ejpe.2016.05.003.
- [190] A. S. Eltaweil, E. M. Abd El-Monaem, G. M. El-Subruiti, B. M. Ali, M. M. Abd El-Latif, and A. M. Omer, "Graphene oxide incorporated cellulose acetate beads for efficient removal of methylene blue dye; isotherms, kinetic, mechanism and co-existing ions studies," *J. Porous Mater.*, 2022, doi: 10.1007/s10934-022-01347-6.
- [191] I. K. Basha, E. M. Abd El-Monaem, R. E. Khalifa, A. M. Omer, and A. S. Eltaweil, "Sulfonated graphene oxide impregnated cellulose acetate floated beads for adsorption of methylene blue dye: optimization using response surface methodology," *Sci. Rep.*, vol. 12, no. 1, pp. 1–17, 2022, doi: 10.1038/s41598-022-13105-4.
- [192] S. Al-anssari, A. Barifcani, S. Wang, L. Maxim, and S. Iglauer, "Journal of Colloid and Interface Science Wettability alteration of oil-wet carbonate by silica nanofluid," *J. Colloid Interface Sci.*, vol. 461, pp. 435–442, 2016, doi: 10.1016/j.jcis.2015.09.051.
- [193] S. Tanvir and L. Qiao, "Surface tension of Nanofluid-type fuels containing suspended nanomaterials," pp. 1–10, 2012.
- [194] G. K. Pothula, R. K. Vij, and A. Bera, "An overview of chemical enhanced oil

- recovery and its status in India," *Pet. Sci.*, no. xxxx, 2023, doi: 10.1016/j.petsci.2023.01.001.
- [195] M. Liu, J. K. Beattie, and A. Gray-weale, "The Surface Relaxation of Water," 2012.
- [196] M. Amadu and M. J. Pegg, "Analytical derivation of a pH dependent contact angle equation and the relationship to industrial processes of energy concerns," *J. Pet. Sci. Eng.*, 2019, doi: 10.1016/j.petrol.2018.11.036.
- [197] J. Song and M. W. Kim, "Excess Charge Density and its Relationship with Surface Tension Increment at the Air Electrolyte Solution Interface," pp. 1856–1862, 2011.
- [198] M. Amirpour, S. Reza, H. Esfandyari, and S. Ahmadi, "Experimental investigation of wettability alteration on residual oil saturation using nonionic surfactants: Capillary pressure measurement," *Petroleum*, vol. 1, no. 4, pp. 289–299, 2015, doi: 10.1016/j.petlm.2015.11.003.
- [199] S. Li, L. Hendraningrat, O. Torsæter, and T. Ntnu, "IPTC 16707 Improved Oil Recovery by Hydrophilic Silica Nanoparticles Suspension : 2- Phase Flow Experimental Studies," pp. 1–15, 2013.
- [200] A. Bardhan, "SPE-204263-STU Graphene as a Surfactant Carrier: A Performance Study for Enhanced Oil Recovery Applications Surfactant EOR – Mechanism & Problems Surfactant Adsorption," 2020.
- [201] A. V. Minakov, M. I. Pryazhnikov, Y. N. Suleymana, V. D. Meshkova, and D.V. Guzei, "Experimental study of nanoparticle size and material effect on the

- oil wettability characteristics of various rock types," *J. Mol. Liq.*, vol. 327, p. 114906, 2021, doi: 10.1016/j.molliq.2020.114906.
- [202] E. Virga, E. Spruijt, W. M. De Vos, and P. M. Biesheuvel, "Wettability of Amphoteric Surfaces: The Effect of pH and Ionic Strength on Surface Ionization and Wetting," *Langmuir*, vol. 34, no. 50, pp. 15174–15180, 2018, doi: 10.1021/acs.langmuir.8b02875.
- [203] A. Vázquez-quesada, R. I. Tanner, and M. Ellero, "Shear Thinning of Noncolloidal Suspensions," vol. 108001, no. September, pp. 1–5, 2016, doi: 10.1103/PhysRevLett.117.108001.
- [204] H. Kesarwani, A. Saxena, and S. Sharma, "Novel Jatropha Oil Based Emulsion Drilling Mud Out performs Conventional Drilling Mud: A comparative study," Energy Sources, Part A Recover. Util. Environ. Eff., Jan. 2020, doi: 10.1080/15567036.2020.1827095.
- [205] N. Yekeen, A. M. Ali Elakkari, J. A. Khan, M. Ali, A. Al-Yaseri, and H. Hoteit, "Experimental and Computational Fluid Dynamics Investigation of Mechanisms of Enhanced Oil Recovery via Nanoparticle-Surfactant Solutions," *Energy and Fuels*, 2023, doi: 10.1021/acs.energyfuels.3c00136.
- [206] N. Yekeen, A. A. Malik, A. K. Idris, N. I. Reepei, and K. Ganie, Foaming properties, wettability alteration and interfacial tension reduction by saponin extracted from soapnut (Sapindus Mukorossi) at room and reservoir conditions, vol. 195. Elsevier B.V., 2020.
- [207] A. P. Tchameni, L. D. W. Djouonkep, R. D. Nagre, and X. Wang, "Thermo-

- responsive polymer-based Janus biogenic-nanosilica composite, part B: Experimental study as a multi-functional synergistic shale stabilizer for water-based drilling fluids," *J. Mol. Liq.*, vol. 395, p. 123921, 2024, doi: https://doi.org/10.1016/j.molliq.2023.123921.
- [208] L. D. Wandji Djouonkep *et al.*, "Enhanced amphoteric polymer filtration reducer with vinyl-functionalized nanosilica for high-salt and ultra-high temperature water-based drilling environments," *Geoenergy Sci. Eng.*, vol. 236, p. 212743, 2024, doi: https://doi.org/10.1016/j.geoen.2024.212743.
- [209] P. Pandey and A. Choubey, "Green Synthesized ZnO@CuO Nanocomposites Using Achyranthes aspera Leaves Extract for Dielectric Applications," *J. Alloys Compd.*, vol. 970, p. 172492, 2023, doi: 10.1016/j.jallcom.2023.172492.
- [210] Y. Yang, T. Cheng, H. Wu, Z. You, D. Shang, and J. Hou, "Enhanced Oil Recovery Using Oleic Acid-Modified Titania Nanofluids: Underlying Mechanisms and Oil-Displacement Performance," *Energy and Fuels*, vol. 34, no. 5, pp. 5813–5822, 2020, doi: 10.1021/acs.energyfuels.0c00594.
- [211] S. Ranjan, N. Dasgupta, and E. Lichtfouse, *Nanoscience in Food and Agriculture 3*, vol. 23. 2016.
- [212] N. Yekeen, T. Xin Kun, A. Al-Yaseri, F. Sagala, and A. Kamal Idris, "Influence of critical parameters on nanoparticles-surfactant stabilized CO2 foam stability at sub-critical and supercritical conditions," *J. Mol. Liq.*, vol. 338, p. 116658, 2021, doi: 10.1016/j.molliq.2021.116658.
- [213] J. Hou, J. Du, H. Sui, and L. Sun, A review on the application of nanofluids in

- enhanced oil recovery, vol. 16, no. 8. 2022.
- [214] D. Liu, X. Zhang, F. Tian, X. Liu, J. Yuan, and B. Huang, "Review on nanoparticle-surfactant nanofluids: formula fabrication and applications in enhanced oil recovery," *J. Dispers. Sci. Technol.*, vol. 43, no. 5, pp. 745–759, 2022, doi: 10.1080/01932691.2020.1844745.
- [215] W. Al-Shatty, M. Campana, S. Alexander, and A. R. Barron, "Interaction of Surface-Modified Alumina Nanoparticles and Surfactants at an Oil/Water Interface: A Neutron Reflectometry, Scattering, and Enhanced Oil Recovery Study," ACS Appl. Mater. Interfaces, vol. 14, no. 17, pp. 19505–19514, 2022, doi: 10.1021/acsami.2c02228.
- [216] N. Lashari, T. Ganat, S. Kalam, T. A. Chandio, T. Sharma, and S. Qureshi, "Impact of a novel HPAM/GO-SiO2 nanocomposite on interfacial tension: Application for enhanced oil recovery," *Pet. Sci. Technol.*, vol. 40, no. 3, pp. 290–309, 2022, doi: 10.1080/10916466.2021.1993915.
- [217] N. Yekeen, M. A. Manan, A. K. Idris, A. M. Samin, and A. R. Risal, "Experimental investigation of minimization in surfactant adsorption and improvement in surfactant-foam stability in presence of silicon dioxide and aluminum oxide nanoparticles," *J. Pet. Sci. Eng.*, vol. 159, pp. 115–134, 2017, doi: 10.1016/j.petrol.2017.09.021.
- [218] H. Kesarwani, M. Belal Haider, R. Kumar, and S. Sharma, "Performance evaluation of deep eutectic solvent for surfactant polymer flooding," *J. Mol. Liq.*, vol. 362, p. 119734, 2022, doi: 10.1016/j.molliq.2022.119734.

- [219] N. M. Briggs *et al.*, "Multiwalled Carbon Nanotubes at the Interface of Pickering Emulsions," *Langmuir*, vol. 31, no. 48, pp. 13077–13084, 2015, doi: 10.1021/acs.langmuir.5b03189.
- [220] N. Briggs *et al.*, "Stable pickering emulsions using multi-walled carbon nanotubes of varying wettability," *Colloids Surfaces A Physicochem. Eng. Asp.*, vol. 537, pp. 227–235, 2018, doi: 10.1016/j.colsurfa.2017.10.010.
- [221] N. Yekeen, E. Padmanabhan, A. H. Syed, T. Sevoo, and K. Kanesen, "Synergistic influence of nanoparticles and surfactants on interfacial tension reduction, wettability alteration and stabilization of oil-in-water emulsion," *J. Pet. Sci. Eng.*, vol. 186, no. November 2019, p. 106779, 2020, doi: 10.1016/j.petrol.2019.106779.
- [222] T. Arya *et al.*, "Influence of bio-resource-derived graphene oxide on the mechanical and thermal properties of poly(vinyl alcohol) nanocomposites," *Polym. Compos.*, 2023, doi: 10.1002/pc.27808.
- [223] C. Tewari, Y. Kim, Y. Kim, S. Ryu, H. Jeong, and Y. Jung, "Development of fluorescent epoxy composite with carbon-based nanomaterial additives derived from agricultural waste," *J. Vinyl Addit. Technol.*, 2023, doi: 10.1002/vnl.22032.
- [224] P. Sahu, R. P. Verma, C. Tewari, N. Sahoo, and B. Saha, "Environmental application of amine functionalised magnetite nanoparticles grafted graphene oxide chelants," *Environ. Sci. Pollut. Res.*, vol. 29, pp. 1–14, 2022, doi: 10.1007/s11356-022-21407-3.

- [225] C. Tewari, Y. Kim, H. Muramatsu, M. Endo, Y. Kim, and Y. Jung, "Development and Optimization of Water-Soluble Double-Walled Carbon Nanotubes by Effective Surface Treatment of Inner Walls," *Langmuir*, vol. 39, 2023, doi: 10.1021/acs.langmuir.3c00092.
- [226] C. Tewari *et al.*, "Can graphene-based composites and membranes solve current water purification challenges a comprehensive review," *Desalination*, vol. 567, p. 116952, 2023, doi: 10.1016/j.desal.2023.116952.
- [227] C. Tewari *et al.*, "Waste plastics derived reduced graphene oxide-based nanocomposite with Fe3O4 for water purification and supercapacitor applications," *J. Ind. Eng. Chem.*, 2023, doi: 10.1016/j.jiec.2023.09.038.
- [228] T. Somanathan, K. Prasad, K. K. Ostrikov, A. Saravanan, and V. M. Krishna, "Graphene oxide synthesis from agro waste," *Nanomaterials*, vol. 5, no. 2, pp. 826–834, 2015, doi: 10.3390/nano5020826.
- [229] R. S. Kumar, K. R. Chaturvedi, S. Iglauer, J. Trivedi, and T. Sharma, "Impact of anionic surfactant on stability, viscoelastic moduli, and oil recovery of silica nanofluid in saline environment," *J. Pet. Sci. Eng.*, vol. 195, no. July, p. 107634, 2020, doi: 10.1016/j.petrol.2020.107634.
- [230] S. Al-Anssari, M. Arif, S. Wang, A. Barifcani, and S. Iglauer, "Stabilising nanofluids in saline environments," *J. Colloid Interface Sci.*, vol. 508, no. August, pp. 222–229, 2017, doi: 10.1016/j.jcis.2017.08.043.
- [231] Y. Zhang *et al.*, "Investigation on interfacial/surface properties of bio-based surfactant N-aliphatic amide-N,N-diethoxypropylsulfonate sodium as an oil

- displacement agent regenerated from waste cooking oil," *J. Mol. Liq.*, vol. 223, pp. 68–74, 2016, doi: 10.1016/j.molliq.2016.08.026.
- [232] Z. Y. Qi, Y. F. Wang, and X. L. Xu, "Effects of interfacial tension reduction and wettability alteration on oil recovery by surfactant imbibition," *Adv. Mater. Res.*, vol. 868, pp. 664–668, 2014, doi: 10.4028/www.scientific.net/AMR.868.664.
- [233] J. Hou and L. Sun, "Synergistic effect of nanofluids and surfactants on heavy oil recovery and oil-wet calcite wettability," *Nanomaterials*, vol. 11, no. 7, 2021, doi: 10.3390/nano11071849.
- [234] H. Kesarwani and S. Sharma, "Adsorption Behaviour of Karanj Oil Surfactant

 Role of Different Adsorbent Surfaces," 83rd EAGE Annu. Conf. Exhib., vol.

 2022, no. 1, pp. 1–5, Jun. 2022, doi: 10.3997/2214-4609.202210619.
- [235] H. Vatanparast, F. Shahabi, A. Bahramian, A. Javadi, and R. Miller, "The role of electrostatic repulsion on increasing surface activity of anionic surfactants in the presence of hydrophilic silica nanoparticles," *Sci. Rep.*, vol. 8, no. 1, pp. 1–11, 2018, doi: 10.1038/s41598-018-25493-7.
- [236] M. Y. Rezk and N. K. Allam, "Impact of Nanotechnology on Enhanced Oil Recovery: A Mini-Review," *Ind. Eng. Chem. Res.*, vol. 58, no. 36, pp. 16287– 16295, 2019, doi: 10.1021/acs.iecr.9b03693.
- [237] J. K. Beattie *et al.*, "PH and the surface tension of water," *J. Colloid Interface Sci.*, vol. 422, pp. 54–57, 2014, doi: 10.1016/j.jcis.2014.02.003.
- [238] S. Hoeiland, T. Barth, A. M. Blokhus, and A. Skauge, "The effect of crude oil

- acid fractions on wettability as studied by interfacial tension and contact angles," *J. Pet. Sci. Eng.*, vol. 30, no. 2, pp. 91–103, 2001, doi: 10.1016/S0920-4105(01)00106-1.
- [239] Z. Ylmaz, S. Aktemur, H. D. Buzoglu, and M. Gümüsderelioglu, "The effect of temperature and pH variations on the surface tension of EDTA solutions," *J. Endod.*, vol. 37, no. 6, pp. 825–827, 2011, doi: 10.1016/j.joen.2011.03.012.
- [240] P. D. Cratin, "Mathematical Modeling of Some pH-Dependent Surface and interfacial Properties of Steaic Acid," *J. Dispers. Sci. Technol.*, vol. 14, no. 5, pp. 559–602, 1993, doi: 10.1080/01932699308943427.
- [241] J. F. Danielli and P. R. S. L. B, "The relations between surface p H, ion concentrations and interfacial tension," *Proc. R. Soc. London. Ser. B Biol. Sci.*, vol. 122, no. 827, pp. 155–174, 1937, doi: 10.1098/rspb.1937.0018.
- [242] H. Hartridge, R. A. Peters, and P. R. S. L. A, "Interfacial tension and hydrogenion concentration," *Proc. R. Soc. London. Ser. A, Contain. Pap. a Math. Phys. Character*, vol. 101, no. 711, pp. 348–367, 1922, doi: 10.1098/rspa.1922.0050.
- [243] A. Bera, K. Ojha, and A. Mandal, "Synergistic effect of mixed surfactant systems on foam behavior and surface tension," *J. Surfactants Deterg.*, vol. 16, no. 4, pp. 621–630, 2013, doi: 10.1007/s11743-012-1422-4.
- [244] A. Samanta, A. Bera, K. Ojha, and A. Mandal, "Effects of alkali, salts, and surfactant on rheological behavior of partially hydrolyzed polyacrylamide solutions," *J. Chem. Eng. Data*, vol. 55, no. 10, pp. 4315–4322, 2010, doi: 10.1021/je100458a.

- [245] M. Rahimi and M. Vadi, "Langmuir, Freundlich and Temkin Adsorption Isotherms of Propranolol on Multi-Wall Carbon Nanotube," *J. Mod. Drug Discov. Drug Deliv. Res.*, pp. 1–3, 2014.
- [246] M. J. Tempkin and V. Pyzhev, "Recent modifications to Langmuir isotherms," vol. 12, pp. 217–222, May 2023.
- [247] C. B. Vidal *et al.*, "Adsorption of polycyclic aromatic hydrocarbons from aqueous solutions by modified periodic mesoporous organosilica," *J. Colloid Interface Sci.*, vol. 357, no. 2, pp. 466–473, 2011, doi: 10.1016/j.jcis.2011.02.013.
- [248] Q. S. Liu, T. Zheng, P. Wang, J. P. Jiang, and N. Li, "Adsorption isotherm, kinetic and mechanism studies of some substituted phenols on activated carbon fibers," *Chem. Eng. J.*, vol. 157, no. 2–3, pp. 348–356, 2010, doi: 10.1016/j.cej.2009.11.013.
- [249] M. A. Islam, M. A. Chowdhury, M. S. I. Mozumder, and M. T. Uddin, "Langmuir Adsorption Kinetics in Liquid Media: Interface Reaction Model," *ACS Omega*, vol. 6, no. 22, pp. 14481–14492, 2021, doi: 10.1021/acsomega.1c01449.
- [250] W. G. Anderson, "Wettability Literature Survey Part 1: Rock-Oil-Brine Interactions and the Effects of Core Handlding on Wettability.," Soc. Pet. Eng. AIME, SPE, 1985.
- [251] P. Muller, G. Sudre, and O. Théodoly, "Wetting transition on hydrophobic surfaces covered by polyelectrolyte brushes," *Langmuir*, vol. 24, no. 17, pp.

- 9541–9550, 2008, doi: 10.1021/la801406x.
- [252] A. O. Mmbuji, R. Cao, Y. Li, X. Xu, and E. X. Ricky, "Nanoparticle-Assisted Surfactant / Polymer Formulations for Enhanced Oil Recovery in Sandstone Reservoirs: From Molecular Interaction to Field Application," 2023, doi: 10.1021/acs.energyfuels.3c02742.
- [253] S. Kumar, N. Saxena, and A. Mandal, "Journal of Industrial and Engineering Chemistry Synthesis and evaluation of physicochemical properties of anionic polymeric surfactant derived from Jatropha oil for application in enhanced oil recovery," *J. Ind. Eng. Chem.*, vol. 43, pp. 106–116, 2016, doi: 10.1016/j.jiec.2016.07.055.
- [254] A. Bera, S. Shah, M. Shah, J. Agarwal, and R. K. Vij, "Mechanistic study on silica nanoparticles-assisted guar gum polymer flooding for enhanced oil recovery in sandstone reservoirs," *Colloids Surfaces A Physicochem. Eng. Asp.*, vol. 598, p. 124833, 2020, doi: 10.1016/j.colsurfa.2020.124833.
- [255] I. M. Mahbubul, R. Saidur, and M. A. Amalina, "Latest developments on the viscosity of nanofluids," *Int. J. Heat Mass Transf.*, vol. 55, no. 4, pp. 874–885, 2012, doi: 10.1016/j.ijheatmasstransfer.2011.10.021.
- [256] M. A. Haruna, J. Gardy, G. Yao, Z. Hu, N. Hondow, and D. Wen, "Nanoparticle modified polyacrylamide for enhanced oil recovery at harsh conditions," *Fuel*, vol. 268, p. 117186, 2020, doi: https://doi.org/10.1016/j.fuel.2020.117186.
- [257] Z. Hu, M. Haruna, H. Gao, E. Nourafkan, and D. Wen, "Rheological Properties

- of Partially Hydrolyzed Polyacrylamide Seeded by Nanoparticles," *Ind. Eng. Chem. Res.*, vol. 56, no. 12, pp. 3456–3463, 2017, doi: 10.1021/acs.iecr.6b05036.
- [258] E. Nourafkan, M. A. Haruna, J. Gardy, and D. Wen, "Improved rheological properties and stability of multiwalled carbon nanotubes/polymer in harsh environment," *J. Appl. Polym. Sci.*, vol. 136, no. 11, p. 47205, 2019, doi: https://doi.org/10.1002/app.47205.
- [259] M. A. Haruna, S. Pervaiz, Z. Hu, E. Nourafkan, and D. Wen, "Improved rheology and high-temperature stability of hydrolyzed polyacrylamide using graphene oxide nanosheet," *J. Appl. Polym. Sci.*, vol. 136, no. 22, p. 47582, 2019, doi: https://doi.org/10.1002/app.47582.
- [260] S. O. Olayiwola and M. Dejam, "A comprehensive review on interaction of nanoparticles with low salinity water and surfactant for enhanced oil recovery in sandstone and carbonate reservoirs," *Fuel*, vol. 241, no. December 2018, pp. 1045–1057, 2019, doi: 10.1016/j.fuel.2018.12.122.
- [261] H. F. Asl, G. Zargar, A. K. Manshad, M. A. Takassi, J. A. Ali, and A. Keshavarz, "Effect of SiO2 nanoparticles on the performance of L-Arg and L-Cys surfactants for enhanced oil recovery in carbonate porous media," *J. Mol. Liq.*, vol. 300, p. 112290, 2020, doi: 10.1016/j.molliq.2019.112290.